

# **The Remote Sensing of Fires and their Effects on Soil Properties in the uKhahlamba Drakensberg Park**

A thesis submitted in fulfilment of the  
requirements for the degree of  
MASTER OF SCIENCE  
at  
Rhodes University  
November 2018

By  
Natasha Jade Moore

Supervisor:  
Prof. K.I. Meiklejohn (Rhodes University)



**RHODES UNIVERSITY**  
*Where leaders learn*

## ABSTRACT

Fires are a common and natural occurrence globally and specifically on the African continent. The Drakensberg Mountains are home to southern Africa's high-altitude fire-climax grasslands, where fire is the dominant management tool. Fire is used to maintain the grasslands in the uKhahlamba Drakensberg Park (UDP) World Heritage Site, located on the eastern escarpment of the KwaZulu-Natal Drakensberg. This study aimed to investigate the spatial and temporal frequency of fires using remote sensing, and to investigate the effect of fire frequency on soil properties in the UDP. Remote sensing offers a set of supportive tools for the management of this sensitive vegetation and specifically to assess the frequency and spatial extent of fires. Field assessments can then be used to assess the impact of fires. Remotely sensed data were used to determine fire frequency and the spatial extent of fires in the UDP. The Moderate Resolution Imaging Spectroradiometer (MODIS) and Visible Infrared Imaging Radiometer Suite (VIIRS) active fire detection point data were processed to investigate the temporal resolution of fires. Landsat 5 and 8 imagery were utilised for conducting Normalised Burn Ratios (NBR) to determine the spatial extent of the burn scars of fires. The results from the remotely sensed data were used to select study sites for accessing the effects of fire frequency on soil properties. The remote sensing results showed the main fire season in the UDP was from May to October, and annual burn scars from the available Landsat data for 1998 to 2017 ranged from 22.5% to 57.67% of the UDP. Remote sensing was shown to be an effective tool for monitoring fires in the UDP, with a combination of satellite data producing the best results. Soil properties were highly varied across the UDP. Environmental factors were shown to have a more significant influence on soil properties than fire frequency. This study highlighted the complex nature and diversity of fires and soils across the UDP.

## ACKNOWLEDGEMENTS

Thank you to the following people for the support and input into my research project:

To Professor Ian Meiklejohn, my supervisor, for all his input into my project, his patience and for calming my nerves. To my mom, Geraldine Moore, who climbed mountains for me (literally) and accompanied me on all my fieldwork and was a dedicated fieldwork scribe. To Abe Ngoepe, the Senior Technical Officer for the Geography Department, who provided me with my fieldwork equipment and helped me with my soil laboratory work. To Hans-Peter Bakker, from Rhodes University, for running the statistical tests for my soil samples and giving up his time to always be available.

Thank you to the South African National Space Agency (SANSA) for supporting me and funding my two years of studies. Thank you to Ezemvelo KZN Wildlife for accepting my research project and granting me with a permit to access and collect my soil samples in the uKhahlamba Drakensberg Park.

Finally, thank you to the Rhodes University Geography Department for being a welcoming and supportive place for all my years of studies.



## TABLE OF CONTENTS

<b>CHAPTER 1: INTRODUCTION .....</b>	<b>1</b>
1.1 BACKGROUND.....	1
1.2 MOTIVATION.....	2
1.3 AIMS AND OBJECTIVES .....	3
<b>CHAPTER 2: LITERATURE REVIEW .....</b>	<b>4</b>
2.1 INTRODUCTION .....	4
2.2 FIRE .....	4
2.2.1 Fires in South Africa .....	4
2.2.2 Fires in the Drakensberg .....	5
<i>Fire Studies in the Drakensberg</i> .....	6
<i>What Is Already Known About Fires in the Drakensberg?</i> .....	7
2.2.3 Fire Management in the uKhahlamba Drakensberg Park.....	7
<i>uKhahlamba Drakensberg Park: Annual Fire Reports</i> .....	9
2.3 REMOTE SENSING.....	10
2.3.1 Remote Sensing of Fires.....	10
2.3.2 Remote Sensing Studies.....	12
2.3.3 Active Fire Detection.....	14
2.3.4 Burn Area Detection.....	17
2.3.5 Accuracy and Validation Methods .....	19
2.3.6 Remote Sensing in Protected Areas.....	19
2.4 SOILS.....	20
2.4.1 Soil Formation .....	20
2.4.2 Effects of Fire on Soil Properties .....	22
<i>Soil Organic Matter</i> .....	23
<i>Soil pH</i> .....	24
<i>Other Soil Properties</i> .....	24
2.5 SOILS AND FIRE VARIABILITY .....	25
<b>CHAPTER 3: STUDY AREA .....</b>	<b>27</b>
3.1 SETTING.....	27
3.2 HISTORY AND CONSERVATION .....	28
3.3 LANDSCAPE AND GEOLOGY .....	28
3.4 CLIMATE AND WEATHER.....	31
3.5 VEGETATION.....	32
3.6 SOILS.....	36
3.7 SOCIAL ASPECTS.....	37
<b>CHAPTER 4: METHODOLOGY.....</b>	<b>38</b>
4.1 INTRODUCTION .....	38
4.2 REMOTE SENSING.....	38
4.2.1 Data Collection.....	38
<i>Fire Frequency</i> .....	38
<i>Spatial Extent</i> .....	39
4.2.2 Data Analysis.....	41
<i>Data Pre-processing</i> .....	41
<i>Fire Frequency</i> .....	42
<i>Spatial Extent</i> .....	43

<i>Accuracy Assessments</i> .....	44
4.2.3 Study Site Selection.....	45
4.3 SOILS.....	48
4.3.1 Field work.....	48
4.3.2 Limitations of Site Selection.....	52
4.3.3 Soil Laboratory Analysis .....	55
<i>Soil Moisture Content</i> .....	55
<i>Soil Colour</i> .....	56
<i>Soil Organic Matter</i> .....	56
<i>Soil pH</i> .....	56
<i>Soil Texture</i> .....	57
4.3.4 Statistical Analysis.....	57
<i>Statistical Tests</i> .....	59
<b>CHAPTER 5: RESULTS .....</b>	<b>61</b>
5.1 REMOTE SENSING.....	61
5.1.1 Fire Frequency.....	62
<i>MODIS Active Fire Data</i> .....	62
<i>VIIRS Active Fire Data</i> .....	66
<i>Comparison between MODIS and VIIRS Active Fire Data</i> .....	69
5.1.2 Spatial Extent .....	73
<i>Burn Scar Band Combinations</i> .....	73
<i>Normalised Burn Ratio</i> .....	73
<i>Accuracy of Normalised Burn Ratio</i> .....	79
5.1.3 Comparison: MODIS vs VIIRS vs Landsat.....	81
5.2 SOILS.....	85
5.2.1 Overview .....	85
<i>Soil Moisture</i> .....	87
<i>Soil Colour</i> .....	87
<i>Soil Texture</i> .....	88
5.2.2 Soil statistics.....	89
<i>Soil Strength</i> .....	90
<i>Soil pH</i> .....	91
<i>Soil Organic Matter</i> .....	91
<b>CHAPTER 6: DISCUSSION.....</b>	<b>94</b>
6.1 INTRODUCTION .....	94
6.2 REMOTE SENSING .....	94
6.2.1 Fire Frequency.....	94
6.2.2 Spatial Extent .....	95
6.2.3 Evaluating Remote Sensing in the UDP.....	97
6.3 SOILS.....	99
6.3.1 Soils in the UDP .....	100
6.3.2 Influencing Factors on Soil Properties .....	102
6.3.3 Overview .....	104
<b>CHAPTER 7: CONCLUSIONS .....</b>	<b>105</b>
7.1 FUTURE RECOMMENDATIONS.....	106
<b>REFERENCES .....</b>	<b>108</b>

<b>APPENDICES .....</b>	<b>120</b>
APPENDIX A: SOIL DATA .....	120
APPENDIX B: SOIL DATA GRAPHS .....	124
APPENDIX C: SOIL STATISTICAL DATA.....	126
APPENDIX D: SITE COMPARISON PHOTOGRAPHS .....	130

## LIST OF FIGURES

<i>Figure 2.1. Veldfire risk levels in South Africa. (Source: Forsyth et al., 2010: 13).</i> .....	5
<i>Figure 2.2. MODIS active fire detection. (Source: NASA, 2018).</i> .....	15
<i>Figure 2.3. Validation of MODIS active fire detections compared against an ASTER image from Siberia, 23<sup>rd</sup> July 2002, showing active fire pixels with high (yellow) and nominal (red) confidence ratings. (Source: Csiszar et al., 2006).</i> .....	16
<i>Figure 3.1. Locality Map of the UDP.</i> .....	27
<i>Figure 3.2. Geology and rock formations in the Drakensberg. (Source: Norman and Whitfield, 2006: 293).</i> .....	30
<i>Figure 3.3. Geology of the UDP. (Source: Council for Geoscience, n.d.)</i> .....	30
<i>Figure 3.4. Digital Elevation Model (DEM) of the UDP.</i> .....	31
<i>Figure 3.5. Aspect map of the UDP.</i> .....	31
<i>Figure 3.6. Winter at Giant's Castle in the UDP.</i> .....	32
<i>Figure 3.7. Summer at Giant's Castle in the UDP. (Photograph: Ian Meiklejohn).</i> .....	32
<i>Figure 3.8. Vegetation of the UDP. (Source: Mucina and Rutherford, 2006).</i> .....	33
<i>Figure 3.9. Climate diagrams of the grasslands of the UDP. (Source: Mucina and Rutherford, 2006).</i>	34
<i>Figure 3.10. Comparison of the vegetation and geology of the KwaZulu-Natal Drakensberg. (Source: Bristow, 2010).</i> .....	35
<i>Figure 3.11. Schematic cross-section of the altitudinal vegetation belts and their main vegetation communities illustrated for Cathedral Peak (Northern area of the UDP). (Source: Killick, 1963).</i> .....	36
<i>Figure 3.12. A comparison between the dominant land cover surrounding the southern and northern UDP. (Source: DEA, 2016).</i> .....	37
<i>Figure 4.1. Landsat 5 image (3<sup>rd</sup> September 2007) showing burn scar in the UDP, comparison from left to right: (1) band combinations red (0.630 – 0.680 <math>\mu</math>m), green (0.525 – 0.600 <math>\mu</math>m), blue (0.450 – 0.515 <math>\mu</math>m) showing burn scar in black, (2) band combinations SWIR 2 (2.100 – 2.300 <math>\mu</math>m), NIR (0.845 – 0.885 <math>\mu</math>m), red (0.630 – 0.680 <math>\mu</math>m) showing burn scar in red, (3) Outcome of a NBR showing burn scar in red.</i> .....	44
<i>Figure 4.2. An example of the site selection process in ArcMap in the UDP. (Example from Bushman's Nek, UDP).</i> .....	47
<i>Figure 4.3. Site locations across the UDP.</i> .....	48
<i>Figure 4.4. Fieldwork equipment.</i> .....	50
<i>Figure 4.5. Field work quadrat layout.</i> .....	51

Figure 4.6. Soil sampling equipment approximate depth into soil. ....	51
Figure 4.7. NBR detection errors from clouds and cloud shadows from a Landsat 5 image from 2006 in the UDP. ....	52
Figure 4.8. NBR detection error with rock reflections being classified as annual burn scar. (Example from Cobham, UDP).....	52
Figure 4.9. Geology map layer (1:250000) overlaid with the World Imagery ArcMap basemap showing potential error at a zoomed-up scale. (Example from Garden Castle, UDP). ....	54
Figure 4.10. Soil sectioning process for large soil samples. ....	55
Figure 4.11. Malvern Mastersizer 3000 particle size analysis. ....	57
Figure 5.1. Total annual MODIS active fire data recorded from 2003 to 2017 in the UDP.....	62
Figure 5.2. Fire point data showing the annual MODIS active fire data from 2003 to 2017 in the UDP. ....	63
Figure 5.3. Overall kernel density showing areas of high and low fire frequency recorded by MODIS active fire data from 2003 to 2017 in the UDP. ....	64
Figure 5.4. Annual kernel densities showing the areas of high and low fire frequency recorded by MODIS active fire data from 2003 to 2017 in the UDP. ....	65
Figure 5.5. Total monthly MODIS active fire data recorded from 2003 to 2017 in the UDP. ....	66
Figure 5.6. Total annual VIIRS active fire data recorded from 2012 to 2017 in the UDP. ....	67
Figure 5.7. Fire point data showing the annual VIIRS active fire data from 2012 to 2017 in the UDP. ....	67
Figure 5.8. Overall kernel density showing areas of high and low fire frequency recorded by VIIRS active fire data from 2012 to 2017 in the UDP. ....	68
Figure 5.9. Total monthly VIIRS active fire data recorded from 2012 to 2017 in the UDP. ....	69
Figure 5.10. Comparison between the annual MODIS and VIIRS active fire data recorded from 2012 to 2017 in the UDP. ....	70
Figure 5.11. Comparison between the total monthly MODIS and VIIRS active fire data recorded from 2012 to 2017 in the UDP. ....	71
Figure 5.12. Comparison between kernel density maps for MODIS and VIIRS active fire data recorded from 2012 to 2017 in the UDP. ....	72
Figure 5.13. Landsat 8 image (7 <sup>th</sup> June 2016) showing band combinations red (0.630 – 0.680 $\mu\text{m}$ ), green (0.525 – 0.600 $\mu\text{m}$ ), blue (0.450 – 0.515 $\mu\text{m}$ ) for the southern UDP.....	73
Figure 5.14. Landsat 8 image (7 <sup>th</sup> June 2016) showing band combinations SWIR 2 (2.100 – 2.300 $\mu\text{m}$ ), NIR (0.845 – 0.885 $\mu\text{m}$ ), red (0.630 – 0.680 $\mu\text{m}$ ) for the southern UDP.....	73
Figure 5.15. NBR results showing annual percentage burn and no burn, for the 12 years of available Landsat imagery from 1998 to 2017 in the UDP.....	74
Figure 5.16. Comparisons of NBR burn scar results, for the 12 years of available Landsat imagery from 1998 to 2017 in the UDP. ....	75
Figure 5.17. Overall percentage of overlapping burn scar per number of years of overlap, for the 12 years of available Landsat imagery, from 1998 to 2017 in the UDP. ....	77

Figure 5.18. Combined NBR burn scar results showing areas of overlapping burn scar per number of years of overlap, for the 12 years of available Landsat imagery, from 1998 to 2017 in the UDP. ....	77
Figure 5.19. Overall percentage of overlapping burn scar per number of years of overlap for the last five years of data, from 2013 to 2017 in the UDP.....	78
Figure 5.20. Combined NBR burn scar results showing areas of overlapping burn scar per number of years of overlap for the last five years of data, from 2013 to 2017 in the UDP. ....	78
Figure 5.21. Digitised vector burn scar versus NBR raster burn scar versus for 2017 in the UDP.....	80
Figure 5.22. Comparison between MODIS and VIIRS active fire data and the Landsat 8 image from 14 <sup>th</sup> September 2017 in the UDP.....	82
Figure 5.23. Comparison between MODIS and VIIRS active fire data and NBR showing burn scar for 2017 in the UDP. ....	84
Figure 5.24. Water logged high fire frequency site at Garden Castle (29 <sup>th</sup> December 2018).....	87
Figure 5.25. The 85 soil samples after being oven dried, showing soil colour variations .....	87
Figure 5.26. Sand-silt-clay diagram showing the 85 soil sampling points. Diagram from Gradistat Version 8.0 Grain Size Analysis Program (Blott, 2010). ....	88
Figure 5.27. Correlation matrix of the soil properties. (Source: Bakker, 2018, pers. comm.). ....	89
Figure 5.28. Relative importance graphs, using the LMG metric, for the full regression model for each outcome variable. (Source: Bakker, 2018, pers. comm.). ....	92
Figure 6.1. Comparison between the soil surfaces: Low fire frequency site at Giant's Castle (23 <sup>rd</sup> January 2018) (top); and high fire frequency site at Injisuthi (24 <sup>th</sup> January 2018) (bottom). ....	102
Figure 6.2. Colour variations on the soil surface at the high fire frequency sites at Cathedral Peak (26 <sup>th</sup> January 2018).....	102
Figure 9.1. Soil moisture values (%) for all sites in the UDP. Orange represents high fire frequency sites and green represents low fire frequency sites. ....	124
Figure 9.2. Soil organic matter values (pH) for all sites in the UDP. Orange represents high fire frequency sites and green represents low fire frequency sites. ....	124
Figure 9.3. Soil pH values for all sites in the UDP. Orange represents high fire frequency sites and green represents low fire frequency sites. ....	124
Figure 9.4. Hand penetrometer values (kPa) for all sites in the UDP. Orange represents high fire frequency sites and green represents low fire frequency sites. ....	125
Figure 9.5. Hand shear vane values (kPa) for all sites in the UDP. Orange represents high fire frequency sites and green represents low fire frequency sites. ....	125
Figure 9.6. Particle size values (% sand, silt and clay) for the all sites in the UDP.....	125



## LIST OF TABLES

<i>Table 2.1. The amount of burning that occurred in the UDP for financial years 2014/2015, 2015/2016 and 2016/2017, as recorded in the annual reports from the UDP (Source: EKZNW, 2015; EKZNW, 2016; EKZNW, 2017).</i>	10
<i>Table 2.2. Remote sensing studies in southern Africa.</i>	13
<i>Table 4.1. The dates of the available Landsat 5 and 8 images used for investigating burn scar in the UDP.</i>	40
<i>Table 4.2. Landsat 5 bands. (Source: U.S. Geological Survey, 2018).</i>	41
<i>Table 4.3. Landsat 8 bands. (Source: Barsi et al., 2014; U.S. Geological Survey, 2018).</i>	41
<i>Table 4.4. MODIS active fire data confidence ratings. (Confidence percentage classes from Giglio, 2015).</i>	43
<i>Table 4.5. VIIRS active fire data confidence ratings.</i>	43
<i>Table 4.6. Year of fire occurrence at the low fire frequency sites across the UDP.</i>	54
<i>Table 5.1. Ratio comparisons between annual number of MODIS and VIIRS active fire data from 2012 to 2017 in the UDP.</i>	70
<i>Table 5.2. Summary of NBR analyses comparing annual area of burn and no burn, for the 12 years of available Landsat imagery from 1998 to 2017 in the UDP.</i>	74
<i>Table 5.3. NBR raster burn scar versus digitised vector burn scar for 2017 in the UDP.</i>	79
<i>Table 5.4. Acquisition time of MODIS and VIIRS active fire data from 14<sup>th</sup> September 2017 in areas A, B and C.</i>	81
<i>Table 5.5. Accuracy (%) comparison between MODIS and VIIRS active fire data and the Landsat NBR ratio for 2013 to 2017 in the UDP.</i>	84
<i>Table 5.6. Number of MODIS and VIIRS active fires recorded after the Landsat image date.</i>	84
<i>Table 5.7. Summary of soil property data including all sites, the high fire frequency sites (orange) and the low fire frequency sites (green). The bold and darker shaded writing indicates the higher value between high and low fire frequency.</i>	85
<i>Table 5.8. Summary comparison between the high and low fire frequency sites at each area with the soil property being placed under the high or low fire frequency heading where the soil property was highest or in the similar column if the soil property values showed only a slight difference.</i>	86
<i>Table 5.9. Summary comparison of the number of times a soil property was highest in the high or low fire frequency sites or similar.</i>	86
<i>Table 5.10. Adjusted R<sup>2</sup> values for the full multiple regression models for all four outcome variables.</i>	90
<i>Table 9.1. All soil data in the UDP.</i>	120
<i>Table 9.2. Soil colour for all soil samples in the UDP using the Munsell colour chart.</i>	122
<i>Table 9.3. Particle size values (% sand, silt and clay) for all soil samples in the UDP.</i>	123
<i>Table 9.4. Site photographs comparing high and low fire frequency sites.</i>	130

## EQUATIONS

<i>Equation 1: Normalised Burn Ratio</i> .....	43
<i>Equation 2: Vector versus Raster Accuracy</i> .....	45
<i>Equation 3: % Soil Moisture</i> .....	55
<i>Equation 4: Loss on ignition</i> .....	56

## ABBREVIATIONS

µm	- micrometre
.shp	- shapefile
AIC	- Akaike Information Criterion
APCV	- Annual Precipitation Coefficient of Variation
ASTER	- Advanced Spaceborne Thermal Emission and Reflection Radiometer
AVHRR	- Advanced Very High Resolution Radiometer
AVHRR-GAC	- Advanced Very High Resolution Radiometer Global Area Coverage
BIC	- Bayesian Information Criterion
DEM	- Digital Elevation Model
dnBR	- Differenced Normalised Burn Ratio
EKZNW	- Ezemvelo KwaZulu-Natal Wildlife
EOS	- Earth Observing System
EOSDIS	- Earth Observing System Data and Information
EROS	- Earth Resources Observation and Science
ESA	- European Space Agency
ETM+	- Enhanced Thematic Mapper Plus
FIRMS	- Fire Information for Resource Management System
Gd	- Drakensberg Grassland Bioregion
GEOS	- Geostationary Operational Environmental Satellite
GeoTIFF	- Geographic Tagged Image File Format
GIS	- Geographic Information System
GMT	- Greenwich Meridian Time
GPS	- Global Positioning System
Gs	- Sub-Escarpment Grassland Bioregion
HP	- Hand Penetrometer
HSV	- Hand Shear Vane
kPa	- Kilopascals
L1TP	- Level 1 Precision and Terrain corrected Products
LANCE	- Land, Atmosphere Near real-time Capability for EOS
LMG	- Lindeman, Merenda and Gold
LOI	- Loss On Ignition
MAP	- Mean annual precipitation
MAPE	- Mean Annual Potential Evaporation
m.a.s.l	- Metres above sea level
MASMS	- Mean Annual Soil Moisture Stress
MAT	- Mean Annual Temperature
MFD	- Mean Frost Days
mins	- minutes
MIR	- Middle Infrared

MODIS	- Moderate Resolution Imaging Spectrometer
MSG SEVIRI	- Meteosat Second Generation Spinning Enhanced Visible and Infrared Imager
NASA	- National Aeronautics and Space Administration
NBA	- National Biodiversity Assessment
NBR	- Normalised Burn Ratio
NDVI	- Normalised Difference Vegetation Index
NIR	- Near Infrared
NOAA	- National Oceanic and Atmospheric Administration
NRT	- Near Real-Time
OLI	- Operational Land Imager
QGIS	- Quantum GIS
SANBI	- South African National Biodiversity Institute
SANSA	- South African National Space Agency
SOM	- Soil Organic Matter
S-NPP	- Suomi National Polar-orbiting Partnership
SPOT	- Satellites Pour l'Observation de la Terre
SWIR	- Shortwave Infrared
TIRS	- Thermal Infrared Sensor
TM	- Thematic Mapper
UDP	- uKhahlamba Drakensberg Park
UDP WHS	- uKhahlamba Drakensberg Park World Heritage Site
UNESCO	- United Nations Educational, Scientific and Cultural Organisation
USGS	- United States Geological Survey
UTM	- Universal Transverse Mercator
VIIRS	- Visible Infrared Imaging Radiometer Suite
WGS	- World Geodetic System

## DATA DISCLAIMER

All Moderate Resolution Spectroradiometer (MODIS) and Visible Infrared Imaging Radiometer Suite (VIIRS) active fire data came from the Fire Information for Resource Management System (FIRMS) webpage: I *“acknowledge the use of data and imagery from the Land, Atmosphere Near real-time Capability for EOS (LANCE) Fire Information for Resource Management System (FIRMS) operated by the NASA/GSFC/Earth Science Data and Information System (EDIS) with funding provided by NASA/HQ”*. All Landsat imagery (Landsat 5 and 8) is courtesy of the United States Geological Survey and was downloaded from the United States Geological Survey *‘EarthExplorer’* webpage.

The following online basemap layers were used in ArcMap 10.3 and ArcMap 10.6 for site selection (Figure 4.2):

- OpenStreetMap: Credit: ©OpenStreetMap and contributors, Creative Commons Attribution-Share-Alike licence (CC-BY-SA).
- World Imagery: *“Source: ESRI, DigitalGlobe, GeoEye, Earthstar Geographics, CNES/Airbus DS, USDA, USGS, AeroGRID, IGN, and the GIS User Community”*.

The following Geographic Information System (GIS) data layers were used in creating the uKhahlamba Drakensberg Park (UDP) maps:

- 'Formal protected areas' dataset used for the boundary of the UDP. From the National Biodiversity Assessment 2011 Terrestrial Formal Protected Areas layer. Obtained from the Rhodes University Geography Department. (Source: SANBI, 2012.)
- South African vector datasets: provinces, towns, and rivers. Obtained from the Rhodes University Geography Department.
- South African vegetation (2006), obtained from the Rhodes University Geography Department. (Source: Mucina and Rutherford, 2006).
- South African geology (1:250000), obtained from the Rhodes University Geography Department. Geological Survey of South Africa. (Source: Council for Geoscience, n.d.).
- Vector datasets from South African map grids 2828, 2829 and 2929. Downloaded from the Rhodes University Geography Department map server accessed via their webpage. The data is downloaded in geographic coordinates 'WGS 1984'. The 20 m relief lines (contour lines) were used to create a Digital Elevation Model (DEM). From the DEM, a 20 m slope and aspect map were created.
- South African National Land Cover Data (2013 – 2014), 35 land cover classes, reprojected UTM 35 south. Obtained from the Department of Environmental Affairs (DEA) GIS data downloads webpage. (Source: DEA, 2016).

Geographic coordinates 'WGS 1984' were used for all datasets. All maps were created using projection properties; Universal Transverse Mercator Zone 35 South (UTM 35S), central meridian of 27.

# CHAPTER 1: INTRODUCTION

---

## 1.1 BACKGROUND

Fires are a common and natural occurrence on the African continent, resulting in it being named 'the fire continent' and are regarded as South Africa's most common hazard (Strydom and Savage, 2016). The combination of South Africa's dry, warm climate, and fire-prone vegetation makes veldfires particularly significant environmental phenomena (Moses, 2011). Grasslands are a significant part of South Africa's landscape, making up nearly one third of the total land area, and are noted as significant global biodiversity assets (SANBI, 2013). Less than 3% of these valuable grasslands are formally protected, one area being the uKhahlamba Drakensberg Park (UDP) (SANBI, 2013). The UDP is a protected park located on the eastern escarpment of the KwaZulu-Natal Drakensberg and was designated as a World Heritage Site due to its significant flora and fauna species richness, and cultural significance (Holmes, 2011). The KwaZulu-Natal Drakensberg is home to one of South Africa's largest areas of natural grassland (Everson and Everson, 2016) and southern Africa's high altitude fire-climax grasslands (as referred to by Scotcher and Clarke, 1981) or fire sub-climax (as referred to by Mentis *et al.*, 1974). Protected areas, like the UDP, are significant in maintaining biodiversity and the natural ecological functions of an area (dos Santos *et al.*, 2018).

South African grasslands are fire-prone and fire-dependent, making fire an important ecological factor (SANBI, 2013). Fire is critical for the maintenance, management and health of the grasslands through removing dead plant material, stimulating new growth, hindering the growth of woody species and invasive species, contributing to organic nutrients such as organic matter, as well as covering large areas and reaching inaccessible areas (SANBI, 2013). Problems such as degradation of ecosystems and damage to the natural environment arise when fires occur at inopportune times, are too severe for the environment, or occur too seldom or too frequently (Forsyth *et al.*, 2010; Holmes, 2011; SANBI, 2013). Worldwide, wildfires, across multiple biomes, were identified as one of the biggest challenges for managing protected areas (dos Santos *et al.*, 2018). The importance of a fire management plan is recognised in South Africa through the National Veld and Forest Fire Act, No. 101 of 1998 that provides a national framework to improve the way veldfires are managed (South Africa, 1998; Kruger *et al.*, 2006; Forsyth *et al.*, 2010).

The importance of regular burning in the UDP grasslands has been acknowledged for a long time (Everson, 1985). There is a fire management plan in the UDP that implements controlled burning (EKZNW, 2012). The fire management plan aims to preserve spatial and temporal heterogeneity across the UDP, by burning in a mosaic pattern with varying fire regimes, in order to conserve maximum

biodiversity; and the maintenance of firebreaks to help control the spread of wildfires (EKZNW, 2012; SANBI, 2013).

“Remote sensing is the science of extracting information about an object without being in physical contact with it” (Roy *et al.*, 2013: 77), and is ideally suited to investigating fires by providing information on the location, the spread and area damaged by a fire (Roy *et al.*, 2013). Thus, it provides information on the temporal and spatial frequency of fires. Remote sensing is a valuable monitoring tool (Turner *et al.*, 2015), which can provide a variety of information to protected areas managers that can help inform decisions (Gross *et al.*, 2009), thus helping to promote conservation. Flasse *et al.* (2004) highlight the benefits of remote sensing for fire management, including: the ability to gather the same information at a cheaper price, faster and over a larger area than field work, the ability to view a broader range of the electromagnetic spectrum such as NIR (Near-infrared), a high temporal resolution with consistent coverage, and a high spatial resolution by covering large areas of the earth.

## 1.2 MOTIVATION

While fires have been thoroughly studied across the UDP for a number of decades (e.g. Mentis *et al.*, 1974; Scotcher and Clarke, 1981; Everson and Tainton, 1984; Everson, 1985; Everson *et al.*, 1985; Short *et al.*, 2003a; Short *et al.*, 2003b; Everson and Everson, 2016; McGranahan *et al.*, 2018), the effects of fire studies are dominated by vegetation studies at site specific areas, such as the Cathedral Peak Nature Reserve (Everson and Everson, 2016). Studies on the effects of fires on soils in the UDP are limited to Bijker *et al.* (2001) and Manson *et al.* (2007).

Remote sensing has not been used to investigate fires in the UDP, nor has fires and soils been investigated in a holistic way incorporating the whole UDP. Thus, there is the potential to incorporate remote sensing for investigating fires and grasslands across the UDP, providing spatial and temporal information on fires. In addition, remote sensing provides a monitoring tool that can potentially be incorporated into the fire management plan in the UDP. With fire being a dominant feature in the UDP and the new technological advances in remotes sensing, together with the availability of free open sourced satellite data, there is a great potential for implementing remote sensing as a management tool for promoting continuity for monitoring and conservation in the UDP. This study can be seen as an initial step in evaluating the potential of remote sensing technologies for monitoring of other factors in the UDP, not just fires.

The UDP is a World Heritage Site making conservation and preservation of utmost importance and is part of an important water resources network, making it critical to preserve the landscape, specifically indigenous vegetation and soils (EKZNW, 2012; UNESCO, 2017). Preservation of soils is important as they are considered one of earth’s greatest resources (Alcañiz *et al.*, 2018). Mills and Fey (2004: 394)

states that “the quality of soil and vegetation are interdependent”. Fires during the dormant winter period in the Drakensberg help to maintain high levels of grassland basal cover, which promotes soil conservation (Short *et al.*, 2003a). Soil deteriorates with the loss of vegetation (Mills and Fey, 2004), with fire occurrence being linked to vegetation, and vegetation is linked to soils (Santín and Doerr, 2016). Fires can affect the physical, chemical and biological properties of soils (Zavala *et al.*, 2014; Alcañiz *et al.*, 2018). Soil properties can provide insight into the disturbance that fire can have on an ecosystem (Pereira *et al.*, 2014). It is known that fires can have direct and indirect effects on soil properties that can be short or long term (Zavala *et al.*, 2014). Grasslands and their environments can have varying responses to fire (SANBI, 2013), thus, emphasising the importance of investigating the effects of fires on soils across the whole UDP.

### 1.3 AIMS AND OBJECTIVES

The aim of this research project is to investigate the spatial and temporal frequency of fires using remote sensing, and to investigate the effect of fire frequency on soil properties in the uKhahlamba Drakensberg Park.

In order to achieve the aim, the following objectives were followed:

1. Determine the frequency of fires using remote sensing.
2. Determine the spatial extent of fires using remote sensing.
3. Evaluate whether remote sensing is effective for investigating fires in the UDP.
4. Evaluate the effects of fire frequency on soil properties.

## CHAPTER 2: LITERATURE REVIEW

---

### 2.1 INTRODUCTION

The literature review comprises an up to date summary of the literature on three sections, namely; fire, remote sensing and soils. The fire section contains literature on fires in South Africa, fires in the Drakensberg and fire management in the UDP. The remote sensing section contains literature on what remote sensing is, how remote sensing can be used in fire studies, previous remote sensing studies of fire in southern Africa, methods used for active fire detection, methods used for burn scars analyses, conducting accuracy assessments of remote sensing data, and remote sensing of protected areas. The soil section contains literature on soil formation, the effects of fire on soil properties, and soil and fire variability.

### 2.2 FIRE

#### 2.2.1 Fires in South Africa

The South African landscape is prone to veldfires (Moses, 2011), specifically grasslands which are fire-dependent, making fire an important ecological factor (SANBI, 2013). In South Africa, every year wildfires are responsible for destroying vast areas of veld and forest (Vorster, 2013). Veldfires refer to vegetation fires, with wildfires referring to unwanted veldfires (Kruger *et al.*, 2006). South Africa proclaimed the National Veld and Forest Fire Act, No. 101 of 1998, providing a national framework to improve the way veldfires are managed in South Africa (South Africa, 1998; Kruger *et al.*, 2006; Forsyth *et al.*, 2010). Fires within South Africa's ecosystems are part of the natural environment (Forsyth *et al.*, 2010). Fire is not only an important aspect in the grassland biome of South Africa, but the fynbos biome too (de Klerk, 2008). Prescribed burning is implemented in mountain catchments in the Cape region as a means to rejuvenate fynbos, enhance water yield while sustaining high quality water, regulate alien invasive plants and control potential fire hazards (Richardson *et al.*, 1994).

The spatio-temporal analysis of fires in South Africa by Strydom and Savage (2016) indicate that in the last 10 years, fires were most frequent in the north-eastern and eastern parts of South Africa. A high density of fires occur along mountain ranges, specifically in the mountain grasslands, indicating the potential role of topography and climate in fire occurrence in South Africa (Strydom and Savage, 2016). Due to the eastern half of South Africa experiencing sufficient rainfall, the grasslands are able to support fires every one to two years due to there being sufficient fuel load from the grasslands (Forsyth *et al.*, 2010; Strydom and Savage, 2016). The eastern parts of South Africa experience summer rainfall, making the fire season during the cool, dry winter months, with August and September experiencing the majority of the fires (Strydom and Savage, 2016). According to Strydom and Savage (2016) the link between high fire frequency and grassland vegetation is the ability of grasslands to



grow rapidly in the presence of sufficient rainfall. A high number of fires were located along the Drakensberg mountain range, on the western border of KwaZulu-Natal (Strydom and Savage, 2016). Archibald *et al.*'s (2010) analysis of fire regimes using burn scar from remote sensing in southern Africa from 2001 to 2008 found the area in South Africa with the highest burn scar was the area east of the border between Lesotho and South Africa, where the KwaZulu-Natal Drakensberg and UDP is found. KwaZulu-Natal, where the UDP is located, has the highest veldfire risk level in South Africa with 84.1%, which is classified as extreme (Figure 2.1) (Forsyth *et al.*, 2010) Thus, it is evident that fire is a dominating aspect in the KwaZulu-Natal Drakensberg and highlights the potentials of further

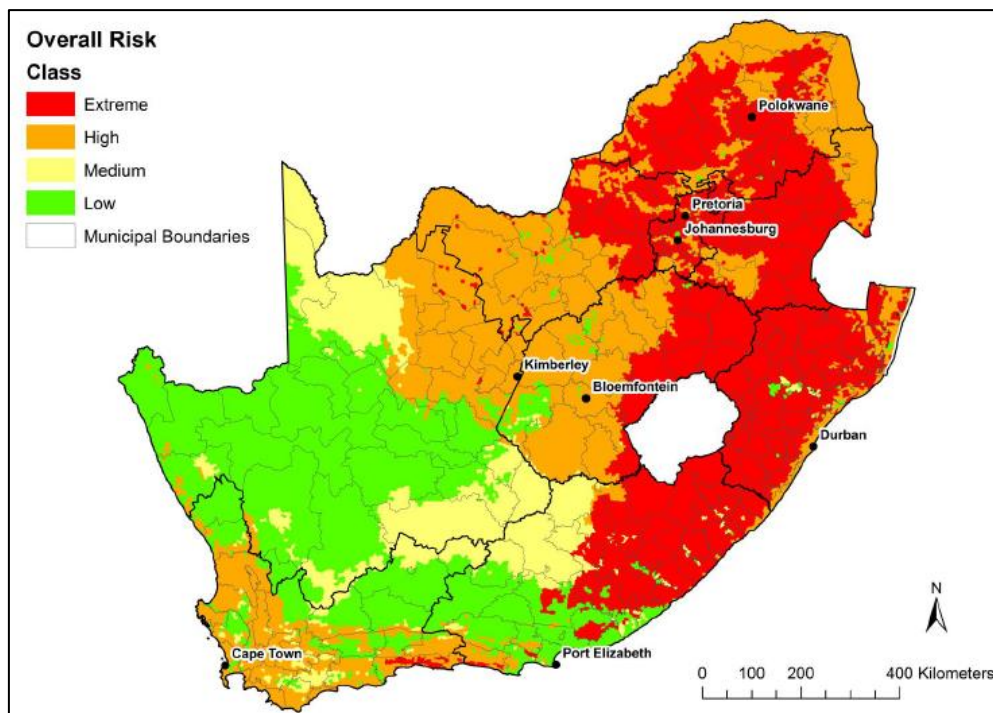


Figure 2.1. Veldfire risk levels in South Africa. (Source: Forsyth *et al.*, 2010: 13).

investigation fire in this area at a larger scale.

### 2.2.2 Fires in the Drakensberg

The Drakensberg is home to southern Africa's high altitude fire-climax grasslands (as referred to by Scotcher and Clarke, 1981) or fire sub-climax (as referred to by Mentis *et al.*, 1974). As fire rejuvenates grasses, in the absence fires, these fire-climax grasslands such as those located in the UDP are at risk of an increase in woody plants, shrubs and forests (Everson, 1985; Forsyth *et al.*, 2010). Acocks (1953) refers to these grasslands areas east of the Drakensberg as 'false' grasslands, meaning that if these grasslands were excluded from fire, their temperature and rainfall conditions would result in forests being supported (Bond *et al.*, 2003). In the Drakensberg, long-term fire exclusion studies resulted in a colonisation of woody vegetation over time (de Villiers and O'Connor, 2011) and decreased production and quality of grasslands (Everson and Everson, 2016). A succession of grasses will occur

when previously fire-protected areas are exposed to regular burning (Bijker *et al.*, 2001). Thus, the necessity and significance of fire in the Drakensberg is highlighted. The term Drakensberg is referring to the KwaZulu-Natal Drakensberg in this study.

#### *Fire Studies in the Drakensberg*

The importance of regular burning in the Drakensberg grasslands has been acknowledged for a long time (Everson, 1985). The effects of fires in the Drakensberg have been thoroughly studied for a number of decades and are still being studied today. The 1970s and 1980s were popular for studying the effects of fires in the Drakensberg. The majority of the studies on fire in the Drakensberg are on the effects of fire on grasslands and veld condition (Mentis *et al.*, 1974; Scotcher and Clarke, 1981; Everson and Tainton, 1984; Everson, 1985; Everson *et al.*, 1985; Short *et al.*, 2003a; Short *et al.*, 2003b; Everson and Everson, 2016; McGranahan *et al.*, 2018), with the effects of fire on woody vegetation (de Villiers and O'Connor, 2011) and shrubs (Smith and Tainton, 1985) having been investigated. Studies specifically investigating the effects of fire on soil in the Drakensberg are limited, with Bijker *et al.* (2001), O'Connor *et al.* (2004) and Manson *et al.* (2007) investigating the effects of fire on both soils and vegetation. Both fauna (Mentis and Rowerowe, 1979) and invertebrates (Arnott 2006: Uys and Hamer, 2007) have been investigated for the effects of fire.

Studies on the effects of fire in the Drakensberg have been conducted across a range of temporal scales. For example, Everson and Everson (2016) investigated long-term effects of a fire regime, Short *et al.* (2003b) considered medium-term changes in grasslands, and de Villiers and O'Connor (2011) looked at the effect of a single fire on woody vegetation. Spatially, fire studies in the Drakensberg are located in three specific areas where the majority of fire studies are conducted. The Cathedral Peak region in the northern Drakensberg (part of the UDP), namely the Cathedral Peak Nature Reserve (formerly the Cathedral Peak Forestry Research Station) and including the Brotherton burning trial, is the most popular area for fire studies in the Drakensberg (Everson and Tainton, 1984; Everson *et al.*, 1985; Smith and Tainton, 1985; Short *et al.*, 2003a; Manson *et al.*, 2007; Uys and Hamer, 2007; de Villiers and O'Connor, 2011; Everson and Everson, 2016). A second documented area, Giant's Castle (part of the UDP) or the Giant's Castle Game Reserve, located in the central Drakensberg (Mentis *et al.* 1974; Scotcher and Clarke, 1981; Bijker *et al.*, 2001; Arnott, 2006). The third area is the southern Drakensberg, specifically in the Underberg region (not part of the UDP) (Short *et al.*, 2003b; O'Connor *et al.*, 2004). In the literature investigated, only one recent study (McGranahan *et al.*, 2018) was conducted in an area different to the three common fire studies areas mentioned above. This study investigated how different types of grasses (specifically C<sub>3</sub> grasses) alter fuel load and fire spread, using Highmoor, Giant's Castle and Monk's Cowl as study sites.

While there are many studies of fires in the grasslands of the UDP, the majority of these studies are conducted in specific burn and no-burn research sites in the central to northern areas of the UDP, for example, Giant's Castle Game Reserve (Bijker *et al.*, 2001), the Brotherton burning trial at Cathedral Peak (Manson *et al.*, 2007), and the Cathedral Peak research catchments (Everson and Everson, 2016). While study areas like these are important for long-term monitoring and limiting site variability, there is a lack of fire studies across the whole UDP and in the southern region of the UDP.

#### *What Is Already Known About Fires in the Drakensberg?*

The UDP has undertaken multiple experimental burning programmes for decades to determine the effects of fires, thus contributing to the current fire management practices in the UDP. For example, in 1952 experimental burning and exclusion plots first started at Cathedral Peak in Catchment IX (de Villiers and O'Connor, 2011), in 1973 at Giant's Castle Game Reserve, experimental biennial summer burn plots (Scotcher and Clarke, 1981) and in 1980 the Brotherton burning trial, located at Cathedral Peak, was established for examining the long-term impacts of fires (Uys and Hamer, 2007). What is already known about the fires in the Drakensberg from other studies is discussed below.

There are many studies on the appropriate time to burn in the Drakensberg. Mentis *et al.* (1974) noted that the natural fire regime in the Drakensberg seemed to be in summer and fire management implemented May to September burns, which still exist today. Biennial summer burn plots showed a decrease in grassland cover but minimum damage to woody vegetation (Scotcher and Clarke, 1981). The benefit of summer fires are the low intensity burns due to the increased moisture (Smith and Tainton, 1985), however, the increased summer rainfall could arguably increase soil erosion (Nel, 2007). The latest study by Everson and Everson (2016) found that the differences in the production of grasslands after 30 years of either annual winter or biennial spring burning were not significant between the two different burning regimes. This suggests that in order to maximise grassland productivity, burning should take place either annually or biennially between winter and spring, which are the dormant winter months in the UDP (Everson and Everson, 2016). This burning regime is thought to be beneficial for the long-term productivity of montane grasslands (Everson and Everson, 2016).

#### **2.2.3 Fire Management in the uKhahlamba Drakensberg Park**

The UDP, being a significant conservation management area and with substantial prior research and knowledge about fire, already has a fire management plan in place (EKZNW, 2012). The current fire management plan in the UDP comes from decades of past research in the Drakensberg such as the fire frequency, fire season, fire behaviour and fire intensity studies done in the 1980s by Scotcher and Clarke (1981), Everson *et al.* (1985) and Smith and Tainton (1985). Previous management objectives

for the Drakensberg include Mentis *et al.* (1974) which refers to the basic management aim in a wildlife reserve, like the Giant's Castle Game Reserve, as maintaining ecological diversity. Everson and Tainton (1984) noted some of the current management goals at that time for the Drakensberg as referenced by Bainbridge and Scott (1981) as: producing high quality water, preserving the soil structure and maintaining species diversity of fauna and flora. Holmes (2011) described the UDP main management practises as emphasising nature conservation, water resources and reducing fire hazards.

The 2012 Integrated Management Plan for the UDP World Heritage Site includes a section under conservation management on fire management in the UDP (EKZNW, 2012). Prescribed burning, implemented by Ezemvelo KwaZulu-Natal Wildlife, takes place in the UDP (Holmes, 2011). Prescribed burning involves burning of the landscape under controlled conditions, with the purpose of decreasing the available fuel loads in the landscape over large areas (Holmes, 2011). Fire has been used as a management tool for a long time, for example Mentis *et al.* (1974). But unsuitable prescribed burning and poor veldfire management can lead to the environment being negatively affected (Forsyth *et al.*, 2010). According to the UDP Integrated Plan document from 2012 (EKZNW, 2012), fire is regarded as the main ecosystem process impacting biodiversity and the fresh water resources in the UDP. The fire management plan in the UDP aims to incorporate the following guiding principles (EKZNW, 2012): giving consideration to the variety of conservation requirements of the significant biodiversity, using burning to preserve the spatial and temporal heterogeneity across the UDP; conducting burning in a way that allows a patch mosaic of grasslands for a landscape with areas of burn and no-burn, following the requirements from the National Veld and Forest Fire Act No. 101 of 1998, for example, implementing firebreaks, and conducting scheduled burns in a safe manner.

The high level of complexity and diversity in the UDP landscape makes creating an ideal fire management plan to meet the multiple conservation objectives challenging (EKZNW, 2012). The UDP adopts an adaptive management approach for revising and evaluating fire management to ensure the best practices are followed (EKZNW, 2017). New information and approaches are being investigated, with suggestions for fire management in the UDP still occurring today. For example, Holmes (2011) developed a fire management environmental decision support system in the UDP using GIS based on the prescribed burning objectives and ideal fire regimes in the UDP. Another example is McGanahan *et al.* (2018) who suggested incorporating information on the frequency, load and fuel moisture of different grassland types (for example C<sub>3</sub> grasses) which can require different burn types with different fuel load conditions to be consistent across different grassland types.

The Fire Management plan (EKZNW, 2012) has a strong emphasis on variability and flexibility in implementation for achieving long-term conservation. The fire season runs from March to September

(EKZNW, 2017). Non-scheduled fires, such as arson, have to be taken into consideration due to their unpredictable nature as these are not part of the set fire plan and may occur anywhere across the UDP (EKZNW, 2012), making the monitoring of fires vital. The purpose of the implementation and maintenance of firebreaks is to help manage controlled burns and help control wildfires by preventing runaway fires, especially during the dry winter season (EKZNW, 2012; EKZNW, 2017). Firebreaks are burnt before mid-winter (by July) every year, and can amount to 10% of the total surface area of a property, and for natural grasslands are burnt around the perimeter (O'Connor *et al.*, 2004). The patchiness effect of grasslands is created by burning different patches of grasslands at different times, creating a landscape which has varying patches of recovery, different fire frequencies and fire conditions (EKZNW, 2012). This results in a landscape which can support a variety of species and ecosystems with varying responses to fire, aiming to conserve the highest level of diversity (EKZNW, 2012). This approach was also highlighted by Arnott (2006) who noted that an effective burning regime consists of multiple fire parameters, not just fire frequency but also fire season and size of the area burning as different patches of grassland being burnt at different stages of ecological succession allows conserving maximum diversity. The patch mosaic effect is created by burning smaller areas, instead of one large burn, with staggered burning times and a 'cool' burn rather than a 'hot' burn (EKZNW, 2012). This emphasises the importance of investigating the impacts of fire frequency across the UDP.

#### *uKhahlamba Drakensberg Park: Annual Fire Reports*

Ezemvelo KZN Wildlife releases an annual report for each financial year (1<sup>st</sup> April to 31<sup>st</sup> March). The annual reports contain information on fire management, which include the area and percentage of burning that was recorded across the UDP (EKZNW, 2015; EKZNW, 2016; EKZNW, 2017). These reports include scheduled burns, firebreaks, and non-scheduled burns which consists of invasive fires, fires from lightning, runaway fires, arson fires, accidental fires, and fires of unknown cause. Fire information from three financial years, 2014/2015, 2015/2016 and 2016/2017, are included in Table 2.1 below.

The scheduled burns in the UDP ranged from a low of 11.0% in 2014/2015 up to a high of 16.91% in 2016/2017 (Table 2.1). Total burned area ranged from a low of 26.4% in 2015/2016 to a high of 44.06% in 2014/2015 (Table 2.1). In 2016/2017, a total of 500 fire events were recorded (EKZNW, 2017). Arson fires is one of the most frequent and widespread illegal activities in the UDP (EKZNW, 2017), with 24 arson incidents recorded in the UDP for 2016/2017, resulting in 22179 ha (9.27%) of the UDP burning from arson (EKZNW, 2017). Arson fires made up the largest area of burn for 2014/2015 with 55674 ha (23.5%) burning, while scheduled burning making up the largest area of burn per year for 2015/2016 and 2016/2017. Non-scheduled burning made up 74.49% of the total burned area for 2014/2015, 50.38% of the total burned area for 2015/2016, and 38.02% of the total burned area for 2016/2017.

The annual reports for 2014/2015 and 2015/2016 noted unscheduled wildfires in the UDP as being problematic and contributed to making the financial year challenging (EKZNW, 2015; EKZNW, 2016).

Table 2.1. The amount of burning that occurred in the UDP for financial years 2014/2015, 2015/2016 and 2016/2017, as recorded in the annual reports from the UDP (Source: EKZNW, 2015; EKZNW, 2016; EKZNW, 2017).

Burn		2014/2015		2015/2016		2016/2017	
		%	Area (ha)	%	Area (ha)	%	Area (ha)
Scheduled burn		11	25557	12.7	30471	16.91	40476
Firebreaks		0.24	564	0.4	868	4.02	9632
Non-scheduled burn	Invasive fire	4.26	9921	0.2	470	0.01	29
	Lightning	0.45	1074	0.8	1924	0.05	131
	Runaway	3.0	7243	0.8	2001	1.44	3441
	Arson	23.5	55674	9.8	23511	9.27	22179
	Accidental	1.61	3685	1.5	3592	1.58	3628
	Unknown	-	-	0.2	435	0.49	1162
Total burn		44.06	103718	26.4	63272	33.77	80678

## 2.3 REMOTE SENSING

### 2.3.1 Remote Sensing of Fires

Remote sensing of fires enables the location, the spread and area damaged by the fire to be determined (Roy *et al.*, 2013), providing information before, during and after fires (Flasse *et al.*, 2004). For example, remote sensing can be utilised to conduct a vegetation analysis before the fire, active fires can be detected and burned areas can be assessed after fires (Flasse *et al.*, 2004). In addition, these satellite images are archived and can be accessed in the future (Vorster, 2013) with remote sensing being able to provide pre-fire information that might not have been possible to obtain otherwise (Morgan *et al.*, 2014) as well as remote sensing data being more objective and repeatable (Chen *et al.*, 2016). Fire regime information such as fire season, frequency, type, intensity of fire, and spatial extent of burn scars (Trollope, 1981), are important aspects to investigate due to changes over time leading to the potential altering of the landscape (Goodwin and Collett, 2014). For fire management to be effective, reliable information is needed (Flasse *et al.*, 2004). Remote sensing is a suitable tool in such situations and is convenient and effective for fire management (Flasse *et al.*, 2004).

Satellites, which provide the remotely sensed data, can be categorised as geostationary or polar-orbiting (Roy *et al.*, 2013). Geostationary satellites orbit synchronously with the earth and are, hence able to maintain a fixed position above the earth, normally overhead of the equator and have a high temporal resolution that makes them beneficial for active fire mapping (Philip, 2007; Roy *et al.*, 2013). For example, Geostationary Operational Environmental Satellites (GOES) have a high temporal

resolution, with their field of view revisit time being every 30 minutes (Chuvieco and Kasischke, 2007). Polar orbiting satellites have a higher spatial resolution and orbit at a closer altitude than those that are geostationary (Philip, 2007). For example, Landsat has a moderate spatial resolution of 30 m and a low temporal resolution of 16 days (Hudak and Brockett, 2004).

Remote sensing can detect fires and burn scar due to changes in vegetation and soil during a fire (Escuin *et al.*, 2008). These changes include depletion of vegetation and charring, which means a loss of chlorophyll and an increase in exposed soil which results in a decrease in surface reflectance in the visible to NIR spectrums (Lentile *et al.*, 2006; Escuin *et al.*, 2008). One of the reasons satellites are able to detect active fires is the increase in radiance in the middle infrared (MIR) bands from the high temperatures associated with fires (Chuvieco and Kasischke, 2007). Analysis of the MIR bands is a standard method for active fire detection with the most suitable for active fire detection being the bands focused on the 3.7  $\mu\text{m}$  wavelength (Chuvieco and Kasischke, 2007). Spectral signatures are able to differentiate between different features on satellite imagery, for example differentiating between smoke and clouds (Jones and Christopher, 2010). Each satellite is designed with specific specifications, including orbits, spectral abilities, and sensing geometry to monitor a wide variety of features on the earth's surface (Roy *et al.*, 2013). Therefore, only a subset of satellites are suitable for monitoring fires (Roy *et al.*, 2013).

The limiting factors to detecting burn scar in dynamic landscapes highlighted by Goodwin and Collett (2014), include land reflectance errors from exposed soils, vegetation structure, soil moisture, cloud cover, cloud shadows and smoke, which prevent the satellite sensors from being able to detect anything, and create gaps in data (Langmann *et al.*, 2009). These limitations highlight the importance of long-term repetitive data, as more available images of an area increase the chances of being able to monitor that area with a clear image (Turner *et al.*, 2015). Influencing factors such as vegetation type and fire severity affect the success of fire scar detection, with both aspects influencing the recovery time of the landscape (Goodwin and Collett, 2014). For example, low severity fires with limited char and high levels of patchiness between burned and non-burned vegetation will be more challenging for satellites to accurately detect (Goodwin and Collett, 2014). For example grasslands, in comparison to large vegetation changes that require moderate to long vegetation recovery, with large amounts of char present will have increased detection rates possibilities with satellites (Goodwin and Collett, 2014).

### 2.3.2 Remote Sensing Studies

Remote sensing has been used in many fire studies across the world, from local to continental and global scale studies, using a variety of satellite sensors with high and low spatial and temporal resolutions, each with benefits and limitations. The two broad uses of remote sensing of fires are active fire detection and assessing burn scar, which are the post-fire effects (Lentile *et al.*, 2006). There are a variety of satellites that can be used for fire management, each with specific accuracy and features (Flasse *et al.*, 2004, Roy *et al.*, 2013).

When it comes to continuous, global coverage, long-term, earth observation data, the Landsat series of satellites and the Advanced Very High Resolution Radiometer (AVHRR), are the stand out satellite imagery providers (Turner *et al.*, 2015). Landsat is a significant earth observation platform due to having the longest record of archived data, dating back to 1972, of medium spatial resolution (30 m) data covering the globe (Hansen and Loveland, 2012). Many fire studies have used Landsat for burn scars analysis, across a variety of vegetation types, including forests (Miller and Yool, 2002; Chen *et al.*, 2016), and savannah (Hudak and Brockett, 2004). AVHRR is used for active fire detection (Barbosa *et al.*, 1999; Lentile *et al.*, 2006) and is used in forest fire assessments (Hernandez-Leal *et al.*, 2006). Since the 2000s, Moderate Resolution Spectroradiometer (MODIS) has been a popular satellite sensor for fire analysis, with both active fire detection algorithms (Giglio *et al.*, 2003; Tanpipat *et al.*, 2009) and burned area products being used (Archibald *et al.*, 2010; Buthelezi *et al.*, 2016).

Remote sensing has been used to investigate fires in Africa. Examples from southern Africa, at both small and large scales utilising a range of remotely sensed data are shown in Table 2.2. The usefulness of remote sensing has been acknowledged for a long time. For example, Edwards *et al.* (1983) noted the effectiveness of satellite imagery in providing useful information for scientific purposes and simple image interpretation techniques with a study using Landsat images from 1981 to monitor veld burns (spatial extent and burn frequency) in the eastern agricultural regions of South Africa. Another satellite sensor mentioned in the literature for South African fire studies is Satellite Pour l'Observation de la Terre (SPOT) (Vorster, 2013). Vorster (2013) noted the advantages of using SPOT is the spatial resolution (20 m for SPOT 4, 10 m for SPOT 5) and revisit period of three to seven days. However, SPOT is limited to few spectral bands (Vorster, 2013). Vorster (2013) found, in South African case studies, Landsat imagery to be a more suitable sensor due to the large imagery archive.



Table 2.2. Remote sensing studies in southern Africa.

Satellite sensor	Spatial resolution	Revisit time	Reference	Study
AVHRR - global area coverage (GAC)	5km	Daily	Barbosa <i>et al.</i> (1999)	Continental scale - investigated biomass burning from vegetation fires in Africa over an eight-year period from 1981 to 1991.
Landsat	30 m	16 days	Edwards <i>et al.</i> (1983)	Used Landsat images from 1981 to monitor veld burns (spatial extent and burn frequency) in the eastern agricultural regions of South Africa.
			Hudak and Brockett (2004)	Landsat 1, 2, 5 and 7 images - map fire scars from 1972-2002 in a semi-arid savannah landscape in the Madikwe Game Reserve on the South Africa and Botswana border.
MODIS active fire detection	1 km	Up to four times daily	de Klerk (2008)	Mapping fires in the fynbos biome
			Strydom and Savage (2016)	Analysing the spatial and temporal frequency of fires across the whole of South Africa
MODIS burnt area products	500 m	Eight days	Archibald <i>et al.</i> (2010)	Investigating fire regimes across southern Africa
			Buthelezi <i>et al.</i> (2016)	Assessed the spatial and temporal variations of fire regimes in different vegetation types in the KwaZulu-Natal province
SPOT 4 SPOT 5	20 m 10 m	Three to seven days	Vorster (2013)	Analysing wildfires in South African case studies

Remote sensing has not been used to investigate fires specifically in the UDP. However, Robinson (2014) used Landsat TM and ETM+ images to produce a burn frequency map (1993 to 2011) of the Sani Pass Region in the Lesotho highlands, near the border of the UDP. Remote sensing has been used in vegetation studies in the UDP before. For example, Shoko *et al.* (2018) investigated the use of the freely available new multi-temporal Sentinel-2A images (spatial resolution 10 m to 60 m and revisit period of 5 to 19 days) to investigate variations in aboveground biomass across C<sub>3</sub> and C<sub>4</sub> grasslands in the Drakensberg. Sentinel-2, with the improved spatial and temporal resolution, improved geographical coverage (290 km swath-width), and is freely available from the European Space Agency (ESA) website, offering a new alternative to remote sensing studies that improves on other sensors limitations, such as MODIS and Landsat (Shoko *et al.*, 2018). However, using Sentinel-2 in this study of fires in the UDP had limitations as there is a lack of available archived data due to Sentinel-2 being a new initiative from 2015 and 2017 (Turner *et al.*, 2015). High resolution aerial imagery has also been used in the northern UDP to monitor bracken fern, using image classifications (Singh, 2013).

### 2.3.3 Active Fire Detection

Some of the first active fire detection data came from data produced by the National Oceanic and Atmospheric Administration (NOAA) AVHRR, with 1 km fire monitoring data and with data dating back to 1979 (Chuvieco and Kasischke, 2007; Roy *et al.*, 2013). The addition of MODIS in the early 2000s led to improved active fire detection due to MODIS having specific fire detection bands, with a total of 36 spectral bands (between 0.405 and 14.385  $\mu\text{m}$ ), with channels 21, 22 and 31 being directly used for active fire detection (Giglio *et al.*, 2003; Chuvieco and Kasischke, 2007; Jones and Christopher, 2010). MODIS active fire detection has been followed by the Visible Infrared Imaging Radiometer Suite (VIIRS) in October 2011 with improved mapping capabilities and fire detection algorithm compared to MODIS (Schroeder *et al.*, 2014).

The MODIS instruments, from the National Aeronautics and Space Administration's (NASA) Earth Observing System (EOS), found on-board the morning-descending Terra (February 2000) and afternoon-ascending Aqua (June 2002) satellites, produces active fire data at 1 km resolution with up to four revisits a day (Giglio *et al.*, 2003, Philip, 2007). The VIIRS, from NASA and NOAA, found on-board the Suomi National Polar-orbiting Partnership (S-NPP) and produces active fire data at 375 m resolution with a temporal resolution of 12 hours or less, with active fire data available from January 2012 (Schroeder *et al.*, 2014). MODIS and VIIRS both have archived active fire detection data (Giglio *et al.*, 2003; Schroeder *et al.*, 2014). Archived fire data is available from the Fire Information for Resource Management System (FIRMS) webpage which is acquired from the United States' NASA's Earth Observing System Data and Information System (EOSDIS), based at the University of Maryland (Strydom and Savage, 2016). FIRMS fire data provides locations of fires as point data and is useful for active fire mapping (Roy *et al.*, 2013; Strydom and Savage, 2016). Active fire detection is best suited to satellite detection with high temporal resolution, such as the daily data from MODIS and VIIRS (Giglio *et al.*, 2003; Schroeder *et al.*, 2014).

The fire detection algorithm for MODIS and VIIRS work by identifying any active fires, using thermal anomalies, within each instrument's swath (Giglio *et al.*, 2003). The detection algorithm identifies pixels as "fire pixels" if during the satellite overpass, there are one or more fires actively burning within the pixel (Giglio *et al.*, 2003). Each pixel, during the satellite overpass, is assigned either: fire, non-fire, missing data, cloud, water or unknown (Giglio *et al.*, 2003). Therefore, a fire pixel does not indicate how many fires are present in the pixel, with multiple fire pixels next to each other could relate to the same fire, and the exact location of the fire is not known as the pixel is placed at the centre of the pixel (1 km<sup>2</sup> for MODIS, 375 m<sup>2</sup> for VIIRS) (NASA, 2018) (Figure 2.2).

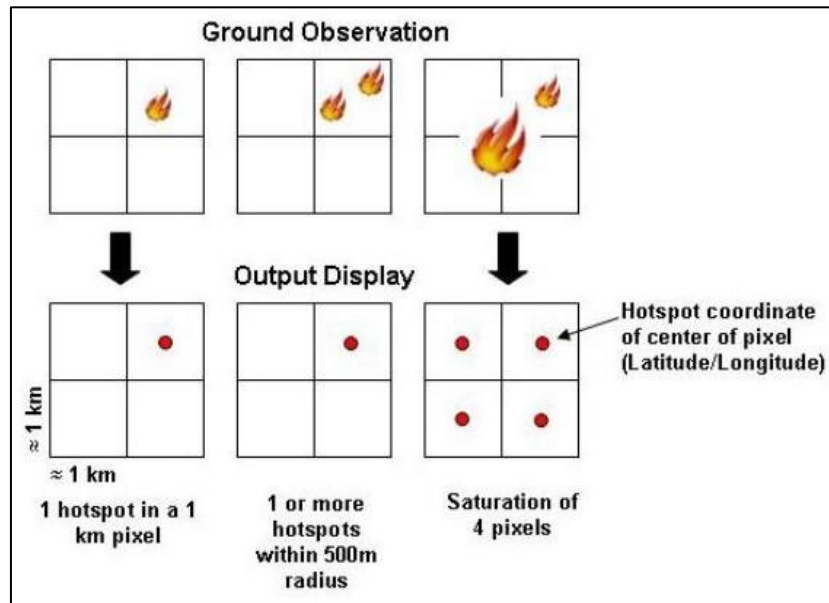


Figure 2.2. MODIS active fire detection. (Source: NASA, 2018).

The current MODIS “Collection 6” algorithm aimed to improve on the “Collection 5” fire product by decreasing false alarms from incorrect detections and omissions from thick smoke obstructions (Giglio *et al.*, 2016). The “version 4” MODIS algorithm found that approximately 100 m<sup>2</sup> was the smallest flaming fire with a minimum 50% chance of detection from both day and night ideal detection conditions (Giglio *et al.*, 2003). However, this is from “version 4” of the algorithm from 2003, and the “Collection 6” algorithm will have improved detection abilities. The limitation of the MODIS FIRMS fire data is that ground-truthing or validation of the fire data from the early 2000s is not possible (Strydom and Savage, 2016). In addition, cloud cover reduces the detection of active fires (Strydom and Savage, 2016) and fires are not detected if the fire is not actively burning or has distinguished during the satellite overpass.

The active fire detection data has a confidence rating for each fire pixel. Csiszar *et al.* (2006) shows an example of MODIS active fire detections, represented on a 1 km grid, with the active fire detections confidence ratings of “high” and “nominal” compared to the matching Advanced Spaceborne Thermal Emission and Reflection Radiometer (ASTER) image of a fire in Siberia, on the 23<sup>rd</sup> July 2002 (Figure 2.3). From Figure 2.3, it is evident that MODIS was able to accurately detect active fires. However, some pixels with active fires were not detected, and some pixels that were detected as fires did not have active burning in the pixel.

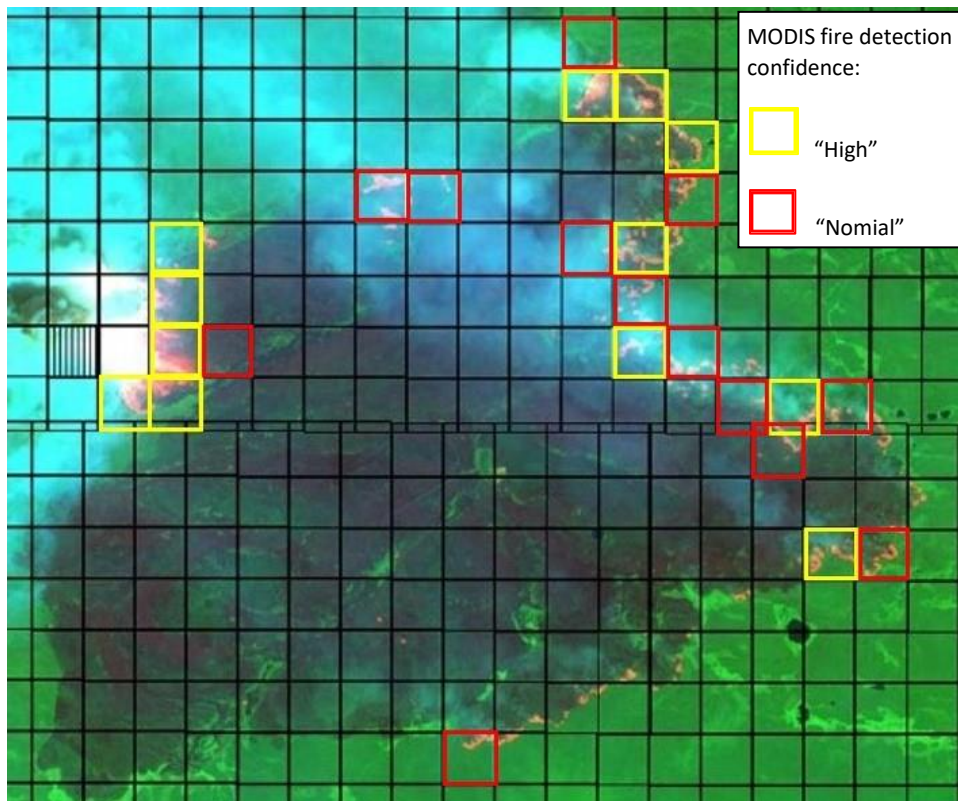


Figure 2.3. Validation of MODIS active fire detections compared against an ASTER image from Siberia, 23<sup>rd</sup> July 2002, showing active fire pixels with high (yellow) and nominal (red) confidence ratings. (Source: Csiszar *et al.*, 2006).

The new VIIRS active fire detection algorithm was designed to improve on the MODIS fire algorithm (Schroeder *et al.*, 2014). The advantages of VIIRS higher spatial resolution of 375 m are the ability to detect smaller, cooler fires and improved mapping of larger fires due to the greater detail (Schroeder *et al.*, 2014; Oliva and Schroeder, 2015). In Schroeder *et al.*'s (2014) comparison of MODIS and VIIRS data, VIIRS had a much greater ability to detect fires that coincided with the Landsat 7 burned areas, while MODIS had omission errors leading to inconsistent fire spread information. Analysis of VIIRS active fire data found different vegetation types to have different accuracies, with forested areas observing the highest accuracy and grasslands and savannahs having the highest omission and commission errors (Oliva and Schroeder, 2015). However, the size, duration and types of burns in different vegetation types are different (Oliva and Schroeder, 2015).

MODIS active fire data has been used in South Africa before, with Strydom and Savage (2016) conducting a spatio-temporal analysis of fires in South Africa and has been evaluated for fire mapping in the fynbos biome in South Africa (de Klerk, 2008). However, it was found to be insufficient in producing a 4-year fire history in the fynbos biome due to MODIS only recording fires at the satellite overpass (de Klerk, 2008). However, since de Klerk's (2008) study, MODIS has improved algorithms and more data is available (Giglio *et al.*, 2016) and fynbos is a different vegetation type to grasslands like in the UDP, therefore will have different detection accuracies (Oliva and Schroeder, 2015). While

MODIS active fire data has been used for investigating fires in South Africa previously (de Klerk, 2008; Strydom and Savage, 2016), the VIIRS active fire data archived data dating back to January 2012 was only released at the beginning of 2018, making VIIRS a new fire detection algorithm which aims to improve on the MODIS active fire algorithm (Schroeder *et al.*, 2014).

#### 2.3.4 Burn Area Detection

Burn area detection or determining the spatial extent of fires using remote sensing has been widely used. In the literature, there are three possible methods to go about determining the spatial extent of burn scar in the UDP, including: image classifications (e.g. supervised or unsupervised classifications), digitising of fires, or using a burn scar detection algorithm using spectral changes post-fire (Miller and Yool, 2002). Fires cause surface changes, therefore selecting suitable wavelengths can take advantage of the reflectance changes (Roy *et al.*, 2013). For example, black char causes a decrease in reflectance (Roy *et al.*, 2013). A challenge of creating an automated approach for burn scar mapping, as highlighted by Goodwin and Collett (2014) is the range of possible fires that can occur along with the diversity of different landscapes and vegetation, all potentially responding in different ways. Therefore, propose the balance between omission and commission of fire scar detection (Goodwin and Collett, 2014). However, the UDP landscape is dominated by grasslands.

The most widely used satellite imagery for mapping and classifying burned areas were from the Landsat sensors (Kritikos *et al.*, 1995, Hudak and Brockett, 2004; Goodwin and Collett, 2014; Chen *et al.*, 2016). This is due to Landsat being freely available, having archived data, while having a medium spatial resolution of 30 m, a temporal frequency of 16 days, and having advanced multispectral abilities with NIR, Shortwave Infrared (SWIR) and thermal bands (Hudak and Brockett, 2004; Goodwin and Collett, 2014).

Image classifications, including supervised (Maximum Likelihood algorithm) and unsupervised classifications have been widely used in fire studies for a long time (Kritikos *et al.*, 1995; Kuntz and Karteris, 1995; Miller and Yool, 2002; Hudak and Brockett, 2004; Chen *et al.*, 2016). All these studies used Landsat imagery and were conducted using forest fires. The advantage of this method is the ability to go beyond just burned and non-burned areas, and further classify other land cover (Kritikos *et al.*, 1995). The vegetation in the UDP is dominated by grasslands which responds differently to fire in comparison to forest vegetation (Goodwin and Collett, 2014), for example grassland vegetation will recover more rapidly. This leads to the question of whether the results of burn scar detection using image classifications in grasslands, like the UDP, will be as effective as forest fire detection. As well as for determining burn scar in the UDP, it is only necessary to differentiate between burned areas and non-burned areas, not further classify land cover classes.

Manual digitising of burn scars using satellite imagery would seem like a viable option, due to the advances in higher resolution imagery and burned areas are usually easily visible due to the dark appearance after a fire (char) and loss of vegetation (Langmann *et al.*, 2009), as well as the combination of NIR and SWIR bands' abilities to highlight burn scar (Chen *et al.*, 2016). Hudak and Brockett (2004) highlight the advantage of digitising of burn scars being that the human brain has recognition abilities that help identify burn scar that automated classification lacks. However, the disadvantages of manually digitising burn scar are that it is subjective and time consuming due to the varying patterns of burn scar (Hudak and Brockett, 2004). Manual digitising of burn scar is a more appropriate option when looking at the burn scars of one fire. With a large amount of burning from multiple fires that takes place in the UDP each year, and looking at burn scars from multiple years, means that digitising of burn scar is not a viable option for this study.

Popular indices used in burn scar detection and assessing the effects of fire are: Normalised Difference Vegetation Index (NDVI) and Normalised Burn Ratio (NBR). NDVI uses the red and NIR regions to detect spectral changes and is used to assess changes in vegetation, post-fire for fire vegetation analysis (Lentile *et al.*, 2006; Escuin *et al.*, 2008). NBR is a widely used index for detecting burned areas, which uses the spectral changes of the surface after a fire using the NIR and MIR regions (Lentile *et al.*, 2006; Roy *et al.*, 2006; Escuin *et al.*, 2008). The NBR is calculated by the difference in NIR and SWIR 2 reflectance divided by the sum of NIR and SWIR 2 (Roy *et al.*, 2006; Miller *et al.*, 2015). López-García and Caselles (1991) found the normalised difference in reflectance in Landsat 5 Thematic Mapper (TM) band 4 (NIR, 0.76-0.90  $\mu\text{m}$ ) and 7 (MIR, 2.08-2.35  $\mu\text{m}$ ) to be the most appropriate to map burnt areas. NBR has widely been used in using Landsat imagery in forested areas (Miller and Yool, 2002; Escuin *et al.*, 2008). The majority of the published NBR studies consulted were conducted in forested areas. However, Vorster (2013) used NBR for fire assessment in case studies in South Africa where plantations and grasslands were present. Robinson (2014) used NDVI and NBR with Landsat imagery to create a fire frequency map in the Lesotho grasslands, within very close proximity of the UDP, with NBR producing better burn scar results than NDVI.

Remote sensing capabilities have been investigated to go beyond just fire detection and burn scar mapping to access the extent of surface changes (Lentile *et al.*, 2006). Multiple studies used remote sensing for assessing the severity of fires or producing burn severity maps, by calculating NBR values pre and post-fire events, thus looking at difference NBR (dNBR) (Lentile *et al.*, 2006; Roy *et al.*, 2006; Escuin *et al.*, 2008; Morgan *et al.*, 2014), and fire risk using NDVI (Hernandez-Leal *et al.*, 2006). Miller and Yool (2002) used supervised and unsupervised classifications, NBR and manual digitising for mapping forests post-fire, finding that including pre and post-fire data improves outcomes. Assessing dNBR would require multiple satellite images. However, for this study on fires in the UDP, only the

spatial extent of fires is investigated over the whole UDP from multiple different fires which occurred at different times, making dNBR inappropriate for this study.

The ideal burn scar mapping method for rangeland managers, suggested by Hudak and Brockett (2004: 3232) is one that is “accurate, efficient, objective and consistent”. Given the vast extent of the UDP, with the majority being grassland and being a dominant fire landscape, together with the success of using NBR with freely available archived Landsat imagery in multiple studies, and the output being simple burned and non-burned pixel classifications, using Landsat with conducting a NBR is deemed the most applicable method for determining the spatial extent of burn scar in the UDP.

### 2.3.5 Accuracy and Validation Methods

Even with all the advances in remote sensing technologies, the results are dependent on accurate interpretations and understanding of the outputs from the remote sensing technologies (Csiszar *et al.*, 2006). Therefore, it is important to note the spatial, temporal and spectral resolutions, and conduct accuracy assessments or include an error matrix (Congalton, 1991; Lentile *et al.*, 2006). Many studies conducted accuracy assessments, using other remote sensing data for validation. For example, Landsat 8 data has been used as reference data for VIIRS active fire data and compared for validation (Schroeder *et al.*, 2014; Oliva and Schroeder, 2015), Landsat TM images were used as a comparison of burned and non-burned areas against AVHRR-GAC vegetation burning (Barbosa *et al.*, 1999), and Escuin *et al.* (2008) conducted an error matrix for overall accuracy of NBR. The limitation of using high spatial resolution imagery for comparison in the validation of active fire data (such as MODIS active fire detection) is the usually low temporal resolution (Csiszar *et al.*, 2006). Landsat imagery has a 16-day revisit period, and differing satellite overpass times can lead to inaccuracies (Schroeder *et al.*, 2014). With the addition of the higher spatial resolution VIIRS active fire detection (375 m<sup>2</sup>), the MODIS active fire detection data (1 km<sup>2</sup>) can be compared against the VIIRS data for an accuracy comparison. As ground-truthing of the fire data in the UDP is not possible, accuracy assessments of the fire data needed to be conducted using comparisons with the other fire data in the UDP.

### 2.3.6 Remote Sensing in Protected Areas

The potential of using remote sensing for monitoring protected areas have been previously considered (Gross *et al.*, 2009, Corbane *et al.*, 2015; dos Santos *et al.*, 2018). Remote sensing can provide an array of information to protected areas managers that can help inform decisions (Gross *et al.*, 2009) by providing information across a range of temporal and spatial scales from a local level up to global studies, as demonstrated earlier in the literature review. This information needs to be at management-relevant scales as protected areas have impacts ranging across multiple spatial scales (Gross *et al.*, 2009). Remote sensing is a valuable monitoring tool, and monitoring is essential to

conservation (Turner *et al.*, 2015). Both Gross *et al.* (2009) and Turner *et al.* (2015) highlighted the limited use of remote sensing satellite data in monitoring and conservation. This was also noted in the UDP, with no prior studies found using remote sensing for investigating fires in the UDP. The closest study being Robinson's (2014) fire frequency study in the Sani Pass region of Lesotho, near the UDP.

The power and potential of remote sensing are evident. However, Corbane *et al.* (2015) highlighted that when it comes to implementing remote sensing techniques in habitat monitoring and conservation, multidisciplinary research is needed with collaboration between all stakeholders in order to fully use remote sensing's potential. It is not sufficient to only implement remote sensing, it is a tool. Turner *et al.* (2015) noted that the important contributing factors to remote sensing being utilised and being appropriate for biodiversity conservation are: data continuity, the ability to look at long-term records adding temporal data; data affordability, the access to freely available data and imagery; and data access, conservation managers and researcher's ability work with and use satellite imagery and processing platforms. However, even with the advances in remote sensing applications, these are limited by the expensive software packages needed (for example, ArcMap), long processing time and expert skills to run the remote sensing software (de Klerk, 2008; Corbane *et al.*, 2015). This is where MODIS active fire products are beneficial with their freely available, easily downloadable data about fire locations (de Klerk, 2008).

## 2.4 SOILS

### 2.4.1 Soil Formation

Jenny (1941:13) described soil as "an exceedingly complex system possessing of a great number of properties" and brought about a new concept of soil formation factors. Jenny (1941) defined the fundamental equation of soil-forming factors as " $s = f(c, o, r, p, t, \dots)$ " where climate (c), organisms (o), topography (r), parent material (p) and time (t) are a function of (f) the soil system. The dots represent any additional soil forming variables that could be included in the soil system (Jenny, 1941). Soil forming factors do not act individually from each other but together (Alijani, 2013; Certini, 2014).

Soils can be defined by using these soil formation factors as "*dynamic natural bodies having properties derived from the combined effects of climate and biotic activities, as modified by topography, acting on parent materials over periods of time*" (Weil and Brady, 2017: 60). The nature of soils that develops in particular areas are influenced by the complex, simultaneous and interdependent actions of the five soil formation factors (Weil and Brady, 2017). The book '*The Nature and Properties of Soils*' by Weil and Brady (2017) was used to summarise the interactions of the five soil formation factors below. These five soil formation features influence soil formation and interact in the following ways:



- Climate largely influences parent material by influencing the weathering that occurs (Weil and Brady, 2017). Precipitation and temperature influence biological, chemical and physical processes on a landscape and the rates at which these processes occur (Weil and Brady, 2017). Precipitation and temperature influences soil moisture, which affects the plant growth and microbial activity, in turn affecting soil organic matter (Weil and Brady, 2017).
- Organisms affecting soil formation can include biota, microbes, natural vegetation, soil fauna and humans (Weil and Brady, 2017). The important one in this study being natural vegetation, which decreases soil erosion rates and largely influences organic matter accumulation (Weil and Brady, 2017). In grasslands, the root systems which are deep and fibrous, mostly contribute to the organic matter in the soils, with fine roots occurring as deep as approximately 1 m in the 'A' soil horizon (Weil and Brady, 2017). Fires in grasslands are common, removing aboveground biomass and adding an accumulation of ash and charcoal to the soil (Weil and Brady, 2017). In forests, the main contribution to organic matter comes from litter accumulation from falling twigs and leaves, and presents a thin 'A' soil horizon, with a distinct 'O' soil horizon (Weil and Brady, 2017). Climate affects the type of natural vegetation that occurs and natural vegetation, in turn influences the soil that forms from the parent material (Weil and Brady, 2017).
- Topography or relief refers to the layout of the land surface and includes elevation, slope, aspect and landscape position (e.g. high ridge) (Weil and Brady, 2017). Steep slopes can encourage erosion, affects the amount of water leaching into soil due to increased water runoff and decreased water entering the soil, and can affect soil depth and alter soil profiles (Weil and Brady, 2017). Aspect influences the absorbance of solar energy on a landscape (Weil and Brady, 2017). In the southern hemisphere, north facing slopes in comparison to south facing slopes, are usually warmer and lower in moisture due to be being more perpendicular to the sun and therefore experiencing increased solar radiation (Weil and Brady, 2017). Slope angle and aspect plays a role in the soil temperature (Weil and Brady, 2017). Topography can reflect the spread of parent materials across a landscape (Weil and Brady, 2017). For example, residual materials found on the summit or upper slopes, colluvium making up the mid to lower slopes, and alluvium deposits collecting at the valley bottom (Weil and Brady, 2017).
- Parent material is brought to the surface of the Earth through geological processes, from which soil forms (Weil and Brady, 2017). Residual parent material forms when the underlying rock is weathered (Weil and Brady, 2017). Parent material can also be transported across a landscape (Weil and Brady, 2017). For example, colluvium, which occurs when rock fragments are separated and transported downslope, usually by gravity, and alluvial deposits, which are

transported by rivers (Weil and Brady, 2017). Parent material influences the soil texture, and the chemical and mineralogical characteristics of soils (Weil and Brady, 2017). Soil texture affects soil permeability with sandy coarser soils having a higher water infiltration rate than clay soils (Weil and Brady, 2017).

- Time represents the period taken for soil formation to begin from the parent materials (Weil and Brady, 2017).

Fire and soil have a mutual relationship, therefore Certini (2014) noted that fire should be considered a soil formation factor. Reasons being that fire can have a significant impact on vegetation with the ability to control vegetation growth, such as the fire climax grasslands in the UDP, as this vegetation grows in soils and most soils have the ability to grow vegetation (Certini, 2014). In addition, fire has short or long-term direct and indirect impacts on soil (Certini, 2014).

#### 2.4.2 Effects of Fire on Soil Properties

The effects of fires on soil properties have been thoroughly reviewed at a worldwide scale, including both wildfires and prescribed burning (Certini, 2005; Zavala *et al.*, 2014; Alcañiz *et al.*, 2018), and studies including forests (Kennard and Gholz, 2001; González-Pérez *et al.*, 2004), semi-arid environments (Novara *et al.*, 2013), and grasslands (Pereira *et al.*, 2014) including across South African grasslands (Fynn *et al.*, 2003). There are two studies in the UDP that investigated the effects of burning on soils (Bijker *et al.*, 2001; Manson *et al.*, 2007). Bijker *et al.* (2001) compared soil properties and vegetation characteristics at regularly burned sites and a long-term no burn plot in the Giant's Castle Game Reserve. Manson *et al.* (2007) investigated the effects of fire season and frequency on soils and landscape functioning in the Cathedral Peak region of the UDP. There are no long-term studies on the effects of fire on soil properties in the Drakensberg and no studies that investigate soils across the whole UDP.

Soil properties affected by fire include physical, chemical and biological properties (Zavala *et al.*, 2014; Alcañiz *et al.*, 2018). The soil properties investigated in fire studies include: physical properties – soil texture, soil water repellency, soil infiltration capacity, soil moisture, soil aggregates, soil strength, soil colour, and bulk density; chemical properties – soil pH, soil organic matter, electrical conductivity, and total carbon and nitrogen. The effects of fire on soils can be short-term, long-term or permanent (Certini, 2005; Zavala *et al.*, 2014). The soil properties used in this study include soil properties used by Bijker *et al.* (2001) to investigate the effects of veld burning in the Giant's Castle Game Reserve, in the central UDP. These include: soil moisture, soil organic matter (SOM), soil texture (particle size), soil surface strength, soil compressive strength, soil colour, and soil pH (Bijker *et al.*, 2001). The above studies showed highly variable responses of soil properties to fire. The effects of fire on soil properties

are influenced by fire properties, which includes fire regime information (season, frequency, type and intensity of fire) (Trollope, 1981), burn severity (peak temperature and burn duration), and environmental factors, including vegetation type, litter accumulation, soil type, climate, topography, aspect and the ecosystem affected (Certini, 2005; Novara *et al.*, 2013; Pereira *et al.*, 2014; Zavala *et al.*, 2014), thus leading to the varying differences between soil property responses.

The effects of fire on soils can be both direct and indirect (Neary *et al.*, 2005). There are a range of additional factors that can influence soil properties, such as soil depth, with the highest temperatures during a fire occur in the top centimetre of soil (Certini, 2014). A variety of soil sampling depths have been used for soil sampling, with multiple studies opting to use more than one sampling depth. For example, O'Connor *et al.* (2004) used 0 - 10 mm and 10 - 20 mm for soil pH and electrical conductivity, and 100 mm deep for total Carbon and Nitrogen. Manson *et al.* (2007) used soil depths 0 - 50 mm and 150 - 200 mm, and Pereira *et al.* (2014) used 0 - 50 mm depth. Manson *et al.* (2007) found that soil properties varied with depth and that, in the case of SOM, burning had the highest impact on the top 0 - 50 mm.

#### *Soil Organic Matter*

SOM is one of the most widely studied soil properties in fire studies (González-Pérez *et al.*, 2004; Certini, 2005; Pereira *et al.*, 2014). The effects of fire on SOM are highly variable (González-Pérez *et al.*, 2004; Alcañiz *et al.*, 2018) with some literature noting both an increase and decrease in SOM (González-Pérez *et al.*, 2004; Zavala *et al.*, 2014). Weil and Brady (2017) states that there is a definite consumption of SOM by fires.

SOM has been found to have increased from fire. For example, in occasionally burnt grasslands or low fire frequency burns (Zavala *et al.*, 2014) where fire can increase nutrients and expose soil surfaces allowing increased access to light encouraging plant growth (Weil and Brady, 2017), or in low severity fires where fuel and organic matter did not combust completely (Novara *et al.*, 2013), or from the addition of charred material and ash (Novara *et al.*, 2013) which is a source of nutrients (Mills and Fey, 2004), or in a regularly burnt area, where an increase in SOM could be from a long-term accumulation of charcoal in the soil (Bijker *et al.*, 2001).

SOM has been found to decrease with exposure to fire, which could be from factors such as combustion during a fire (Zavala *et al.*, 2014). During the burning process, aboveground biomass and the accumulation of leaf litter are combusted, leading to a decrease in the factors that contribute to the organic content of the soil (Mills and Fey, 2004).

The effect of fire on SOM has also been found to not be significant in some cases. For example, SOM levels were not depleted by burning treatments at Cathedral Peak (Manson *et al.*, 2007), and Novara *et al.* (2013) showed the differences in soil organic carbon to be non-significant after a prescribed fire and noted that the slight difference could be due to the two different types of grasslands, leading to different characteristics. Novara *et al.* (2013) investigated soil organic carbon, this study investigated soil organic matter.

SOM has been found to change with time, decreasing immediately after fire (forest), then potentially increasing over time (Certini, 2005). Pereira *et al.* (2014) found the highest SOM value to be in the first two months after the fire. Soil moisture was noted as an important factor in SOM, with González-Pérez *et al.* (2004) noting soil moisture as one of the factors that SOM is dependent on, and Bijker *et al.* (2001) noting that the difference in SOM on south and north facing regularly burnt slopes could be due to temperature and moisture differences.

#### *Soil pH*

Soil pH can have high spatial variability with differences across a landscape occurring from hundreds of metres to a few millimetres or less, with soil depth, and with seasonal variations (Weil and Brady, 2017). Soil pH levels can be affected by plant roots, ash accumulation, and soil movement from erosion factors and topography (Weil and Brady, 2017). Soil pH also had a variety of responses to burning, with both increases and decreases in pH being noted (Zavala *et al.*, 2014; Alcañiz *et al.*, 2018). For example, forest fires were found to increase soil pH as the high temperatures cause soil heating leading to denaturation of organic acids (Certini, 2005), Manson *et al.* (2007) suggests that an increase in soil pH on frequently burnt grasslands could be due to ash neutralising the acidity in the soil, and accumulations of SOM in the soil causing the soil to acidify, decreasing in pH (Weil and Brady, 2017), Bachinger *et al.* (2016) found that in Loskop Dam Nature Reserve in South Africa, between firebreaks and unburnt grasslands, soil pH was not linked to either in the, Bijker *et al.* (2001) found no-burn sites to have the highest soil pH, while Manson *et al.* (2007) found soil pH in the top 50 mm was higher in frequently burnt compared to infrequently burnt (five year and no burn) grasslands.

#### *Other Soil Properties*

Other soil properties effected by fires include soil texture (particle size), soil surface shear strength, soil compressive strength, soil colour and soil moisture. Soil texture was found to be affected by fire through a potential decrease in the finer particles (clay) with bare ground after a fire and possibilities of erosion (e.g. wind), which could lead to an increase in coarser particles in soils (Zavala *et al.*, 2014). Bijker *et al.* (2001) found particle size (soil texture) to be influenced by aspect rather than burning, with north facing slopes being significantly coarser. Soil surface shear strength and soil compressive

strength were found to have an increase in soil strength from regular burning (Bijker *et al.*, 2001). Soil strength was found to be affected by aspect, SOM and soil moisture levels. For example, Bijker *et al.* (2001) noted that lower SOM can be related to lower soil strength values. Soil moisture was found to be affected by aspect, with Bijker *et al.* (2001) finding soil moisture to be significantly higher on south facing slopes. Burning can change soil colour due to accumulation of ash or charcoal (Pereira *et al.*, 2014), ranging from black to white in colour, changing of iron oxides, which causes redness, or organic matter combusting causing blackening (Zavala *et al.*, 2014). SOM does also account for some of the variation in soil colour (Bijker *et al.*, 2001).

## 2.5 SOILS AND FIRE VARIABILITY

Assessing the effects of fires is challenging due the spatial variability that can occur across one fire, as fires do not burn in the same manner across a landscape or differing ecosystems (Morgan *et al.*, 2014), and due to the variable impact fire can have on soils. Additional factors that need to be considered when investigating fire and soil effects are discussed below.

All fires do not burn uniformly, and the effects of fires depend on the fire regime. Fire regime refers to the season, frequency, type and intensity of fire (Trollope, 1981). The effects of fire frequency and fire season have been documented in the UDP previously (Mentis *et al.*, 1974; Scotcher and Clarke, 1981; Everson *et al.*, 1985). The significance of investigating fire behaviour has been acknowledged for a long time, with Trollope (1978) investigating the effects of head and back fires in a South African landscape, after noting the lack of knowledge regarding fire behaviour in South Africa, and Everson *et al.* (1985) investigating the range of fire behaviours that can occur in the UDP. Head and back fires are surface fires burning with the wind (head) or against the wind (back) (Trollope, 1981). The results from Trollope's (1978) study showed that while head fires had a greater rate of spread, flame length and intensity, back fires had a more significant effect on grasslands rate of recovery in a grassland environment with the same environmental conditions (Trollope, 1981). Thus, Trollope (1981) noted the necessity of including fire type when describing fire regime. This highlights that different types of fire can have different effects on landscapes, and thus soils. The time of year a fire occurs can affect the impacts of the fire. For example, a fire during the wet summer season will respond differently to a fire during the dry winter season (Forsyth *et al.*, 2010). There are, thus, inter-seasonal variations in fires (Forsyth *et al.*, 2010). Wildfires and prescribed fire are different in that wildfires may be of greater severity (Alcañiz *et al.*, 2018), have the potential to completely remove vegetation and leave the soil bare and open the soil to erosion effects of rain and wind (Miller *et al.*, 2015), whereas prescribed fires are of low to moderate severity and intensity (Certini, 2005).

Fire and environmental factors have a high level of heterogeneity across a landscape (Alcañiz *et al.*, 2018), resulting in the effects of fires varying greatly. Due to the wide variety of fire and environmental factors across the UDP there is high inter- and intra-variability (Alcañiz *et al.*, 2018), not just between the southern, central and northern UDP, but between each area and even between each sampling site (e.g. soil pH differing a few millimetres apart). For example, the composition of the plant communities, such as the difference between C<sub>3</sub> and C<sub>4</sub> grasslands, can alter the effects of fire behaviour due to fuel types and fuel moisture levels (McGranahan *et al.*, 2018). Uys and Hamer (2007) noted that additional environmental variables that are not directly related to the fire regime could be influencing invertebrate diversity in the UDP. This same concept could be said for soils and vegetation. This highlights the complexity of studying effects of fires on soils across a large diverse landscape like the UDP.

## CHAPTER 3: STUDY AREA

### 3.1 SETTING

The UDP is situated in the KwaZulu-Natal Province of South Africa, located on the western border of KwaZulu-Natal and the eastern border of Lesotho, and forms part of the Drakensberg mountain range, representing the largest protected area along southern Africa's Great Escarpment (EKZNW, 2012) (Figure 3.1). The UDP can be divided into three regions, northern, central and southern (Nel, 2007). The UDP is approximately 242813 ha (the area of the UDP used in the remote sensing analyses was 231393.42 ha as per the NBR results) in extent and ranges from an altitude of approximately 1200 metres above sea level (m.a.s.l) to the highest point in South Africa of 3408 m.a.s.l (EKZNW, 2012) (Figure 3.4). The UDP is approximately 158 km long and 28 km wide at the greatest width (EKZNW, 2012). 'uKhahlamba' translates into 'Barrier of Spears' in Zulu (Norman and Whitfield, 2006).

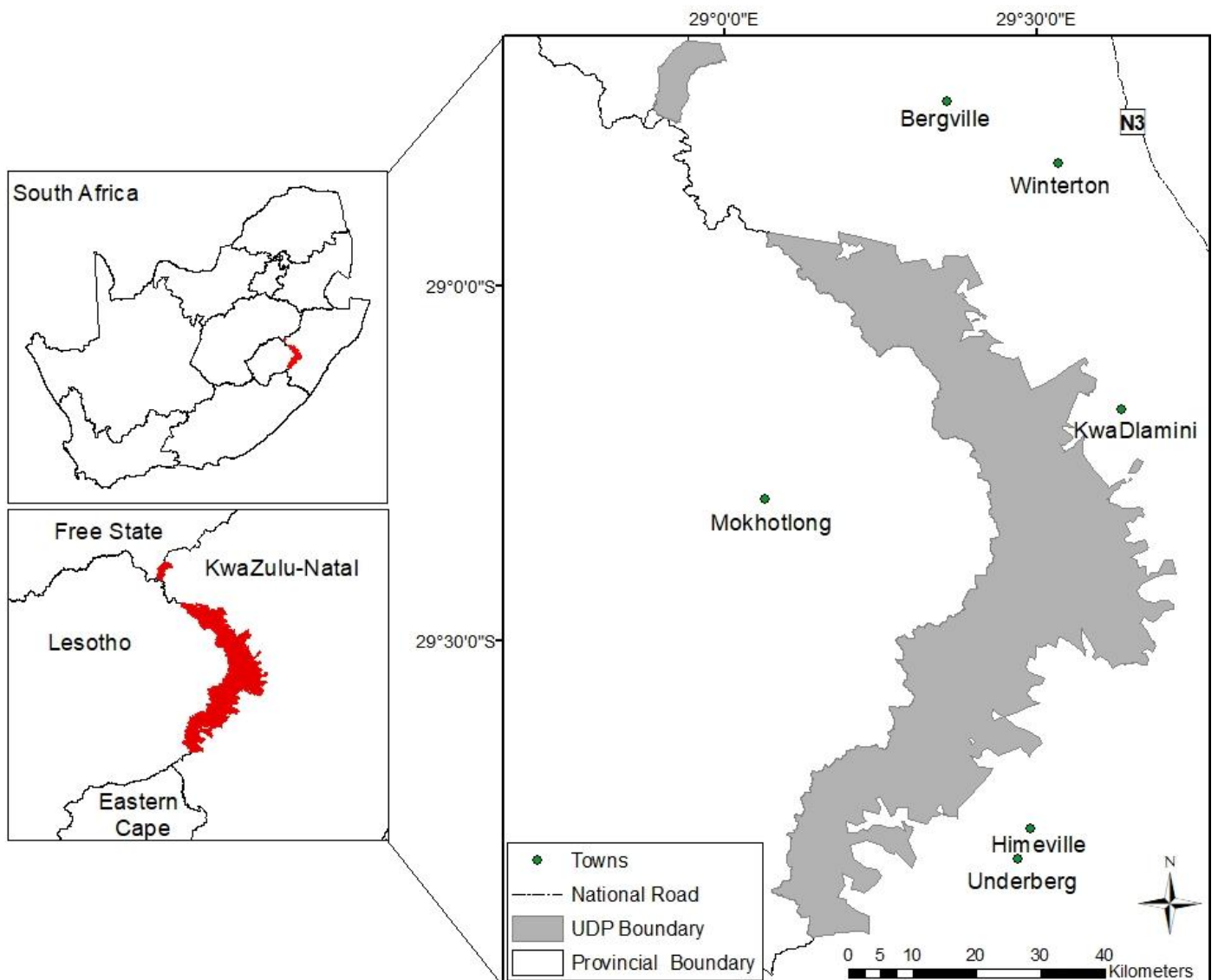


Figure 3.1. Locality Map of the UDP.

### 3.2 HISTORY AND CONSERVATION

The UDP forms part of the transboundary Maloti-Drakensberg Park, along with the Sehlabathebe National Park in Lesotho (UNESCO, 2017). Ezemvelo KwaZulu-Natal Wildlife (EKZNW) manages and controls the UDP (Krüger, 2007), which is of both national and international importance due to the unique cultural and natural values, which led to being listed as a World Heritage Site (EKZNW, 2012; UNESCO, 2017). The UDP is made up of 12 previously protected areas, dating back to 1903, with the area having a long history of conservation management (EKZNW, 2012). On 29<sup>th</sup> November 2000, the United Nations Educational, Scientific and Cultural Organisation (UNESCO) listed the UDP as a World Heritage Site (EKZNW, 2012; UNESCO, 2017). In 1997, the UDP was listed as a Ramsar site due to its important wetlands (Krüger, 2007). The UDP comprises four wilderness areas that make up 48.5% of the total area (Krüger, 2007). They are: Mlamboja (6270 ha), Mdedelelo (27000 ha), Mkhmazi (56155 ha), and Mzimkulu (28340 ha) (Krüger, 2007). These wilderness areas are proclaimed by statute to preserve natural conditions (Krüger, 2006). The importance of the UDP is exemplified by the fact that less than one percent of South Africa has been proclaimed as wilderness areas, with 36% of these wilderness areas being contained within the UDP (Krüger, 2007). The cultural significance is the thousands of San rock art paintings found within the UDP (Prins, 2005 cited in EKZNW, 2012). Thus, there is a big influence on conservation and preservation inside the UDP.

### 3.3 LANDSCAPE AND GEOLOGY

The Great Escarpment, some of which lies within the UDP, is important for South Africa's water supply, forming a watershed for some of southern Africa's largest basins and the source of the Orange River and the uThukela River (EKZNW, 2012; Gordijn, 2014). The uKhahlamba Drakensberg catchment plays an important role in contributing to the flow of the uMzimkhulu and uMkhomazi Rivers as well as their tributaries, with a large number of rivers and wetlands producing high quality water (EKZNW, 2012). According to Gordijn (2014), the Drakensberg mountain range is known as South Africa's "water tower". The Drakensberg's steep slopes, shallow soils and high rainfall, create large amount of runoff which the indigenous vegetation and soils help with the absorption of surface flow (EKZNW, 2012).

The KwaZulu-Natal Drakensberg has steep altitudinal gradients and diverse topography (Hill, 1996). The Drakensberg has two distinct topographical features, namely the High Berg and the Little Berg (Bainbridge, 1999 cited in EKZNW, 2012; Maloti Drakensberg Transfrontier Programme, 2012). The High Berg is made up of the higher altitude areas at the top of the escarpment, the summit plateau, the mountain peaks, and the steep slopes below the escarpment (Bainbridge, 1999 cited in EKZNW, 2012; Maloti Drakensberg Transfrontier Programme, 2012). The Little Berg is located below the High Berg and is made up of the lower altitude areas on the grass covered plateau, spurs, ridges and



sandstone cliffs (Bainbridge, 1999 cited in EKZNW, 2012; Maloti Drakensberg Transfrontier Programme, 2012).

Geologically, the Drakensberg is part of the Karoo Supergroup (McCarthy and Rubidge, 2005; Maloti Drakensberg Transfrontier Programme, 2012). The Drakensberg mountains largely comprise horizontally differentiated strata of the Upper Beaufort Group (or Tarkastad Formation), the Molteno Formation, Elliot Formation and Clarens Formation, with a cap of basaltic lava forming the basalt of the Drakensberg Group/Formation, and Karoo Dolerites in the form of widespread dykes and sills (McCarthy and Rubidge, 2005; Norman and Whitfield, 2006) (Figure 3.2, Figure 3.3). The rocks of the Stormberg Group, placed on top of the Beaufort Group, namely the Molteno, Elliot and Clarens Formations, show an increase in arid conditions gradually from the Molteno Formation to the Clarens Formation (McCarthy and Rubidge, 2005).

The Clarens Formation was formerly known as the Cave Sandstone, reflecting the ability of the Clarens Formation to weather to form caves (McCarthy and Rubidge, 2005). The cliffs of the Clarens Formation comprise fine grained sandstone which are yellowish to pinkish in colour, and siltstone (Norman and Whitfield, 2006). The Elliot Formation comprise mostly of multi-coloured mudstones, with sandstones present too (Norman and Whitfield, 2006). The Molteno Formation comprise of alternating sandstone and shale (Norman and Whitfield, 2006). The Tarkastad Formation (of the Upper Beaufort Group) comprise sandstones which alternate between fine- to medium- grained, and mudstones which are green and bluish in colour (Norman and Whitfield, 2006). On top of the Stormberg Group, the volcanic rocks of the Drakensberg Group are found, which today are only found in the high Drakensberg and Lesotho due to erosion (McCarthy and Rubidge, 2005). The Drakensberg Basalts consists of amygdaloidal lava with whitish amygdales (Norman and Whitfield, 2006; EKZNW, 2012). The Karoo Dolerites have the same composition as the lavas in the Drakensberg Basalts (Norman and Whitfield, 2006). The high ground, known as the High Berg is represented by the Drakensberg Formation basaltic lava cap that eroded into steep and high cliffs and rocky peaks (Norman and Whitfield, 2006). The Little Berg is made up of Clarens, Elliot and Molteno sandstones that sometimes form smaller plateaus, particularly at the top of the Clarens Formation (Norman and Whitfield, 2006).

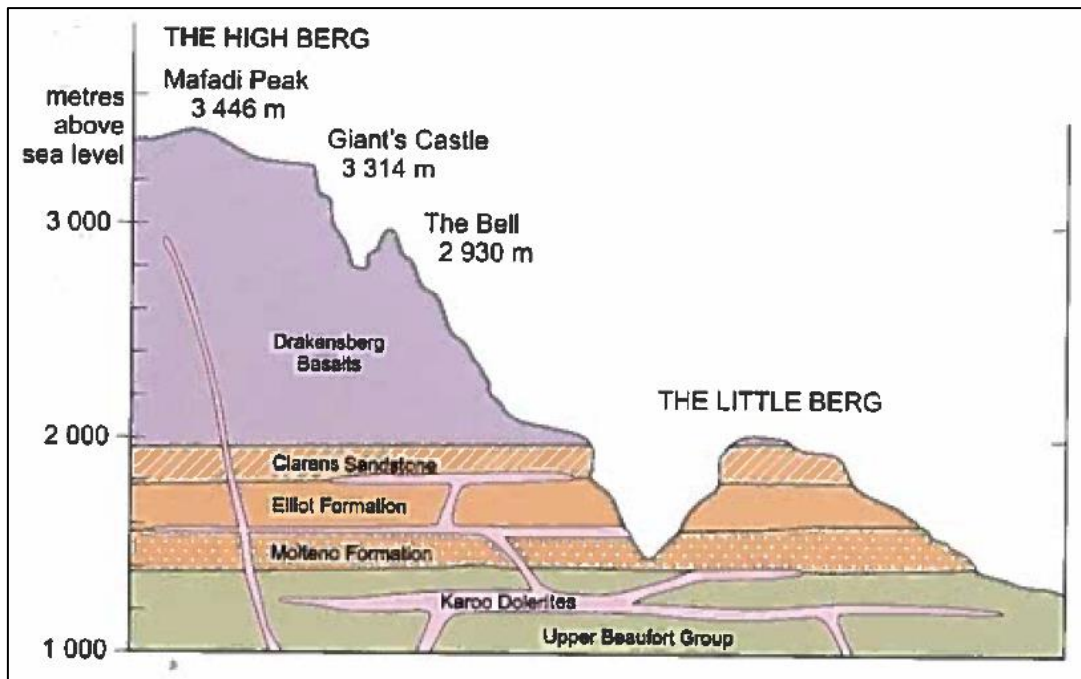


Figure 3.2. Geology and rock formations in the Drakensberg. (Source: Norman and Whitfield, 2006: 293).

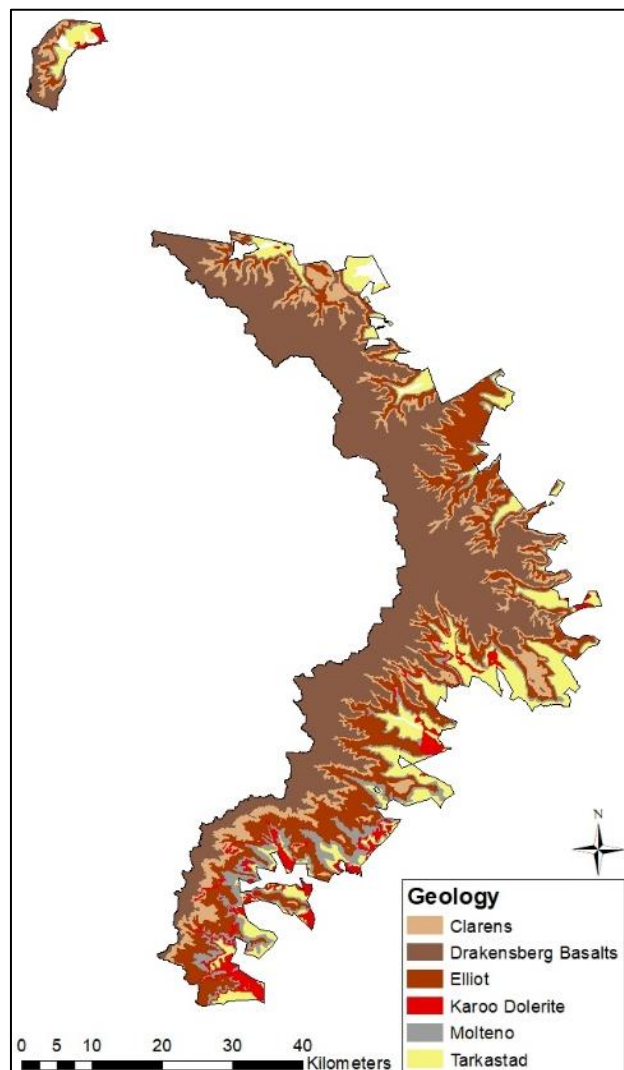


Figure 3.3. Geology of the UDP. (Source: Council for Geoscience, n.d.)

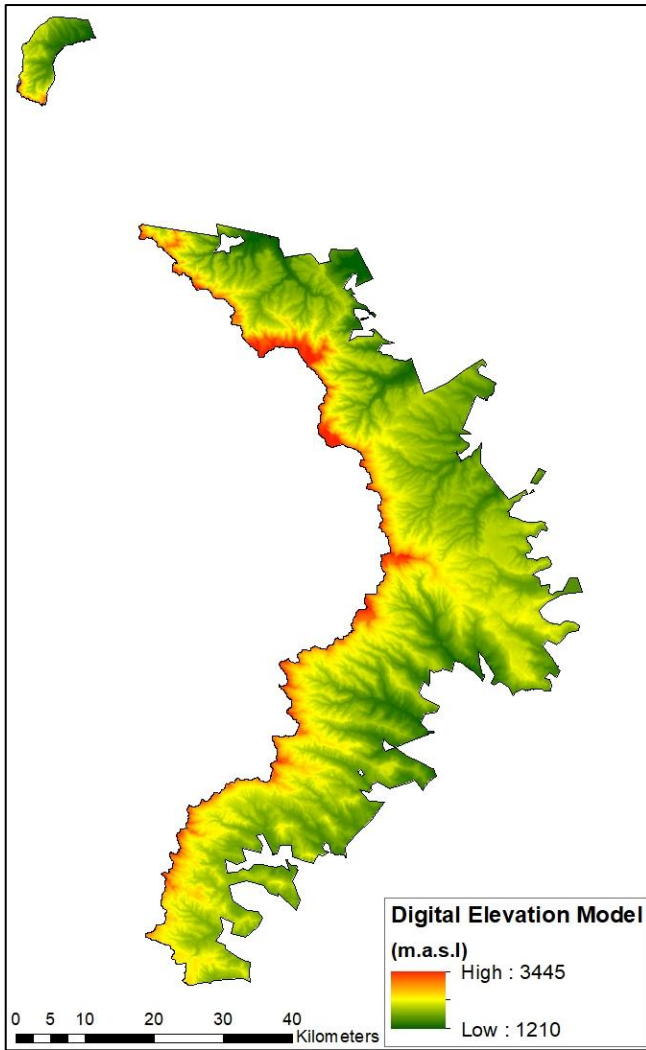


Figure 3.4. Digital Elevation Model (DEM) of the UDP.

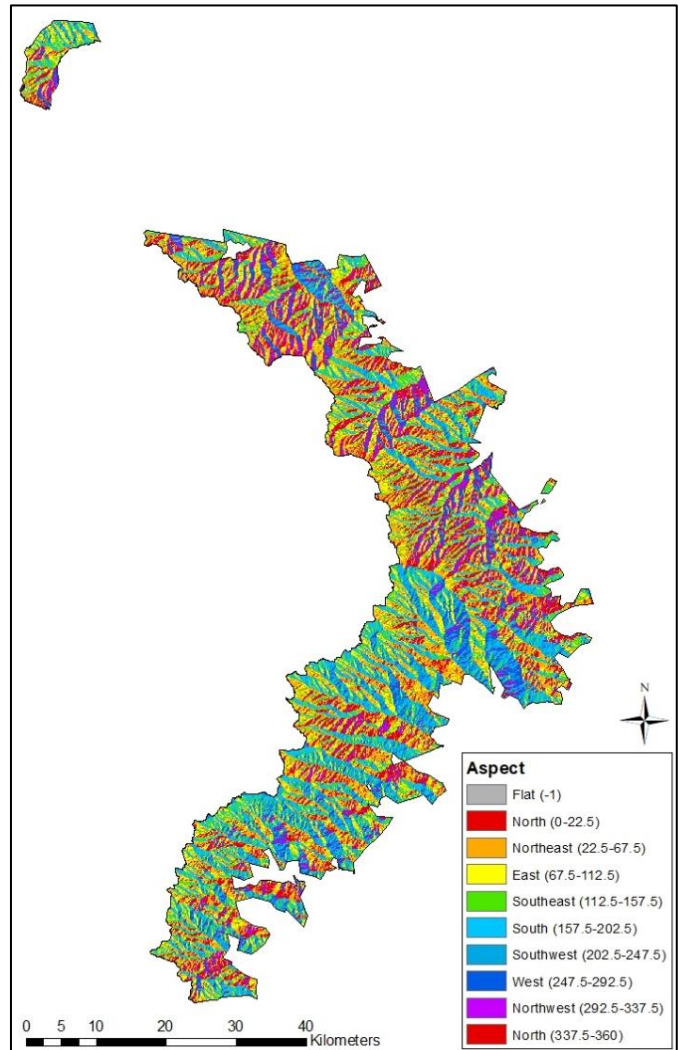


Figure 3.5. Aspect map of the UDP.

### 3.4 CLIMATE AND WEATHER

The KwaZulu-Natal Drakensberg is characterised by summer rainfall and dry winters, with 70% of the annual rainfall between November and March, and 10% falling between May and August (Nel, 2007). Annual precipitation ranges from 1000 mm in the lower foothills up to approximately 1800 mm at the escarpment (Bainbridge, 1999 cited in EKZMW, 2012). An increase in altitude usually corresponds with increased rainfall and decreased temperature (Mucina and Rutherford, 2006). Summer thunderstorms are very common due to the diverse topography, and due to mountainous areas having an orographic impact on rainfall (Mucina and Rutherford, 2006), leading to precipitation varying throughout the Drakensberg (Bainbridge, 1999 cited in EKZMW, 2012). Snowfalls occur mainly in winter, particularly at the high altitudes (Bainbridge, 1999 cited in EKZMW, 2012). The mean annual temperature in the KwaZulu-Natal Drakensberg is approximately 16°C, with significant variations between seasons and daily variations between day and night (Bainbridge, 1999 cited in EKZMW, 2012). Temperatures can reach up to 35°C on the lower altitude north facing slopes during the summer and can reach below freezing at the summit of the escarpment at night time in the winter (Bainbridge, 1999 cited in EKZMW,

2012). Slope aspect affects temperature with the highest temperatures occurring on the north-facing slopes during the summer months at the lower altitudes, and the lowest temperatures occurring at the top of the escarpment during the winter months (Figure 3.5) (Bainbridge, 1999 cited in EKZNW, 2012). There is a strong seasonal variation in vegetation between summer and winter, with the grassland vegetation being green in summer and turning brown in winter (Figure 3.6; Figure 3.7). This is due to the differences in geology and climatology extending across the UDP, such as variations between the high-altitude basalts with higher rainfall and the lower altitude sandstones with lower rainfall, and geomorphological processes being site specific (Grab, 2004 cited in EKZNW, 2012).



Figure 3.7. Summer at Giant's Castle in the UDP. (Photograph: Ian Meiklejohn).



Figure 3.6. Winter at Giant's Castle in the UDP.

### 3.5 VEGETATION

The UDP is located in the grassland biome (Mucina and Rutherford, 2006). More specifically, the Drakensberg Grassland Bioregion ('Gd' as referred to by Mucina and Rutherford, 2006), which majority of UDP falls within, and the Sub-Escarpment Grassland Bioregion ('Gs' as referred to by Mucina and Rutherford, 2006), where the lower foothills lie (Mucina and Rutherford, 2006). The UDP consists of fire-climax grasslands, with patches of shrub and forest located occasionally around the UDP (Scotcher and Clarke, 1981). These shrub and forest patches are normally located in refuge sites in low frequency fire areas (Scotcher and Clarke, 1981). The distribution of vegetation relates to altitude, rainfall, aspect and disturbances such as fire (EKZNW, 2012).

According to Mucina and Rutherford (2006), there are three dominating vegetation types within the UDP, namely:

- uKhahlamba Basalt Grassland (1820 - 3300 m.a.s.l) located at the high altitudes bordering Lesotho,
- Northern Drakensberg Highland Grassland (1460 - 2060 m.a.s.l) found in the lower altitude's northern areas,
- Southern Drakensberg Highland Grassland (1420 - 2080 m.a.s.l) found in the lower altitude's southern areas.

Other grassland vegetation found in the study area includes Drakensberg Foothill Moist Grassland found at the lowest altitudes of the UDP near the boundary with the rest of KwaZulu-Natal, Lesotho Highland Basalt Grassland found on the border with Lesotho, Northern KwaZulu-Natal Moist Grassland, and Southern KwaZulu-Natal Moist Grassland (Mucina and Rutherford, 2006) (Figure 3.8). Other vegetation types found scattered across the UDP in small patches, include: Drakensberg Afroalpine Heathland, Drakensberg Wetlands, Drakensberg-Amathole Afromontane Fynbos, and Northern Afromontane Forest (Mucina and Rutherford, 2006) (Figure 3.8).

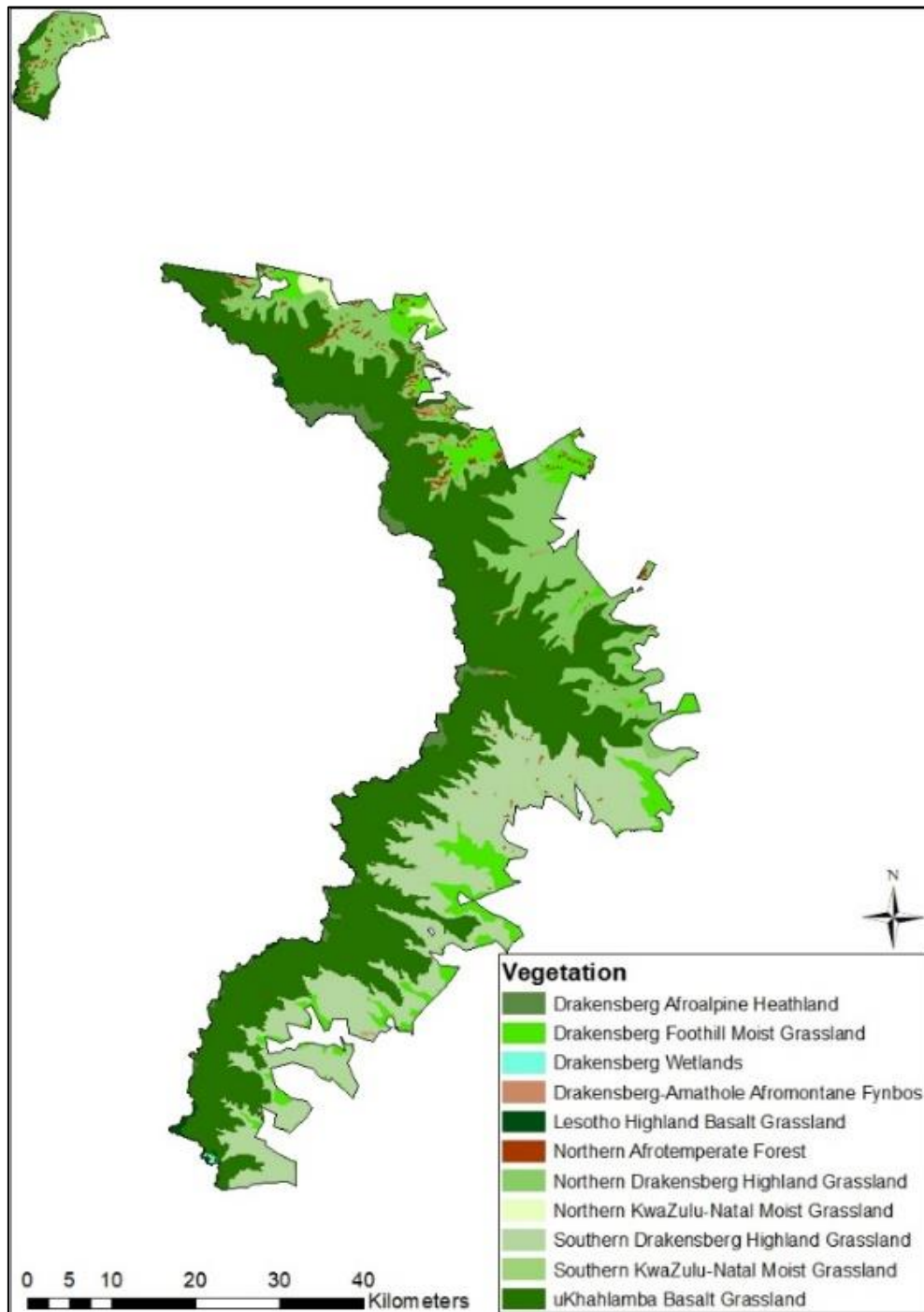


Figure 3.8. Vegetation of the UDP. (Source: Mucina and Rutherford, 2006).

According to Mucina and Rutherford (2006), each of these Drakensberg Grassland Bioregions and Sub-Escarpment Bioregions have their own climatic characteristics. Mucina and Rutherford (2006) created climate graphs representing these differences, including: Mean Annual Precipitation (MAP), Annual Precipitation Coefficient of Variation (APCV) Mean Annual Temperatures (MAT), Mean Frost Days (MFD), Mean Annual Potential Evaporation (MAPE), and Mean Annual Soil Moisture Stress (MASMS) (Figure 3.9). The climate graphs from Mucina and Rutherford (2006) shown below, include the most common vegetation type (uKhahlamba Basalt Grassland) and the four vegetation types that coincided with where soil samples were taken in this study (Figure 3.9).

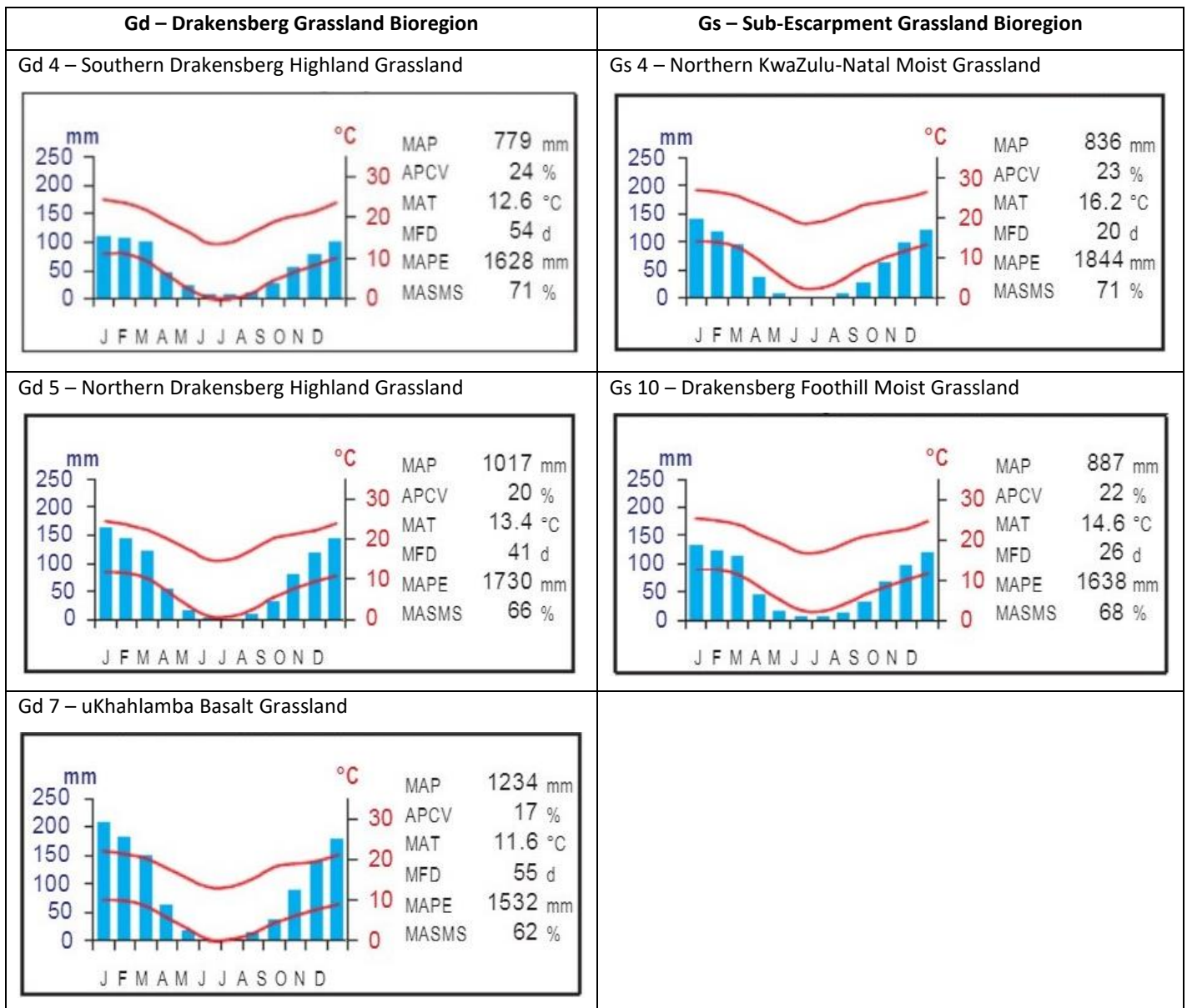


Figure 3.9. Climate diagrams of the grasslands of the UDP. (Source: Mucina and Rutherford, 2006).

When comparing the three main grassland types in the UDP, part of the Drakensberg Grassland Bioregion (left graphs – Figure 3.9), it is evident that the higher altitude grasslands (uKhahlamba Drakensberg Grassland) have a lower MAT and higher MAP when compared to the Southern and Northern Drakensberg Highland Grasslands, with MAP being significantly higher than the Southern Drakensberg Highland Grasslands. The Northern Drakensberg Highland Grasslands have a higher MAT and MAP when compared to the Southern Drakensberg Highland Grasslands, which are located at the same altitudes. The two other grassland types used in comparison are part of the Sub-Escarpment Bioregion (right graphs – Figure 3.9). Both the Northern KwaZulu-Natal Moist Grassland and the Drakensberg Foothill Moist Grassland are found at the lowest altitudes near the boundary of the UDP, with the Drakensberg Foothill Moist Grassland extending higher in the UDP and covering a greater area. Both the Northern Drakensberg KwaZulu-Natal Moist Grassland and the Drakensberg Foothill Moist Grassland have higher MAT than the previously mentioned grassland types, and lower MAP, except for the Southern Drakensberg Highland Grassland which recorded the lowest MAP. This shows the differences occurring across the UDP, and the importance of taking into account inter-site variability for comparisons across the UDP. Figure 3.10 highlights the influence that geology and altitude have on the vegetation of the Drakensberg, indicating the inter-relatedness of vegetation and geology in the UDP.

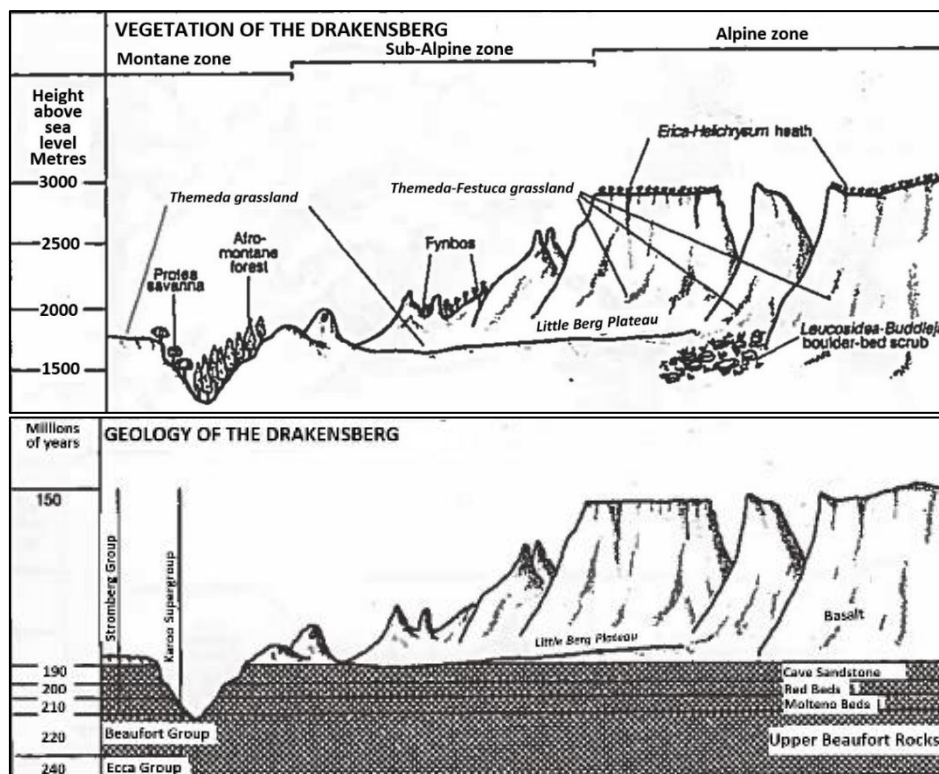


Figure 3.10. Comparison of the vegetation and geology of the KwaZulu-Natal Drakensberg. (Source: Bristow, 2010).

Killick (1963) identified three altitudinal vegetation belts in the KwaZulu-Natal Drakensberg; Montane belt (1280 - 1829 m), Sub-alpine belt (1830 - 2865 m), and Alpine belt (2866 - 3353 m), as shown in Figure 3.11. These zones coincide with the lower river valley system, the rolling foothills and the summit areas (Hill, 1996).

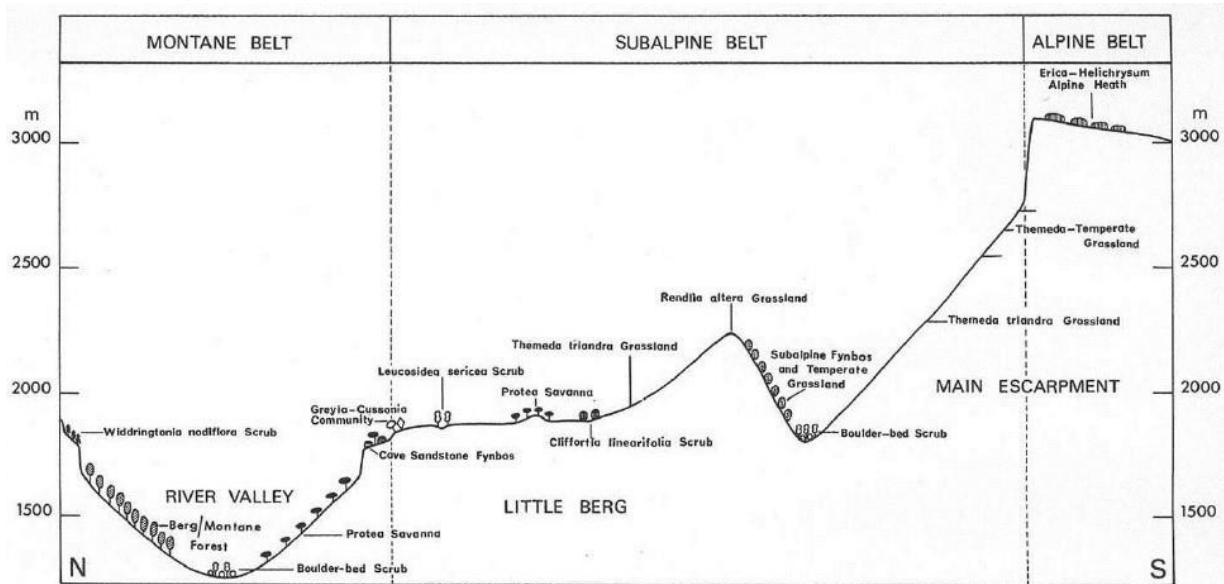


Figure 3.11. Schematic cross-section of the altitudinal vegetation belts and their main vegetation communities illustrated for Cathedral Peak (Northern area of the UDP). (Source: Killick, 1963).

### 3.6 SOILS

The soils of the UDP consist mostly of lithic soils (Fey *et al.*, 2010). Lithic soils range from 15% at the lowest altitudes, with the UDP mostly containing 30-60% of lithic soils, and up to greater than 60% at the top of the escarpment on the border with Lesotho (Fey *et al.*, 2010). Humic soils are also dominant in the UDP, ranging from 15 - 30% in the southern Drakensberg, and between 30 - 60% in the northern Drakensberg (Fey *et al.*, 2010). Oxidic soils are found in the northern Drakensberg only, with some patches in the northern Drakensberg ranging from 1 - 60% (Fey *et al.*, 2010). Other soils found in the UDP, consisting of between 1 - 7% each include: organic soils (throughout the UDP), duplex soils (mostly found in the southern UDP), gleyic soils (found mostly in the southern UDP and the lower altitudes of the northern UDP and not in the central UDP) and cumulic soils (with only a small patch located in the northern UDP area) (Fey *et al.*, 2010).

Lithic soils are regularly associated with steep topography and have a strong connection with their underlying parent rock, which plays a role in lithic soils' physical and chemical properties (Fey *et al.*, 2010). Highlighting the significance and relationship of soils and geology in the UDP. The humic horizon has a significant accumulation of humus or SOM, and often related to a high degree of weathering (Fey *et al.*, 2010). Humic soils are usually found in areas with high rainfall, cool temperatures and a gentle to moderate slope, such as the mid-altitudes of the UDP (Fey *et al.*, 2010).



### 3.7 SOCIAL ASPECTS

The management issues in the UDP include illegal exit and entry points through Lesotho and South Africa, communities surrounding the UDP not being supportive of the UDP, alien and invasive species, increased soil erosion caused by fires and tourists, poaching, and fire management (EKZNW, 2012). It is important to know what is happening in the buffer zone surrounding the UDP boundary, as different land uses and anthropogenic activities occurring close to the UDP boundary can have an effect on the UDP.

According to the Department of Environmental Affairs (DEA) 2013-2014 South African National Land cover dataset (DEA, 2016), there are differing dominant land covers surrounding the northern and southern areas of the UDP (Figure 3.12). The area surrounding the southern UDP is dominated by cultivated commercial farming and plantations. In comparison, the area surrounding the northern UDP has dominant settlements and cultivated subsistence farming, while also having plantations and cultivated commercial farming as land uses.

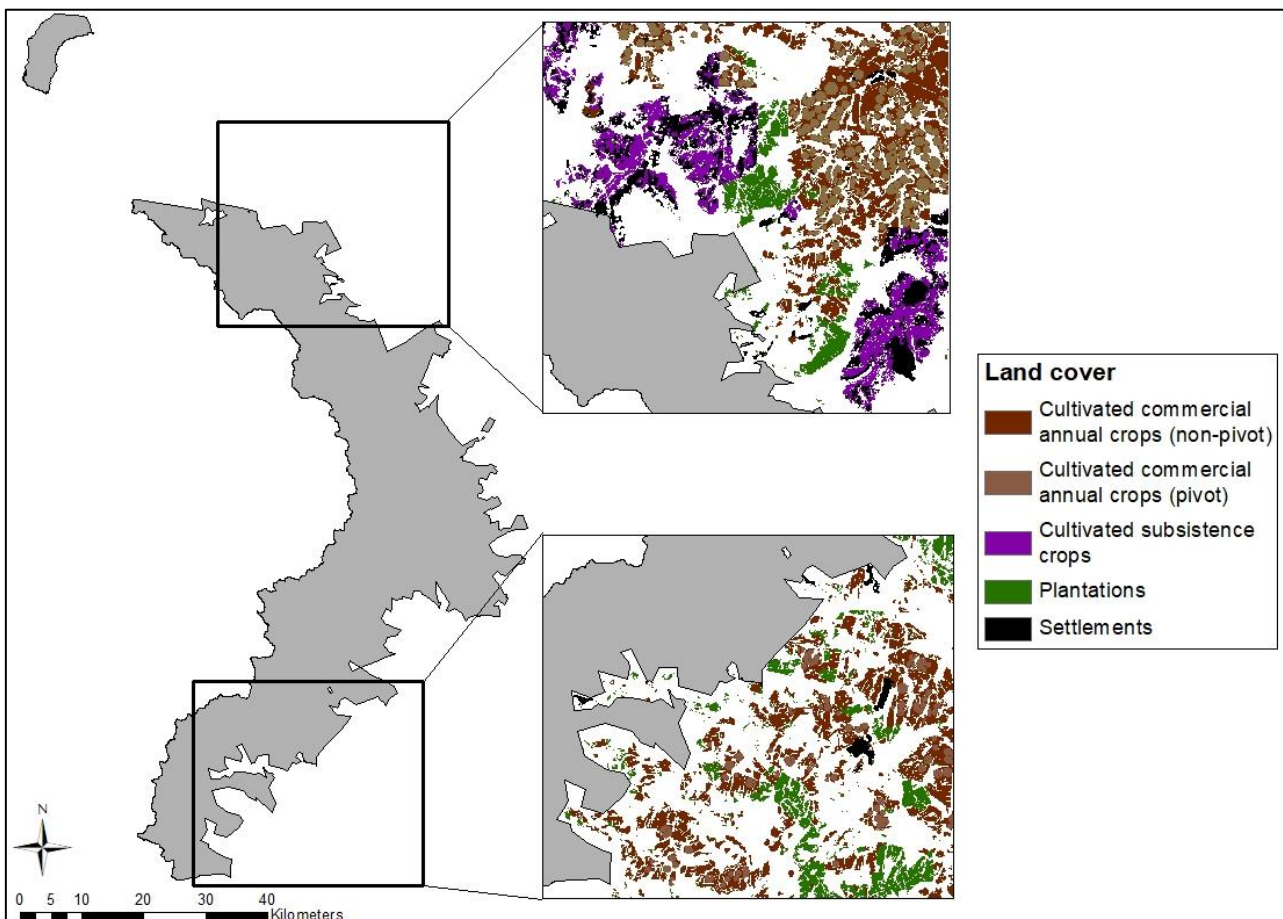


Figure 3.12. A comparison between the dominant land cover surrounding the southern and northern UDP. (Source: DEA, 2016)

## CHAPTER 4: METHODOLOGY

---

### 4.1 INTRODUCTION

The methodology comprises two parts: remote sensing and soils. The remote sensing methods used MODIS and VIIRS active fire detection data for investigating fire frequency across the UDP, and Landsat 5 and 8 for investigating the spatial extent of burn scar in the UDP. For investigating the effects of fire on soil properties, field work was conducted for soil sample collection, followed by soil laboratory analyses. Study sites for soil sampling were selected based on the remote sensing analyses of the spatial extent of fires results, and final site selection occurred in the field.

### 4.2 REMOTE SENSING

#### 4.2.1 Data Collection

ArcMap 10.3 (in 2017) and ArcMap 10.6 (in 2018) were used for all remote sensing processing, including both fire frequency using MODIS and VIIRS data, and Landsat burn scar analysis. ArcMap is the software available for use in the Geography Department at Rhodes University. The same data collection and analyses methods were used for both MODIS and VIIRS active fire detection.

#### *Fire Frequency*

To determine the frequency of fires in the UDP, MODIS active fire detection data and VIIRS active fire detection data were analysed. Archived fire point data from Fire Information for Resource Management System (FIRMS) was downloaded from the NASA Earthdata webpage. FIRMS data are acquired from NASA's EOSDIS, based at the University of Maryland (Strydom and Savage, 2016). FIRMS allow registered users to freely download daily fire hotspot information. MODIS and VIIRS fire point data was downloaded for South Africa in a shapefile in Geographic co-ordinates World Geodetic System (WGS) 1984 datum (WGS84). No near real-time (NRT) data was used for both MODIS and VIIRS data.

The MODIS instruments are found on-board NASA's Terra and Aqua satellites (Giglio *et al.*, 2016). Terra has been collecting MODIS data since February 2000 and Aqua since June 2002 (Giglio *et al.*, 2003). To compare annual fire point data, only years with full datasets were used. Therefore, MODIS active fire data were investigated for 2003 to 2017. The MODIS active fire data used was "Collection 6", standard products (MCD14ML). The 1 km<sup>2</sup> MODIS pixels are classified as a fire pixel if one or more actively burning fires are detected in that pixel during the satellite overpass (Figure 2.1) (Giglio *et al.*, 2016).

The Visible Infrared Imaging Radiometer Suite (VIIRS) instrument is found on-board the Suomi-National Polar-orbiting Partnership (S-NPP) satellite, and was launched in October 2011 (Schroeder *et*

*al.*, 2014). The VIIRS instrument has global coverage every maximum 12 hours, depending on the latitude (Schroeder *et al.*, 2014). VIIRS active fire data was available from 20 January 2012 (Schroeder and Giglio, 2018). The new VIIRS active fire detection algorithm was designed to improve on the MODIS fire algorithm, with a higher spatial resolution of 375 m<sup>2</sup> (Schroeder *et al.*, 2014).

#### *Spatial Extent*

To determine the spatial extent of burn scar in the UDP, Landsat 5 and Landsat 8 imagery was used. Landsat has a 30 m spatial resolution (band dependent – Table 4.2; Table 4.3), with a sun synchronous orbit and a 16-day revisit time (U.S. Geological Survey, 2016). Landsat imagery is freely available for download from the United States Geological Survey (USGS) ‘EarthExplorer’ webpage. The extent of burn scar was investigated for the last 20 years (1998 - 2017).

Initial fire frequency results from the MODIS and VIIRS active fire data, suggest the main fire season in the UDP runs from May to October, with the most fires occurring in June and July (Figure 5.5 and Figure 5.9). Therefore, to investigate burn scars in the UDP using Landsat, the months August, September and October were viewed as the most appropriate to identify burn scars, as it was when they are prominent and would achieve the maximum likelihood of detecting burn scar in the Landsat image. From 1998 to 2017, Landsat images for 12 out of the 20 years were appropriate for detecting burn scar in the UDP (Table 4.1). The main data limitations with finding appropriate Landsat images were cloud cover covering the burn scar or missing data, which has been noted in the literature (Langmann *et al.*, 2009; Goodwin and Collett, 2014.). Some years did not have Landsat images that covered the UDP available. For example, the Landsat 7 Enhanced Thematic Mapper Plus (ETM+) data was not used in this study caused by data gaps due to a technical failure on the satellite (U.S. Geological Survey, 2016). Dates each year differ due to Landsat’s 16-day revisit period and the available data; the closest possible dates for each year were obtained. The ‘best’ Landsat image, which excluded clouds and snow and had visible burn scar was selected per year.

Table 4.1. The dates of the available Landsat 5 and 8 images used for investigating burn scar in the UDP.

Landsat	Year	Date
5	1998	10-Sep
5	1999	28-Aug
5	2000	30-Aug
5	2001	17-Aug
5	2005	29-Sep
5	2006	16-Aug
5	2007	3-Sep
8	2013	3-Sep
8	2014	6-Sep
8	2015	24-Aug
8	2016	26-Aug
8	2017	14-Sep

Two Landsat images (Path 169, Row 80; Path 169, Row 81) were needed to cover the extent of the UDP. The downloaded Landsat images were in map projection Universal Transverse Mercator (UTM) 35S and World Geodetic System (WGS) 1984 datum (U.S. Geological Survey, 2016), leading to UTM 35S being used for all mapping of the UDP. The Landsat images were downloaded in Geographic Tagged Image File Format (GeoTIFF) in compressed files and the data were extracted (U.S. Geological Survey, 2017) using the free 7-Zip package.

For 1998 to 2007, Landsat 5 Thematic Mapper (TM) “Collection 1 Level 1” imagery was used. Landsat 5 TM, in operation from March 1984 to January 2013, contains seven bands: the visible spectrum bands (red, green, blue) and near infrared (NIR), with the Thematic Mapper (TM) sensor including the additional shortwave infrared (SWIR) bands and thermal band (Table 4.2) (U.S. Geological Survey, 2016). For 2013 to 2017, Landsat 8 Operational Land Imager (OLI)/Thermal Infrared Sensor (TIRS) “Collection 1 Level 1” imagery was used. Landsat 8 OLI/TIRS, in operation since February 2013, contains 11 bands; like the Landsat 5 TM, with the addition of OLI adding a 15 m panchromatic band, coastal-aerosol band and cirrus cloud detection, and TIRS containing an additional thermal band (Table 4.3) (U.S. Geological Survey, 2016). This study used the red, green, blue, NIR and SWIR 2 bands from both Landsat 5 and Landsat 8 for burn scar detection.

The data quality of Level 1 Landsat products is known (U.S. Geological Survey, 2017). Both Landsat 5 TM and Landsat 8 OLI/TIRS data used Level 1 Tier 1 category data, meaning that geometric and radiometric quality standards have been fulfilled (U.S. Geological Survey, 2017). Tier 1 products under Collection 1 with processing to Level 1 Precision and terrain corrected products (L1TP) have the highest quality of Level 1 products with correction for relief displacement, ground control points

orthorectification, and radiometric correction, making them considered suitable for pixel-level time series analyses (U.S. Geological Survey, 2017). The radiometry and geometry quality standards help to ensure that changes detected are not due to changes on the sensor (U.S. Geological Survey, 2017).

Table 4.2. Landsat 5 bands. (Source: U.S. Geological Survey, 2018).

Landsat 4-5 TM bands		Wavelengths ( $\mu\text{m}$ )	Resolution (m)
Band 1	Blue	0.45 – 0.52	30
Band 2	Green	0.52 – 0.60	30
Band 3	Red	0.63 – 0.69	30
Band 4	Near Infrared (NIR)	0.76 – 0.90	30
Band 5	Shortwave Infrared (SWIR) 1	1.55 – 1.75	30
Band 6	Thermal	10.40 – 12.50	120*(30)
Band 7	Shortwave Infrared (SWIR) 2	2.08 – 2.35	30

Table 4.3. Landsat 8 bands. (Source: Barsi et al., 2014; U.S. Geological Survey, 2018).

Landsat 8 OLI/TIRS bands		Wavelengths ( $\mu\text{m}$ )	Resolution (m)
Band 1	Ultra-Blue (coastal/aerosol)	0.433 – 0.453	30
Band 2	Blue	0.450 – 0.515	30
Band 3	Green	0.525 – 0.600	30
Band 4	Red	0.630 – 0.680	30
Band 5	Near Infrared (NIR)	0.845 – 0.885	30
Band 6	Shortwave Infrared (SWIR) 1	1.560 – 1.660	30
Band 7	Shortwave Infrared (SWIR) 2	2.100 – 2.300	30
Band 8	Panchromatic	0.500 – 0.680	15
Band 9	Cirrus	1.360 – 1.390	30
Band 10	Thermal Infrared (TIRS) 1	10.60 – 11.19	100* (30)
Band 11	Thermal Infrared (TIRS) 2	11.50 – 12.51	100* (30)

#### 4.2.2 Data Analysis

##### *Data Pre-processing*

In ArcMap, the 'clip tool' under geoprocessing tools was used to clip the MODIS and VIIRS active fire data which was downloaded for the whole of South Africa, to the UDP border. In order to analyse the MODIS and VIIRS active fire data annually and monthly, the data was pre-processed by exporting the shapefile attribute tables to Microsoft Excel to separate the date data into separate day, month and year columns. The data was then imported back into ArcMap.

For each downloaded Landsat 5 and 8 image, the top and bottom images that covered the UDP were utilised in ArcMap, and the following bands were added for each year: blue, green, red, NIR and SWIR 2 (Table 4.2; Table 4.3). In the image analysis toolbar, a composite image of the individual bands was

created for each Landsat image. The two Landsat images for each year were mosaicked together in the image analysis toolbar, and the 'extract by mask' tool was used to clip the mosaicked Landsat image to the boundary of the UDP. Resulting in one Landsat image per year of suitable data in the UDP.

### *Fire Frequency*

The MODIS and VIIRS data were analysed using annual and monthly periods. MODIS and VIIRS point data were analysed annually using point comparisons and density diagrams, specifically kernel densities, showing the areas of the highest and lowest concentrations of fire points across the UDP. Kernel density estimation is a non-parametric statistical method (Koutsias *et al.*, 2004) which, in this study, used fire point data to estimate the fire probability densities or fire occurrence zones like used by Koutsias *et al.* (2014). An overall kernel density was analysed for 2003 to 2017 for MODIS and 2012 to 2017 for VIIRS. The 'kernel density tool' from the Arctoolbox, under spatial analyst was used to create the kernel density (Settings: Type = percent clip; min = 0.5, max = 0.5).

Due to the different spatial resolutions (1 km<sup>2</sup> for MODIS and 375 m<sup>2</sup> for VIIRS) the data is not directly comparable, and was therefore compared looking at patterns and ratios for 2012 to 2017. The ratio of MODIS points to VIIRS points was calculated by dividing the annual number of VIIRS points by the annual number of MODIS points.

The limitations of using MODIS and VIIRS active fire detection are the pixel resolutions as well as a detected fire point relating to at least one fire occurring in that pixel, with the potential for multiple fire points to be related to one large fire and not necessarily many fires (Figure 2.1) (Giglio *et al.*, 2003). Both MODIS and VIIRS active fire data comes with a detection confidence rating for each individual fire point. The purpose of this is for users to get an indication of the quality of the data (Giglio, 2015). MODIS active fire data confidence estimates are given as a percentage from 0% to 100% (Giglio, 2015). These percentages relate to three fire confidence classes: low, nominal or high (Table 4.4) (Giglio, 2015). VIIRS active fire data confidence estimates are not given as a percentage but as one of the three fire confidence ratings (Schroeder and Giglio, 2018). Using all the fire points, from all three confidence classes, results in maximum fire detection but with the possibility of false alarms (Giglio, 2015). As this study is looking at using available fire data, the confidence ratings were acknowledged and calculated for all the years' data (Table 4.4; Table 4.5) but all fire pixels, no matter the confidence rating, were used in the fire point analyses for MODIS and VIIRS active fire data. Out of the total 8056 MODIS fire points detected from 2003 to 2017, 23 had a 0% rating and 911 had a 100% confidence, with an average confidence of 69.78% (Table 4.4). Out of the total 10479 VIIRS fire points detected from 2012 to 2017, 2.72% had a low confidence rating and 9.19% had a high confidence rating (Table 4.5). For

fire management and scientific study purposes, Schroeder and Giglio (2018) acknowledges the VIIRS active fire data used in this study to be considered of good enough quality, while acknowledging the data's known limitations.

Table 4.4. MODIS active fire data confidence ratings. (Confidence percentage classes from Giglio, 2015).

MODIS			
Confidence percentage (%)	Confidence category	Number of points	Percentage (%)
0 – 29	Low	431	5.35
30 – 79	Nominal	4558	56.58
80 – 100	High	3067	38.07

Table 4.5. VIIRS active fire data confidence ratings.

VIIRS		
Confidence category	Number of points	Percentage (%)
Low	285	2.72
Nominal	9231	88.09
High	963	9.19

#### *Spatial Extent*

Burn scars in the UDP were examined using different band combinations of Landsat to highlight burn scars to investigate the spatial extent of fires in the UDP. The ideal band combinations for investigating burn scar were determined to be SWIR 2, NIR and red (Figure 4.1), as suggested in the literature review (Chen *et al.*, 2016). The options for investigating burn scar in the UDP were: image classifications using supervised and unsupervised classifications or Normalised Burn Ratio (NBR). Both methods were attempted in ArcMap, using a Landsat 8 image from the UDP. It was determined that the NBR method was the most suitable option for investigating burn scar in the UDP, as highlighted in the literature review. NBR was used to determine the spatial extent of fires by detecting burn scar in the UDP, for all the years of Landsat imagery.

A NBR was applied to all the available Landsat images (Figure 4.1). The standard methods for calculating NBR were used (Roy *et al.*, 2006; Miller *et al.*, 2015). NBR was calculated using the spatial analyst 'raster calculator' tool in ArcMap. The NBR equation is:

$$\text{Equation 1: Normalised Burn Ratio} = \frac{(\text{Near Infrared} - \text{Shortwave Infrared 2})}{(\text{Near Infrared} + \text{Shortwave Infrared 2})}$$

NBR was calculated based on the Landsat 30 m pixel resolution, by detecting each 30 m pixel as 'burn' or 'no burn' (Figure 4.1). The same process was followed for both Landsat 5 and 8. The resulting NBR is the number of pixels that were detected as 'burn' and 'no burn', allowing for the amount of burn scar detected to be quantified (Figure 4.1). The percentage burn is based on the number of pixels

calculated as burn out of a total 2571038 (30 m<sup>2</sup>) pixels that make up the whole UDP. The area of burn scar in squared metres (m<sup>2</sup>) was determined by multiplying the number of burn pixels by the area of one pixel (30 m<sup>2</sup>). The ‘raster calculator’ in ArcMap was used to determine areas of the UDP where burn scar detected by NBR overlapped for all 12 years of available Landsat data and to detect the areas where no burn scar occurred in the UDP. This analysis shows where the areas of high and low fire frequency occurred.

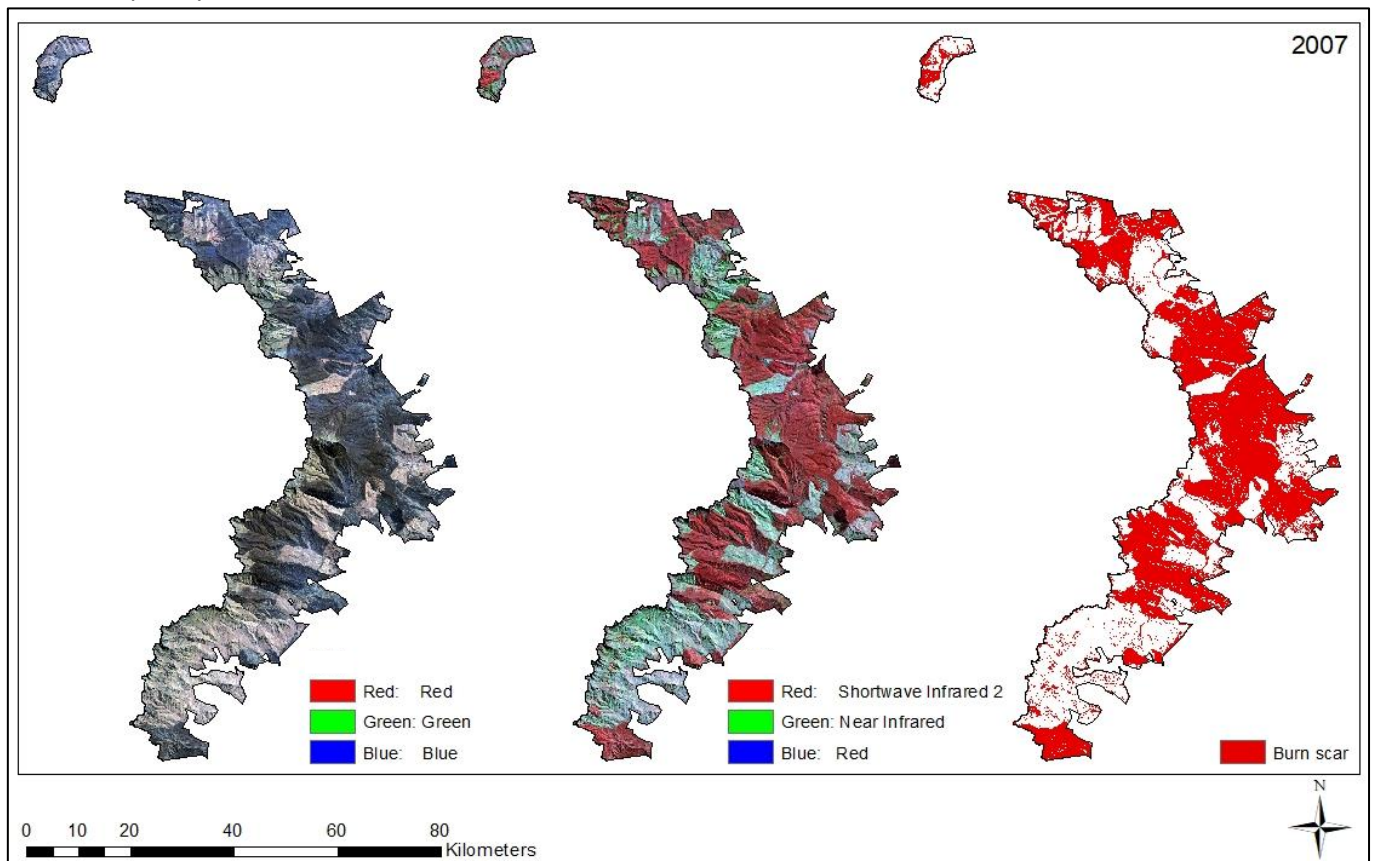


Figure 4.1. Landsat 5 image (3<sup>rd</sup> September 2007) showing burn scar in the UDP, comparison from left to right: (1) band combinations red (0.630 – 0.680 μm), green (0.525 – 0.600 μm), blue (0.450 – 0.515 μm) showing burn scar in black, (2) band combinations SWIR 2 (2.100 – 2.300 μm), NIR (0.845 – 0.885 μm), red (0.630 – 0.680 μm) showing burn scar in red, (3) Outcome of a NBR showing burn scar in red.

#### Accuracy Assessments

An important aspect of interpreting the results of the fire frequency and spatial extent of burn scar is conducting an accuracy assessment of the remote sensing data to provide an indication of the extent to which the fire data can be considered reliable. Congalton (1991) highlights the importance of providing an accuracy assessment and an error matrix. This is particularly relevant in this study to compare fire data from MODIS, VIIRS and the NBR, which all have an automated classification element at three different scales.

Fire points from one day of MODIS and VIIRS data from the UDP were compared to a corresponding Landsat 8 satellite image. Schroeder *et al.*, (2014) conducted an accuracy comparison between VIIRS



active fire data and Landsat. The time of the fire point detection was compared to visible smoke on the Landsat image, highlighting the differing satellite overpass times as noted by Schroeder *et al.* (2014). Annual MODIS and VIIRS fire points were compared to the NBR results by conducting an overlay analysis. In ArcMap, the 'Extract values to point' tool was used to calculate the number of MODIS and VIIRS points that overlapped with burn scar from the NBR results. The fire points that occurred after the Landsat image acquisition date were excluded from the comparison. A percentage was calculated for the number of MODIS and VIIRS fire points that overlapped with the Landsat NBR burn scar to give an accuracy of fire points to actual burn scar.

An example of digitising burn scar for the Landsat image was conducted for 2017, to compare with the NBR burn scar results. In ArcMap, the NBR burn scar pixels were converted from their raster format to a vector polygon format, and the burn scar polygons were manually edited using the Landsat 8 image as a background layer. The burn scars were not manually digitised from scratch, but edited using the NBR results. The percentage area of burn scar calculated using the pixels of burn scar from the NBR results was compared to the percentage area of burn scar calculated using the polygons of burn scar. The accuracy comparison was calculated as:

$$\text{Equation 2: Vector versus Raster Accuracy} = \frac{(\% \text{ Burn vector})}{(\% \text{ Burn Raster})} \times 100$$

This accuracy assessment acts as an error estimate. The same study area for each year of NBR burn scar calculations (used the same UDP boundary was used). Therefore, the known NBR errors, for example detecting rock reflections and outcrops as burn scar (Figure 4.4), are assumed to occur every year as the rock outcrops are constant across all my years of data.

#### 4.2.3 Study Site Selection

The remote sensing data analyses involved the selection of appropriate study sites for soil sampling based on areas of low and high fire frequency, to investigate the effect fire has on soils. The fire regime information included in site selection was fire frequency (high and low) and the environmental factors included in site selection were aspect, slope and geology. Site selection using remotely sensed fire frequency maps has been used before. For example, Robinson (2014) used fire frequency maps, created using NBRs from Landsat imagery, and included environmental factors of slope, aspect, altitude and topographical settings, to identify suitable monitoring sites in the Sani Pass region of Lesotho, near the UDP.

Using ArcMap, possible sites were determined using the combined NBR results, to achieve an unbiased site selection. For high frequency fire areas, areas where fires overlapped for all 12 years of burn scar data were used. For low fire frequency fire areas, areas which had burn scar for one out of the 12

years of burn scar data were used. One year of burn scar was used instead of areas with zero years of burn scar, as the NBR results for zero years of burn scar were located on areas of forest, buildings, car parks and camping grounds. Accessibility of sites was also an important factor to consider in site selection. First, general areas of the UDP were selected for study areas. The areas selected were known parts of the UDP that had road access, hiking paths and had EKZNV huts and rangers present. The locations were spread across the whole UDP, adding a spatial variation element. Nine areas were selected, including: Bushman's Nek, Garden Castle, Cobham, Kamberg, Giant's Castle, Injisuthi, Monks Cowl, Cathedral Peak and the Royal Natal National Park (Figure 4.6). Possible study sites for each area of the UDP was determined by loading GIS layers: NBR (fire frequency), geology, aspect, slope, and two ArcMap base layers (World imagery and Open street map) (see data disclaimer) (Figure 4.2). Geology, aspect and slope were considered to select sites that had similar environmental factors, as these factors play a role in soil formation (Weil and Brady, 2017), and to avoid steep slopes that were inaccessible. Open street map showed the roads, hiking paths and rivers (Figure 4.2). The World imagery basemap showed an aerial satellite view, which made it easier to detect rocks, hiking paths, camping areas and forests (Figure 4.2). The minimum size of the possible sampling areas selected in ArcMap prior to field work was 30 m<sup>2</sup> as this is the pixel size used for the NBR results and the Landsat imagery. Gross *et al.* (2009) highlighted the need for ground-truthing remote sensing data, however, this is costly and not all areas are always accessible. This study was not able to ground-truth the remote sensing data. Therefore, multiple possible high fire frequency and low fire frequency study sites were selected per area. This was to take into account field variation, and the difficulty in selecting sites from GIS data with the potential for errors with GIS data. The co-ordinates of the centre of the polygon for each possible site were determined in ArcMap and used to find the sites during field work. Final site selection took place in the field.

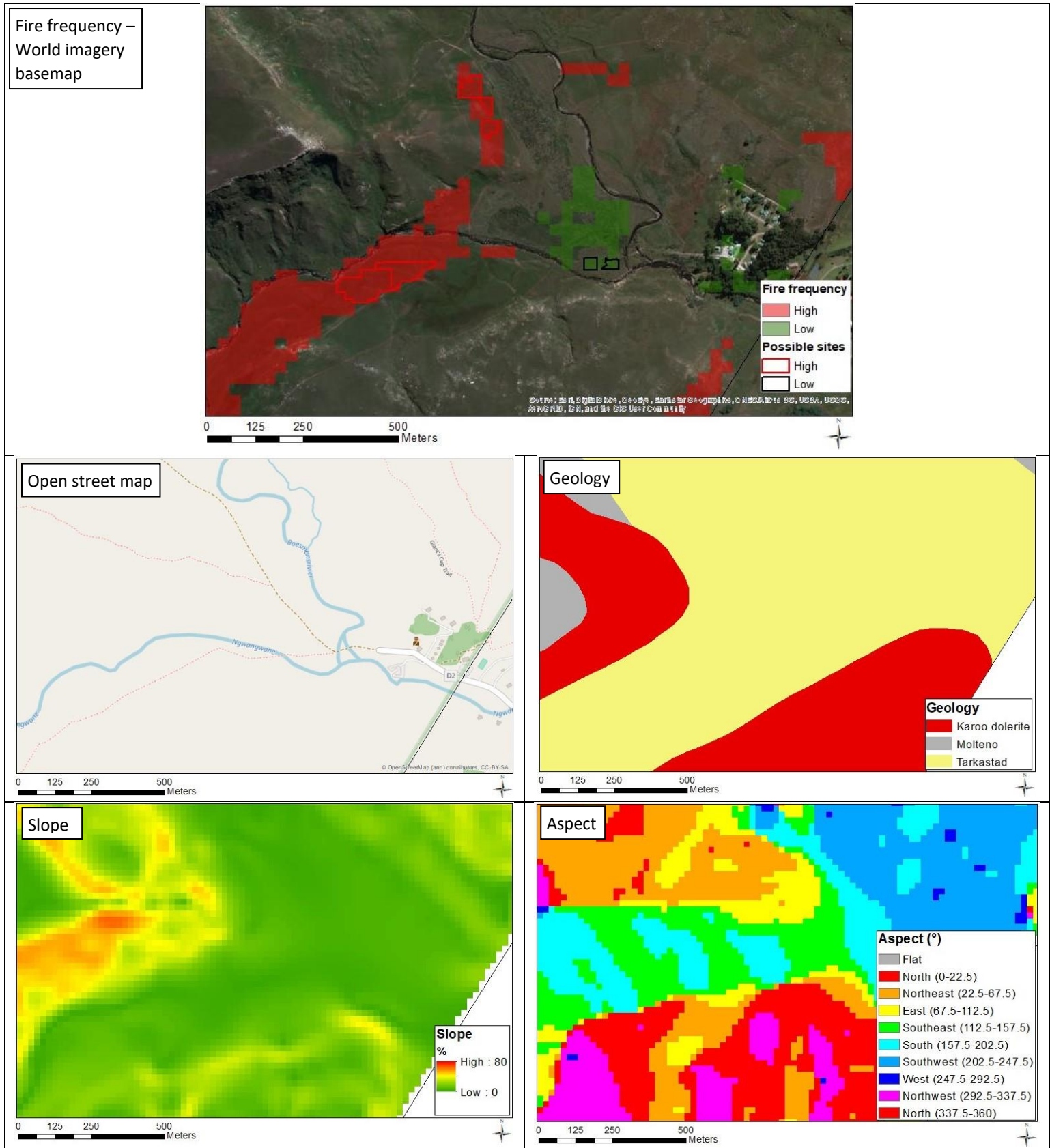


Figure 4.2. An example of the site selection process in ArcMap in the UDP. (Example from Bushman's Nek, UDP).

## 4.3 SOILS

### 4.3.1 Field work

Field visits and soil sampling took place over one month in December 2017 and January 2018. The first part of the field work was selecting the high and low fire frequency sampling sites in each area from the possible sample sites. These possible sites were established using ArcMap prior to going into the field, and located in the field by using the coordinates of the point at the centre of the possible site, using a Garmin Global Positioning System (GPS) (GPSMAP 64s) (Figure 4.4). Final site selection occurred in the field. Nine areas across the UDP were sampled, with nine high fire frequency sites and eight low fire frequency sites (Royal Natal did not have a low fire frequency site), with 17 sites in total across the UDP (Figure 4.3).

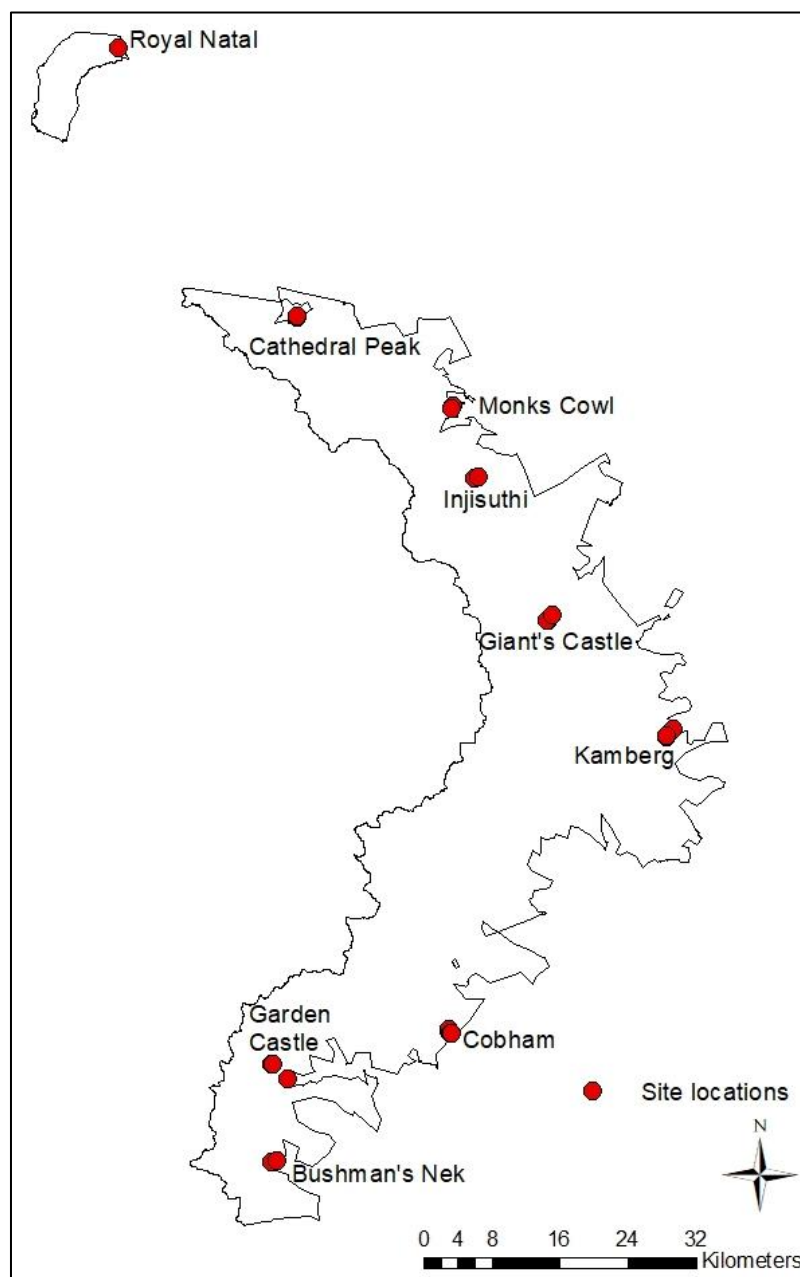
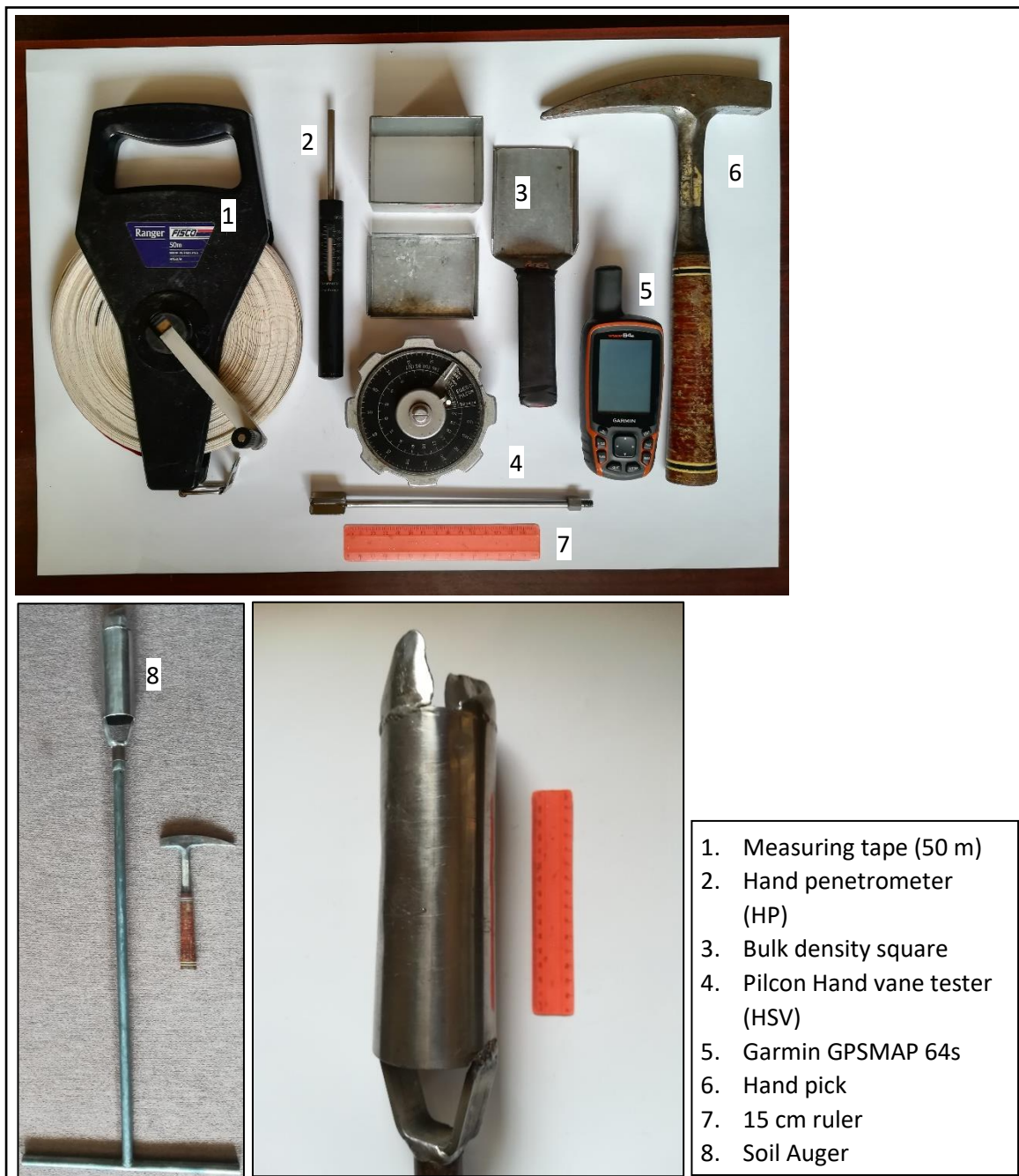


Figure 4.3. Site locations across the UDP.

Site selections were conducted using NBR results with a pixel resolution of 30 m (due to Landsat 5 and 8 having a spatial resolution of 30 m). To increase the chances of placing the sampling quadrat within the correct designed sampling zone selected in ArcMap in the field and to take into account variability in the field, soil sampling was conducted using 20 m x 20 m quadrats. A quadrat method was used, which has been used for vegetation and soil studies in the Drakensberg (Everson and Clarke, 1987; Bijker *et al.* 2001; O'Connor *et al.*, 2004) and deemed suitable for soil sampling in this study. As well as being suitable with the square pixels from the NBR results used for site selection. A total of 17 x 20 m<sup>2</sup> quadrats were conducted across the UDP for soil sampling (Figure 4.5). A measuring tape was used to measure out the quadrats with wooden poles being used to mark the four corners and centre. The date, time, weather, and site description were recorded at each site. The geology, aspect, slope and vegetation category were recorded from data layers in ArcMap. The soil samples and soil measurements were taken as close to the pole markers as possible. A Garmin GPS was used to take the coordinates of each soil sample.

Five soil samples were taken at each quadrat, one in each corner and one in the centre of the quadrat, giving a total of 85 soil samples (Figure 4.5). The method allowed for unbiased sample selection. Soil samples were taken at two depths from the upper 200 mm of soil (Figure 4.6) (Bijker *et al.*, 2001). The literature showed depth to be an important element in soil sampling as multiple studies using more than one sample depth (O'Connor *et al.*, 2004; Manson *et al.*, 2007), with fire impacting the top few centimetres the most (Certini, 2014) and a deeper sample allowing for a comparison. A bulk density square was used to collect four soil samples (140 cm<sup>3</sup>) at each site (the four corner samples) from the upper 50 mm of soil (Figure 4.4; Figure 4.6). The bulk density square was pushed into the ground as far as the ground would allow. If the bulk density square could not be pushed into the ground due to ground hardness or roots, the soil was loosened with a hand pick and the soil dug up and the bulk density square was filled. A soil auger was used to collect one soil sample at each site, the centre sample, from the upper 200 mm of soil (Figure 4.6). The soil auger was twisted into the ground until the soil reached the top of the auger. In very rocky areas where the soil auger could not get into the ground, the soil auger soil sample site was shifted to the nearest point where the soil auger could go into the ground. In this instance, a new GPS point was taken, with the HP and HSV reading being taken at the soil auger site. This resulted in 68 bulk density square soil samples and 17 soil auger soil samples. The samples were stored in labelled sealed bags until laboratory analyses took place in February 2018. Five hand penetrometer (HP) and five hand shear vane (HSV) measurements were taken at each site (at each corner and the centre) using the same soil strength measurements used by Bijker *et al.* (2001) (Figure 4.4; Figure 4.5). The HP was pushed into the ground until the base of the instrument touched the soil surface (Figure 4.6), recording the 'effort' or penetrometer resistance to get the instrument

into the ground in kilopascals (kPa), or soil compressive strength (Bijker *et al.*, 2001). A Pilcon Hand Vane Tester (English Drilling Equipment Co. Ltd.) was used to take the HSV readings which measures the shear strength of cohesive soils (Grabowski, 2014) or simply the force at which the soil fails, measured in kPa. The 19 mm diameter HSV was pushed half way into the ground ( $\pm 12$  cm depth – Figure 4.6) and the vane head was rotated clockwise at a constant rate until the soil gave way (where the arrow stopped moving) (Grabowski, 2014) (Figure 4.4). The soil sampling equipment was cleaned and alcohol swabbed between sites.



1. Measuring tape (50 m)
2. Hand penetrometer (HP)
3. Bulk density square
4. Pilcon Hand vane tester (HSV)
5. Garmin GPSMAP 64s
6. Hand pick
7. 15 cm ruler
8. Soil Auger

Figure 4.4. Fieldwork equipment.

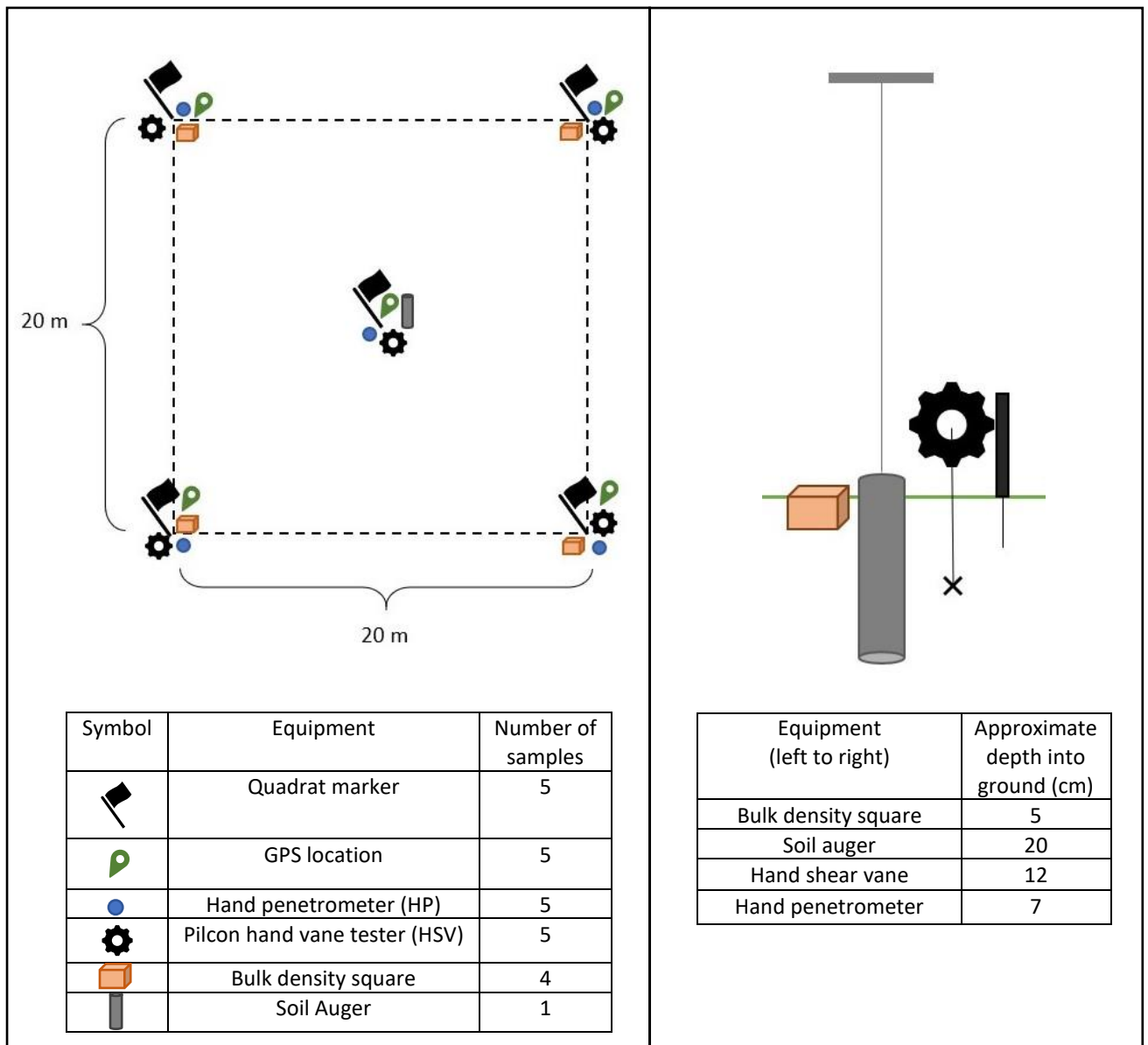


Figure 4.5. Field work quadrat layout.

Figure 4.6. Soil sampling equipment approximate depth into soil.

#### 4.3.2 Limitations of Site Selection

The first limitation with site selection was detection errors from the NBR results which were used to select the high and low fire frequency sites. The NBR did not detect burn scar in clouds or cloud shadow areas in the UDP (Figure 4.7), also noted in the literature as limitations of remote sensing's abilities by Langmann *et al.* (2009) and Goodwin and Collett (2014). The blue polygons (Figure 4.7) are showing clouds in white and shadow from clouds in black (left), with no burn scar being detected (right). From the accuracy assessment of digitising fires versus the NBR results (Figure 5.21), it was found that the NBR was detecting reflective rocks as annual burn scar (Figure 4.8). Possible rock reflections had to be checked when selecting high fire frequency burn sites.

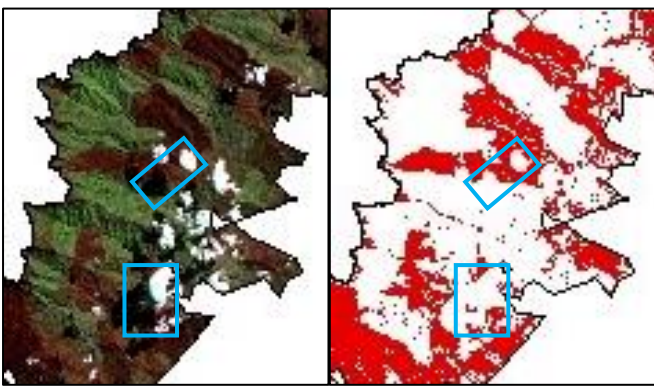


Figure 4.7. NBR detection errors from clouds and cloud shadows from a Landsat 5 image from 2006 in the UDP.

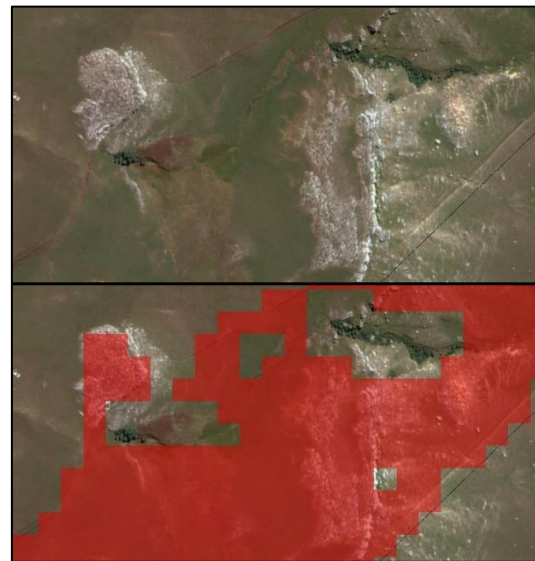


Figure 4.8. NBR detection error with rock reflections being classified as annual burn scar. (Example from Cobham, UDP)

Selecting appropriate and consistent study sites was challenging. From the NBR results, it was noted that the area for selecting high fire frequency sites covered 2.27% of the UDP, while the area for selecting low fire frequency sites covered 6.84% (Figure 5.17; Figure 5.18). This created a challenge for selecting appropriate study sites with limited area available, which was further reduced by taking into account accessibility and environmental factors, leaving only a small percentage of the UDP suitable for soil sampling. Due to the large extent of the UDP and the high variability across the UDP and at site locations, it is not possible to select all sites with the same slope, aspect, geology, and vegetation category, while simultaneously fulfilling the fire frequency requirements.

The importance of ground-truthing was highlighted with field site selection. Site selections in ArcMap can be thorough with checking slope, aspect, geology, accessibility with hiking paths and roads, and using satellite imagery to investigate at the area; however, field variability can still be very high. In the field it was discovered that not all possible sites were accessible, for example, possible Giant's Castle



low fire frequency sites and possible Injisuthi high fire frequency sites were on very steep slopes or cliffs. This could be due to an error with the NBR incorrectly indicating reflective rocks as burn scar (Figure 4.8) or a resolution error as the slope map used for site selection had a 20 m pixel resolution (Figure 4.2). Some sites had to be shifted to avoid things such as hiking paths, and all possible options for low fire frequency sites at Cobham were located on a horse paddock and a new site had to be selected in the field. One of the Cathedral Peak high fire frequency sites had two large trees. This could be an error from the NBR results detecting the trees as annual burning, as large trees would not be present if the area was burnt annually. It is challenging to determine the actual state of the landscape from ArcMap as map data can be deceiving and difficult to interpret. For example, the Injisuthi low fire frequency site was very overgrown and difficult to access, leading to a new site having to be selected in the field. It was not possible to create a 20 x 20 m quadrat due to not being able to walk through the whole site, the closest possible area to what would have been the four corners were used for taking the soil samples. Therefore, even with the advances in remote sensing, ground-truthing remote sensing data is important.

Using a 30 m resolution data leads to pixelation errors, which are most notable on edges such as the boundary of the UDP, as seen in the of slope map in Figure 4.2. Due to the discrepancies caused by the 30 m pixelation of the site selection method used, and site variability in the field. In ArcMap, the exact GPS points from the soil sampling resulted in some of the sampling points falling outside the stated one year (low fire frequency) and 12 year (high fire frequency) burn areas. ArcMap shows some of the one year burn exact point locations to fall within a more fire frequent zone, even though the other four points in the 20 m<sup>2</sup> quadrat fell within the one year burn area. Due to missing years of Landsat imagery, in which the low fire frequency areas could have burned, all low fire frequency sites potentially do not have the exact same number of fires. Therefore, the categories low fire frequency and high fire frequency are used. There is however, a definite difference in number of years burned between the classifications of high and low fire frequency. These point issues could be due to pixelation issues due to the 30 m resolution. Therefore, the year of fire occurrence in the low fire frequency sites (Table 4.6) are the year that showed all 5 points from the 20 m<sup>2</sup> site to have burned. For example, Injisuthi low fire frequency site had to be reselected in the field due to an error (mentioned above). All five points show 2013 to have burned, however, points one, three and five showed burning in 1998 and 2006 as well, making a total of three fires. However this is still a low fire frequency site in comparison to the 12 years of the high fire frequency sites.

Table 4.6. Year of fire occurrence at the low fire frequency sites across the UDP.

Sites	Year of fire occurrence
Bushman's Nek	2005
Garden Castle	2000
Cobham	2013
Kamberg	2016
Giant's Castle	2000
Injisuthi	2013
Monks Cowl	2006
Cathedral Peak	2015
Royal Natal	-

The geology of the sites was determined from a geology layer of South Africa created at 1:250000. Therefore, the accuracy of the geology layer used at a 30 m pixel resolution site level is limited (Figure 4.9).

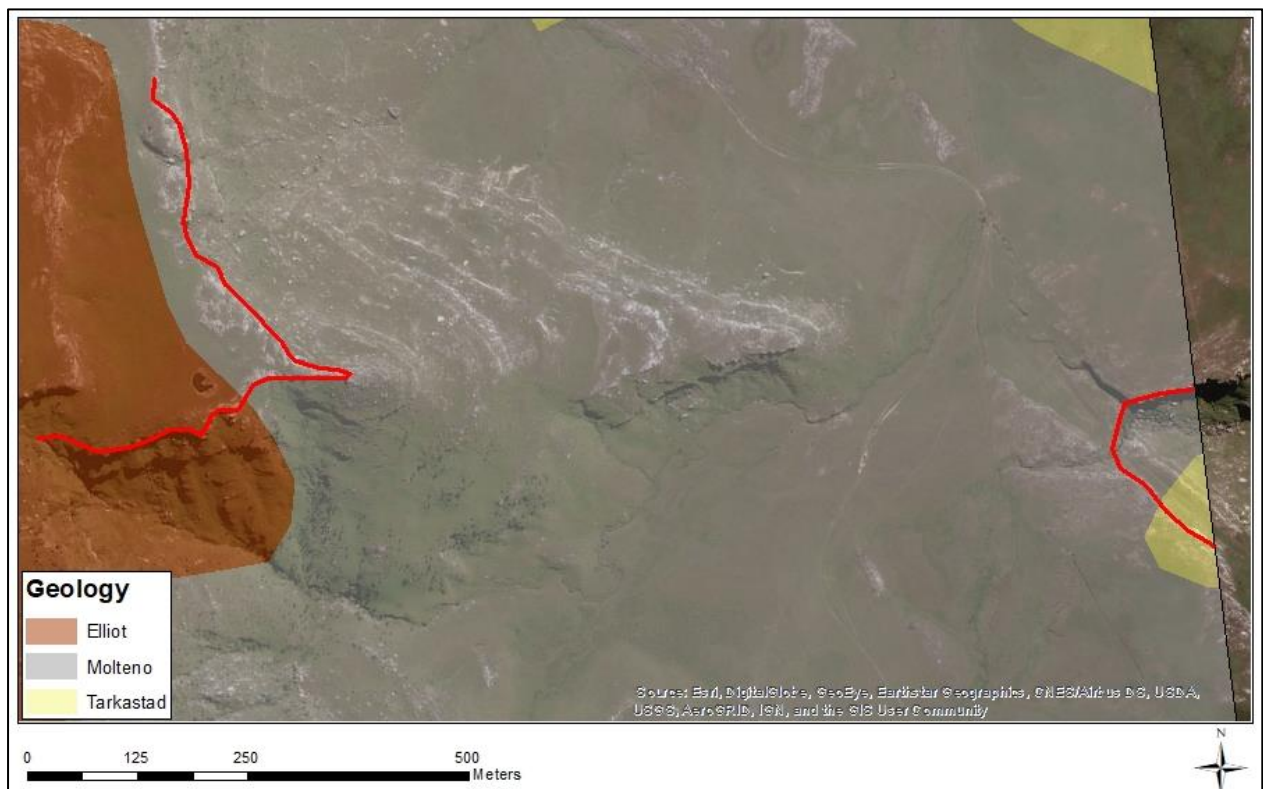


Figure 4.9. Geology map layer (1:250000) overlaid with the World Imagery ArcMap basemap showing potential error at a zoomed-up scale. (Example from Garden Castle, UDP).

### 4.3.3 Soil Laboratory Analysis

The soil laboratory work included investigating the soil physical properties and soil chemical properties. The soil laboratory analyses conducted, according to the methods of Bijker *et al.* (2001), were soil moisture content, soil colour, SOM, soil pH and soil texture (particle size analysis). The 85 soil samples were kept in zip lock bags from collection in the field, until opened for the soil laboratory analyses, to prevent moisture loss. The first soil laboratory analysis conducted was soil moisture content as the soil needed to be weighed when wet from the sealed bags. All the samples were then oven dried at 105°C for 24 hours (Bijker *et al.*, 2001; Pereira *et al.*, 2014). The samples were ground using a pestle and mortar and passed through a 2 mm sieve. For the 68 bulk density square samples, the whole sample was ground and sieved, then divided into three parts for SOM, pH and particle size analysis. For the 17 soil auger samples, the samples were sectioned due to the large size of the samples, and a representative portion of the sample were ground and sieved for use in SOM, pH and particle size analysis. The process of sectioning the samples involved thoroughly mixing each sample, spreading the sample out into a square and dividing the sample into four equal parts (Figure 4.10). Two diagonally opposite parts of the separated sections were used for the soil laboratory analyses. The sectioning process was repeated twice if the soil sample was large. The laboratory sampling methods for soil moisture content, soil colour, SOM and soil pH were taken from 'Techniques for Soil Analysis' from the Department of Geography, Rhodes University (Weaver, 1990).

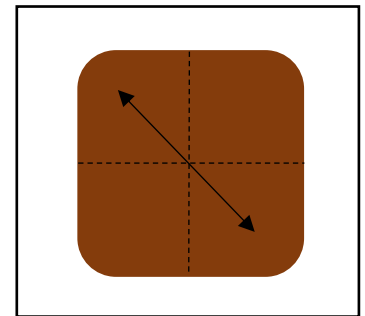


Figure 4.10. Soil sectioning process for large soil samples.

#### Soil Moisture Content

The gravimetric method was used to calculate percentage of soil moisture (Weaver, 1990). Soil moisture content requires a wet sample weight and a dry sample weight (Weaver, 1990). Foil containers were used to place the soil in for oven drying. The foil containers were placed in the oven at 105°C and placed in the desiccator prior to putting the wet sample in to remove moisture. The empty foil container weight was recorded. The soil samples were emptied individually from the sealed bags into the foil containers and were weighed using an electronic balance (two decimal places) to get a wet sample value. As mentioned in the introduction above, the samples were oven dried at 105°C for 24 hours (Bijker *et al.*, 2001; Pereira *et al.*, 2014). The samples were placed in a desiccator to cool before re-weighing the samples to get a dry sample weight. The soil moisture content is in relation to weight loss on drying, meaning the percentage of soil moisture is expressed as the weight of the dry sample (Weaver, 1990). The equation to determine percentage of soil moisture content is:

$$\text{Equation 3: \% Soil Moisture} = \left( \frac{(\text{wet sample weight}) - (\text{dry sample weight})}{(\text{dry sample weight})} \right) \times 100$$

### *Soil Colour*

Soil colour was determined using the Munsell colour chart (Munsell Colour, 2010). Samples were described based on the hue, value and chroma of the soil (Munsell Colour, 2010). Soil colour was determined after the samples had been oven dried and before the samples were ground and sieved.

### *Soil Organic Matter*

To determine the SOM content of the soil, a weight loss on ignition (LOI) test was conducted. LOI is a widely used method for quantifying SOM, which uses heat to remove SOM (Pereira *et al.*, 2014; Hoogsteen *et al.*, 2015). To calculate LOI, a before ignition weight and after ignition weight were recorded (Weaver, 1990). The silica crucibles used for LOI were pre-ignited in the Muffle Furnace at 450°C and weighed. A portion (filled up the crucible to the maximum) of the oven dried, grinded and sieved sample was weighed using a Mettler AJ 100 Analytical Balance (four decimal places). The samples were placed in a Muffle Furnace at 450°C for 24 hours (Weaver, 1990). The limitation of this method in determining SOM content is the possibility of a loss of carbon dioxide and water during the ignition process contributing to the weight LOI value (Weaver, 1990). The samples were cooled in a desiccator and re-weighed. The equation to determine weight LOI is:

$$\text{Equation 4: Loss on ignition: } \left( \frac{W_2 - W_3}{W_2 - W_1} \right) \times 100$$

Where:

$W_1$  = Mass of crucible,

$W_2$  = Mass of crucible and sample (before ignition),

$W_3$  = Mass of crucible and sample (after ignition)

### *Soil pH*

The pH of soil indicates the degree of soil acidity or alkalinity, measured on a logarithmic scale (Weil and Brady, 2017). The pH of soil is seen as a significant measure of soil properties due to pH notably influencing chemical processes (Weil and Brady, 2017). Soil pH was measured using a Eutech pH 700 which involves placing a pH electrode into a soil water suspension (Weil and Brady, 2017). The Eutech pH 700 was calibrated using buffer solutions. Soil pH was determined using 20 g of the ground and sieved sample (Weaver, 1990). The sample was placed into a 100 ml beaker and 50 ml of distilled water was added before it was stirred well (Weaver, 1990). After 50 mins, the sample was stirred again, and after another 10 mins, the sample was stirred vigorously (Weaver, 1990). While swirling the sample, the pH rod and thermometer from the Eutech pH 700 were placed into the sample and when the Eutech pH 700 read 'Ready', the pH and temperature reading was recorded.

### Soil Texture

Soil texture refers to the proportion of soil particles (Weil and Brady, 2017). Soil texture plays a role in suitability of soil for different uses and soil behaviour (Weil and Brady, 2017). As well as particle size analysis giving insight into the transport and deposition of sediments (Briggs, 1977). Before particle size analysis could be determined, the organic matter from the soil samples had to be removed (Harada and Inoko, 1977). This process involved digesting the soil samples in hydrogen peroxide ( $H_2O_2$ ) (Harada and Inoko, 1977; Gray *et al.*, 2010). To do this, one third of a tablespoon of the sieved sample was placed in a 400 ml beaker and approximately 120 ml of hydrogen peroxide ( $H_2O_2$ ) was added to each beaker. The beakers were placed on a hot plate and the samples were left to digest. Depending on the amount of organic matter in the different samples (shown by bubbling), more  $H_2O_2$  was added if necessary, until there was no reaction was occurring (Harada and Inoko, 1977). Once the  $H_2O_2$  had evaporated, a dispersant solution was added to each beaker. Particle size analysis was determined using a laser diffraction method (Blott and Pye, 2006). A Malvern Mastersizer 3000 laser diffraction size analyser and Hydro EV was used (Figure 4.11).

Standard methods were used for the Malvern Mastersizer 3000. The Malvern Mastersizer 3000 produces analysis documents for each soil sample, with information about the particle size classes ( $\mu m$ ) and the volume density (%) of each particle, such as the frequency diagrams shown in Blott and Pye (2006).



Figure 4.11. Malvern Mastersizer 3000 particle size analysis.

#### 4.3.4 Statistical Analysis

The soil sample data were recorded, and calculations for soil moisture and SOM were conducted using Microsoft Excel. Particle size analysis was conducted using Gradistat Version 8.0 Grain Size Analysis Program (Blott, 2010) which is based on Microsoft Excel. The results output from the Mastersizer 3000, including the particle size classes ( $\mu m$ ) and volume density (%), were input into the Gradistat programme in Excel for all 85 samples. The results show the percentage of sand, silt and clay per sample, and use the Folk and Ward (1957) methods showing the mean, mode, sorting and skewness values (Blott and Pye, 2001).

The soil statistical tests were run in RStudio (RStudio Team, 2015) by statistician Hans-Peter Bakker. The soil statistical analyses were used to investigate the objective of evaluating the effects of fire frequency on soil properties. Therefore, the effects that high and low fire frequency have on the measured soil values were investigated, while controlling for the possible influencing variables or environmental factors. The five measured numeric soil variables were: hand penetrometer (HP) (kPa),

hand shear vane (HSV) (kPa), soil organic matter (SOM) (%), pH, and soil moisture (%). The factors that were controlled for were: area, aspect, elevation (m.a.s.l), geology, particle size analysis (% sand, silt and clay), slope (°), vegetation, and method of soil collection (referred to as 'type' in the raw statistical data and referred to as 'depth' below).

The controlled factors outcomes were: The nine areas were simplified to 'southern Drakensberg', 'central Drakensberg' and 'northern Drakensberg'; sites were numbered 1 - 17; samples were numbered 1 – 85; simplified aspect (north, south, east); geology (Tarkastad, Molteno, Karoo Dolerite, Elliot, Clarens); vegetation (Drakensberg Foothill Moist Grassland, Northern Drakensberg Highland Grassland and Northern KwaZulu-Natal Moist Grassland, Southern Drakensberg Highland Grasslands); and sample collection method referring to sampling depths (bulk density square or soil auger).

The geology and vegetation values were determined from GIS layers in ArcMap (see data disclaimer). Slope, aspect and elevation values were determined in ArcMap. A Digital Elevation Model (DEM) was created using the 20 m contour lines for the UDP. From the DEM, 20 m slope and aspect maps were created. In ArcMap, the 'extract values to points' tool was used to determine the slope, aspect and elevation values of each GPS point from the soil sampling. No interpolation was used, the point value was given the pixel value. There were obvious issues with this method, as seen with some of the slope values. Therefore, six slope values were edited by removing the slope value and replacing the slope value with the average of the other slope values for that site. The edited slope values were: two values (points 42, 44) from Giant's Castle high fire frequency, two values (points 57,58) from Injisuthi low fire frequency, and two values (points 62, 64) from Monks Cowl high fire frequency sites. For example, Monks Cowl high fire frequency sites slope readings ranged from 3.97° to 26.08° over a 20 m quadrat, which is assumed due to errors with using pixels, and were therefore edited.

Due to two errors with the HSV values (error with data recording), points 64 and 79 data entries were excluded. Point 35 was excluded due to the soil auger site having to be shifted due to the presence of rocks, resulting in a different location for soil sample collection and soil readings (HSV, HP). Only complete data entries were used in the statistical analyses. During the statistical analyses, it was found that point 58 had significant influence or was causing undue influence on the model (Bakker, 2018, *pers. comm.*). The difference between point 58 and the other points from the sites was the aspect value, with point 58 being categorised with an east aspect with the other points being categorised with a south aspect. This is assumed to be due to the method of assigning aspect values due to pixelation errors. Therefore point 58 was excluded. Resulting in a total of 81 data points being used in the statistical analyses.

The data was cleaned and the minimum, maximum, medium, mean, and the first and third quartiles were calculated for all numeric values, and the categorical values were counted (Bakker, 2018, *pers. comm.*). As the particle size analysis results for percentage sand, silt and clay add up to 100%, the percentages are dependent on each other, and therefore silt was not included in the analyses (Bakker, 2018, *pers. comm.*).

#### *Statistical Tests*

A multivariate analysis approach was used as there are multiple variables that are obtained for each selected soil property outcome (Afif *et al.*, 2012). The statistical tests applied included a correlation matrix, and regression analyses including simple linear regressions and multiple regressions (Bakker, 2018, *pers. comm.*). The correlation matrix was used to look at the spread of the data and the relationships between variables. The linear regressions were used to interpret the extent to which burning was a factor in the selected soil properties. The challenge in interpreting the soil results was the many factors influencing soil properties, such as geology and slope etc.

A correlation matrix indicates the correlation coefficients, which are a measure of the linear relationship of the variables (Everitt and Dunn, 2001). From the outcome of the correlation matrix, there is a strong positive correlation between SOM and soil moisture, making it unnecessary to include both soil properties in the regression analyses, and soil moisture was excluded from further analyses (Afifi *et al.*, 2012; Bakker, 2018, *pers. comm.*).

The regression analyses involved running two separate regression models for each of the selected soil property outcome variables. The selected outcome variables were: HP, HSV, pH and SOM. The models run for each outcome variable included (Bakker, 2018, *pers. comm.*):

1. A multiple linear regression to determine the relationship of each outcome variable and all the predictor variables, with relative importance plots.
2. A multiple linear regression using a model with the five “best” subsets of the predictor variables, determined using a Bayesian information criterion (BIC) as a criterion including relative importance plots and diagnostic plots.

Due to soil variability and inter-site variability being high across the UDP, two models were run. This acknowledges the possibility that each predictor variable will have a different influence on the outcome variable, with some factors being significant and others being non-significant. Simple and multiple regression models have been shown to be suitable in analysing soil data for a long time (Indorante *et al.*, 1989; Dahal and Routray, 2011).

The BIC is a widely used tool for statistical model selection, based on the empirical log-likelihood (Neath and Cavanaugh, 2012). Simply, the BIC is able to facilitate the selection of a suitable model by, from a large dataset, favouring a model that seems the most plausible from the given dataset (Neath and Cavanaugh, 2012) after comparing all possible alternatives (Bakker, 2018, *pers. comm.*). The models selected by the BIC criterion can have a varying number of variables selected in the “best” model for different outcome variables. The “best” model is identified from the BIC criterion with the lowest value (Neath and Cavanaugh, 2012). The advantages of using the BIC for model selection was consistency, computational ease, and that it is seen as an effective scientific measure for model selection (Neath and Cavanaugh, 2012). Where a BIC criterion did not select ‘burn’ as a variable, an Akaike Information Criterion (AIC) criterion was run to test if ‘burn’ was selected as a variable using a different criterion (Bakker, 2018, *pers. comm.*). Both BIC and AIC are common penalised model selection criteria, with the same aim of selecting the “best” model (Kuha, 2004). The information criteria are similar but have different assumptions (Kuha, 2004).

Relative importance graphs were produced for both the multiple regression including all predictor variables and the multiple regression using the predictor variables selected from the BIC models, for each outcome variable (Bakker, 2018, *pers. comm.*). The relative importance relates to the amount of variation each variable contributes to the total variation ( $R^2$ ) in each multiple regression model (Grömping, 2006). The relative importance graphs help to investigate which predictor variables are having the greatest influence on predicting the outcome variable in the regression models. One of the six methods Grömping (2006) looks at for assessing relative importance includes the Lindeman, Merenda and Gold (LMG) method (Lindeman *et al.*, 1980 cited in Grömping, 2006), which is one of the recommended methods by Grömping (2006). The LMG variables sum to the total of  $R^2$  (Grömping, 2006). Grömping (2006) highlighted a negative factor with relative importance being the influence that the order of the predictor variables has on the relative importance results. According to Grömping (2006), the LMG method uses simple unweighted averages, along with its sequential sums of squares, to avoid this ordering influence.

Diagnostic plots were run for the “best” models used in the second regression models (Bakker, 2018, *pers. comm.*). Diagnostic plots were used to interpret if the model used worked well for the data (Kim, 2015). The diagnostic plots looked at included: residuals versus fitted, normal Q-Q, scale-location, and residuals versus leverage. The diagnostic plots show if residuals have non-linear patterns, are normally distributed, have uniform variance or are equally spread across the range of predictor variables, and identifies outliers that are influential (Kim, 2015).



## CHAPTER 5: RESULTS

---

The results section is divided into two parts: remote sensing and soils. The remote sensing section includes: fire frequency results using MODIS active fire data from 2003 to 2017, and VIIRS active fire data from 2012 to 2017, a comparison between the MODIS and VIIRS results, and the spatial extent of burn scar results using NBRs from Landsat 5 and Landsat 8 covering 12 years of available imagery from 1998 to 2017. The remote sensing accuracy assessment includes a comparison between digitised burn scar and the Landsat NBR results for 2017, a one day comparison between MODIS and VIIRS active fire data and a Landsat image, and a comparison between the MODIS and VIIRS active fire data and the corresponding Landsat image and NBR results. The soil section includes: an overview of the soil field work and soil laboratory results, including soil moisture content, soil colour, soil organic matter content, soil texture (particle size analysis), and the statistical analyses of the effect of fire frequency on soil properties.

### 5.1 REMOTE SENSING

The MODIS and VIIRS active fire points refers to the number of pixels containing fires, not the actual number of fires. Therefore, a fire point corresponds to at least one active fire detected within that pixel, 1 km<sup>2</sup> for MODIS and 375 m<sup>2</sup> for VIIRS (see Figure 2.2). Multiple fire points next to each other could relate to the same fire. MODIS active fire data, hereafter referred to as MODIS data. VIIRS active fire data, hereafter referred to a VIIRS data.

### 5.1.1 Fire Frequency

#### *MODIS Active Fire Data*

The total number of MODIS data (1 km<sup>2</sup> pixel resolution) recorded in the UDP from 2003 to 2017 was 8056, with an annual average of 537.07 and standard deviation of 105.83 (Figure 5.1; Figure 5.2). Frequencies ranged from the highest annual MODIS data of 877 fire points in 2007, which was significantly higher than the other years, to the lowest annual of 417 fire points in 2015 (Figure 5.1). MODIS data showed that fires occur across the whole UDP every year, including the southern, central and northern UDP (Figure 5.2). Annual fires follow an 'up and down' pattern or increase and decrease pattern in consecutive years (Figure 5.1)

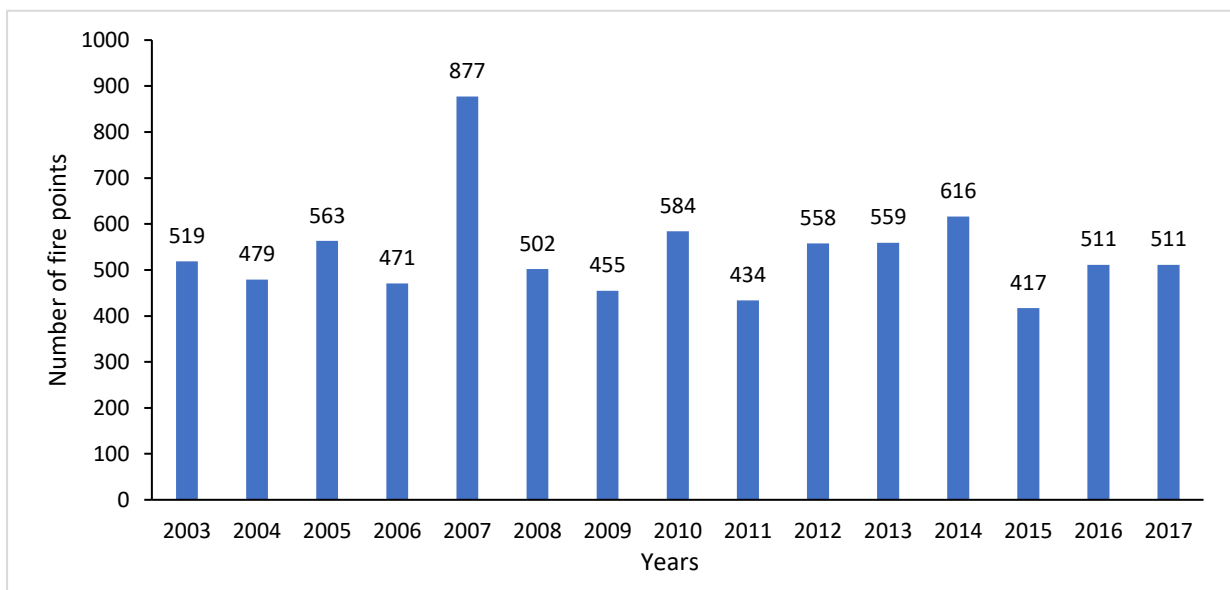


Figure 5.1. Total annual MODIS active fire data recorded from 2003 to 2017 in the UDP.

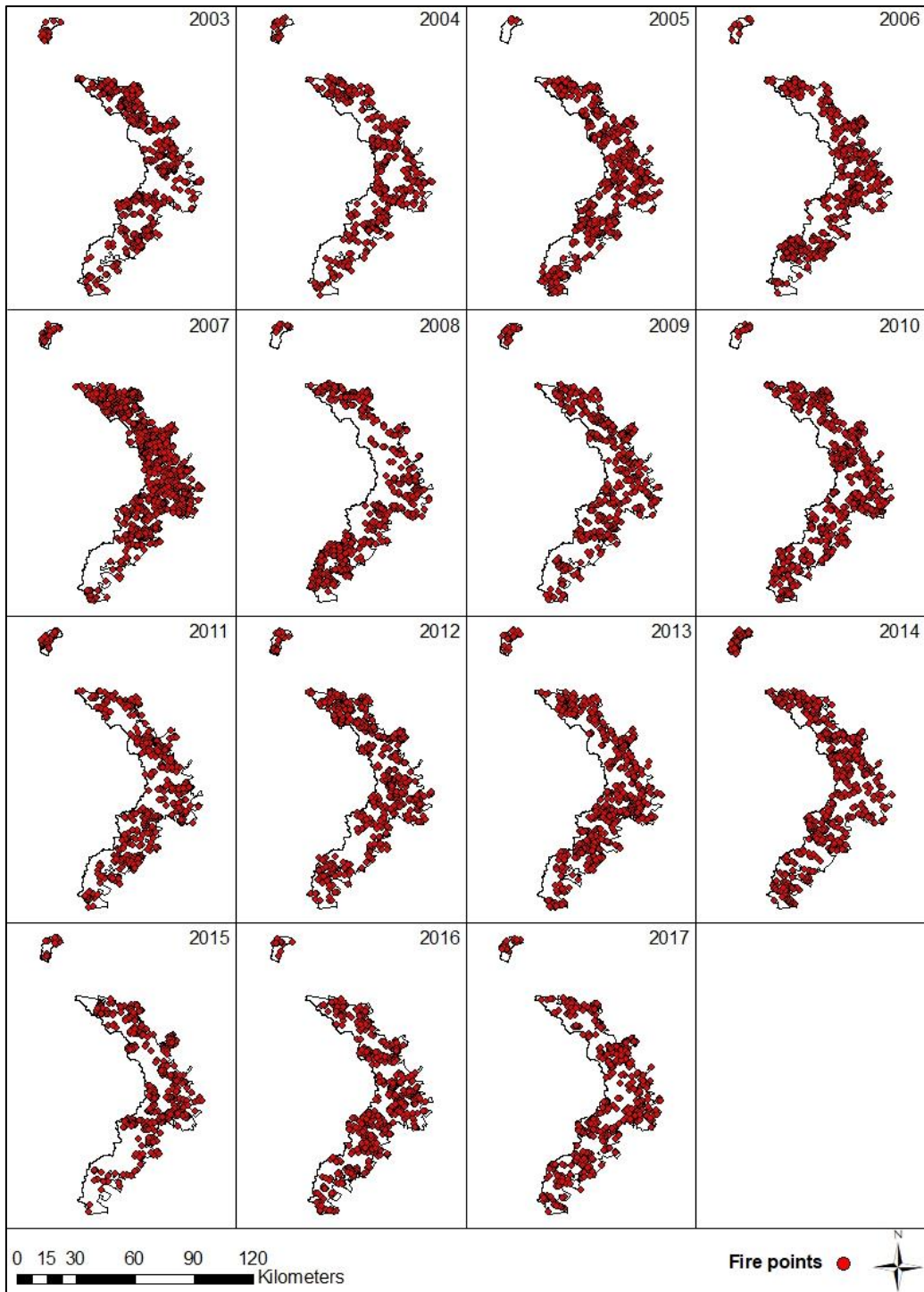


Figure 5.2. Fire point data showing the annual MODIS active fire data from 2003 to 2017 in the UDP.

The kernel density analysis using the MODIS data showed the areas of high concentrations of active fire points in red and the lowest concentrations of active fire points in green across the UDP (Figure 5.3; Figure 5.4). The overall kernel density map for MODIS data from 2003 to 2017 shows the southern UDP to have the lowest fire frequency (green), the central UDP to have a moderate fire frequency (yellow and orange), and the northern central and more northern areas of the UDP to have the highest fire frequency (red) (Figure 5.3). The annual kernel densities show the majority of the lowest fire frequency areas (green) are located in the very northern area of the UDP (Royal Natal) and the very southern area of the UDP, with only 2005 and 2008 showing high fire concentrations (red areas) in the southern UDP (Figure 5.4).

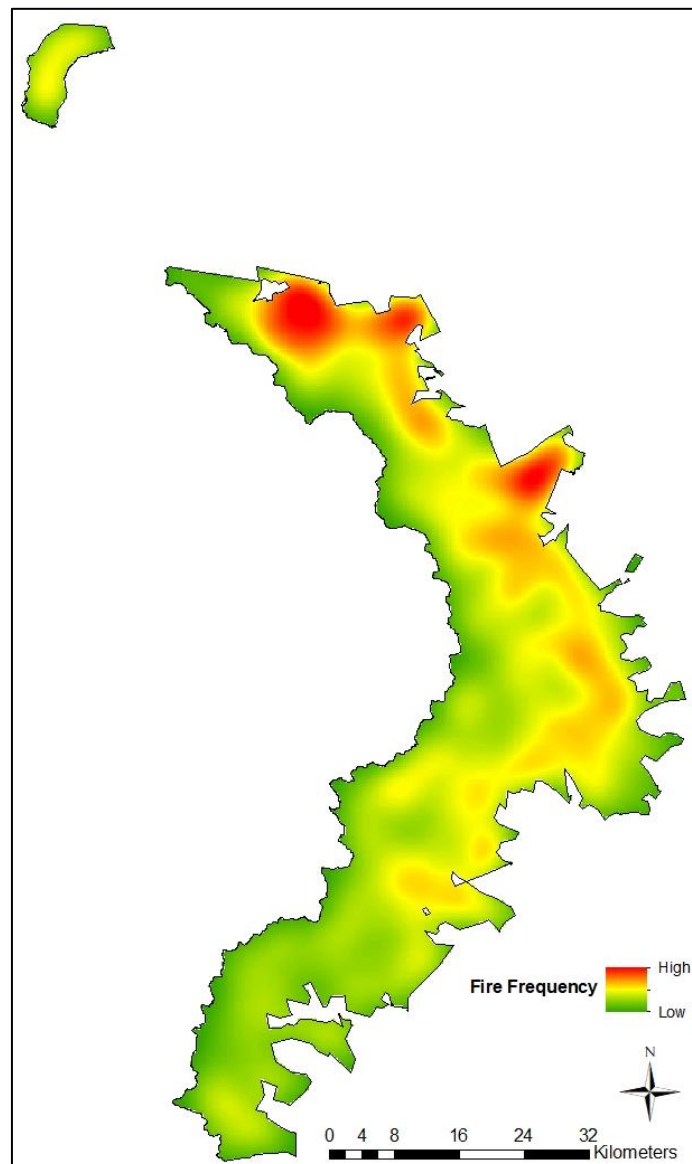


Figure 5.3. Overall kernel density showing areas of high and low fire frequency recorded by MODIS active fire data from 2003 to 2017 in the UDP.

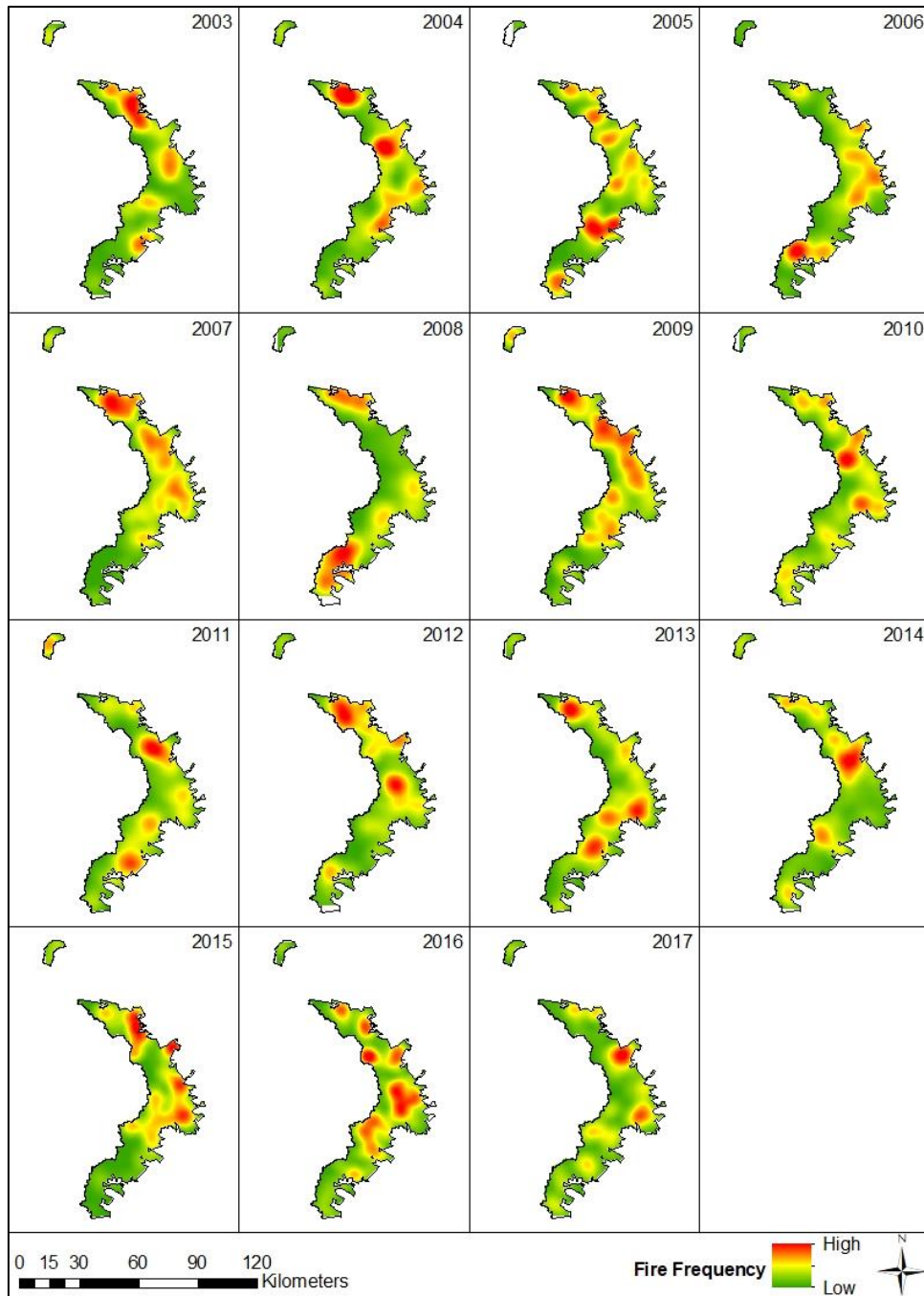


Figure 5.4. Annual kernel densities showing the areas of high and low fire frequency recorded by MODIS active fire data from 2003 to 2017 in the UDP.

The monthly MODIS data show the main fire season is from May to October, falling over the dry winter season, with very few fires being recorded from November to April, during the high rainfall season (Figure 5.5). The highest monthly total was recorded in June with 2662 fire points, representing 33.04% of the total fire points from 2003 to 2017. Neither January nor March had any fires recorded, with December and February recording two and three fires respectively from 2003 to 2017.

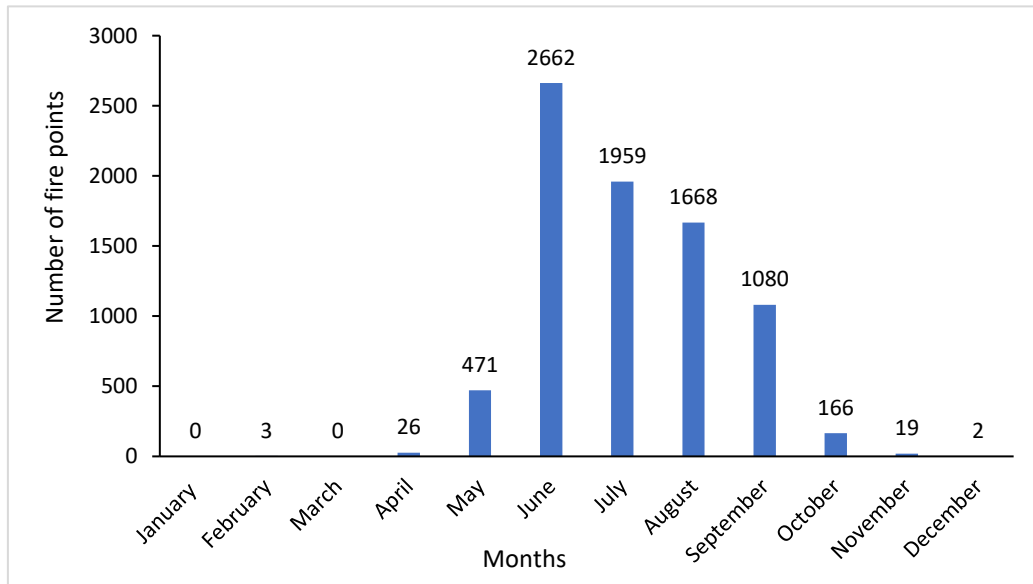


Figure 5.5. Total monthly MODIS active fire data recorded from 2003 to 2017 in the UDP.

#### VIIRS Active Fire Data

The total number of VIIRS data (375 m<sup>2</sup> pixel resolution) recorded in the UDP from 2012 to 2017 was 10479, with an annual average of 1746.5 and a standard deviation of 326.76 (Figure 5.6). Frequencies ranged from the highest annual VIIRS data from 2012 to 2017 of 2196 fire points in 2014, to the annual lowest of 1137 fire points in 2015 (Figure 5.6). From 2012 to 2014, there was an increase in recorded VIIRS data, with a significant lower number of fire points for 2015 (Figure 5.6), corresponding to the MODIS data (Figure 5.1). Looking at the VIIRS data, fires occur across the whole UDP every year from 2012 to 2017, including the southern, central and northern UDP (Figure 5.7), corresponding to the MODIS data (Figure 5.2).

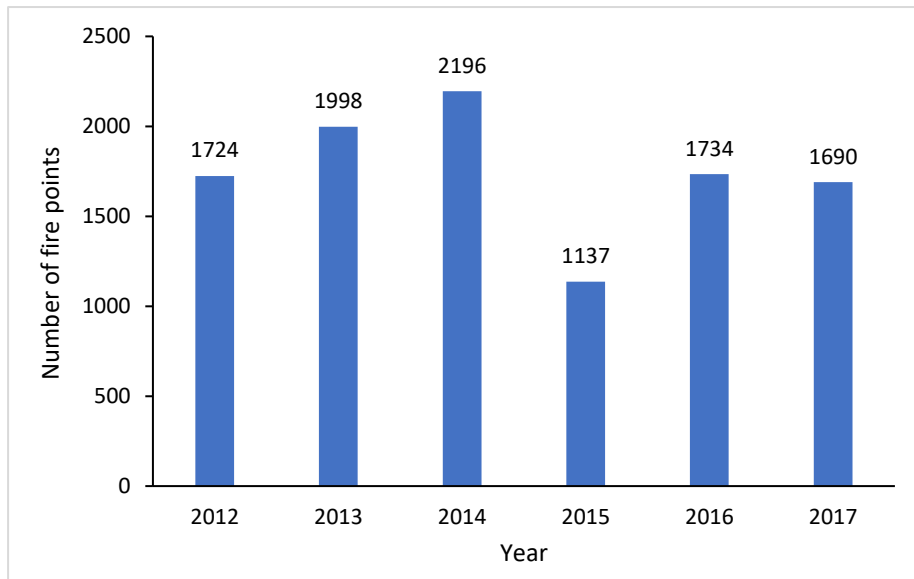


Figure 5.6. Total annual VIIRS active fire data recorded from 2012 to 2017 in the UDP.

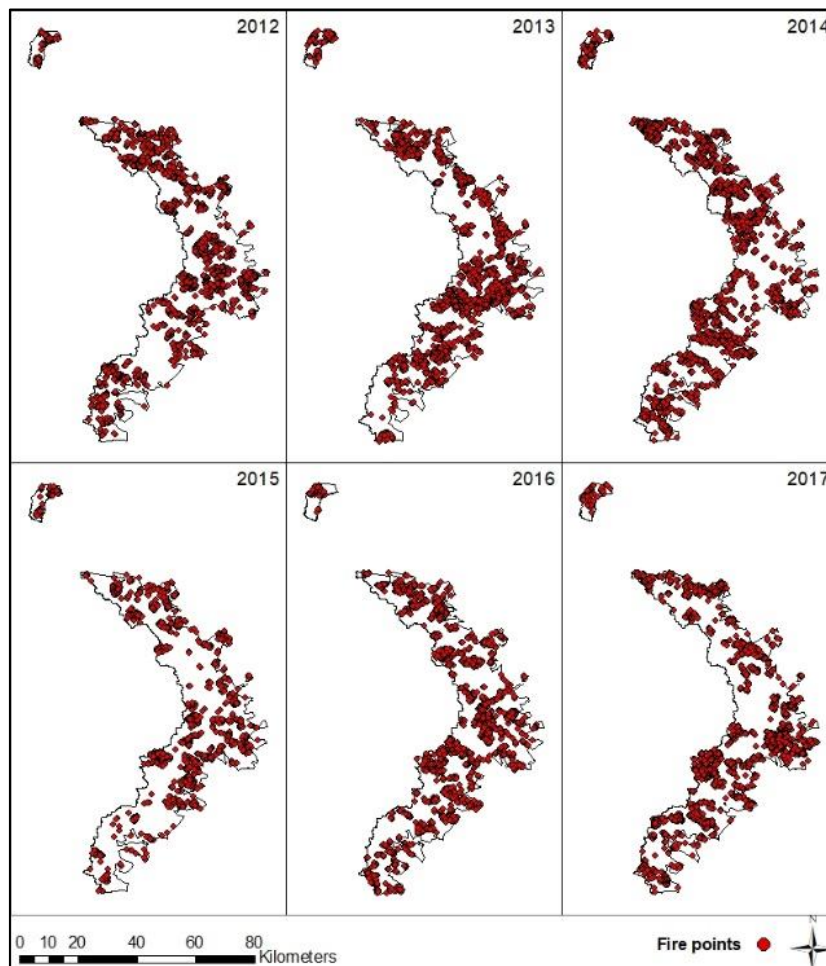
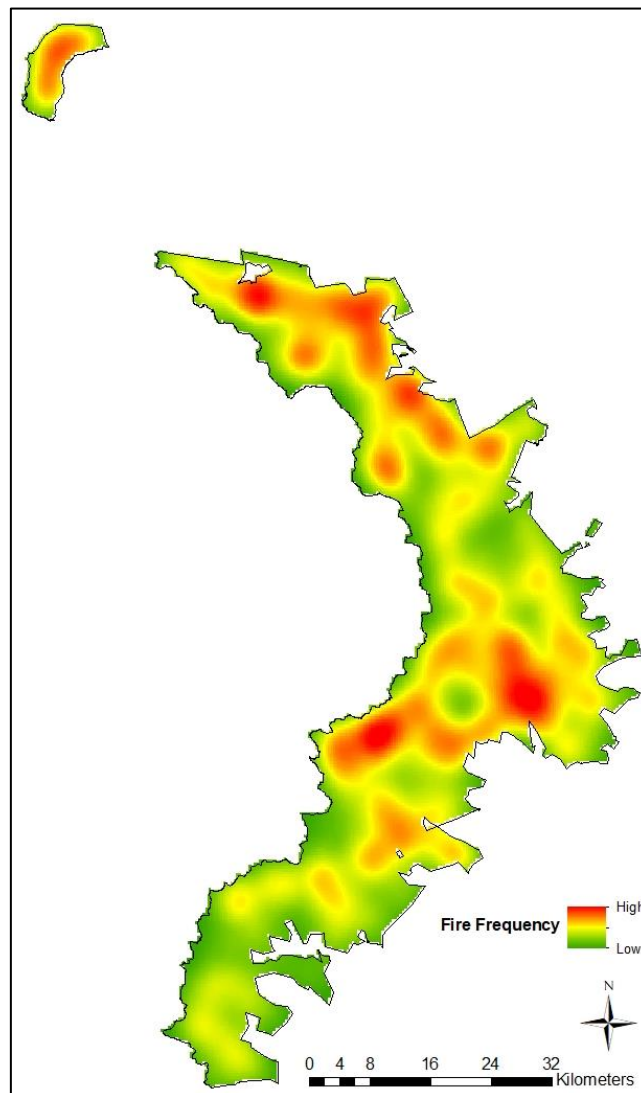


Figure 5.7. Fire point data showing the annual VIIRS active fire data from 2012 to 2017 in the UDP.

The overall kernel density map for the VIIRS data from 2012 to 2017 (Figure 5.8) showed the southern UDP to have the lowest fire frequency (green) with the highest fire frequencies being found in the central and northern areas of the UDP, and Royal Natal showed a moderate fire frequency (orange).



*Figure 5.8. Overall kernel density showing areas of high and low fire frequency recorded by VIIRS active fire data from 2012 to 2017 in the UDP.*

The results of the monthly VIIRS data show that the main fire season is from May to October, falling over the dry winter season, with very few fires being recorded from November to April, the high rainfall season (Figure 5.9). The highest monthly total was recorded in July with 3338 fire points, representing a total of 31.85% of the total fire points from 2012 to 2017 (Figure 5.9). There were no fire points recorded in January, February or March, while December recorded eight fire points from 2012 to 2017 (Figure 5.9).



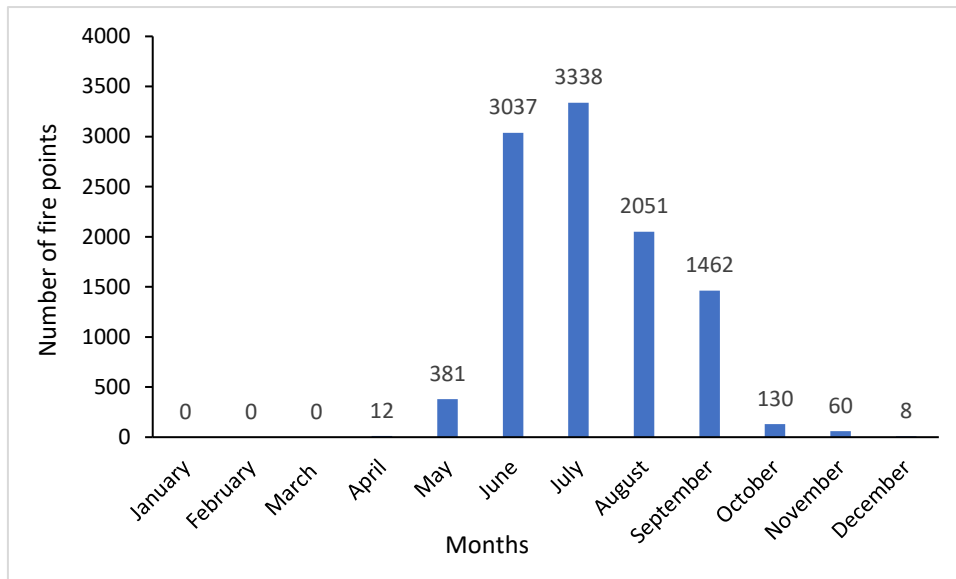


Figure 5.9. Total monthly VIIRS active fire data recorded from 2012 to 2017 in the UDP.

#### Comparison between MODIS and VIIRS Active Fire Data

MODIS and VIIRS data were compared from 2012 to 2017, as these are the years that VIIRS active fire detection data was available. The difference between MODIS and VIIRS data is the pixel resolution at which the data is recorded, with MODIS was recorded at 1 km<sup>2</sup> and VIIRS was recorded at 375 m<sup>2</sup>. Therefore, the data is not directly relatable, and comparisons looked at patterns and ratios, as stated in the Methodology section above.

Comparing annual MODIS and VIIRS data from 2012 to 2017 indicates the data to follow similar trends as shown graphically on a line graph, with VIIRS data for 2012 and 2015 showing a lower record of fire points in comparison to the pattern of fire points by MODIS data (Figure 5.10). The difference in pixel resolution between MODIS and VIIRS relates to a MODIS fire pixel being 2.67 times the size of VIIRS fire pixel. The ratio of annual MODIS data to VIIRS data, averages showed a 1:3.30 ratio, with VIIRS recording approximately just over three times the amount of fire points than MODIS (Table 5.1).

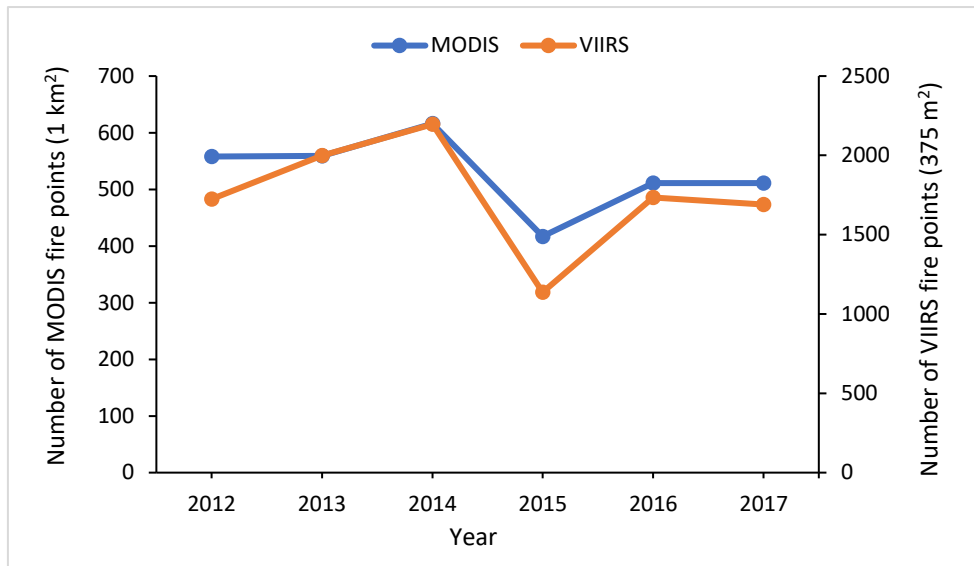


Figure 5.10. Comparison between the annual MODIS and VIIRS active fire data recorded from 2012 to 2017 in the UDP.

Table 5.1. Ratio comparisons between annual number of MODIS and VIIRS active fire data from 2012 to 2017 in the UDP.

Year	MODIS - Number of fire points	VIIRS - Number of fire points	Ratio MODIS:VIIRS
2012	558	1724	1: 3.09
2013	559	1998	1: 3.57
2014	616	2196	1: 3.56
2015	417	1137	1: 2.73
2016	511	1734	1: 3.39
2017	511	1690	1: 3.31
Total	3172	10479	1: 3.30

Monthly comparisons between MODIS and VIIRS data for 2012 to 2017 showed MODIS data recorded June to have the highest number of fire points, while VIIRS recorded July as the highest (Figure 5.11). A similar pattern is shown between the monthly MODIS and VIIRS data, which is expected as the fire detections are occurring across the same area (UDP) (Figure 5.11).

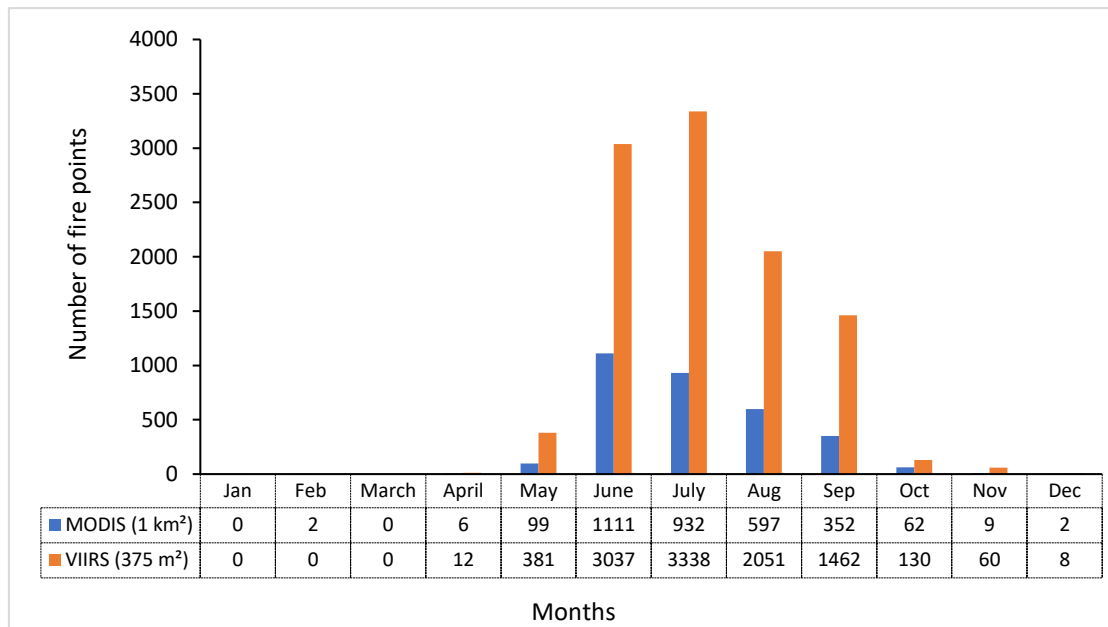


Figure 5.11. Comparison between the total monthly MODIS and VIIRS active fire data recorded from 2012 to 2017 in the UDP.

The comparison between the kernel density maps for MODIS and VIIRS data are similar but display different and additional areas for the fire ‘hotspots’, or areas of high fire point concentrations (red areas) (Figure 5.12). Considering that both satellites are capturing data of the same fires in the same areas, although the kernel densities show differing results, VIIRS would be considered more accurate due to the higher spatial resolution. For example, in 2015 VIIRS shows the high concentrations (red areas) to be located more central UDP than MODIS. In 2014, VIIRS shows multiple areas of high concentrations (red area), while MODIS only shows one distinct red area. In 2016, MODIS shows multiple areas of high concentrations (red areas), while VIIRS shows a much smaller area of red areas (Figure 5.12).

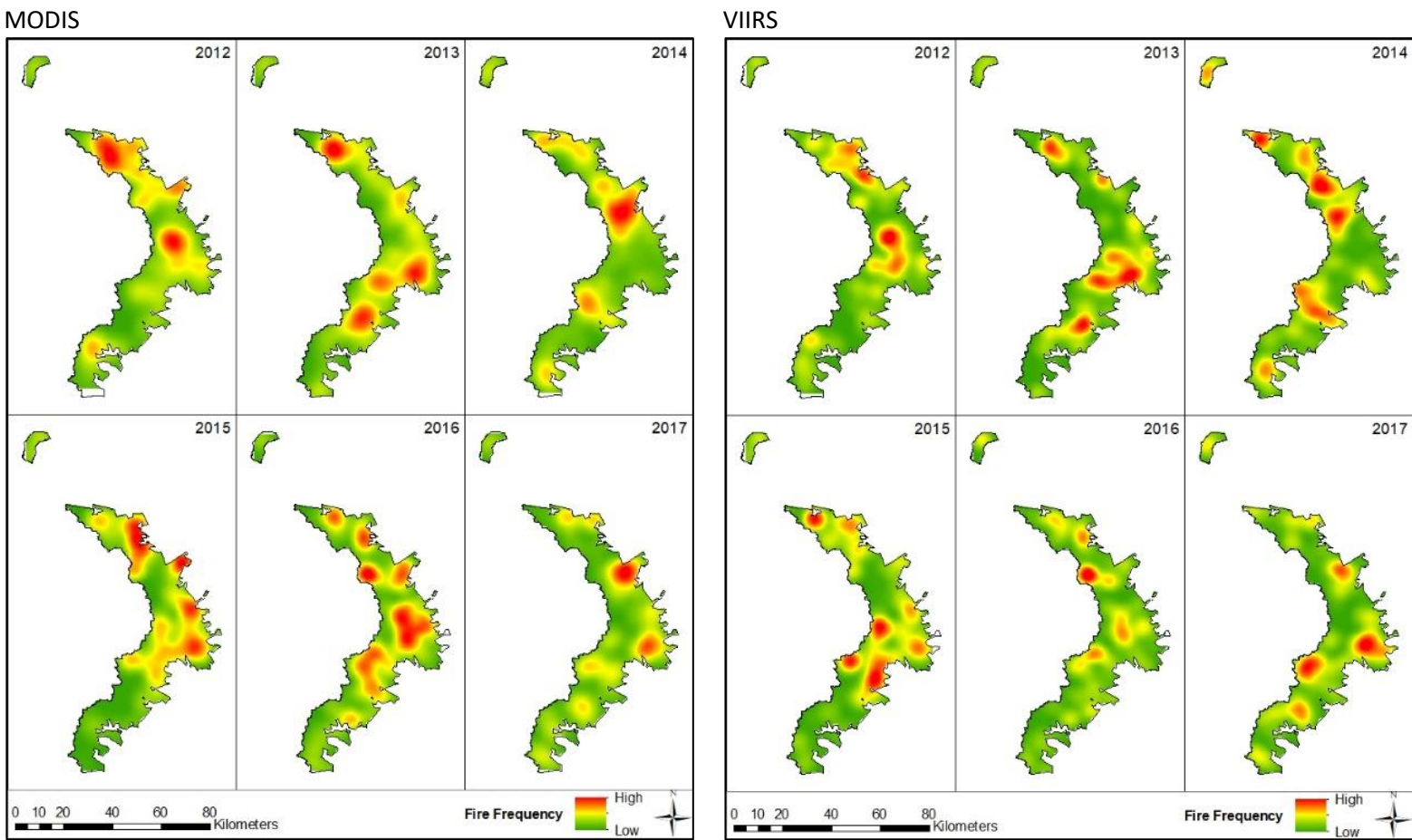


Figure 5.12. Comparison between kernel density maps for MODIS and VIIRS active fire data recorded from 2012 to 2017 in the UDP.

## 5.1.2 Spatial Extent

### *Burn Scar Band Combinations*

Using a Landsat 8 image, the standard colour composite of band combinations red (0.630 – 0.680  $\mu\text{m}$ ), green (0.525 – 0.600  $\mu\text{m}$ ) and blue (0.450 – 0.515  $\mu\text{m}$ ), a ‘normal’ visible spectrum (Figure 5.13) shows: burn scar in black with faint visible fire breaks (bottom left), smoke from the two fires in white (bottom of image), farm land in shades of green, and the grasslands as brownish due to the image being taken during the dry winter time (Figure 5.13). The band combinations of SWIR 2 (2.100 – 2.300  $\mu\text{m}$ ), NIR (0.845 – 0.885  $\mu\text{m}$ ) and red (0.630 – 0.680  $\mu\text{m}$ ), deemed the most suitable band combinations for highlighting burn scar (Figure 5.14) shows burn scar in bright red, with the long linear fire breaks standing out in red, smoke from the two fires shown in blue, active fires shown in orange, farm land in bright shades of green, and the grasslands as faint green and pinkish (Figure 5.14). Both images showed rock faces and shadows in black and were not detected as burn scar (Figure 5.13; Figure 5.14). However, as noted during the site selection from NBR, in some cases, rock reflections were detected as burn scar (Figure 4.4).

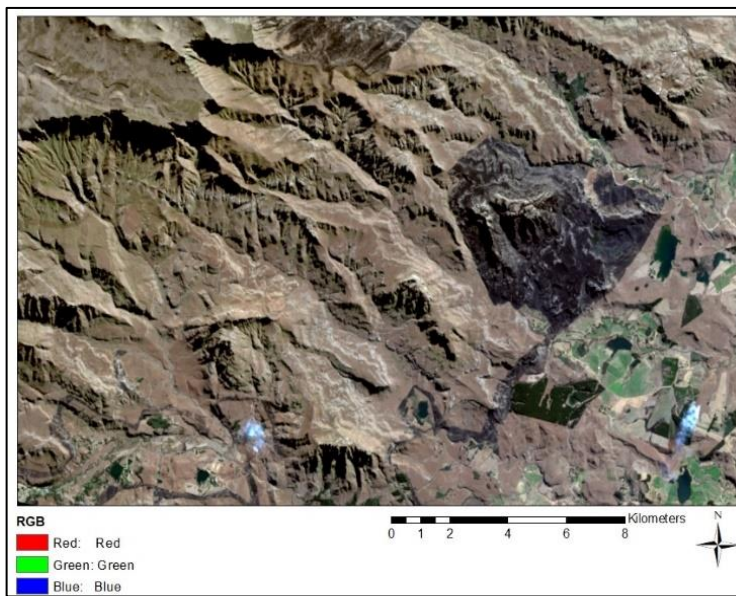


Figure 5.13. Landsat 8 image (7<sup>th</sup> June 2016) showing band combinations red (0.630 – 0.680  $\mu\text{m}$ ), green (0.525 – 0.600  $\mu\text{m}$ ), blue (0.450 – 0.515  $\mu\text{m}$ ) for the southern UDP

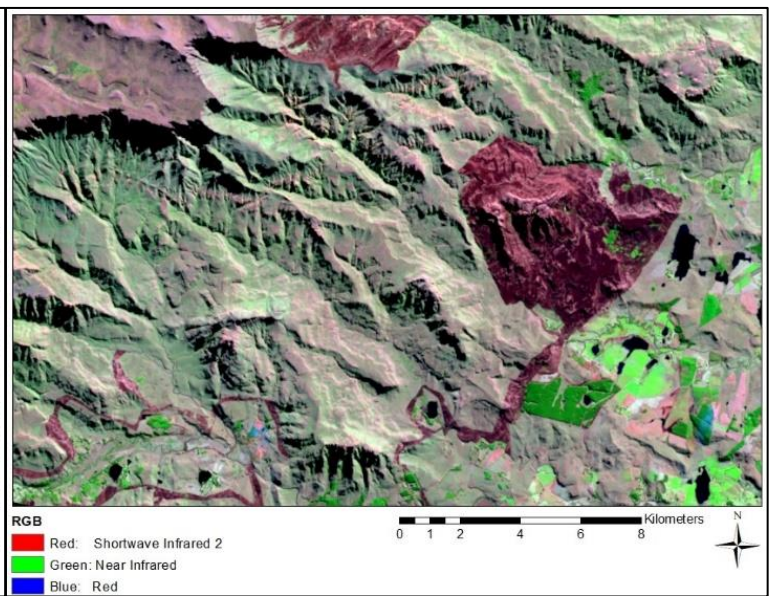


Figure 5.14. Landsat 8 image (7<sup>th</sup> June 2016) showing band combinations SWIR 2 (2.100 – 2.300  $\mu\text{m}$ ), NIR (0.845 – 0.885  $\mu\text{m}$ ), red (0.630 – 0.680  $\mu\text{m}$ ) for the southern UDP.

### *Normalised Burn Ratio*

The spatial extent of burn scar in the UDP determined using NBRs from the available Landsat images (Table 4.1), showed the burn scar to range from a low of 22.5% (52058.52 ha) in 2015, to a high of 57.67% (133453.44 ha) in 2007, with an average of 36.04% (83398.04 ha) (Table 5.2; Figure 5.15; Figure 5.16). 2007 was the only year to have more than half the UDP comprising of burn scar, with 1998 just less than half with 49.96% (Table 5.2; Figure 5.15). The highest levels of burn scar in 2007 matched the highest MODIS data results, which recorded 2007 with the highest fire points (Figure

5.1). In the last five years (2012 to 2017), 2013 and 2014 had larger burn areas with large patches of burn scar, while 2015, 2016 and 2017 had less burn areas with smaller more fragmented areas of burn scar (Figure 5.16). It is evident that large areas of the UDP are being burnt every year (Figure 5.16). Like with the fire point data from MODIS (Figure 5.2) and VIIRS (Figure 5.7), the burn scar maps show burning happening across the whole UDP every year, including southern, central and northern UDP, as well as different areas burning in consecutive areas (Figure 5.16).

Table 5.2. Summary of NBR analyses comparing annual area of burn and no burn, for the 12 years of available Landsat imagery from 1998 to 2017 in the UDP.

Landsat year	Burn area (ha)	No burn area (ha)	Total area (ha)	% Burn	% No burn
1998	115603.56	115789.86	231393.4	49.96	50.04
1999	71348.85	160044.57	231393.4	30.83	69.17
2000	86489.37	144904.05	231393.4	37.38	62.62
2001	53930.52	177462.9	231393.4	23.31	76.69
2005	104911.47	126481.95	231393.4	45.34	54.66
2006	63337.95	168055.47	231393.4	27.37	72.63
2007	133453.44	97939.98	231393.4	57.67	42.33
2013	86936.94	144456.48	231393.4	37.57	62.43
2014	93622.95	137766.42	231393.4	40.46	59.54
2015	52058.52	179334.9	231393.4	22.5	77.5
2016	67664.34	163729.08	231393.4	29.24	70.76
2017	71422.92	159970.5	231393.4	30.87	69.13

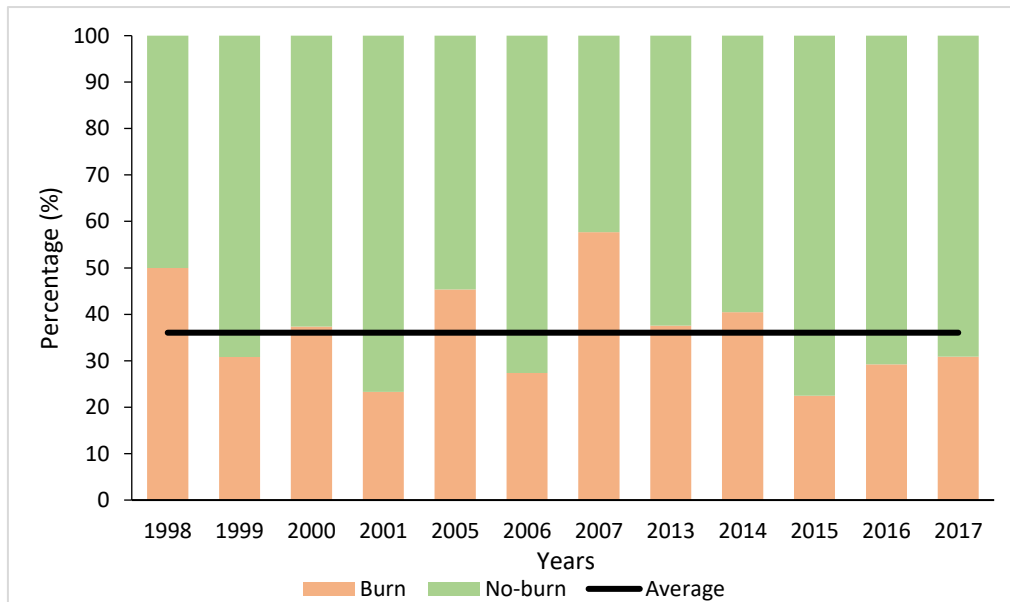


Figure 5.15. NBR results showing annual percentage burn and no burn, for the 12 years of available Landsat imagery from 1998 to 2017 in the UDP.

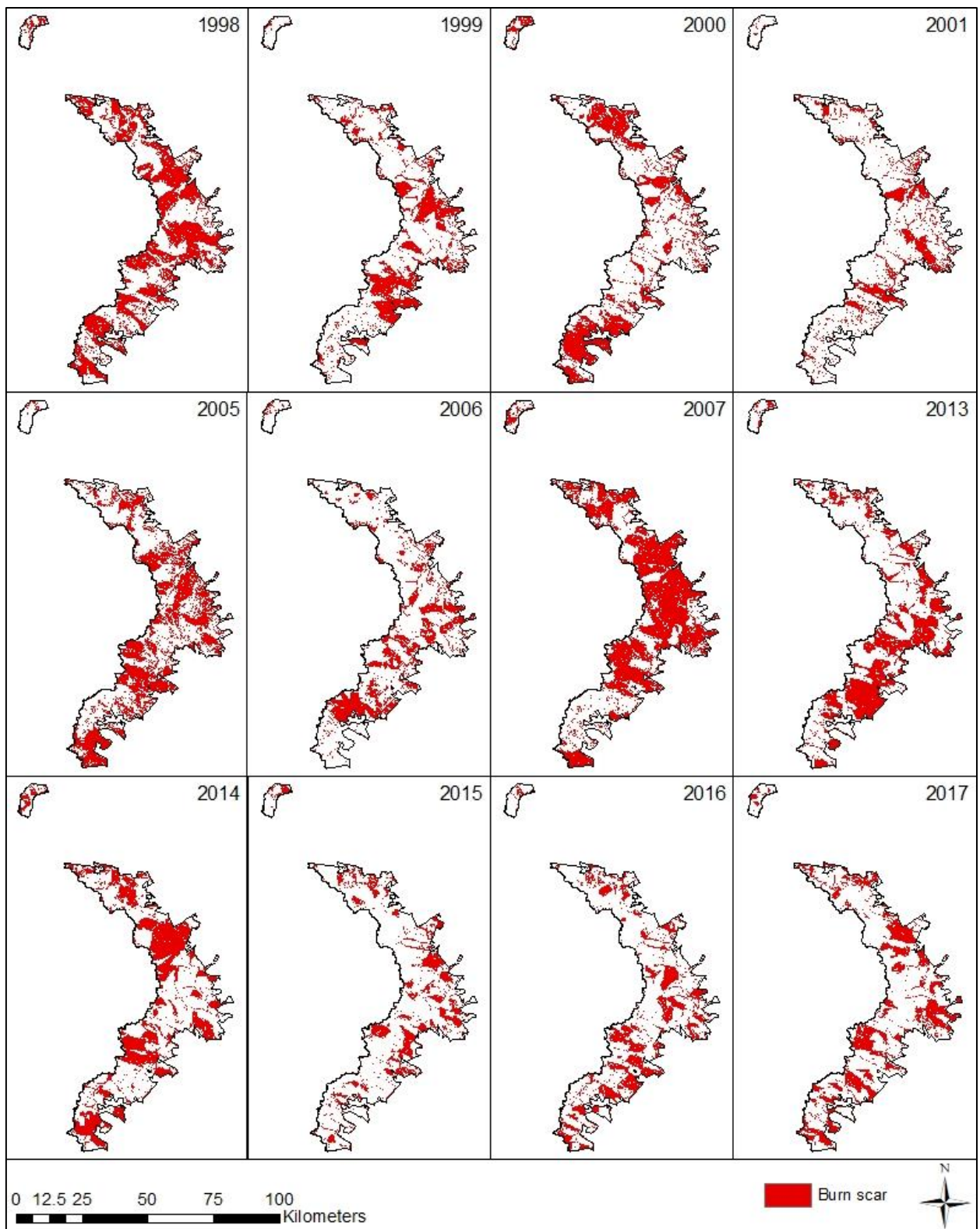


Figure 5.16. Comparisons of NBR burn scar results, for the 12 years of available Landsat imagery from 1998 to 2017 in the UDP.

When considering the annual burn scar areas in the UDP (Figure 5.16), together with the map of annual overlapping of NBR burn scar results from 1998 to 2017 (Figure 5.18) showing that 5.31% of the UDP did not record any burn scar (dark green areas) (Figure 5.17); it is evident that there is significant burning occurring in the UDP. However, from the maps of annual overlapping of burn scar areas (Figure 5.18; Figure 5.20), it is evident that annual overlapping of burn scar areas is limited. For example, for the 12 years of available data from 1998 - 2017 (Figure 5.18), 2.27% of the UDP burnt for all 12 years (dark red), with 25.27% of the UDP burning for between six to 12 years (shades of red), while 62.56% of the UDP were burnt for between two to five years (shades of green). This shows the most common number of years of overlapping burn scar to be two to five years out of the 12 years of data.

In the last five years of NBR data (2013 – 2017), 5.46% of burn scar areas overlapped for all five years (dark red areas) with 19.00% of the UDP showing no records of burning (dark green areas) (Figure 5.19; Figure 5.20). There was 4.25% of burn scar overlapping for four years and 8.54% overlapping for three years; resulting in 18.25% of the UDP burnt in more than three out of the last five years of data (shades of red on the map) (Figure 5.19; Figure 5.20). The largest percentage of overlapping burn scar in the UDP burnt for one year in the last five with 34.79%. Second was two years of burning in the last five years with 27.96%, resulting in 62.75% of the UDP burning one or twice in the last five years of data (shades of green on the map) (Figure 5.19; Figure 5.20).

It is evident from the combined NBR burn scar maps (Figure 5.18; Figure 5.20) that visually there are more green shades on the maps than red shades. Additionally, the corresponding graphs (Figure 5.17; Figure 5.19) showed the percentage overlapping of burn scar follow the same pattern of increased percentages of less overlapping (green) and decreased percentages of more overlapping (red), with both graphs reaching a peak in the green shades and dropping to the lowest percentages of overlap just before the maximum overlap of years, with a slight increase in percentage of overlap towards the maximum overlap. Green indicates less overlapping of burn scar, highlighting the mosaicking pattern of burning in the UDP. It is evident from the combined NBR burn scar maps (Figure 5.18; Figure 5.20) that the areas that burn every year are fire breaks, following thin linear movements (red areas). The higher altitudes of the UDP (left of the maps) are dominated by darker shades of green which means that those areas have had the least burn scar (have not burnt or have burnt only once or twice), possibly due to the fact that these areas are less accessible or not accessible at all due to the steep topography (Figure 5.18, Figure 5.20). The lower altitudes of the UDP (right of the maps) have more of the lighter shades of green and red, meaning that they have burnt a 'moderate' number of years (Figure 5.18; Figure 5.20).





1998 - 2017

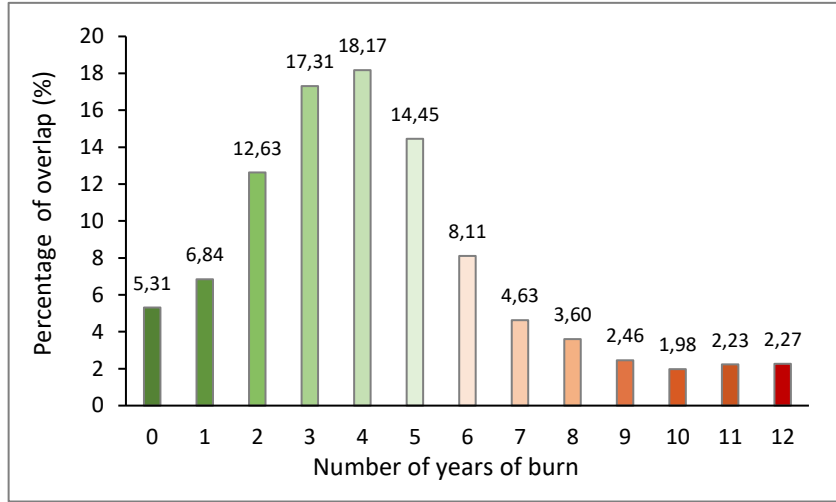


Figure 5.17. Overall percentage of overlapping burn scar per number of years of overlap, for the 12 years of available Landsat imagery, from 1998 to 2017 in the UDP.

Years burned

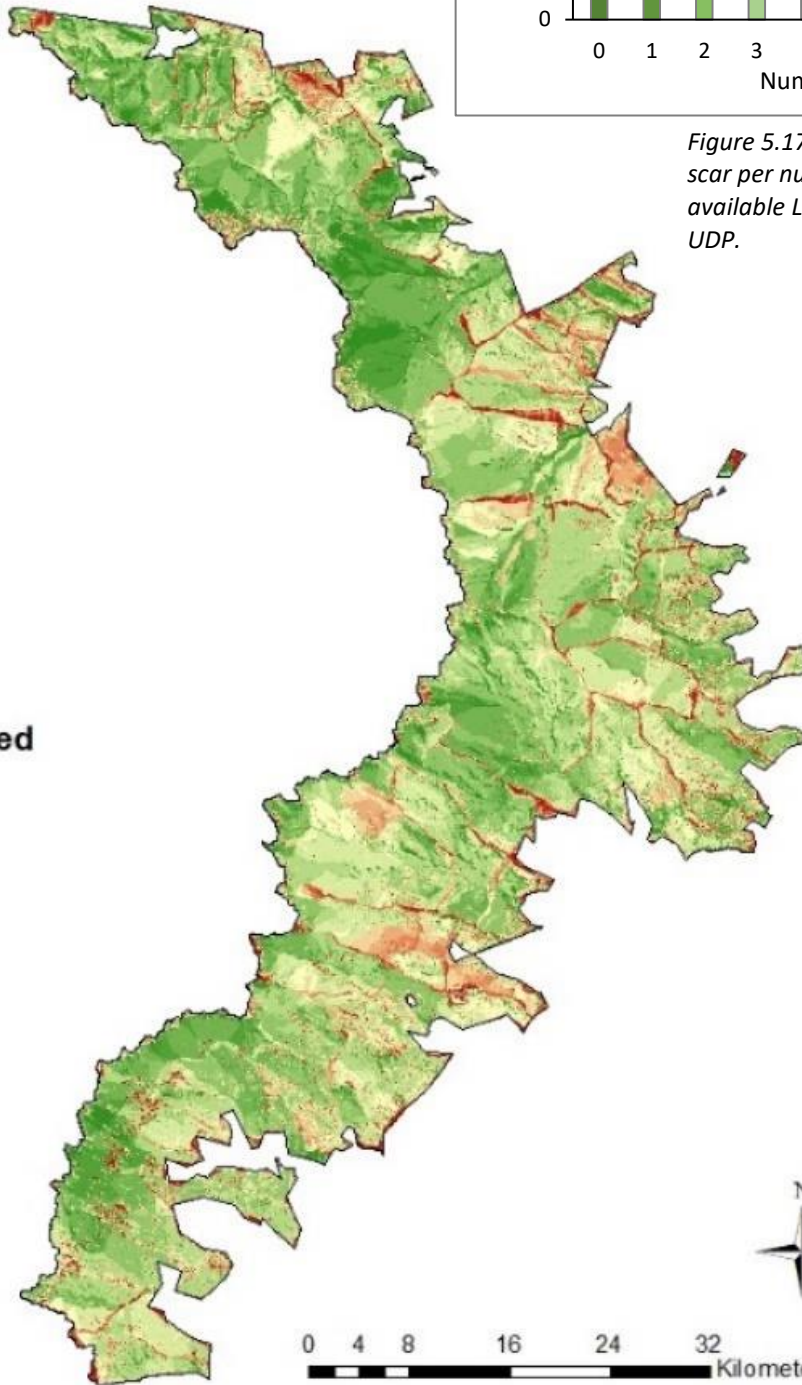
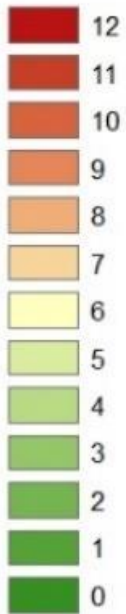


Figure 5.18. Combined NBR burn scar results showing areas of overlapping burn scar per number of years of overlap, for the 12 years of available Landsat imagery, from 1998 to 2017 in the UDP.



**2013 - 2017**

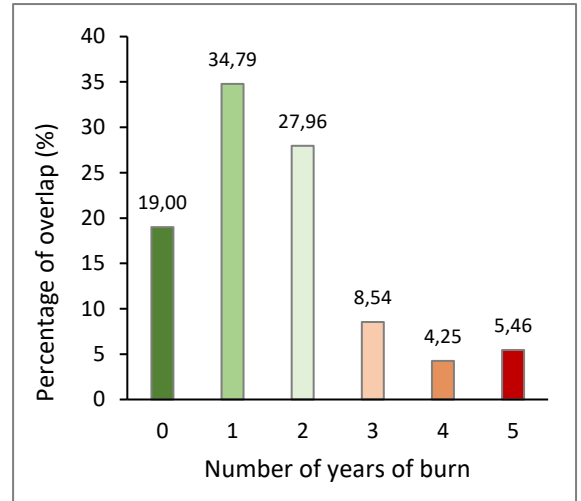


Figure 5.19. Overall percentage of overlapping burn scar per number of years of overlap for the last five years of data, from 2013 to 2017 in the UDP.

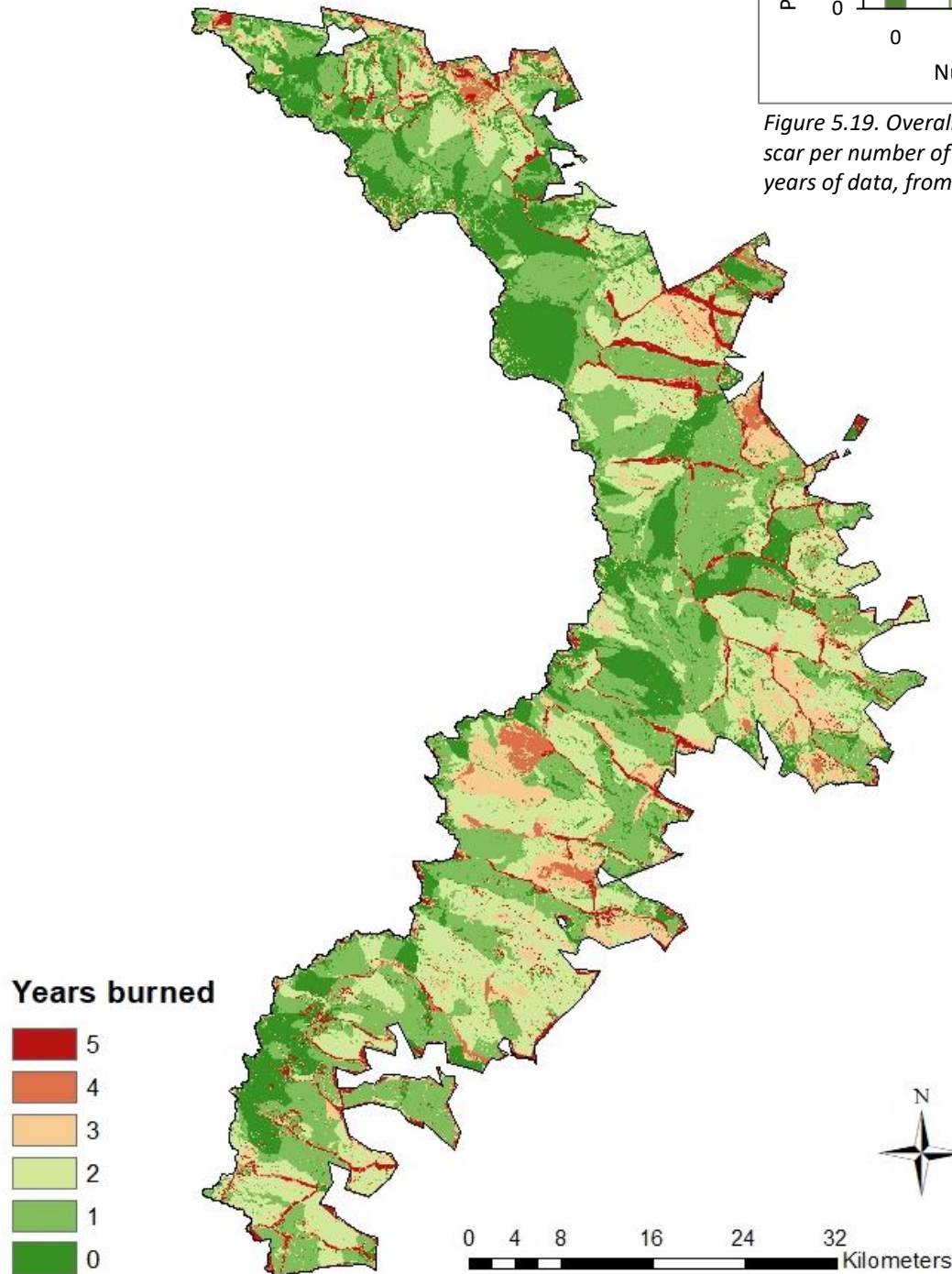


Figure 5.20. Combined NBR burn scar results showing areas of overlapping burn scar per number of years of overlap for the last five years of data, from 2013 to 2017 in the UDP.

### *Accuracy of Normalised Burn Ratio*

An accuracy estimation of the NBR burn scar results was determined by comparison to an example of digitised burn scar. This was a vector versus raster burn scar comparison. The NBR percentage of burn scar was calculated in relation to the area of the UDP calculated using raster (30 m<sup>2</sup> pixels), with the digitised percentage of burn scar calculated in relation to the area of the UDP calculated using the actual polygon border of the UDP. This means that the percentage of burn scar was calculated using different total areas of the UDP (Table 5.3). For 2017, the NBR showed 30.87% of burn scar, with the manually edited digitised method showing 29.60% of burn scar (Table 5.3; Figure 5.21). This produces a 95.89% accuracy of the NBR results in relation to the digitised burn scar for 2017 (Table 5.3). Some error is expected due to pixilation of the NBR method. It is evident from the zoomed-up burn scar vector versus raster comparison maps (Figure 5.21) that the large patches of burn scar are correctly detected by NBR, with many of the NBR errors coming from small pixel errors that could be assumed to be rock reflections or trees being incorrectly detected as burn scar (e.g. Figure 4.8).

*Table 5.3. NBR raster burn scar versus digitised vector burn scar for 2017 in the UDP.*

<b>2017</b>	<b>Raster</b>		<b>Vector</b>	
	<b>Area (ha)</b>	<b>%</b>	<b>Area (ha)</b>	<b>%</b>
Burn	71422.92	30.87	68475.96	29.60
No burn	159970.5	69.13	162874.87	70.40
Total	231393.42	100	231350.82	100
Accuracy (%)	95.89			

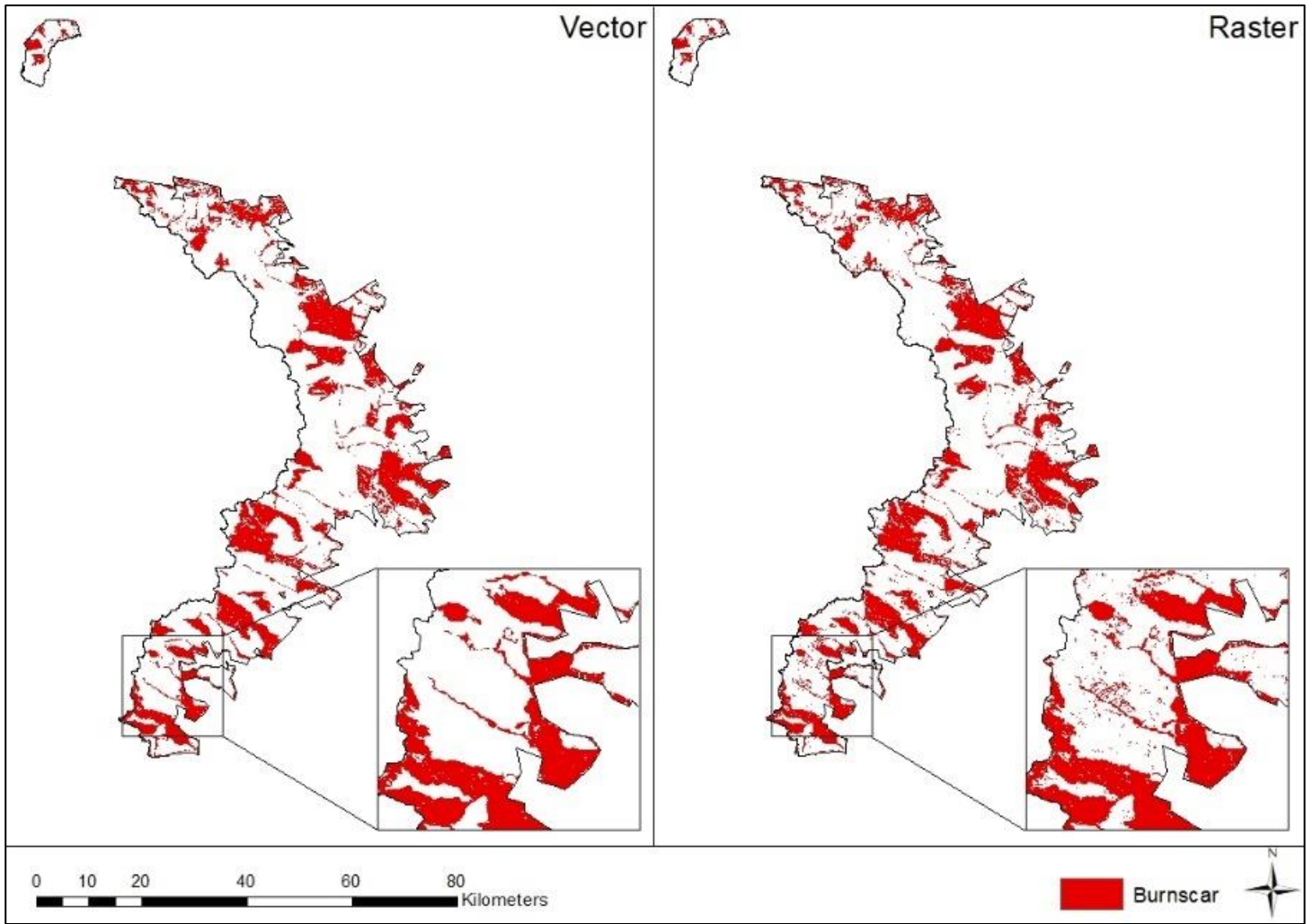


Figure 5.21. Digitised vector burn scar versus NBR raster burn scar versus for 2017 in the UDP.

### 5.1.3 Comparison: MODIS vs VIIRS vs Landsat

A comparison was made between the MODIS and VIIRS data, and the Landsat 8 image for 14<sup>th</sup> September 2017 (Figure 5.22). The Landsat 8 image, used as the reference image, was taken at 07:57:02 GMT (top Landsat image) and 07:57:26 GMT (bottom Landsat image). There are three areas on the map of the UDP showing active MODIS and VIIRS active fire data points (A,B and C) with two of these areas (A and C) showing visible smoke on the image. MODIS data recorded 10 points: four points at 07:26 GMT (terra) (C) and six points at 11:43/11:44 GMT (A, B and C) (Table 5.4). VIIRS data recorded 15 points: 12 points at 12:18 GMT (A, B and C) and three points at 23:34 GMT (A and C) (Table 5.4).

The visible smoke at (A) and (C) coincide with the MODIS and VIIRS data. The no visible smoke at (B) could mean that the fire/s only started after the Landsat image was taken and therefore only detected later in the day by MODIS and VIIRS but not earlier in the morning by Landsat. VIIRS had a later overpass than MODIS on the 14<sup>th</sup> September, which could provide an explanation for why MODIS only records one point at (B) and VIIRS records three points (two at 23:34 GMT).

The MODIS and VIIRS data from 13<sup>th</sup> September 2017 (the day before) shows points recorded in the faint smoke area shown on the Landsat image between (A) and (C), meaning that the smoke on the Landsat image could be from fires the day before which had extinguished or were too faint to be detected by MODIS and VIIRS on the 14<sup>th</sup> September 2017.

MODIS detected fires at (C) at 07:26 GMT, before the Landsat overpass, indicating why there is smoke evident in the Landsat image, with MODIS and VIIRS detecting fires in (C) later in the day too.

The green point in (C) shows a MODIS fire point, recorded at 11:43 GMT on the 14<sup>th</sup> September 2017, which is located just outside the UDP boundary, and is not included due to being outside the boundary. The point's distance to the UDP boundary ranges from approximately 107 - 135 m away. However, due to the MODIS 1 km<sup>2</sup> pixel resolution there is a chance that the fire did actually occur in the UDP.

*Table 5.4. Acquisition time of MODIS and VIIRS active fire data from 14<sup>th</sup> September 2017 in areas A, B and C.*

Active fire data	A		B		C	
	Time (GMT)	No. of points	Time (GMT)	No. of points	Time (GMT)	No. of points
MODIS	11:44 (Aqua)	2	11:43 (Aqua)	1	07:26 (Terra)	4
					11:43 (Aqua)	3
VIIRS	12:18	4	12:18	1	12:18	7
	23:34	1	23:34	2		

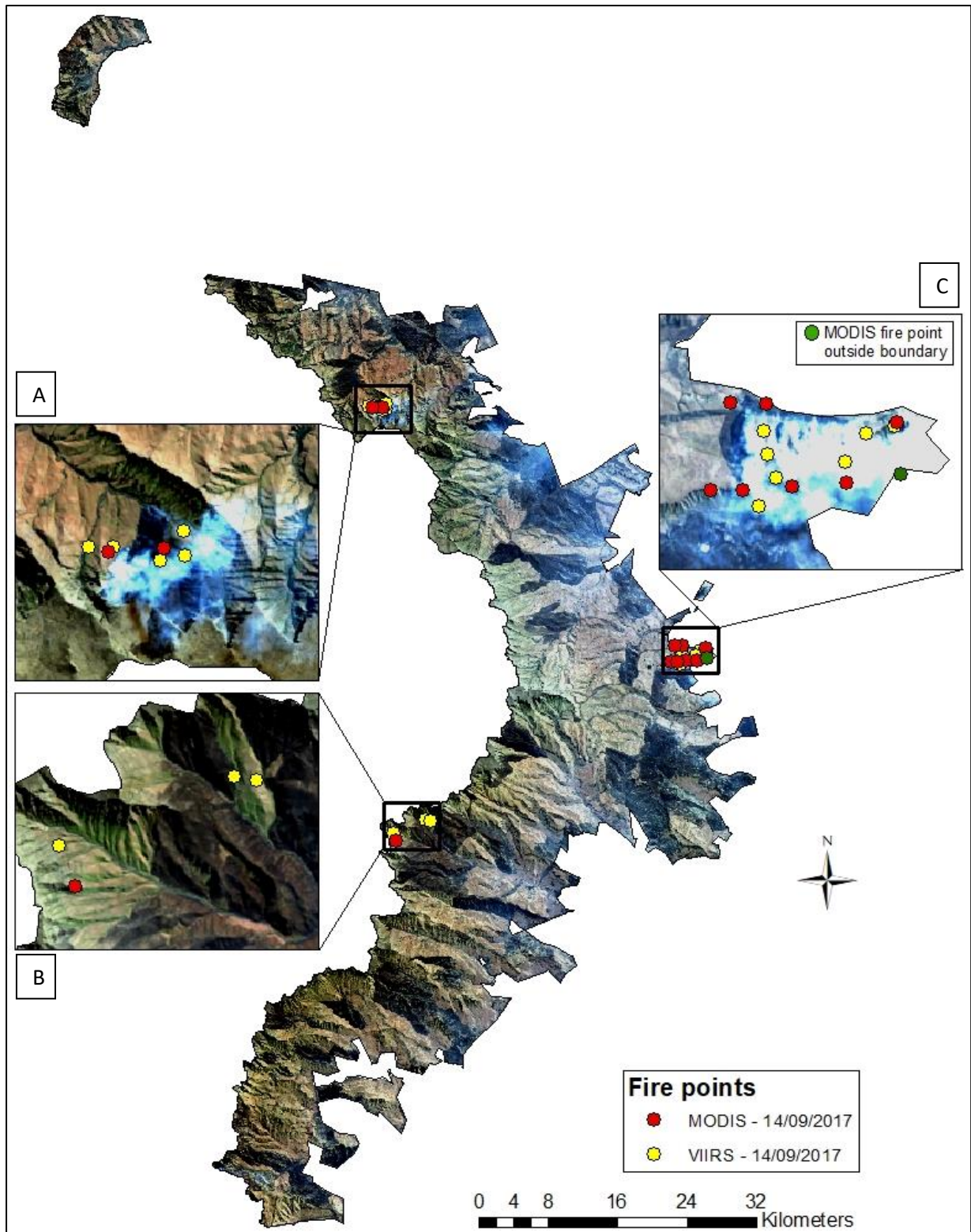


Figure 5.22. Comparison between MODIS and VIIRS active fire data and the Landsat 8 image from 14<sup>th</sup> September 2017 in the UDP.

For 2017, MODIS recorded 511 active fires, VIIRS recorded 1690 active fires, and Landsat 8 NBR recorded 71422.92 ha (30.87%) of burn scar (Figure 5.23). When comparing MODIS and VIIRS data with the NBR results from the Landsat 8 image from 2017 visually on the maps below (Figure 5.23), the active fire data from MODIS and VIIRS (red points) detected fires in the same locations as where the burn scar was located on the Landsat 8 image (red areas). An accuracy determination based on the percentage of active fire data points from MODIS and VIIRS overlapping with the NBR results from the Landsat burn scar for 2017 resulted in 62.70% of MODIS fire points and 76.30% of VIIRS fire points overlapping with the Landsat NBR burn scar results (Table 5.5). From 2013 to 2017, MODIS data overlapped with the Landsat burn scar from a low of 55.03% in 2015 to a high of 72.85% in 2014. VIIRS data overlapped with the Landsat burn scar from a low of 74.84% in 2015 to a high of 83.06% in 2013 (Table 5.5). The Landsat image for 2017 was taken on 14<sup>th</sup> September 2017, and the MODIS and VIIRS data recorded fire points for the whole year. MODIS recorded seven fire points after this date, while VIIRS recorded 57 fires points after this date (Table 5.6), and were, therefore were not included in the above 2017 accuracy comparison. Fire points detected by MODIS and VIIRS after the Landsat image acquisition dates were excluded from all the accuracy comparisons (Table 5.6).

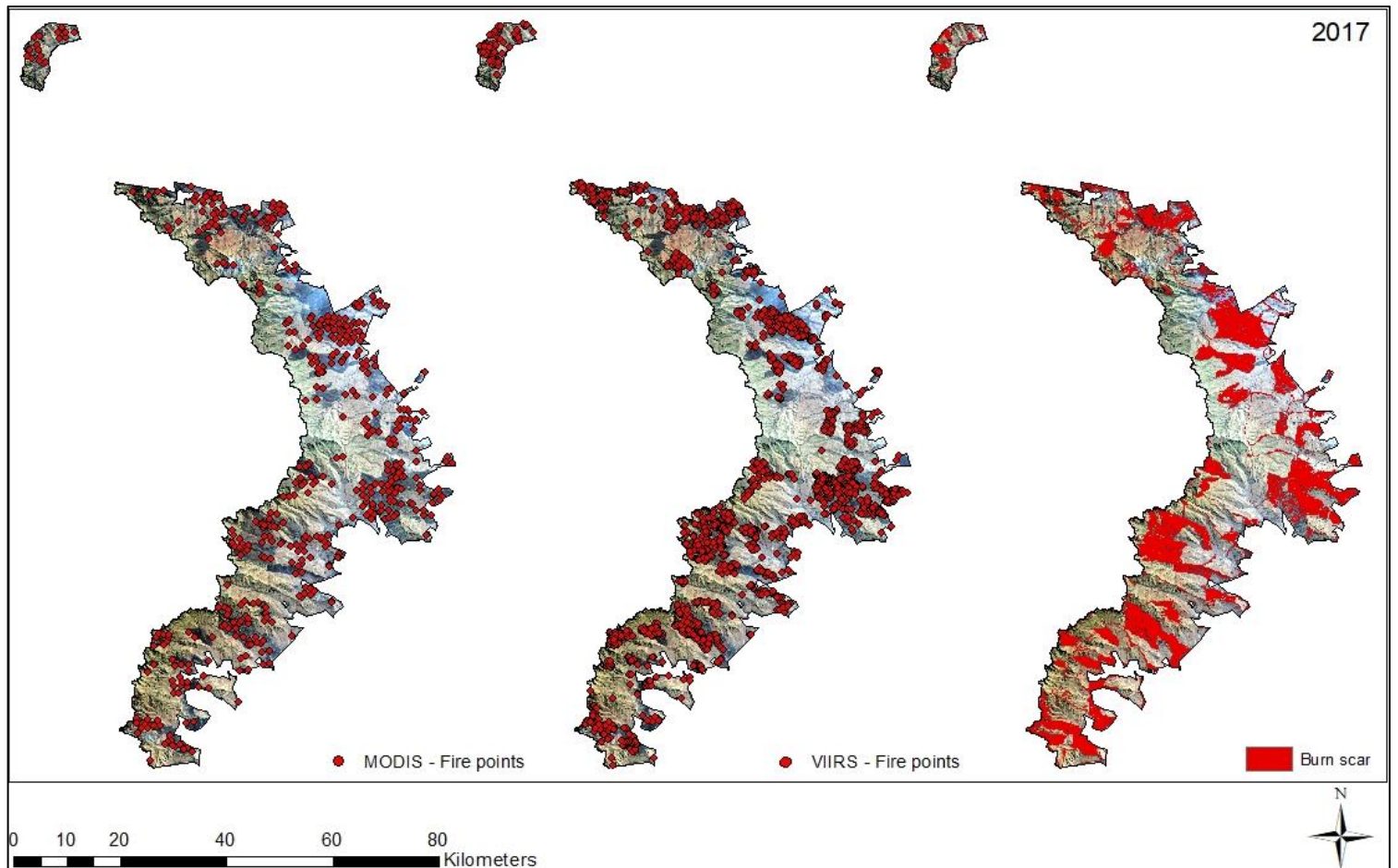


Figure 5.23. Comparison between MODIS and VIIRS active fire data and NBR showing burn scar for 2017 in the UDP.

Table 5.5. Accuracy (%) comparison between MODIS and VIIRS active fire data and the Landsat NBR ratio for 2013 to 2017 in the UDP.

Year	MODIS (%)	VIIRS (%)
2013	66.34	83.06
2014	72.85	82.48
2015	55.03	74.84
2016	61.82	78.91
2017	62.70	76.30

Table 5.6. Number of MODIS and VIIRS active fires recorded after the Landsat image date.

Year	Date Landsat	Landsat % Burn	MODIS – total fires	MODIS – fires after date	VIIRS – total fires	VIIRS – fires after date
2005	29-Sep	45.34	563	11	-	-
2006	16-Aug	27.37	471	140	-	-
2007	3-Sep	57.67	877	70	-	-
2013	3-Sep	37.57	559	45	1998	209
2014	6-Sep	40.46	616	45	2196	232
2015	24-Aug	22.5	417	99	1137	215
2016	26-Aug	29.24	511	160	1734	577
2017	14-Sep	30.87	511	7	1690	57



## 5.2 SOILS

### 5.2.1 Overview

When comparing the soil results from all 85 soil samples, there was a wide range of variability across all soil properties (See full dataset and graphs in Appendix A and Appendix B). There were no obvious distinct patterns, with both inter- and intra-site variation being high across the UDP. Looking at an overview of the results (Table 5.7), there were large ranges in the values. Soil strength values showed that HP ranged from 900 - 4200 kPa and that HSV ranged from 14 - 154 kPa. Soil pH ranged from 3.18 - 5.07, showing the soils in the UDP to be acidic. Soil moisture ranged from 12.28 - 279.71%. SOM ranged from 4.92 - 51.01%. Soil texture results from the particle size analysis showed the soils to be majority silt, with silt ranging from 48.88 - 81.33%. When comparing between sand and clay, some samples had higher clay content and some higher sand content, with sand ranging from 0.82 - 43.09% and clay from 4.38 - 34.61%.

Comparing the average of soil properties against high and low fire frequency sites (Table 5.7) without taking into account additional factors, such as environmental factors (e.g. geology), the high fire frequency sites averaged higher values for HP, HSV, soil moisture, SOM and sand content. The low fire frequency sites averaged higher pH values, and silt and clay content.

Table 5.7. Summary of soil property data including all sites, the high fire frequency sites (orange) and the low fire frequency sites (green). The bold and darker shaded writing indicates the higher value between high and low fire frequency.

Soil property	All sites (85)		High fire frequency sites (45)		Low fire frequency sites (40)	
HP (kPa)	2251.79 ± 743.18	900 – 4200	<b>2459.09 ± 804.66</b>	900 - 4200	2023.75 ± 599.79	1000 - 3200
HSV (kPa)	68.13 ± 32.21	14 - 154	<b>76.91 ± 35.91</b>	14 - 140	58.46 ± 24.54	21 - 154
pH	3.92 ± 0.46	3.18 - 5.07	3.74 ± 0.28	3.18 - 4.6	<b>4.12 ± 0.53</b>	3.19 - 5.07
Soil moisture (%)	47.01 ± 47.14	12.28 - 279.71	<b>53.79 ± 63.20</b>	12.28 - 279.71	39.38 ± 12.98	15.18 - 65.56
SOM (%)	15.08 ± 9.19	4.92 - 51.01	<b>16.37 ± 11.76</b>	4.92 - 51.01	13.62 ± 4.64	6.36 - 26.02
Sand (%)	16.88 ± 9.39	0.82 - 43.09	<b>18.61 ± 9.52</b>	1.18 - 40.18	14.93 ± 8.97	0.82 - 43.09
Silt (%)	64.07 ± 7.29	48.88 - 81.33	62.46 ± 8.08	48.88 - 80.40	<b>65.89 ± 5.86</b>	50.47 - 81.33
Clay (%)	19.05 ± 6.52	4.38 - 34.61	18.93 ± 6.46	10.82 - 34.61	<b>19.18 ± 6.67</b>	4.38 - 32.51

Soil properties from each area and comparisons of soil properties between the high and low fire frequency locations, produced varied results. Some sites had distinctly higher and lower soil property values between high and low fire frequency sites, while some soil properties were similar or only showed a slight difference (Table 5.8; Table 5.9). Soil pH was the only soil property to show a trend, with pH being higher or similar in low fire frequency sites than high fire frequency sites, but never higher in high fire frequency sites (Table 5.9). The other soil properties (HP, HSV, soil moisture and SOM) all had varied results with higher values recorded in high fire frequency sites, higher values in

low fire frequency sites and values that were similar, with all sites being split almost half-half with either 3 or 4 out of 8 sites falling under the highest value in high or low fire frequency sites (Table 5.9).

The most common environmental difference between sites was slope, with six out of the eight areas having varied slopes between the high and low fire frequency sites (Table 5.8). The southern Drakensberg had the highest SOM and soil moisture values, with Garden Castle having much higher SOM and soil moisture values than all the other sites. Cobham had the highest clay content and lowest sand content. Injisuthi recorded the highest soil pH values.

Table 5.8. Summary comparison between the high and low fire frequency sites at each area with the soil property being placed under the high or low fire frequency heading where the soil property was highest or in the similar column if the soil property values showed only a slight difference.

Site	Differences	High fire frequency	Low fire frequency	Similar/slight difference
<b>Bushman's Nek</b>	<ul style="list-style-type: none"> <li>Vegetation</li> </ul>	<ul style="list-style-type: none"> <li>Soil moisture</li> <li>SOM</li> </ul>	<ul style="list-style-type: none"> <li>HP</li> <li>HSV</li> <li>pH</li> </ul>	
<b>Garden Castle</b>	<ul style="list-style-type: none"> <li>Altitude</li> <li>Slope</li> </ul>	<ul style="list-style-type: none"> <li>Soil moisture</li> <li>SOM</li> </ul>	<ul style="list-style-type: none"> <li>HP</li> <li>HSV</li> <li>pH</li> </ul>	
<b>Cobham</b>	<ul style="list-style-type: none"> <li>Aspect</li> <li>Slope</li> </ul>	<ul style="list-style-type: none"> <li>HP</li> <li>HSV</li> </ul>	<ul style="list-style-type: none"> <li>pH</li> </ul>	<ul style="list-style-type: none"> <li>Soil moisture</li> <li>SOM</li> </ul>
<b>Kamberg</b>	<ul style="list-style-type: none"> <li>Altitude</li> <li>Slope</li> <li>Vegetation</li> </ul>	<ul style="list-style-type: none"> <li>HP</li> <li>HSV</li> <li>SOM</li> </ul>		<ul style="list-style-type: none"> <li>pH</li> <li>Soil moisture</li> </ul>
<b>Giant's Castle</b>	<ul style="list-style-type: none"> <li>Geology</li> <li>Slope</li> </ul>		<ul style="list-style-type: none"> <li>pH</li> <li>Soil moisture</li> <li>SOM</li> </ul>	<ul style="list-style-type: none"> <li>HP</li> <li>HSV</li> </ul>
<b>Injisuthi</b>	<ul style="list-style-type: none"> <li>Altitude</li> <li>Aspect</li> <li>Geology</li> </ul>	<ul style="list-style-type: none"> <li>HP</li> <li>HSV</li> <li>Soil moisture</li> <li>SOM</li> </ul>	<ul style="list-style-type: none"> <li>pH</li> </ul>	
<b>Monk's Cowl</b>	<ul style="list-style-type: none"> <li>Slope</li> </ul>	<ul style="list-style-type: none"> <li>HP</li> <li>HSV</li> </ul>	<ul style="list-style-type: none"> <li>pH</li> <li>Soil moisture</li> <li>SOM</li> </ul>	
<b>Cathedral Peak</b>	<ul style="list-style-type: none"> <li>Slope</li> </ul>		<ul style="list-style-type: none"> <li>HP</li> <li>HSV</li> <li>Soil moisture</li> <li>SOM</li> </ul>	<ul style="list-style-type: none"> <li>pH</li> </ul>

Table 5.9. Summary comparison of the number of times a soil property was highest in the high or low fire frequency sites or similar

Soil property	High fire frequency	Low fire frequency	Similar/ slight difference
HP	4	3	1
HSV	4	3	1
pH	-	6	2
Soil moisture	3	3	2
SOM	4	3	1

### Soil Moisture

As the soil moisture percentages are in relation to dry weight, it is possible to get values greater than 100% when the samples are very wet. This was found at the Garden Castle high fire frequency site, which was saturated with water during sampling and could have been saturated peat wetland (Figure 5.24). Soil moisture values are not an accurate value. The samples for this study were collected in the wet season, with some collected while it was raining or the day after a rain event. Some of the samples were taken a month apart (December and January). In order to get accurate soil moisture values, multiple samples would need to be taken repeatedly to provide temporal coverage over all seasons.



Figure 5.24. Water logged high fire frequency site at Garden Castle (29<sup>th</sup> December 2018).

### Soil Colour

Soil colour was varied across the UDP (Figure 5.25). See Appendix A for soil colours. Soil colour across the UDP ranged from black, very dark grey, very dark greyish brown, dark brown, dark yellowish brown, dark greyish brown, dark yellowish brown to brown. The most common hue was 10YR with 79 out of the 85, with the other two hues being 7.5YR with five samples and 2.5Y with one sample.



Figure 5.25. The 85 soil samples after being oven dried, showing soil colour variations

Giant's Castle and Royal Natal had the 7.5 hue which is redder in colour compared to the 10YR hue. The six soil samples described as black in colour were found at Bushman's Nek and Garden Castle, where the site was water logged (Figure 5.24). The most common Munsell colour code (Munsell Colour, 2010) in the UDP was 10YR 3/2 with 20 samples and 10YR 4/3 with 19 samples. According to Weil and Brady (2017), soil colour gives an indication of other soil properties and does not have a significant effect on soil behaviour. Therefore, with the varied soil colour results across the UDP, soil colour was not included in the statistical analyses.

### Soil Texture

The particle size ranges used in the Gradistat program were: sand (63  $\mu\text{m}$  - 2.0 mm), silt (2  $\mu\text{m}$  - 63  $\mu\text{m}$ ), and clay (< 2  $\mu\text{m}$ ) (Udden, 1914 and Wentworth, 1922 cited in Blott, 2010). See Appendix A for particle size values. The sand-silt-clay diagram shows the soil samples to be sandy silt and silt, making the soils silty loam (Figure 5.26). Folk and Ward's (1957) descriptions from Gradistat (Blott and Pye, 2001), the same methods described in Briggs (1977), showed the soils to be silt dominated (48.88 – 81.33 %), ranging from fine silt to very coarse silt with the majority mean (50 out of 85 samples) being medium silt. The samples sorting was mostly very poorly sorted (79 out of 85 samples). The sample skewness ranged from very fine skewed to coarse skewed, with the majority being symmetrical (42 out of 85 samples). Sample kurtosis values were mainly platykurtic (73 out of 85 samples) which means that the distribution curve is more flat than a normal distribution (Briggs, 1977), and mesokurtic (11 out of 85 samples) which means that the samples have a normal distribution (Briggs, 1977).

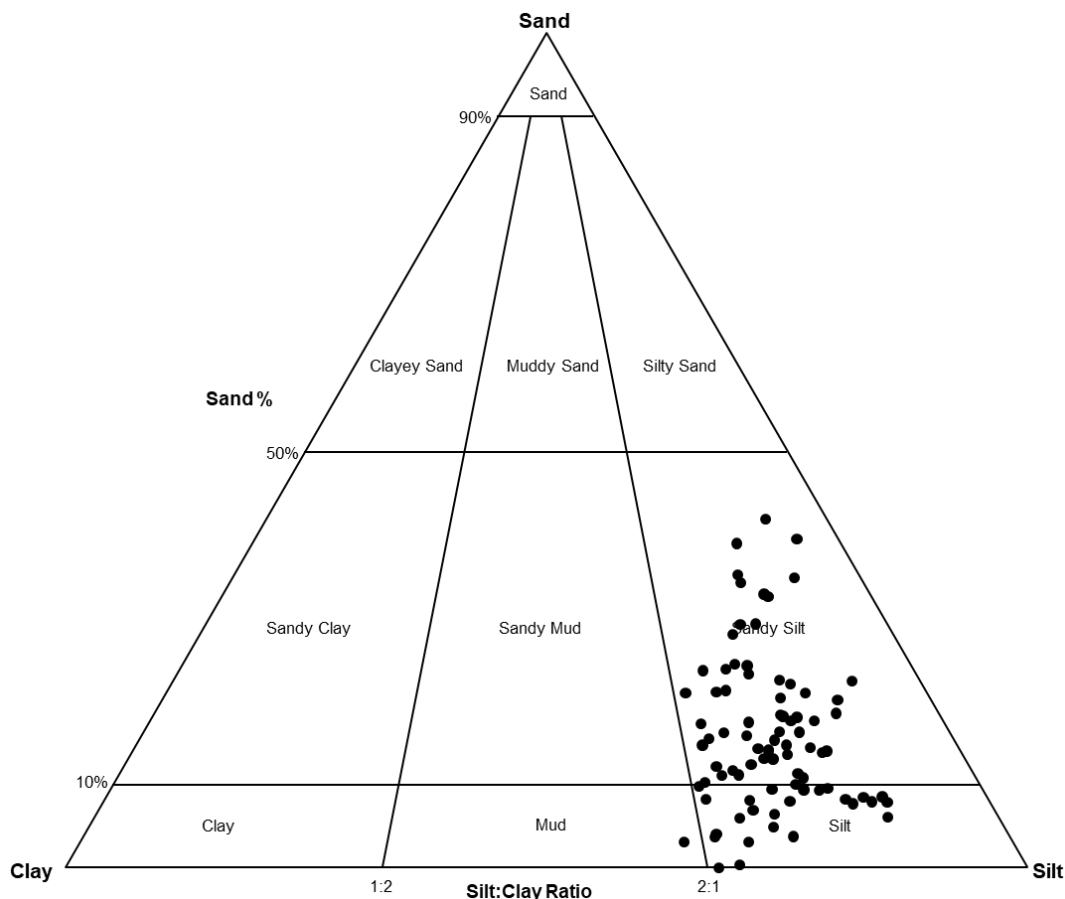


Figure 5.26. Sand-silt-clay diagram showing the 85 soil sampling points. Diagram from Gradistat Version 8.0 Grain Size Analysis Program (Blott, 2010).

### 5.2.2 Soil statistics

The correlation matrix shows a strong positive correlation between SOM and soil moisture (dark blue) (Figure 5.27). Therefore, soil moisture was excluded from further analyses, as mentioned in the methodology. The correlation matrix shows that there is a close positive relationship between HP and HSV, and sand and SOM to be negatively correlated.

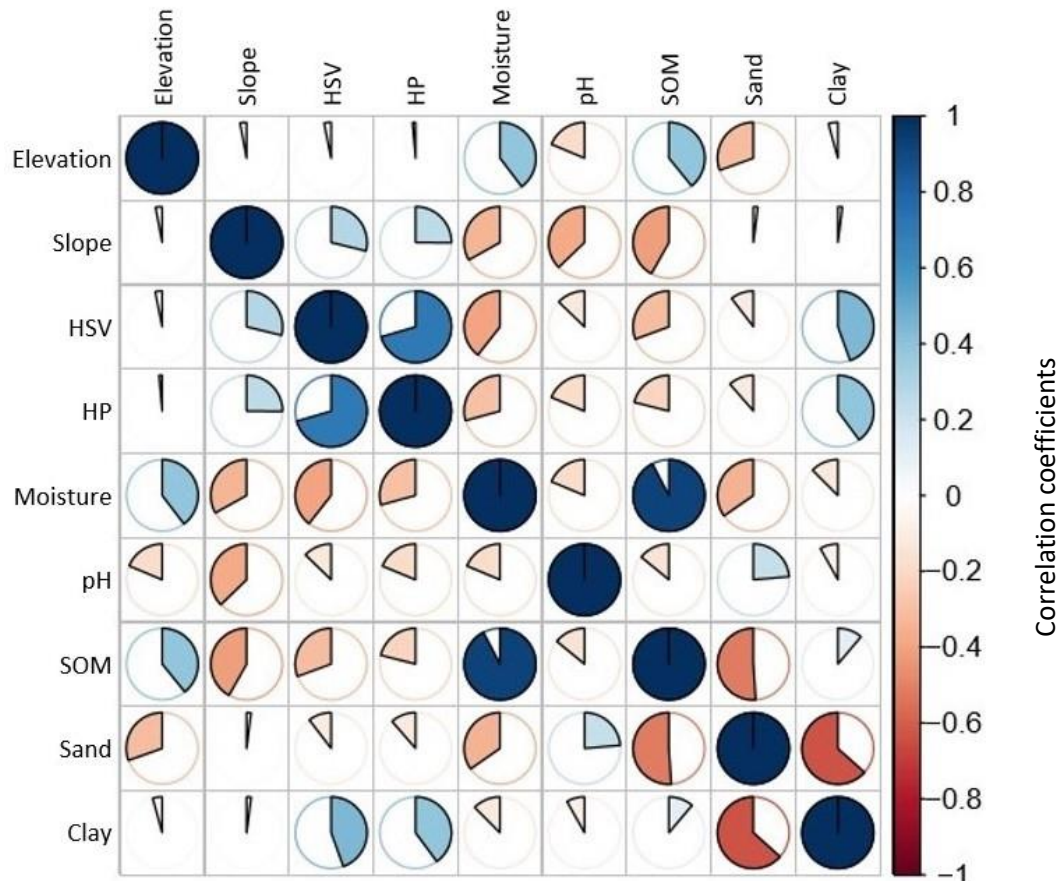


Figure 5.27. Correlation matrix of the soil properties. (Source: Bakker, 2018, pers. comm.).

Broadly, the full regression models, comparing the outcome variables to all predictor values, burn was shown to be significant for SOM (p-value < 0.05). Burn was not significant for HP and HSV (p-value > 0.05). With burn being significant at the 90% confidence level for pH (p-value = 0.088). SOM had the highest adjusted R<sup>2</sup> value (77.51%) (Table 5.10). The adjusted R<sup>2</sup> considers the number of variables in the model and is, therefore, a more appropriate value for the full regression models (Bakker, 2018, pers. comm.). HP had the lowest adjusted R<sup>2</sup> value, followed by HSV (Table 5.10). This means that burn and the other predictor variables for HSV and HP explain the variance in the model less than the models for SOM and pH. SOM and pH have relatively high adjusted R<sup>2</sup> values. This means that the predictor variables are important in explaining SOM and pH. SOM has the highest R<sup>2</sup> value, meaning that the model with all the predictor variables was good at predicting SOM and make up most of the factors influencing SOM.

Table 5.10. Adjusted R<sup>2</sup> values for the full multiple regression models for all four outcome variables.

Outcome variable	Adjusted R <sup>2</sup> (%)
HP	42.83
HSV	50.92
pH	73.16
SOM	77.51

A broad overview of the full regression models above did not take into consideration the relative importance graphs and the “best” model. A further explanation of the regression models for each outcome variable follows, including the influence of individual predictor values, relative importance graphs, and the regression model for the “best” model with diagnostic plots. See Appendix C for raw soil statistical data from R.

#### *Soil Strength*

Soil strength analyses includes the regression models for HP and HSV.

For HP, the full regression model including all predictor variables had an adjusted R<sup>2</sup> value of 42.83%. The significant variables (p-value < 0.05) for HP were depth and aspect (north). Geology (Tarkastad) being significant at the 90% level. However, depth cannot be a factor for HP, as the same sampling method was used for all soil samples. Burn was not significant (p-value > 0.05) for HP. The LMG metric relative importance graphs (Figure 5.28) for the full regression model showed aspect and vegetation to be the most significant, followed by geology. Elevation had the lowest contribution to variance. Burn was not significant in the relative importance graphs.

The regression model with the five “best” subsets of the predictor variables for HP selected burn. The other selected variables were area (north), depth, geology (Tarkastad), aspect (north), vegetation (southern Drakensberg highland grassland), elevation and clay. The significant variables (p-value < 0.05) were aspect (north) and vegetation (southern Drakensberg highland grassland). Burn was not significant (p-value > 0.05). The relative importance graphs show aspect and vegetation to have the biggest contribution to variance, with burn and elevation having low contributions to the variance.

For HSV, the full regression model, including all predictor variables, had an adjusted R<sup>2</sup> value of 50.92%. The significant variables (p-value < 0.05) for HSV were vegetation (northern Drakensberg Highland Grassland), sand, geology (Tarkastad), clay and aspect (north). Burn was not significant (p-value > 0.05). The LMG metric relative importance graphs (Figure 5.27) for the full regression model showed vegetation to have the highest contribution to variance, followed by geology and aspect. Analyses showed that sand had a low contribution to variance. Depth and elevation had the lowest contributions to variance. Burn did not have a significant contribution (had a low contribution) to variance in the relative importance graphs.

The regression model with the five “best” subsets of the predictor variables was not run for HSV. This was due to ‘burn’ not being selected as a subset predictor variable using the BIC criterion for the “best” five model (Bakker, 2018, *pers. comm.*). Following this, another model was run using the BIC criterion with any number of “best” models, with ‘burn’ still not being selected.

#### *Soil pH*

For the full regression model, including all predictor variables, pH had an adjusted R<sup>2</sup> value of 73.16%. The significant variables (p-value < 0.05) for pH were geology (Tarkastad, Molteno, Elliot and Karoo Dolerite), depth and aspect (south). Burn was significant at the 90% level. The LMG metric relative importance graphs (Figure 5.28) for the full regression model showed geology and aspect to have the highest contribution to variance, followed by vegetation and burn. Burn was shown to be one of the top four contributors to variance.

The regression model with the five “best” subsets of the predictor variables using the BIC criterion did not select burn as a predictor variable. Therefore, an AIC criterion was used to select the five “best” subsets of the predictor variables, of which burn was one. This indicates that burn could still be an important variable in pH even though pH was not selected using the BIC criterion (Bakker, 2018, *pers. comm.*) The other selected variables were area (southern), depth, geology (Elliot, Karoo Dolerite, Molteno, Tarkastad), aspect (north and south), vegetation (southern Drakensberg Highland Grassland), and elevation. The significant variables (p-value < 0.05) were geology (Tarkastad, Karoo Dolerite, Molteno and Elliot), area (south), aspect (south), and depth. Burn was significant at the 90% level. The relative importance graphs show geology and aspect, like the relative importance graphs from the full model, to have the largest contribution to variance. Depth has the lowest contribution to variance, followed by elevation. Burn had a low contribution to variance.

#### *Soil Organic Matter*

The full regression model for SOM, including all predictor variables had an adjusted R<sup>2</sup> value of 77.51%. The significant variables (p-value < 0.05) for SOM were sand, burn, geology (Tarkastad, Elliot, Molteno), slope, vegetation (northern Drakensberg Highland Grassland, KwaZulu-Natal Moist Grassland) and clay. Burn was a significant variable for SOM. The LMG metric relative importance graphs (Figure 5.28) for the full regression model, showed sand to have the highest percentage contribution to variance, followed by vegetation and slope. Burn did not show a large contribution to variance, with depth having the lowest contribution to variance.

The regression model with the five “best” subsets of the predictor variables selected burn. The other selected variables were geology (Molteno), vegetation (southern Drakensberg Highland Grassland), slope, and sand. The significant variables (p-value < 0.05) were sand, slope, burn, vegetation (Southern

Drakensberg Highland Grassland), and geology (Elliot and Tarkastad). The relative importance graphs show sand, vegetation and slope to have the largest contribution to variance, while burn had the lowest contribution to variance.

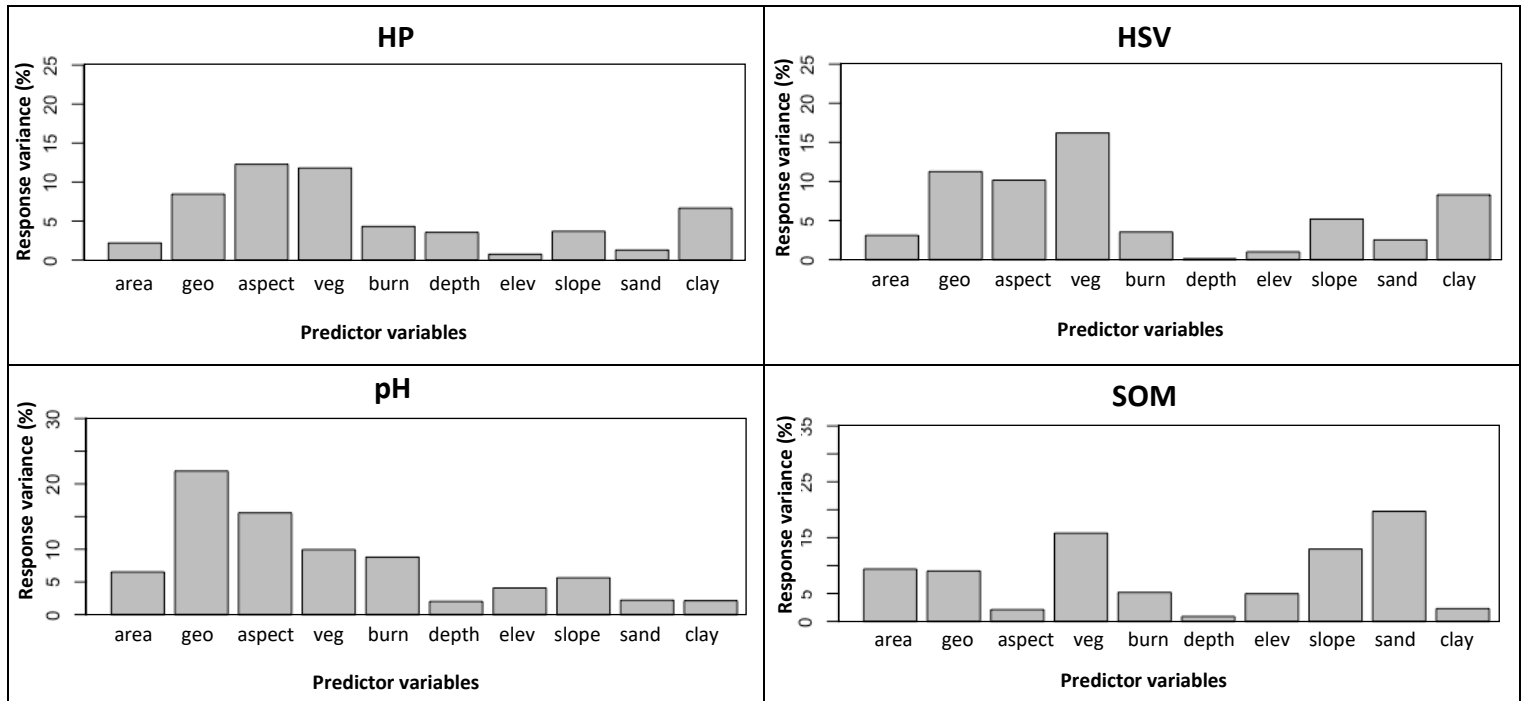


Figure 5.28. Relative importance graphs, using the LMG metric, for the full regression model for each outcome variable. (Source: Bakker, 2018, pers. comm.).

The diagnostic plots for HP, pH and SOM showed the residuals to be normally distributed and there were no outliers that were influential to the regression results. HP and pH showed a linear relationship and more uniform variance, with SOM showing the potential of a non-linear relationship and not showing uniform variance. This could be due to additional variables that were not included in the model influencing soil properties or from some of the potential outliers detected (Bakker, 2018, pers. comm.).

Comparing all four outcome variables (HP, HSV, pH and SOM), burn had the largest significance for SOM and pH. With HSV and HP, which looks at the physical properties of soil, having the least significance to burn. Therefore, for HP, in comparison to all the predictor variables and the “best” model, burn was not seen as a significant predictor variable and had a low contribution to variance. For HSV, burn was not a significant predictor variable. Burn was only found to be a significant variable in the SOM regression models, including the full and “best” model. Burn was not a significant variable in HP or HSV. Burn was significant at the 90% level for the pH full model but not in the “best” model. In the relative importance graphs for the full models and “best” models, burn had a low contribution to variance for all outcome variables. However, across all four variables, pH showed burn to have the



largest contribution to variance in the relative importance graphs. Therefore, other variables present in the models have a larger influence on the outcome variables models than burn. When incorporating information for the full model, “best” model and relative importance graphs; HP highlights ‘aspect’ to be important, HSV highlights vegetation to be important, pH highlights geology and aspect to be important, and SOM highlights sand (particle size), vegetation and slope to be important. With geology having the strongest relationship with pH.

For the full regression models, the relative importance graphs (Figure 5.28) showed vegetation to have a large (significant) contribution to variance for all four outcome variables. Therefore, vegetation can be considered an important contributing factor in affecting soil properties in the UDP. Geology, aspect and vegetation had the highest three percentages of variances in the relative importance graphs for HP, HSV and pH (Figure 5.28). The relative importance graphs showed depth to have the least contribution to variance for HSV, pH and SOM. With depth and elevation having the overall lowest contribution to variance across all four outcome variables.

## CHAPTER 6: DISCUSSION

---

### 6.1 INTRODUCTION

This research project aimed to investigate the spatial and temporal frequency of fires, using remote sensing, and to investigate the effect of fire frequency on soil properties in the UDP. The objectives of this study were to use remote sensing to determine the frequency and spatial extent of fires, evaluate the effectiveness of implementing remote sensing in the UDP, and to evaluate the effects of fire frequency on selected soil properties. Fire frequency and the spatial extent of fires were investigated using freely available, open source remote sensing data from MODIS, VIIRS and Landsat. The remote sensing fire results were used to select study sites for soil sampling collection comparing high and low fire frequency sites across the UDP. Soil samples were analysed to investigate the impact of fire frequency, taking into account the different environmental factors that occur across the UDP. Given the large extent and diversity of the Drakensberg landscape, and the many factors influencing soil formation factors in an area, comparing the effects of fire on soil properties across the whole UDP was challenging.

### 6.2 REMOTE SENSING

The remote sensing results showed fires to be a dominant factor in the UDP, with high fire frequency and large areas of burn scar. The remote sensing fire results from this study coincided with what the fire management plan in the UDP states (EKZNW, 2012). The regularity of fire was evident with high fire frequencies and records of fires across the whole UDP.

#### 6.2.1 Fire Frequency

The fire frequency results from both MODIS and VIIRS data showed fires to occur across the whole UDP annually, with annual fires following an 'up and down' pattern or increase and decrease pattern in consecutive years. This is expected as prescribed burning is implemented across the whole UDP but the same areas in the UDP are not burned every year (EKZNW, 2012). The MODIS and VIIRS data showed burning to occur from May to October over the dormant winter months where annual rainfall is the lowest. This shows winter and spring burning, with majority of the burning taking place in winter. There were very few fires or no fires detected during the summer high rainfall period. The MODIS data showed June to have the highest fire frequency and VIIRS showed July to have the highest fire frequency. Firebreaks are burnt annually before mid-winter (by July) (O'Connor *et al.*, 2004), accounting for the high fire frequencies in June and July.

MODIS fire data showed 2007 to have the highest frequency of fires and the NBR results showed 2007 to have the largest amount of burned area. Strydom and Savage (2016) also found 2007 to have the

highest fire frequency across South Africa, and noted a possible reason being that 2006 was a relatively warm La Niña event, leading to increased growth in vegetation from the combination of increased rainfall and air temperatures, possibly leading to increased occurrence of fires in 2007 (Strydom and Savage, 2016).

The annual MODIS and VIIRS kernel densities (Figure 5.4; Figure 5.12) show a variety of different areas across the UDP to receive the highest fire frequencies in different years. It was expected that fire frequency patterns in consecutive years would differ, as different areas are burned each year. The overall kernel density map for MODIS (Figure 5.3) showed the southern UDP to have the lowest fire frequency and the northern central UDP (Cathedral Peak region) to have the highest fire frequency. VIIRS (Figure 5.8) showed the southern UDP to have the lowest fire frequency, and the central and northern UDP to have a moderate to high fire frequency. A possible reason for the higher fire frequency in the northern areas of the UDP and lower fire frequency in the southern UDP could be the influence of differing land cover types in the areas surrounding the UDP (Figure 3.12). Commercial crops and plantations surrounding the southern UDP would have a specific emphasis on avoiding fires due to the economic losses of agriculture.

Comparing MODIS and VIIRS active fire data, there are expected differences due to spatial resolutions, with MODIS having a 1 km<sup>2</sup> spatial resolution and VIIRS having a 375 m<sup>2</sup> spatial resolution, as well as VIIRS having improved fire detection abilities (Schroeder *et al.*, 2014). Therefore, it is expected that VIIRS will have more recorded fire points and be of higher accuracy. However, the power of MODIS lies in the archived nature of the data, going back to the early 2000s. The annual fire point comparisons showed MODIS and VIIRS to follow a similar pattern, although the limitations between the two datasets is evident with different highest monthly values and differing kernel density fire hotspot locations (Figure 5.12).

### 6.2.2 Spatial Extent

The Landsat imagery used for burn scar detection in the UDP was successful. The main limitation of Landsat imagery in this study was missing imagery or clouds obscuring the imagery, the amount of processing of data by the user that is required and finding an appropriate Landsat image at the end of the burn season. Burn scar was so prominent in the UDP, with large areas of the UDP being covered in burn scar at the end of the burning season, that the burn scar is easily visible with the human eye (Figure 4.1; Figure 5.14). Band combinations (SWIR 2, NIR and red) were effective in detecting burn scar from the UDP landscape, with large patches of burn being detected, faint firebreaks being detected, and the differentiation between rock faces and shadows, and burn scar (Figure 5.14). However, a limitation with the NBR which was determined during site selection, was the detection of

reflective rocks as burn scar (Figure 4.8). The detection of reflective rocks as burn scar as in Figure 4.8 and not Figure 5.13 could be due to the scale differences, with Figure 4.8 being at much larger scale which would make the 30 m pixel resolution error detection easier. The accuracy comparison between the digitised vector burn scar and raster NBR burn scar showed the NBR method of burn scar detection to successfully detect burn scars (Figure 5.21). The errors picked up were mostly small clusters of pixels, which could be due to rock reflections, with the main areas of burn scar correctly detected.

Using a NBR for burn scar detection was a successful and appropriate method for burn scar detection in the UDP. The visual process of NBR is shown in Figure 4.1. It shows the success of NBR's ability to detect visual burn scar and quantify burn scar by detecting burnt 30 m pixels. The combined NBR results showing an overlapping map for all years of data (Figure 5.18) and for the last five years of data (Figure 5.20) provided an overall view of fire in the UDP. It is evident that annual firebreaks are only taking up a small area of the UDP and that annual overlapping of burn scar is limited, with 62.56% of the UDP burnt for between two to five years out of the 12 years of data (Figure 5.17; Figure 5.18) and 62.75% of the UDP burnt once or twice in the last five years of data (Figure 5.19; Figure 5.20). These overlapping results show the NBR's ability to quantify annual burn scar, an easy method for monitoring the extent of burn scar in the UDP. The higher altitudes of the UDP were shown to have less frequent overlapping burn scars than the lower altitudes of the UDP (Figure 5.18; Figure 5.20). This correlates to SANBI's (2013) 'Grassland Ecosystem Guidelines' which indicate that best management practice for South Africa's high-altitude grasslands alpine areas are being burnt every five to seven years, and the lower escarpment areas being burnt every two to four years. This is due to slower growth rates in higher altitude grasslands (SANBI, 2013).

The accuracy comparison between MODIS and VIIRS data and Landsat NBR burn scar, highlighted a limitation with the Landsat NBR burn scar method. This being the Landsat image acquisition dates from August and September. It was previously highlighted that MODIS and VIIRS data recorded many fire points after the date at which the burn scar was calculated (Table 5.6). Therefore, the burn scar calculated for each year using the Landsat images did not include the whole year's possible burn scar across the UDP. Due to the limitation of finding appropriate Landsat images with cloud cover, missing data and the 16-day revisit period, and due to not being able to use Landsat images too late into the year in the UDP, due to the grasslands recovering, burn scar fading and the rainy season having increased cloud cover. It is not likely to obtain one Landsat image that shows 100% of the burn scar in the UDP for the whole year. A possible solution is to use multiple Landsat images from the whole year and calculate the NBR for each Landsat image, then combine the NBR results into one burn scar map for the year.

The NBR burn scar results for 2014, 2015 and 2016 (Table 5.2), in comparison to the burn records in the annual reports from the UDP (Table 2.1), show a lower percentage burn per year than the annual reports. With all three years ranging from a 3.6 - 4.53% decrease compared to the annual reports. A possible reason for the differing percentage burns could be that NBR was calculated using 30 m resolution, which will result in pixelation errors. The Landsat 8 images used for determining NBR for all three years were taken in August or September (Table 4.1) while MODIS recorded between 45 and 160 fire points and VIIRS recorded between 215 and 577 fire points (Table 5.6) after the Landsat images were taken for the respective years. Therefore, the NBR burn scar results did not include the whole year's burn scar. The annual reports worked on the financial year (April to March) and the NBR results worked on a calendar year (January to December), potentially causing slight variations but not significant ones as the dominant fire season is from May to September. This comparison shows the NBR scar results to show quite an accurate representation of the burn scar in the UDP.

### 6.2.3 Evaluating Remote Sensing in the UDP

The success of using remote sensing for investigating fires in the UDP can be seen in the overlapping burn scar results from NBRs using Landsat imagery, specifically in the last five years (Figure 5.20), and in the accuracy comparison between MODIS and VIIRS overlapping with the NBR results from Landsat imagery (Figure 5.23).

The fire management plan in the UDP (EKZWN, 2012) incorporates annual firebreaks and prescribed burning in a patch mosaic effect on the grasslands which is created by burning different patches of grasslands at different times, creating a landscape of varying patches of recovery. The overlapping NBR results from the last five years' (Figure 5.20) coincide with what the fire management plan states (EKZWN, 2012). The annual firebreaks are evident across the UDP and the mosaic overlapping patchiness effect on the grasslands is evident across the whole UDP, with differing patches of the number of years of burn, including areas that have not been burned which act as refuge sites (Figure 5.20). This highlighting the success of using NBRs of Landsat imagery to map burn scar in the UDP and the potential of being a valuable monitoring tool.

The advantages of MODIS and VIIRS active fire detection is the high temporal resolution with daily data available, the archived nature of MODIS data, easy access to the data, and limited processing of the data required (Giglio *et al.*, 2003; Schroeder *et al.*, 2014). They provided valuable data for looking at the spatial and temporal spread of fires across the UDP. The limitations of MODIS and VIIRS active fire data spatial resolution was highlighted throughout the research project. Additionally, with the limitations of not knowing the exact location of the fire as the fire pixel is placed at the centre of either the 1 km<sup>2</sup> or 375 m<sup>2</sup> pixel and does not indicate the number of fires present (Giglio *et al.*, 2003).

Comparing one day of MODIS and VIIRS active fire data with the corresponding Landsat image (Figure 5.22) showed that MODIS and VIIRS were not suitable for determining the spatial extent of fires or the perimeter of a fire at a larger scale. Due to their limited spatial resolution. However, the percentage accuracy comparison between MODIS and VIIRS overlapping with the NBR results from Landsat (Figure 5.23) at a smaller scale looking at the whole UDP show the MODIS and VIIRS fire points to be located on top of the NBR burn scar showing the abilities of MODIS and VIIRS active fire point to give an indication of the spatial extent of fires in the UDP. The VIIRS accuracy ranged from 74.84 - 83.06% and the MODIS accuracy ranged from 55.05 - 72.85%, with the differences being due to the pixel resolution (Table 5.23). Therefore, the fire points could give an idea of spatial extent of fires, as a high concentration of points could be from one fire. The same results were found by Schroeder *et al.* (2014) who noted VIIRS had a greater ability to detect fires that coincided with Landsat 7 burned areas than MODIS.

While the remote sensing imagery from this study was beneficial for looking at fires at an across UDP scale, the limitations and inaccuracies of the spatial resolution of the remote sensing data used was shown when the NBR results were used for soil site selections (as noted in the methodology section), which occurred at a much larger scale. The errors determined from the remote sensing site selection methods (Figure 4.7; Figure 4.8) highlighted the importance of ground-truthing remote sensing data. Therefore, it is important to note the scale at which the imagery will be used. For monitoring, remote sensing alone does not give us an indication of what is happening at the plot scale, but field observations do provide this (Gross *et al.*, 2015). The extensive spatial and temporal data, from remote sensing, including information on possibly inaccessible areas, together with field observations would provide an improved monitoring approach (Gross *et al.*, 2015).

Selecting remote sensing imagery options for the UDP, the cost of imagery is an important consideration as continuation of monitoring could be very costly, making freely available imagery being the best option (Turner *et al.*, 2015). The freely available MODIS and VIIRS active fire data appeal for use in the UDP due to no pre-processing required, increasing the potential for wider use of the data (Turner *et al.*, 2015). A limitation in this study was the expensive software package used (ArcMap) making it less accessible, although other GIS platforms like QGIS can be used.

The flexible and variable approach to fire management in the UDP (EKZNW, 2012) and high level of non-scheduled burning (for example arson) taking place in the UDP every year, as noted in the annual reports (Table 2.1), creates a high level of uncertainty about the areas that burned in the UDP. The locations of where burning from arson are taking place in the UDP are not known in this study. However, there is a likelihood that arson and human involved incidents occur near roads, hiking trails

and camp sites, due to accessibility. Remote sensing would be able to provide a monitoring tool to keep track of the fires and quantify the burn scar.

Turner *et al.* (2015) noted that the important contributing factors to remote sensing being utilised and appropriate for biodiversity conservation are: data continuity, data affordability and data access, which a combination of MODIS and VIIRS active fire data and Landsat imagery, can provide for the UDP. This aim of this research study did not include remote sensing at the plot scale and did not attempt to find an alternative to field monitoring; remote sensing and field monitoring are complementary and create greater value when used together. The aim of this study was to get an idea of the frequency and spatial extent of fire across the whole UDP using remote sensing. The temporal and spatial information gathered from remote sensing; with consistent and complete spatial coverage of an area (Corbane *et al.*, 2015), is so valuable to conservation efforts that the possibilities for the UDP outweigh the limitations of remotely sensed data.

The effects of fires extend across a wide range of spatial and temporal scales (Lentile *et al.*, 2006). This is where remote sensing can be beneficial in investigating fires across the whole UDP, using both active fire detection and burn scar mapping. This study highlighted that the use of a combination of different satellite sensors will benefit assessment of fires in the UDP. The benefits of MODIS and VIIRS active fire data in the UDP, being the high temporal resolution (daily), freely available, easily assessable, long archived MODIS data and the limited data processing in comparison to performing NBRs on Landsat imagery. With the advances of the VIIRS data, there is improved detection abilities. Landsat offered successful burn scar detection at 30 m resolution. The power of MODIS and Landsat being the archived nature of the data. The power and potential of using free, open sourced remote sensing data were highlighted in this study, which can create data that can be easily shared. This study brought the new idea of looking at fires across the whole UDP with remote sensing.

### 6.3 SOILS

The objective for the soil analyses was to evaluate the effects of fire frequency on soil properties across the UDP. The soil sampling sites were selected using GIS based on the NBR burn scar results, accessibility, geology, slope and aspect. Due to the high variability across the UDP and the method used to select study sites, there were very limited suitable areas to select study sites that fitted all the same criteria (Figure 4.2). An evaluation of this method was explained in the methodology. As soils have many influencing factors, a multiple regression model was run with a selection of possible influencing variables which indicated the significance of each variable in the different soil properties. The investigation into the effects of fire frequency on soils in the UDP results showed the selected soil properties (soil strength – HP and HSV, soil pH and SOM) to be highly variable across the whole UDP.

Therefore, due to the many influencing factors across the UDP, including environmental factors and fire regime information (Certini, 2005; Novara *et al.*, 2013; Pereira *et al.*, 2014; Zavala *et al.*, 2014), it is not possible to conclude that the differing soil properties were due to fire frequency alone.

### 6.3.1 Soils in the UDP

The overview of the soil sample results showed that there was a wide range of soil property results across all soil properties (Table 5.7). Some sites recorded distinctly higher and lower soil property values between high and low fire frequency sites and some soil properties were similar or only showed a slight difference (Table 5.8; Table 5.9). The literature review highlighted the varying results for the effects of fire on soil properties (Certini, 2005; Zavala *et al.*, 2014; Alcañiz *et al.*, 2018), specifically SOM and soil pH, and how influential soil formation environmental factors can be on the variation in soil properties across the same area (Weil and Brady, 2017). The results show the same variation of results across the UDP. This demonstrates the strong influence of environmental factors in the UDP and how site-specific soils are.

Soils have not been investigated across the whole UDP before, and only site specific examples are available (Bijker *et al.*, 2001; Mason *et al.*, 2007). It was known that there would be variability issues with soils due to the complex, simultaneous and interdependent actions of the five soil formation factors (Jenny, 1941), as noted by Weil and Brady (2017), and to the diverse nature of the UDP.

Across all sites and soil properties, burn was found to be the most significant across all statistical tests in SOM. SOM and soil moisture were found to be positively correlated in the UDP, also noted by (González-Pérez *et al.* 2004). pH showed burn to have the largest contribution to variance in the relative importance graphs compared to the other outcome variables (Figure 5.28) but the regression analyses did not show burn to be significant. Soil pH was higher in six out of the eight low fire frequency sites, and similar in the other two sites (Table 5.9). Bijker *et al.* (2001) also noted the no-burn site at Giant's castle had the highest soil pH. The soil property results showed a strong correlation between soil moisture and SOM, as noted in the literature (Bijker *et al.*, 2001; González-Pérez *et al.*, 2004). The soil strength values, soil compressive and shear strength (HP and HSV) were shown to be highly varied and inconsistent across the UDP (See Appendix A and B), with HSV and HP averaging higher values in high fire frequency sites in the UDP (Table 5.7). This was also noted by Bijker *et al.* (2001) whose results showed significant differences in soil strength values at Giant's Castle, and that regular burning increases soil strength. Bijker *et al.* (2001) also noted that soil strength (HP and HSV) could be due to SOM levels, however, the correlation matrix for this study did not show a positive correlation for HP and HSV with SOM (Figure 5.27). The regression analyses in this study showed burn to be non-significant in HP and HSV values in the UDP.



From the soil statistical analyses results, vegetation was highlighted as an important contributor to all soil properties measured (HP, HSV, pH and SOM). Geology, aspect and vegetation had the highest three percentages of variances in the relative importance graphs for HP, HSV and pH (Figure 5.27). In the case of SOM, slope and particle size were important contributors to variance. The significant factor with the grassland vegetation classes used in this study from Mucina and Rutherford (2006), was the varying temperature and precipitation values attached to each Drakensberg grassland category (Figure 3.9). For example, the southern Drakensberg Highland Grassland averaged 779 mm of MAP, where the northern Drakensberg Highland Grassland averaged 1017 mm of MAP, highlighting the significant effect that climate has on soil properties in the UDP. Novara *et al.* (2013) noted differences in soil organic carbon could be due to different grasses, highlighting the possible variability in the UDP due to the varying grassland vegetation categories. Vegetation and geology categories in the Drakensberg are interrelated, with vegetation zones and geologies following similar altitudinal patterns (Figure 3.10). The UDP consists mostly of lithic soils (Fey *et al.*, 2010). Lithic soils are regularly associated with steep topography and have a strong connection with their underlying parent rock, therefore playing a role in lithic soils physical and chemical properties (Fey *et al.*, 2010). This highlights the significance and relationship of soils and geology in the UDP. Therefore, we can assume that the soils are related to their parent material in the UDP. The statistical results did not show elevation to be significant for the soil properties. However, elevation is an important factor in the geology and vegetation classifications, and in turn an important factor in the UDP. The relative importance graphs showed depth to have the least contribution to variance for HSV, pH and SOM, and a low contribution to HP. This is not an accurate representation of comparing soil sampling depth in the UDP, due to the soil auger sample from the upper 200 mm of soil being mixed and only a proportion of sample used for analyses.

The most common difference between the high and low fire frequency sites in each area was slope (Table 5.9). Alijani (2013) noted slope to be an important factor in differentiating between soils. The effect of slope can be highlighted by looking at the soil properties for Cathedral Peak where the low fire frequency site had a very steep slope. The significant difference in soil properties between the high fire frequency site was the particle size analysis, with the low fire frequency site on the steep slope having a significantly higher sand content. This could be due to the finer particles being carried down the steep slope by wind or water, leading to an increase in coarser particles, and thus sand (Zavala *et al.*, 2014).

Litter accumulation is greatest in areas which are infrequently burned (Manson *et al.*, 2007). A 910 x 910 mm quadrat photo was taken at the centre of each site as an additional observation to investigate the vegetation coverage (Appendix D). It is evident that the low fire frequency sites had more

vegetation cover than the high fire frequency sites, with the most notable difference being that high fire frequency sites have more exposed soils and that there was a large amount of litter accumulation on the low fire frequency site (Figure 6.1). A result may be more erosion on the high fire frequency sites, as the exposed soils on the high fire frequency sites were present in the photographs taken in December and January during the summer rainfall season. In high fire frequency sites, an accumulation of charcoal on the soil surface is probable (Bijker *et al.*, 2001). This was noted in the UDP (Figure 6.1; Figure 6.2). The high fire frequency site at Injisuthi (Figure 6.1) showed a darkened top layer of soil, with bare ground and roots where the soils sample was taken. The low fire frequency site at Giant’s castle (Figure 6.1) showed large litter accumulation that acts as a protective layer for the soil.



Figure 6.1. Comparison between the soil surfaces: Low fire frequency site at Giant's Castle (23<sup>rd</sup> January 2018) (top); and high fire frequency site at Injisuthi (24<sup>th</sup> January 2018) (bottom).



Figure 6.2. Colour variations on the soil surface at the high fire frequency sites at Cathedral Peak (26<sup>th</sup> January 2018).

### 6.3.2 Influencing Factors on Soil Properties

Consulted literature described varying responses of soil properties to fire. These differences can be due to fire heterogeneity or other influencing factors (Alcañiz *et al.*, 2018). It is known that the factors that affect soil properties from Jenny’s (1941) soil formation equation are climate, organisms, topography, parent material and time. The factors included in this study were: climate, where the

precipitation and temperature data were included within the vegetation classifications with the different grassland vegetation classes from Mucina and Rutherford (2006) (Figure 3.9); organisms, which looked at natural vegetation categories and SOM; topography including slope, aspect and altitude; and parent material, including geology. Environmental factors which could have affected soil properties and were not considered in this study were soil type, topography and position on the landscape. Alijani (2013) found different landform (e.g. high ridge) as one of the main contributing factors for differentiating between soils, which were not considered in this study. It can be assumed that soil type is related to geology, as noted earlier. The other significant factor in this study being fire. Important factors of a fire regime include season, frequency, type and intensity (Trollope, 1981). This study only considered fire frequency and the spatial extent of burn scar, while fire type, behaviour and intensity are beyond the scope of this study, and are noted above as important factors that can influence differing soil properties. Additional possible factors that could have affected soil samples in the UDP are discussed below.

The collected soil sample sites were from locations that were spread across the whole UDP. Sites had a variety of slopes, aspects, geology, vegetation categories, elevations, fire frequencies (high/low), and topographical positions. Broad category aspect values (north, south and east) were used for differentiating sites, whereas Everson and Tainton (1984) used exact aspect degree values. The sampling sites had a variety of slopes, with some sites having steeper slopes. Together with the summer rainfall, there is the potential for runoff to cause erosion and to wash the top layer of soil away (Nel, 2007), thus altering the accuracy of the soil property results. There is also a possibility of an accumulation of increased SOM at the bottom of slopes due to runoff. The Drakensberg experiences summer thunderstorms, resulting in heavy rainfall (Nel, 2007). My soil samples were taken during December and January (summer), leading to the possibility of soil loss from the layer of soil, thus potentially affecting my soil samples.

It is known that the UDP burns firebreaks annual, which can be seen in the NBR results, and has produced a mosaic patchiness prescribed burning regime (EKZNW, 2012). Prescribed burns are usually of low to moderate severity and intensity (Certini, 2005). However, it cannot be assume that all the burnt grasslands were of low to moderate severity. Soil and fire variability was highlighted in the literature review. The annual fire reports in the UDP, note there is a large amount of non-scheduled burning, including large areas of where arson has been responsible for fires (Table 2.1). Therefore, the intensity and severity of the burning on the soil sampling sites are unknown. Since it is known that a patch mosaic burn regime (small patches) is implemented in the UDP (EKZNW, 2012), even landscapes right next to each other could have different burn types, noting the high inter- and intra-variability (Alcañiz *et al.*, 2018) that can occur in the UDP.

The low fire frequency sites did not all burn in the same period over the last 20 years (Table 4.6). Therefore, there is a variety of time since burn, meaning different sites have had a variety of recovery times. This adds to the factors that could affect soil properties, with soil properties such as SOM having been noted to change over time after a fire (Pereira *et al.*, 2014). Additionally, there was monthly variation as burning takes place from May through to October (Figure 5.5).

### 6.3.3 Overview

This study showed an overview of soils across the UDP. This research highlights the complexity of the UDP landscape and the variety of different effects that fires can have on a range environmental factors. The literature showed the varying responses of soil properties to fires across a variety of landscapes (Kennard and Gholz, 2001; González-Pérez *et al.*, 2004; Certini, 2005; Novara *et al.*, 2013; Pereira *et al.*, 2014; Zavala *et al.*, 2014; Alcañiz *et al.*, 2018). These differences were evident across the UDP. Due to the variation in soil sampling sites (inter- and intra-variation) and environmental factors across the UDP, the results were too varied to confirm the effects of fire frequency on soil properties. Manson *et al.*'s (2007) investigation of the effects of burning on soil properties in moist montane grasslands on the Brotherton trial at Cathedral Peak, concluded that the resulting soil properties were not large enough to be play a role in influencing fire management decisions in the Drakensberg. This is highlighted by the fact that there are a lot of vegetation studies of fire and limited soils studies in the UDP (Bijker *et al.*, 2001; Manson *et al.*, 2007). However, soil properties are important to investigate due their importance in vegetation health thus promoting biodiversity (Mills and Fey, 2004; Alcañiz *et al.*, 2018).

It is evident that the effects of fire on soil properties are site specific and need to be looked at in each individual area, such as at the experimental burning plots in the UDP, including the Brotherton burning trial at Cathedral Peak (Manson *et al.*, 2007), and the Cathedral Peak research catchments (Everson and Everson, 2016). It is challenging to make a generalised statement across the whole UDP. An improved method to test soil comparisons would be to take samples before the fire and then after the fire from the same site (Novara *et al.*, 2013). There were no baseline soil results to compare the soil results to. In order to build up a knowledge base of the effects of fire on soil in the UDP, a long-term study is needed.

Therefore, this suggests using a fire management approach that uses management at a finer scale that groups areas together based on environmental factors and implementing a burning regime that compliments those environmental conditions. This will promote conserving maximum biodiversity and promote conservation. Remote sensing and GIS would complement implementing this approach.

## CHAPTER 7: CONCLUSIONS

---

The significant role and dominant presence of fires in the fire-climax grasslands of the UDP, allowed for the opportunity to investigate the effectiveness of using remote sensing to access fires, and investigate the effects of fires on soils, a vital element to promoting vegetation health and upholding the significant biodiversity in the UDP. The literature showed that while fires have been thoroughly studied for a number of decades in the UDP, there were no studies accessing fires in the UDP using remote sensing and there were limited studies on the effects of fire on soils in the UDP (Bijker *et al.*, 2001; Manson *et al.*, 2007). Given the significance of the UDP as a biodiversity hotspot with the flora and fauna species richness, and cultural importance (Holmes, 2011), combined with the abilities of remote sensing to provide spatial and temporal information about fires that could improve monitoring methods (Gross *et al.*, 2009) in the UDP. This study aimed to investigate the spatial and temporal frequency of fires, using remote sensing, and to investigate the effect of fire frequency on soil properties in the UDP. The objectives of this study were to use remote sensing to determine the frequency and spatial extent of fires, evaluate the effectiveness of implementing remote sensing in the UDP, and to evaluate the effects of fire frequency on selected soil properties. Therefore, remote sensing provided the spatial and temporal fire information to investigate the effects of fire frequency on soils at the site level across the UDP. All the objectives were achieved and provided an overview of fires and soils across the UDP.

The MODIS and VIIRS active fire data and Landsat imagery were successful in determining the frequency and spatial extent of fires in the UDP. The UDP has a high fire frequency and the dominant fire season is from May to October, with large areas of annual burn scar ranging from 22.5% to 57.67% of the UDP annually. VIIRS active fire data performed better than MODIS active fire data and therefore should be used for continued active fire monitoring in the UDP. The Landsat imagery was limited at the site scale due to the 30 m spatial resolution and 16-day revisit period, but was successful at detecting and accessing burn scar using a NBR from the available images across the whole UDP. The NBR results highlighted the mosaic burning pattern implemented in the UDP (EKZNW, 2012). Using the remote sensing fire data for fieldwork soil sample collections highlighted the importance of ground-truthing remote sensing data. The limited spatial resolution of the MODIS, VIIRS and Landsat data used in this study is not ideal for site scale investigations. This study highlighted the benefit of using a combination of satellites to investigate fires and the power and potential of using free open sourced satellite data. MODIS and VIIRS active fire data provided high temporal resolution and Landsat provided high spatial resolution. The remote sensing data provided fire data information across the UDP that decades of fire studies in the UDP have not produced. The nature of remote sensing data

will offer an ideal monitoring tool for the flexible and variable approach to fire management in the UDP (EKZNW, 2012). Remote sensing was shown to be a valuable addition to investigating both the temporal and spatial extent of fires in the UDP.

The investigation into the effects of fire frequency on soils in the UDP results showed the selected soil properties (HP and HSV, soil pH and SOM) to be highly variable across the whole UDP and to show no clear differences in soil properties specifically due to fire. Out of the four soil properties measured, SOM had the strongest influence on burn, however was not significant across all statistical tests. Therefore, due to the many influencing factors across the UDP, including environmental factors and fire regime information (Certini, 2005; Novara *et al.*, 2013; Pereira *et al.*, 2014; Zavala *et al.*, 2014), it is not possible to conclude that the differing soil properties were due to fire frequency alone. The environmental factors with the important contributors to soil properties in the UDP were vegetation (including temperature and climate), geology and aspect.

This research highlights the inter- and intra-site variability across the UDP and the complexity of investigating soils, with a variety of different effects that fires can have on a range of environmental factors. Therefore, this suggests using a fire management approach that uses management at a finer scale which groups areas together based on environmental factors and implementing a burning regime that complements those environmental conditions. This will promote conserving maximum biodiversity and promote conservation. Remote sensing and GIS would complement implementing this approach.

## 7.1 FUTURE RECOMMENDATIONS

Remote sensing capabilities continually improve with higher resolution data becoming more easily accessible. Other satellite imagery with improved resolution abilities that can be used to investigate fires in the UDP are Sentinel-2 (spatial resolution 10 m to 60 m and revisit period of 5 to 19 days), which has been used in the UDP before (Shoko *et al.*, 2018). Sentinel-2 improves on the spatial resolution of Landsat and is freely available from the European Space Agency (ESA) website from 2015 and 2017 (Turner *et al.*, 2015). Another new imagery option and future options being Planet Labs (Planet Team, 2017). Which offer imagery options for researchers and scientists (Planet Team, 2018). Planet Lab's satellites cover the globe daily, have spatial resolutions of 3 m, 5 m and 0.72 m, and include a NIR band which promotes fire detections (Planet Team, 2018). However, given the absence of SWIR bands in the imagery supplied by Planet Labs, NBR cannot be calculated using their datasets, thereby limiting its effectiveness. However, the high spatial and temporal resolution and near-real time nature of the data will be beneficial for fire detection and fire spatial extent. Remote sensing capabilities have been investigated to go beyond just fire detection and burn scar mapping to access

the extent of surface changes (Lentile *et al.*, 2006). A dNBR uses pre and post-fire NBR values to assess burn severity (Lentile *et al.*, 2006; Roy *et al.*, 2006; Escuin *et al.*, 2008; Morgan *et al.*, 2014). This can further remote sensing fire investigations to look at burn severity in the UDP.

Investigating the effects of fires on soil properties requires a long-term study where the same sites are used for soil sampling over a period of time. This will enable consistent environmental factors for comparisons and create baseline data for soil studies in the UDP.

## REFERENCES

---

- Acocks, J.P.H. 1953. Veld types of South Africa. *Memoirs of the Botanical Survey of South Africa*, 28: 1-192.
- Afifi, A., May, S. and Clark, V.A. 2012. *Practical Multivariate Analysis* (fifth edition). Boca Raton: Taylor and Francis Group.
- Alcañiz, M., Outerio, L., Francos, M. and Úbeda, X. 2018. Effects of prescribed fires on soil properties: A review. *Science of the Total Environment*, 613-614: 944-957.
- Alijani, Z. and Sarmadian, F. 2013. Predicting soil map using Jenny equation. *Journal of Biodiversity and Environmental Sciences*, 3(12): 125-134.
- Archibald, S., Scholes, R.J., Roy, D.P., Roberts, G. and Boschetti, L. 2010. Southern African fire regimes as revealed by remote sensing. *International Journal of Wildland Fire*, 19: 861-878.
- Arnott, W.L. 2006. *The effect of burning frequency on invertebrate and indigenous flowering forb diversity in a Drakensberg grassland ecosystem*. Pietermaritzburg: University of KwaZulu-Natal. (MSc Dissertation) [pdf].
- Bachinger, L.M. Brown, L.R. and van Rooyen, M.W. 2016. The effects of fire-breaks on plant diversity and species composition in the grasslands of the Loskop Dam Nature Reserve, South Africa. *African Journal of Range and Forage Science*, 33(1): 21-32.
- Bainbridge, W.R. 1999. *Nomination Proposal for the Drakensberg Park*. Alternatively known as uKhahlamba Park to be listed as a World Heritage Site. Prepared by the KwaZulu-Natal Nature Conservation Services and Amafa.
- Bainbridge, W.R. and Scott, D.F. 1981. *Policy Memorandum for the Drakensberg State Forests*. Department report, Department of Environmental Affairs and Fisheries.
- Bakker, H.-P. 2018. Statistician, Rhodes University. Personal Communication. June 2018.
- Barbosa, P.M., Stroppiana, D., Grégoire, J.-M. and Pereira, J.M.C. 1999. An assessment of vegetation fire in Africa (1981-1991): Burned areas, burned biomass, and atmospheric emissions. *Global Geochemical Cycles*, 13(4): 933-950.
- Barsi, J.A., Lee, K., Kvaran, G., Markham, B.L. and Pedelty, J.A. 2014. The Spectral Response of the Landsat-8 Operational Land Imager. *Remote Sensing*, 6(10): 10232-10251.
- Bijker, H.J., Sumner, P.D., Meiklejohn, K.I. and Bredenkamp, G.J. 2001. Documenting the Effects of Veld Burning on Soil and Vegetation Characteristics in Giant's Castle Game Reserve, KwaZulu-Natal Drakensberg. *South African Geographical Journal*, 83(1): 28-33.
- Blott, S.J. 2010. *Gradistat Version 8.0. A Grain Size Distribution and Statistics Package for the Analysis of Unconsolidated Sediments by Sieving or Laser Granulometer*. Berkshire, UK: Kenneth Pye Associates Ltd.



- Blott, S.J. and Pye, K. 2001. Gradistat: A Grain Size Distribution and Statistics Package for the Analysis of Unconsolidated Sediments. *Earth Surface Processes and Landforms*, 26: 1237-1248.
- Blott, S.J. and Pye, K. 2006. Particle size distribution analysis of sand-sized particles by laser diffraction: an experimental investigation of instrument sensitivity and the effects of particle shape. *Sedimentology*, 53: 671-685.
- Bond, W.J., Midgley, G.F. and Woodward, F.I. 2003. What controls South Africa vegetation – climate or fire? *South African Journal of Botany*, 69(1): 79-91.
- Briggs, D. 1977. Sources and Methods in Geography: Sediments. Butterworth, London.
- Bristow, D. 2010. *Best Walks of the Drakensberg (fifth edition)*. Cape Town: Struik Travel and Heritage.
- Buthelezi, N.L.P., Mutanga, O., Rouget, M. and Sibanda, M. 2016. A spatial and temporal assessment of fire regimes on different vegetation types using MODIS burnt area products. *Bothalia*, 46(2): 1-9.
- Certini, G. 2005. Effects of fire on properties of forest soils: a review. *Oecologia*, 143(1): 1-10.
- Certini, G. 2014. Fire as a Soil-Forming Factor. *Ambio*, 43: 191-195.
- Chen, W., Moriya, K., Sakai, T., Koyama, L. and Cao, C.X. 2016. Mapping a burned forest area from Landsat TM data by multiple methods. *Geomatics, Natural Hazards and Risk*, 7(1): 384-402.
- Chuvieco, E. and Kasischke, E.S. 2007. Remote sensing information for fire management and fire effects assessment. *Journal of Geophysical Research*, 112(G01S90): 1-8.
- Congalton, R.G. 1991. A Review of Assessing the Accuracy of Classifications of Remotely Sensed Data. *Remote Sensing of Environment*, 37: 35-46.
- Corbane, C., Lang, S., Pipkins, K., Alleaume, S., Deshayes, M., Millán, V.E.G., Strasser, T., Borre, J.V., Toon, S. and Michael, F. 2015. Remote sensing for mapping natural habitats and their conservation status – New opportunities and challenges. *International Journal of Applied Earth Observation and Geoinformation*, 37: 7-16.
- Council for Geoscience. n.d. 1:250000 geology map of South Africa. Geological Survey of South Africa.
- Csiszar, I.A., Morissette, J.T. and Giglio, L. 2006. Validation of Active Fire Detection From Moderate-Resolution Satellite Sensors: The MODIS Example in Northern Eurasia. *IEEE Transactions on GeoScience and Remote Sensing*, 44(7): 1757-1764.
- Dahal, H. and Routary, J.K. 2011. Identifying Associations Between Soil and Production Variations Using Linear Multiple Regression Models. *The Journal of Agricultural and Environment*, 12: 27-37.

- DEA, 2016. *GIS Data Downloads – National Land Cover Data for SA*. [Online].  
[https://egis.environment.gov.za/data\\_egis/data\\_download/current](https://egis.environment.gov.za/data_egis/data_download/current). [Accessed: 15<sup>th</sup> May 2018].
- de Klerk, H. 2008. A pragmatic assessment of the usefulness of the MODIS (Terra and Aqua) 1-km active fire (MOD14A2 and MYD14A2) products for mapping fires in the fynbos biome. *International Journal of Wildland Fire*. 17: 166-178.
- de Villiers, A.D. and O'Connor, T. 2011. Effect of a single fire on woody vegetation in Catchment IX, Cathedral Peak, KwaZulu-Natal Drakensberg, following extended partial exclusion of fire. *African Journal of Range and Forage Science*, 28(3): 111-120.
- dos Santos, J.F.C., Romeiro, J.M.N., de Assis, J.B., Torres, F.T.P. and Gleriani, J.M. 2018. Potentials and limitations of remote fire monitoring in protected areas. *Science of Total Environment*, 616-617: 1347-1355.
- Edwards, D., de Vos, W.H., Hartkopt, D., Hattingh, D.J., Scheepers, J.J. and Wilby, A.F. 1983. Monitoring of veld burns using satellite imagery. *Proceedings of the Annual Congresses of the Grassland Society of Southern Africa*, 18(1): 131-134.
- Escuin, S., Navarro, R. and Fernández, P. 2008. Fire severity assessment by using NBR (Normalised Burn Ratio) and NDVI (Normalised Difference Vegetation Index) derived from Landsat TM/ETM images. *International Journal of Remote Sensing*, 29(4): 1053-1073.
- Everson, C.S. 1985. *Ecological effects of fire in the montane grasslands of Natal*. Pietermaritzburg: University of Natal (PhD Dissertation) [pdf].
- Everson, C.S. and Clarke, G.P.Y. 1987. A comparison of six methods of botanical analysis in the montane grasslands of Natal. *Vegetatio*, 73: 47-51.
- Everson, C.S. and Everson, T. 2016. The long-term effects of fire regime on primary production of montane grasslands in South Africa. *African Journal of Range and Forage Science*, 33(1): 33-41.
- Everson, C.S. and Tainton, N.M. 1984. The effect of thirty years of burning on the Highland Sourveld of Natal, *Journal of Grassland Society of Southern Africa*, 1(3): 15-20.
- Everson, T.M., Smith, F.R. and Everson, C.S. 1985. Characteristics of fire behaviour in the montane grasslands of natal. *Journal of the Grassland Society of Southern Africa*, 2(3): 13-21.
- Everitt, B.S. and Dunn, G. 2001. *Applied Multivariate Data Analysis (second edition)*. London: Arnold
- EKZNW. 2012. *uKhahlamba Drakensberg Park World Heritage Site: Integrated Management Plan*. [Online]. Available:  
[http://www.kznwildlife.com/Documents/ApprovedProtectedAreaManagementPlans/ukhahlamba\\_drakensberg\\_park\\_whs\\_imp\\_f\\_14062013.pdf](http://www.kznwildlife.com/Documents/ApprovedProtectedAreaManagementPlans/ukhahlamba_drakensberg_park_whs_imp_f_14062013.pdf). [Accessed: 1st May 2017].

- EKZNW. 2015. *Annual Integrated Report 2014/2015*. [Online]. Available: <http://www.kznwildlife.com/downloads.html>. [Accessed: 18th July 2018].
- EKZNW. 2016. *Annual Integrated Report 2015/2016*. [Online]. Available: <http://www.kznwildlife.com/downloads.html>. [Accessed: 18th July 2018].
- EKZNW. 2017. *Annual Report 2016/2017*. [Online]. Available: <http://www.kznwildlife.com/downloads.html>. [Accessed: 18th July 2018].
- Fey, M., Hughes, J., Lambrechts, J. and Dohse, T. 2010. Chapter 2. The soil groups: distribution, properties, classification, genesis and use. *In* Fey, M. (ed.). *Soils of South Africa*. Cape Town: Cambridge University Press, 17-147.
- Flasse, S.P., Trigg, S.N., Ceccato, P.N., Perryman, A.H., Hudak, A.T., Thompson, M.W., Brockett, B.H., Dramé, M., Ntabeni, T., Frost, P.E., Landman, T. and Le Roux, J.L. 2004. Chapter 8. Remote Sensing of vegetation fires and its contribution to a fire management information system. *In* Goldammer, J.G and de Ronde, C. (ed.). *Wildland Fire Management Handbook for Sub-Saharan Africa*. Global Fire Monitoring Centre (GFMC), 158-211.
- Folk, R.I. and Ward, W.C. 1957. Brazos River bar: a study in the significance of grain size parameters. *Journal of Sedimentary Petrology*, 27: 3-26.
- Forsyth, G.G., Kruger, F.J. and Le Maitre, D.C. 2010. National Veldfire Risk Assessment: Analysis of Exposure of Social, Economic and Environmental Assets to Veldfire Hazards in South Africa. CSIR Report No: CSIR/NRE/ECO/ER/2010/0023/C.
- Fynn, R.W.S., Haynes, R.J. and O'Connor, T.G. 2003. Burning causes long-term changes in soil organic matter content of a South African grassland. *Soil Biology and Biochemistry*, 35: 677-687.
- Giglio, L. 2015. *MODIS Collection 6 Active Fire Product User's Guide – Revision A*. [Online]. Available: [https://cdn.earthdata.nasa.gov/conduit/upload/3865/MODIS\\_C6\\_Fire\\_User\\_Guide\\_A.pdf](https://cdn.earthdata.nasa.gov/conduit/upload/3865/MODIS_C6_Fire_User_Guide_A.pdf) [Accessed: 20<sup>th</sup> May 2018].
- Giglio, L., Descloitres, J., Justice, C.O. and Kaufman, Y.J. 2003. An Enhanced Contextual Fire Detection Algorithm for MODIS. *Remote Sensing of Environment*, 87: 273-282.
- Giglio, L., Schroeder, W. and Justice, C.O. 2016. The collection 6 MODIS active fire detection algorithm and fire products. *Remote Sensing of Environment*, 178: 31-41.
- González-Pérez, J.A., González-Vila, F.J., Almendros, G. and Knicker, H. 2004. The effect of fire on soil organic matter – a review. *Environment International*, 30: 855-870.
- Goodwin, N.R. and Collett, L.J. 2014. Development of an automated method for mapping fire history captured in Landsat TM and ETM + time series across Queensland, Australia. *Remote Sensing of Environment*, 148: 206-221.

- Gordijn, P. 2014. How did grassland respond to fire treatments in the Cathedral Peak catchments? eNewsletter – South African Environmental Observation Network (SAEON) Grasslands-Forests-Wetlands Node.
- Grab, S. 2004. *Geology of the UDP WHS*. Unpublished report.
- Grabowski, R.C. 2014. Section 1.3.1: Measuring the shear strength of cohesive sediment in the field. In Clark, L.E. and Nield, J.M. (ed.), *Geomorphological Techniques (Online Edition)*. British Society for Geomorphology, London, UK. ISSN: 2047-0371.
- Gray, A.B., Pasternack, G.B. and Watson, E.B. 2010. Hydrogen peroxide treatment effects on the particle size distribution of alluvial and marsh sediments. *The Holocene*, 20(2): 293-301.
- Grömping, U. 2006. Relative Importance for Linear Regression in R: The Package relaimpo. *Journal of Statistical Software*, 17(1): 1-27.
- Gross, J.E., Goetz, S.J. and Cihlar, J. 2009. Application of remote sensing to parks and protected area monitoring: Introduction to the special issue. *Remote Sensing of Environment*, 113: 1343-1345.
- Hansen, M.C. and Loveland, T.R. 2012. A review of large area monitoring of land cover change using Landsat data. *Remote Sensing of Environment*, 122: 66-74.
- Harada, Y. and Inoko, A. 1977. The oxidation products formed from: Soil organic matter by hydrogen peroxide treatment. *Soil Science and Plant Nutrition*. 23(4): 513-521.
- Hernandez-Leal, P.A., Arbelo, M. and Gonzalez-Calvo, A. 2006. Fire risk assessment using satellite data. *Advances in Space Research*, 37: 741-746.
- Hill, T.R. 1996. Description, classification and ordination of the dominant vegetation communities, Cathedral Peak, KwaZulu-Natal Drakensberg. *South African Journal of Botany*, 62(5): 263-269.
- Holmes, C. 2011. *A Fire Management Environmental Decision Support System for the uKhahlamba Drakensberg Park World Heritage Site*. Pietermaritzburg: University of KwaZulu-Natal. (Master of Science) [pdf].
- Hoogsteen, M.J.J., Lantinga, E.A., Bakker, E.J., Groot, J.C.J. and Tittonell, P.A. 2015. Estimating soil organic carbon through loss of ignition: effects of ignition conditions and structural water loss. *European Journal of Soil Science*, 66: 320-328.
- Hudak, A.T., and Brockett, B.H. 2004. Mapping fire scars in a southern African savannah using Landsat imagery. *International Journal of Remote Sensing*, 25(16): 3231-3243.
- Indorante, S.J., Maatta, J.M., Hammer, R.D. and Brown, J.R. 1989. Multiple Regression Analysis of Soil Properties on Eroded and Native Deep Loess Missouri Soils. *Conference on Applied Statistics in Agriculture*, 103-115.

- Jenny, H. 1941. *Factors of Soil Formation: A System of Quantitative Pedology*. New York: McGraw-Hill.
- Jones, T.A. and Christopher, S.A. 2010. Satellite and Radar Remote Sensing of Southern Plains Grass Fires: A Case Study. *Journal of Applied Meteorology and Climatology*, 49: 2133-2146.
- Kennard, D.K. and Gholz, H.L. 2001. Effects of high- and low-intensity fires on soil properties and plant growth in a Bolivian dry forest. *Plant and Soil*, 234: 119-129.
- Killick, D.J.B. 1963. An account of the plant ecology of the Cathedral Peak area of the Natal Drakensberg. *Memoir, Botanical Survey of South Africa*, 34.
- Kim, B. 2015. *Understanding Diagnostic Plots for Linear Regression Analysis*. Online. Available: <https://data.library.virginia.edu/diagnostic-plots/>. [Accessed: 30<sup>th</sup> June 2018].
- Koutsias, N., Kalabokidis, K.D. and Allgöwer, B. 2004. Fire occurrence patterns at the landscape level: beyond positional accuracy of ignition points with kernel density estimation methods. *Natural Resource Modeling*, 17(4): 359-375.
- Koutsias, N., Balatsos, P. and Kalabokidis, K. 2014. Fire occurrence zones: kernel density estimation of historical wildfire ignitions at the national level, Greece. *Journal of Maps*, 10(4): 630-639.
- Kritikos, G., Charalambidis, A., Karteris, M. and Schroeder, M. 1995. Assessment of forest fire damages in Attiki using remote sensing and GIS techniques. *EARSeL Advances in Remote Sensing*, 4(3): 47-53.
- Krüger, S. 2006. *The Challenge of Wilderness Fire Stewardship in a Time of Change: A South African Perspective*. *International Journal of Wilderness*, 12(1): 44- 47
- Krüger, S. 2007. Wilderness Stewardship Challenges in the uKhahlamba Drakensberg Park World Heritage Site. In Watson, A., Sproull, J. and Liese, D. (ed.), *Science and stewardship to protect and sustain wilderness values: eighth World Wilderness Congress symposium*, Proceedings RMRS-P-49.
- Kruger, F.J., Forsyth, G.G., Kruger, L.M., Slater, K., Le Maitre, D.C. and Matshate, J. 2006. Classification of Veldfire Risk in South Africa for the Administration of the Legislation regarding Fire Management. In Viegas, D.X. (ed.). *Conference Proceedings: 5<sup>th</sup> International Conference on Forest Fire Research*.
- Kuha, J. 2004. AIC and BIC: Comparisons of Assumptions and Performance. *Sociological Methods & Research*, 33(2): 188-229.
- Kuntz, S. and Karteris, M. 1995. Fire risk modelling based on satellite remote sensing and GIS. *EARSeL Advances in Remote Sensing*, 4(3): 39-46.

- Langmann, B., Duncan, B., Textor, C., Trentmann, J. and van der Werf, G.R. 2009. Vegetation fire emissions and their impact on air pollution and climate. *Atmospheric Environment*, 43: 107-116.
- Lentile, L.B., Holden, Z.A., Smith, A.M.S., Falkowski, M.J., Hudak, A.T., Morgan, P., Lewis, S.A., Gessler, P.E. and Benson, N.C. 2006. Remote sensing techniques to assess active fire characteristics and post-fire effects. *International Journal of Wildland Fire*, 15: 319-345.
- Lindeman, R.H., Merenda, P.F. and Gold, R.Z. 1980. *Introduction to Bivariate and Multivariate Analysis*. Glenview, IL: Scott, Foresman and Company.
- López-García, M.J. and Caselles, V. 1991. Mapping burns and natural reforestation using thematic Mapper data. *Geocarto International*, 6(1): 31-37.
- Maloti Drakensberg Transfrontier Programme. 2012. Maloti Drakensberg Transfrontier Park: uKhahlamba Drakensberg Park World Heritage Site/Sehlabathebe National Park – Joint Management Plan. Version 1.1.
- Manson, A.D., Jewitt, D. and Short, A.D. 2007. Effects of season and frequency of burning on soils and landscape functioning in a moist montane grassland. *African Journal of Range and Forage Science*, 24(1): 9-18.
- McCarthy, T. and Rubidge, B. 2005. *The Story of Earth and Life: A southern African perspective on a 4.6-billion-year journey*. Cape Town: Struik Publishers.
- McGranahan, D.A., Archibald, S., Kirkman, K.P. and O'Connor, T.G. 2018. A native C<sub>3</sub> grass alters fuels and fire spread in montane grassland of South Africa. *Plant Ecology*, 219: 621-632.
- Mentis, M.T., Meiklejohn, M.J. and Scotcher, J.S.B. Veld burning in Giant's Castle Game Reserve, Natal Drakensberg. *Proc. Grassld. Soc. Sth. Afr.*, 9: 26-31.
- Mentis, M.T. and Rowerowe, D.T. 1979. Fire and faunal abundance and diversity in the natal Drakensberg. *Proceedings of the Annual Congresses of the Grassland Society of Southern Africa*, 14(1): 75-77.
- Miller, J.D. and Yool, S.R. 2002. Mapping forest post-fire canopy consumption in several overstory types using multi-temporal Landsat TM and ETM data. *Remote Sensing of Environment*, 82: 481-496.
- Miller, M.E., Billmire, M., Elliot, W.J., Endsley, K.A. and Robichaud, P.R. 2015. Rapid Response Tools and Datasets for Post-fire Modelling: Linking Earth Observations and Process-based Hydrological Models to Support Post-fire Remediation. *The International Archives of the Photogrammetry, Remote Sensing and Spatial Information Sciences*, XL-7/W3. 36<sup>th</sup> International Symposium on Remote Sensing of Environment, 11-15 May 2015, Berlin, Germany.

- Mills, A.J. and Fey, M.V. 2004. Declining soil quality in South Africa: effects of land use on soil organic matter and surface crusting. *South African Journal of Plant and Soil*, 21(5): 388-398.
- Morgan, P., Keane, R.E., Dillon, G.K., Jain, T.B., Hudak, A.T., Karau, E.C., Sikkink, P.G., Holden, Z.A. and Strand, E.K. 2014. Challenges of assessing fire and burn severity using field measures, remote sensing and modelling. *International Journal of Wildland Fire*, 23: 1045-1060.
- Moses, K.M. 2011. An overview of strategies to improve integrated fire management in South Africa with special reference to Fire Protection Associations. The 5<sup>th</sup> International Wildland Fire Conference, Sun City, South Africa.
- Mucina, L. and Rutherford, M.C. 2006. *The Vegetation of South Africa, Lesotho and Swaziland*. Strelitzia 19. South African National Biodiversity Institute, Pretoria. ISBN: 978-1919976-21-1.
- Munsell Colour. 2010. *Munsell Soil-Colour Charts: with genuine Munsell colour chips*. Grand Rapids, Michigan: Munsell Colour.
- NASA. 2018. *FIRMS Frequently Asked Questions - What does a MODIS active fire detection mean on the ground?* [Online]. Available: <https://earthdata.nasa.gov/faq/firms-faq> [Accessed: 20<sup>th</sup> May 2018].
- Neary, D.G., Ryan, K.C., DeBano, L.F., Landsberg, J.D. and Brown, J.K. 2005. Chapter 1: Introduction. In Neary, D.G., Ryan, K.C. and DeBano, L.F. (ed.). *Wildland fire in ecosystems: effects on fire on soil and water*. General Technical Report RMRS-GTR-42-vol.4. U.S. Department of Agriculture, Forest Service, Rocky Mountain Research Station, Ogden, UT.
- Neath, A.A. and Cavanaugh, J.E. 2012. The Bayesian information criterion: background, derivation, and applications. *Wiley Interdisciplinary Reviews Computational Statistics*, 4: 199-203.
- Nel, W. 2007. *On climate of the Drakensberg: rainfall and surface-temperature attributes and associated geomorphic effects*. Pretoria: University of Pretoria. (Doctor of Philosophy) [pdf].
- Norman, N. and Whitfield, G. 2006. *Geological journeys: A traveller's guide to South Africa's rocks and landforms*. Cape Town: Struik Publishers.
- Novara, A., Gristina, L., Rühl, J., Pasta, S., D'Angelo, G., La Mantia, T. and Pereira, P. 2013. Grassland fire effect on soil organic carbon reservoirs in a semiarid environment. *Solid Earth*, 4: 381-385.
- O'Connor, T.G., Uys, R.G. and Mills, A.J. 2004. Ecological effects of fire-breaks in the montane grasslands of the southern Drakensberg, South Africa. *African Journal of Range and Forage Science*, 21(1): 1-9.
- Oliva, P. and Schroeder, W. 2015. Assessment of VIIRS 375 m active fire detection product for direct burned area mapping. *Remote Sensing of Environment*, 160: 144-155.

- Pereira, P., Úbeda, X., Mataix-Solera, J., Oliva, M. and Novara, A. 2014. Short-term changes in soil Munsell colour value, organic matter content and soil water repellency after a spring grassland fire in Lithuania. *Solid Earth*, 5: 209-225.
- Philip, S. 2007. *Active Fire Detection Using Remote Sensing Based Polar-orbiting And Geostationary Observations: An Approach Towards Near Real-Time Fire Monitoring*. Netherlands: International Institute for Geo-information Science and Earth Observation. (MSc Dissertation) [pdf].
- Planet Team. 2017. *Planet Application Program Interface: In Space for Life on Earth*. San Francisco, CA.
- Planet Team. 2018. *Planet Imagery and Archive*. [Online]. Available: <https://www.planet.com/products/planet-imagery/>. [Accessed: 29<sup>th</sup> November 2018].
- Prins, F. 2005. Section 2. Cultural context of the UDP WHS. In EKZNW, 2012. *uKhahlamba Drakensberg Park World Heritage Site – South Africa: Integrated Management Plan*. 47-49. Cultural specialist, Maloti Drakensberg Transfrontier Project, Howick.
- Richardson, D.M., van Wilgen, B.W., Le Maitre, D.C., Higgins, K.B. and Forsyth, G.G. 1994. A Computer-Based System for Fire Management in the Mountains of the Cape Province, South Africa. *International Journal of Wildland Fire*, 4(1): 17-32.
- Robinson, K. 2014. *Assessment of the effects of fire and associated grazing on the recovery of Merxmuellera drakensbergensis in the Sani Pass region, Lesotho*. University of the Witwatersrand. (PhD Dissertation) [pdf].
- Roy, D.P., Boschetti, L. and Smith, A.M.S. 2013. Chapter 5. Satellite Remote Sensing of Fires. In Belcher, C.M. (ed.), *Fire Phenomena and the Earth System: An Interdisciplinary Guide to Fire Science*. Chichester: Wiley-Blackwell, 77-94.
- Roy, D.P., Boschetti, L. and Trigg, S.N. 2006. Remote Sensing of Fire Severity: Assessing the Performance of the Normalized Burn Ratio. *IEEE Geoscience and Remote Sensing Letters*, 3(1): 112-116.
- RStudio Team. 2015. *RStudio: Integrated Development for R*. RStudio, Inc., Boston, MA. [Online]. Available: <http://rstudio.com> [Accessed: June 2018].
- SANBI. 2012. *NBA 2011 Terrestrial Formal Protected Areas (vector geospatial dataset)*. [Online]. Available: <http://bgis.sanbi.org/SpatialDataset/Detail/412>. [Accessed: n.d.]
- SANBI. 2013. *Grasslands Ecosystem Guidelines: landscape interpretation for planners and managers*. Compiled by Cadman, M., de Villiers, C., Lechmere-Oertel, R. and McCulloch, D. South African National Biodiversity Institute, Pretoria. 139 pages.



- Santín, C. and Doerr, S.H. 2016. Fire effects on soils: the human dimension. *Philosophical Transactions of the Royal Society B*, 371, 20150171.
- Schroeder, W. and Giglio, L. 2018. *NASA VIIRS Land Science Investigator Processing System (SIPS) Visible Infrared Imaging Radiometer Suite (VIIRS) 375 m and 750 m Active Fire Products*. Product User's Guide Version 1.4.
- Schroeder, W., Oliva, P., Giglio, L. and Csiszar, I.A. 2014. The New VIIRS 375 m active fire detection data product: Algorithm description and initial assessment. *Remote Sensing of Environment*, 143: 85-96.
- Scotcher, J.S.B. and Clarke, J.C. 1981. Effects of certain burning treatments on veld conditions in giant's castle game reserve. *Proceedings of the Annual Congresses of the Grassland Society of Southern African*, 16(1): 121-127.
- Shoko, C., Mutanga, O., Dube, T. and Slotow, R. 2018. Characterizing the spatio-temporal variations of C3 and C4 dominated grasslands aboveground biomass in the Drakensberg, South Africa. *International Journal of Applied Earth Observation and Geoinformation*, 68: 51-60.
- Short, A.D., Everson, T.M. and Everson, C.S. 2003a. The effect of twenty years of burning on the species diversity and basal cover of a moist montane grassland in KwaZulu-Natal, South Africa. *Proceedings of the VII<sup>th</sup> International Rangelands Congress*, 26<sup>th</sup> July – 1<sup>st</sup> August 2003, Durban, South Africa.
- Short, A.D., O'Connor, T.G. and Hurt, C.R. 2003b. Medium-term changes in grass composition and diversity of Highland Sourveld grassland in the southern Drakensberg in response to fire and grazing management. *African Journal of Range and Forage Science*, 20(1): 1-10.
- Singh, K., Forbes, A. and Akombelwa, M. 2013. The Evaluation of High Resolution Aerial Imagery for Monitoring of Bracken Fern. *South African Journal of Geomatics*, 2(4): 296-308.
- Smith, F.R. and Tainton, N.M. 1985. Effects of season of burn on shrub survival, regeneration and structure in the Natal Drakensberg. *Journal of the Grassland Society of Southern Africa*, 2(2): 4-10.
- South Africa. 1998. *National Veld and Forest Fire Act 101 of 1998*. [Online]. Available: <http://www.gov.za/sites/www.gov.za/files/a101-98.pdf>. [Accessed: 25 May 2017].
- Strydom, S. and Savage, M.J. 2016. A spatio-temporal analysis of fires in South Africa. *South African Journal of Science*, 112 (11-12).
- Tanpipat, V., Honda, K. and Nuchaiya, P. 2009. MODIS Hotspot Validation over Thailand. *Remote Sensing*, 1: 1043-1054.

- Titshall, L.W., O'Connor, T.G. and Morris, C.D. 2000. Effect of long-term exclusion of fire and herbivory on the soils and vegetation of sour grassland. *African Journal of Range and Forage Science*, 17(1-3): 70-80.
- Trollope, W.S.W. 1978. Fire behaviour – A preliminary study. *Proceedings of the Annual Congresses of Grassland Society of Southern Africa*, 13(1): 123-128.
- Trollope, W.S.W. 1981. Recommended terms, definitions and units to be used in fire ecology in South Africa. *Proceedings of the Annual Congresses of the Grassland Society of Southern Africa*, 16(1): 107-109.
- Turner, W., Rondinini, C., Pettorelli, N., Mora, B., Leidner, A.K., Szantoi, Z., Buchanan, G., Dech, S., Dwyer, J., Herold, M., Koh, L.P., Leimgruber, P., Taubenboeck, H., Wegmann, M., Wikelski, M. and Woodcock, C. 2015. Free and open-access satellite data are key to biodiversity conservation. *Biological Conservation*, 182: 173-176.
- Udden, J.A. 1914. Mechanical composition of clastic sediments. *Bulletin of the Geological Society of America*, 25: 655-744.
- UNESCO. 2017. *Maloti-Drakensberg Park*. [Online]. Available: <http://whc.unesco.org/en/list/985>. [Accessed: 23 May 2017].
- U.S. Geological Survey. 2016. *Landsat – Earth Observation Satellites (version 1.1)*. U.S. Geological Survey Fact Sheet 2015 – 3081. [Online]. Available: <https://pubs.usgs.gov/fs/2015/3081/fs20153081.pdf>. [Accessed: 20<sup>th</sup> May 2018].
- U.S. Geological Survey. 2017. Landsat Collection 1 Level Product Definition. Version 1.0. Earth Resources Observation and Science (EROS), Sioux Falls, South Dakota. Document Number LSDS-1656.
- U.S. Geological Survey. 2018. *What are the band designations for the Landsat satellites?* [Online]. Available: <https://landsat.usgs.gov/what-are-band-designations-landsat-satellites>. [Accessed: 20<sup>th</sup> May 2018].
- Uys, C. and Hamer, M. 2007. The effect of long-term fire treatments on invertebrates: results from experimental plots at Cathedral Peak, South Africa. *African Journal of Range and Forage Science*, 24(1): 1-7.
- Vorster, W.A. 2013. *Assessment and Analysis of Wildfires with the aid of Remote Sensing and GIS*. University of South Africa. (MSc Dissertation) [pdf].
- Weaver, A. 1990. *Techniques for Soil Analysis*. Rhodes University, Department of Geography. Revised by: Glyn Armstrong and Kate Rowntree (1992).
- Weil, R.R. and Brady, N.C. 2017. *The Nature and Properties of Soils* (fifteenth edition, global edition). Harlow: Pearson.

Wentworth, C.K. 1922. A scale of grade and class terms for clastic sediments. *Journal of Geology*, 30: 377-392.

Zavala, L.M., de Celis, R. and Jordán, A. 2014. How wildfires affect soil properties. A brief review. *Cuadernos de Investigación Geográfica*, 40(2): 311-331.

# APPENDICES

## APPENDIX A: SOIL DATA

Table 9.1. All soil data in the UDP.

Area - Sampling date	Site	Sample Number	Co-ordinates (Decimal Degrees)		Fire Frequency	Geology	Aspect	Vegetation	Elevation (m.a.s.l)	Slope (°)	Hand shear vane (kPa)	Hand Penetrometer (kPa)	Soil Moisture (%)	pH	Soil Organic Matter (%)
			East	South											
Bushman's Nek (BN)  Southern Drakensberg (31/12/2017)	1	1	29,20196	-29,84487	High	Tarkastad	North	Southern Drak Highland Grassland	1778,12	5,70	140	4200	19,11	3,88	9,76
	1	2	29,20174	-29,84483	High	Tarkastad	North	Southern Drak Highland Grassland	1777,97	6,02	38	900	68,45	3,87	23,64
	1	3	29,20184	-29,84468	High	Tarkastad	North	Southern Drak Highland Grassland	1776,04	5,57	25	900	59,96	3,59	17,26
	1	4	29,20204	-29,84473	High	Tarkastad	North	Southern Drak Highland Grassland	1778,23	5,45	46	2200	65,74	4,1	23,29
	1	5	29,2019	-29,84479	High	Tarkastad	North	Southern Drak Highland Grassland	1778,12	5,70	56	1800	59,89	3,69	18,65
	2	6	29,20795	-29,84411	Low	Tarkastad	North	Drak Foothill Moist Grassland	1768,84	5,38	76	2400	49,62	4,34	13,40
	2	7	29,20814	-29,84411	Low	Tarkastad	North	Drak Foothill Moist Grassland	1768,34	5,82	84	2900	41,84	4,18	11,29
	2	8	29,20819	-29,84427	Low	Tarkastad	North	Drak Foothill Moist Grassland	1769,93	7,44	64	2700	37,27	4,13	8,91
	2	9	29,20802	-29,84428	Low	Tarkastad	North	Drak Foothill Moist Grassland	1770,47	6,61	58	2300	37,57	4,08	9,77
	2	10	29,20806	-29,8442	Low	Tarkastad	North	Drak Foothill Moist Grassland	1768,34	5,82	55	2200	39,28	4,09	9,65
Garden Castle (GC)  Southern Drakensberg (29/12/2017, 04/01/2018)	3	11	29,21858	-29,75692	High	Molteno	North	Southern Drak Highland Grassland	1840,00	3,40	21	1800	152,44	3,18	43,38
	3	12	29,21845	-29,75702	High	Molteno	North	Southern Drak Highland Grassland	1841,11	3,16	20	1200	224,22	3,35	44,38
	3	13	29,21829	-29,75689	High	Molteno	North	Southern Drak Highland Grassland	1840,00	3,45	26	1800	279,71	3,41	51,01
	3	14	29,21844	-29,75678	High	Molteno	North	Southern Drak Highland Grassland	1840,00	3,45	14	1500	248,62	3,83	49,17
	3	15	29,21844	-29,7569	High	Molteno	North	Southern Drak Highland Grassland	1840,00	3,45	20	1200	202,58	3,39	38,06
	4	16	29,1997	-29,74198	Low	Molteno	North	Southern Drak Highland Grassland	1910,68	12,61	45	1600	43,27	3,5	15,69
	4	17	29,19987	-29,74199	Low	Molteno	North	Southern Drak Highland Grassland	1910,34	13,55	66	2200	46,90	3,47	17,83
	4	18	29,19983	-29,74216	Low	Molteno	North	Southern Drak Highland Grassland	1915,24	13,53	71	2400	46,20	3,7	14,22
	4	19	29,19965	-29,74212	Low	Molteno	North	Southern Drak Highland Grassland	1915,29	13,07	50	1700	48,44	3,65	17,17
	4	20	29,19976	-29,74204	Low	Molteno	North	Southern Drak Highland Grassland	1910,34	13,55	61	1100	53,00	3,43	15,11
Cobham (CH)  Southern Drakensberg (02/01/2018)	5	21	29,41567	-29,70542	High	Karoo Dolerite	East	Drak Foothill Moist Grassland	1636,58	12,56	140	4000	46,39	3,75	19,74
	5	22	-29,41577	29,70555	High	Karoo Dolerite	East	Drak Foothill Moist Grassland	1634,87	11,73	113	3900	35,82	3,67	18,66
	5	23	29,41563	-29,70567	High	Karoo Dolerite	East	Drak Foothill Moist Grassland	1639,20	13,31	135	3600	49,25	3,83	21,60
	5	24	29,41551	-29,70552	High	Karoo Dolerite	East	Drak Foothill Moist Grassland	1643,47	15,81	125	2800	43,98	3,92	21,83
	5	25	29,41563	-29,70553	High	Karoo Dolerite	East	Drak Foothill Moist Grassland	1639,20	13,31	102	2700	60,53	3,7	21,02
	6	26	29,41336	-29,70145	Low	Karoo Dolerite	North	Drak Foothill Moist Grassland	1621,43	1,98	73	2200	49,93	4,68	20,18
	6	27	29,41336	-29,70127	Low	Karoo Dolerite	North	Drak Foothill Moist Grassland	1620,83	1,55	58	1900	38,28	3,91	18,27
	6	28	29,41361	-29,70131	Low	Karoo Dolerite	North	Drak Foothill Moist Grassland	1620,90	1,62	51	1700	57,37	4,37	21,80
	6	29	29,41355	-29,70149	Low	Karoo Dolerite	North	Drak Foothill Moist Grassland	1621,43	1,98	44	1300	64,99	3,99	26,02
	6	30	29,41349	-29,70138	Low	Karoo Dolerite	North	Drak Foothill Moist Grassland	1620,83	1,55	67	1300	44,09	4,27	12,94
Kamberg (KB)  Central Drakensberg (22/01/2018)	7	31	29,66902	-29,38495	High	Tarkastad	North	Northern Drak Highland Grassland	1716,74	6,16	133	3300	27,38	3,4	12,12
	7	32	29,66923	-29,38498	High	Tarkastad	North	Northern Drak Highland Grassland	1716,65	6,37	92	2700	32,20	3,46	14,39
	7	33	29,6692	-29,38516	High	Tarkastad	North	Northern Drak Highland Grassland	1718,67	4,94	69	2900	39,23	3,46	20,54
	7	34	29,669	-29,38512	High	Tarkastad	North	Northern Drak Highland Grassland	1718,69	4,76	140	3900	21,57	3,46	8,67
	7	35	29,66914	-29,38502	High	Tarkastad	North	Northern Drak Highland Grassland	1716,65	6,37			33,05	3,34	8,82
	8	36	29,67674	-29,37704	Low	Tarkastad	North	Drak Foothill Moist Grassland	1688,17	14,23	26	3200	31,51	3,75	12,51
	8	37	29,67693	-29,37694	Low	Tarkastad	North	Drak Foothill Moist Grassland	1683,86	10,38	53	1800	37,61	3,59	11,93
	8	38	29,67702	-29,37712	Low	Tarkastad	North	Drak Foothill Moist Grassland	1689,06	13,51	68	2800	18,07	3,19	7,70
	8	39	29,67683	-29,37719	Low	Tarkastad	North	Drak Foothill Moist Grassland	1688,17	14,23	44	1800	18,89	3,62	8,82
	8	40	29,67691	-29,37708	Low	Tarkastad	North	Drak Foothill Moist Grassland	1688,17	14,23	64	1600	30,07	3,29	10,10

<b>Giant's Castle (GI)</b> Central Drakensberg (23/01/2018)	9	41	29,52699	-29,25896	High	Elliot	North	Northern Drak Highland Grassland	1772,24	17,51	92	2200	24,05	3,86	7,68
	9	42	29,5272	-29,25893	High	Elliot	North	Northern Drak Highland Grassland	1771,23	17,04	70	2200	19,53	4,01	5,07
	9	43	29,5272	-29,25909	High	Elliot	North	Northern Drak Highland Grassland	1778,74	16,10	69	2250	25,63	4,12	9,01
	9	44	29,527	-29,2591	High	Elliot	North	Northern Drak Highland Grassland	1777,57	17,04	98	3200	24,92	4,1	7,18
	9	45	29,52709	-29,25896	High	Elliot	North	Northern Drak Highland Grassland	1772,24	17,51	107	3000	19,18	3,61	5,08
	10	46	29,52211	-29,26476	Low	Clarens	North	Northern Drak Highland Grassland	1747,43	6,88	71	2200	65,56	4,92	19,22
	10	47	29,52198	-29,26487	Low	Clarens	North	Northern Drak Highland Grassland	1747,43	6,88	75	2700	56,57	5	20,67
	10	48	29,52181	-29,26479	Low	Clarens	North	Northern Drak Highland Grassland	1747,72	6,02	72	2700	38,02	4,68	15,42
<b>Injisuthi (IN)</b> Central Drakensberg (24/01/2018)	11	51	29,43052	-29,11562	High	Elliot	East	Drak Foothill Moist Grassland	1562,53	4,03	68	2200	29,46	3,97	18,40
	11	52	29,43065	-29,11574	High	Elliot	East	Drak Foothill Moist Grassland	1561,32	4,15	74	2400	31,45	3,78	16,86
	11	53	29,43054	-29,11588	High	Elliot	East	Drak Foothill Moist Grassland	1563,12	3,19	100	3000	42,15	4,3	18,19
	11	54	29,43039	-29,11576	High	Elliot	East	Drak Foothill Moist Grassland	1562,53	4,03	70	3000	37,60	4,6	16,36
	11	55	29,43053	-29,11575	High	Elliot	East	Drak Foothill Moist Grassland	1562,53	4,03	66	2800	34,64	3,71	13,68
	12	56	29,43464	-29,11432	Low	Tarkastad	South	Drak Foothill Moist Grassland	1472,92	1,52	21	1100	30,63	5,06	14,71
	12	57	29,43481	-29,11442	Low	Tarkastad	South	Drak Foothill Moist Grassland	1473,72	1,48	59	1600	33,44	4,92	11,57
	12	58	29,43468	-29,11446	Low	Tarkastad	East	Drak Foothill Moist Grassland	1473,44	1,48	21	1400	23,83	4,87	7,79
	12	59	29,4345	-29,11447	Low	Tarkastad	South	Drak Foothill Moist Grassland	1472,20	1,40	34	1000	17,12	4,79	8,02
	12	60	29,43464	-29,11444	Low	Tarkastad	South	Drak Foothill Moist Grassland	1472,92	1,52	27	1200	15,18	5,07	6,36
<b>Monks Cowl (MC)</b> Northern Drakensberg (25/01/2018)	13	61	29,40212	-29,04003	High	Tarkastad	North	Drak Foothill Moist Grassland	1400,03	11,98	64	2400	37,14	3,75	13,08
	13	62	29,4023	-29,03996	High	Tarkastad	North	Drak Foothill Moist Grassland	1393,52	12,02	93	2600	35,09	3,78	11,61
	13	63	29,40242	-29,04008	High	Tarkastad	North	Drak Foothill Moist Grassland	1400,24	12,11	97	2050	33,22	3,95	12,52
	13	64	29,40222	-29,04016	High	Tarkastad	North	Drak Foothill Moist Grassland	1402,33	12,02		2300	29,06	3,51	10,59
	13	65	29,40227	-29,04006	High	Tarkastad	North	Drak Foothill Moist Grassland	1400,03	11,98	44	2600	34,11	3,62	10,89
	14	66	29,40116	-29,04285	Low	Tarkastad	North	Drak Foothill Moist Grassland	1402,55	9,06	56	2050	47,99	3,85	12,83
	14	67	29,40099	-29,04274	Low	Tarkastad	North	Drak Foothill Moist Grassland	1401,85	6,91	48	2300	45,57	3,97	15,41
	14	68	29,40107	-29,04256	Low	Tarkastad	North	Drak Foothill Moist Grassland	1400,00	3,74	80	3200	40,69	3,86	18,30
	14	69	29,40128	-29,04264	Low	Tarkastad	North	Drak Foothill Moist Grassland	1399,99	4,92	32	1600	59,66	4,62	20,51
<b>Cathedral Peak (CP)</b> Northern Drakensberg (26/01/2018)	15	71	29,21259	-28,94789	High	Molteno	North	Drak Foothill Moist Grassland	1472,44	14,45	49	2300	15,93	3,68	5,24
	15	72	29,21279	-28,94785	High	Molteno	North	Drak Foothill Moist Grassland	1472,23	14,56	57	2100	25,56	4,12	8,78
	15	73	29,21284	-28,94799	High	Molteno	North	Drak Foothill Moist Grassland	1476,28	9,33	43	1300	16,42	4,1	5,82
	15	74	29,21263	-28,94806	High	Molteno	North	Drak Foothill Moist Grassland	1476,45	9,09	58	2500	12,28	3,83	5,49
	15	75	29,21271	-28,94795	High	Molteno	North	Drak Foothill Moist Grassland	1472,23	14,56	70	1900	18,67	3,62	4,92
	16	76	29,21204	-28,94922	Low	Molteno	North	Drak Foothill Moist Grassland	1492,85	19,76	35	2000	33,37	4,38	8,22
	16	77	29,21227	-28,94918	Low	Molteno	North	Drak Foothill Moist Grassland	1493,17	18,94	90	1700	30,00	3,81	11,90
	16	78	29,21229	-28,94932	Low	Molteno	North	Drak Foothill Moist Grassland	1500,12	17,97	96	2600	26,03	3,81	10,43
	16	79	29,21212	-28,9494	Low	Molteno	North	Drak Foothill Moist Grassland	1500,12	17,97		2000	28,33	3,69	7,96
<b>Royal Natal (RN)</b> Northern Drakensberg (27/01/2018)	17	81	28,9915	-28,66676	High	Karoo Dolerite	East	Northern KZN Moist Grassland	1373,98	10,34	69	3200	17,83	3,46	7,87
	17	82	28,99137	-28,66662	High	Karoo Dolerite	East	Northern KZN Moist Grassland	1375,52	9,67	85	1500	18,83	3,76	9,16
	17	83	28,99151	-28,6665	High	Karoo Dolerite	East	Northern KZN Moist Grassland	1372,30	10,75	112	2900	21,71	3,66	10,42
	17	84	28,99165	-28,66663	High	Karoo Dolerite	East	Northern KZN Moist Grassland	1372,30	10,75	96	2600	24,35	3,73	9,40
	17	85	28,99152	-28,66664	High	Karoo Dolerite	East	Northern KZN Moist Grassland	1373,98	10,34	101	2400	21,57	3,48	7,46

Table 9.2. Soil colour for all soil samples in the UDP using the Munsell colour chart

Area - Sampling date	Site	Sample Number	Colour	
			Munsell chart code	Name
Bushman's Nek (BN)  Southern Drakensberg (31/12/2017)	1	1	10YR 3/3	Dark brown
	1	2	10YR 3/1	Very dark gray
	1	3	10YR 3/1	Very dark gray
	1	4	10YR 2/1	Black
	1	5	10YR 2/1	Black
	2	6	10YR 4/2	Dark grayish brown
	2	7	10YR 4/2	Dark grayish brown
	2	8	10YR 4/2	Dark grayish brown
	2	9	10YR 4/2	Dark grayish brown
	2	10	10YR 3/1	Very dark gray
Garden Castle (GC)  Southern Drakensberg (29/12/2017, 04/01/2018)	3	11	10YR 2/1	Black
	3	12	10YR 2/1	Black
	3	13	10YR 2/1	Black
	3	14	10YR 2/1	Black
	3	15	2.5Y 2.5/1	Black
	4	16	10YR 3/2	Very dark grayish brown
	4	17	10YR 3/2	Very dark grayish brown
	4	18	10YR 3/2	Very dark grayish brown
	4	19	10YR 3/2	Very dark grayish brown
	4	20	10YR 3/2	Very dark grayish brown
Cobham (CH)  Southern Drakensberg (02/01/2018)	5	21	10YR 3/2	Very dark grayish brown
	5	22	10YR 4/3	Brown
	5	23	10YR 3/3	Dark brown
	5	24	10YR 3/3	Dark brown
	5	25	10YR 3/2	Very dark grayish brown
	6	26	10YR 4/3	Brown
	6	27	10YR 4/3	Brown
	6	28	10YR 4/3	Brown
	6	29	10YR 4/3	Brown
	6	30	10YR 4/3	Brown
Kamberg (KB)  Central Drakensberg (22/01/2018)	7	31	10YR 3/2	Very dark grayish brown
	7	32	10YR 3/2	Very dark grayish brown
	7	33	10YR 3/2	Very dark grayish brown
	7	34	10YR 4/3	Brown
	7	35	10YR 4/2	Dark grayish brown
	8	36	10YR 3/2	Very dark grayish brown
	8	37	10YR 4/3	Brown
	8	38	10YR 4/3	Brown
	8	39	10YR 4/3	Brown
	8	40	10YR 3/2	Very dark grayish brown
Giant's Castle (GI)  Central Drakensberg (23/01/2018)	9	41	10YR 4/4	Dark yellowish brown
	9	42	10YR 4/4	Dark yellowish brown
	9	43	10YR 4/4	Dark yellowish brown
	9	44	10YR 4/4	Dark yellowish brown
	9	45	7.5 YR 4/4	Brown
	10	46	10YR 3/3	Dark brown
	10	47	10YR 3/3	Dark brown
	10	48	10YR 3/3	Dark brown
	10	49	7.5 YR 3/4	Dark brown
	10	50	7.5 YR 3/4	Dark brown
Injisuthi (IN)  Central Drakensberg (24/01/2018)	11	51	10YR 3/4	Dark yellowish brown
	11	52	10YR 3/3	Dark brown
	11	53	10YR 3/3	Dark brown
	11	54	10YR 3/3	Dark brown
	11	55	10YR 3/3	Dark brown
	12	56	10YR 3/1	Very dark gray
	12	57	10YR 3/1	Very dark gray
	12	58	10YR 3/2	Very dark grayish brown
	12	59	10YR 3/2	Very dark grayish brown
	12	60	10YR 4/2	Dark grayish brown
Monks Cowl (MC)  Northern Drakensberg (25/01/2018)	13	61	10YR 4/3	Brown
	13	62	10YR 4/3	Brown
	13	63	10YR 4/3	Brown
	13	64	10YR 4/3	Brown
	13	65	10YR 4/4	Dark yellowish brown
	14	66	10YR 3/2	Very dark grayish brown
	14	67	10YR 3/2	Very dark grayish brown
	14	68	10YR 3/2	Very dark grayish brown
	14	69	10YR 3/2	Very dark grayish brown
	14	70	10YR 3/2	Very dark grayish brown
Cathedral Peak (CP)  Northern Drakensberg (26/01/2018)	15	71	10YR 4/4	Dark yellowish brown
	15	72	10YR 4/3	Brown
	15	73	10YR 4/3	Brown
	15	74	10YR 4/4	Dark yellowish brown
	15	75	10YR 4/4	Dark yellowish brown
	16	76	10YR 4/3	Brown
	16	77	10YR 4/3	Brown
	16	78	10YR 3/2	Very dark grayish brown
	16	79	10YR 5/3	Brown
	16	80	10YR 4/3	Brown
Royal Natal (RN)  Northern Drakensberg (27/01/2018)	17	81	7.5 YR 4/4	Brown
	17	82	10YR 4/4	Dark yellowish brown
	17	83	10YR 4/4	Dark yellowish brown
	17	84	10YR 4/4	Dark yellowish brown
	17	85	7.5 YR 4/4	Brown

Table 9.3. Particle size values (% sand, silt and clay) for all soil samples in the UDP.

Area - Sampling date	Site	Sample Number	Particle size (%)								
			Sand	Silt	Clay						
Bushman's Nek (BN)  Southern Drakensberg (31/12/2017)	1	1	30,33	54,16	15,50	Injisuthi (IN)  Central Drakensberg (24/01/2018)	11	51	15,72	57,50	26,78
	1	2	14,97	70,94	14,09		11	52	10,73	59,63	29,64
	1	3	19,57	69,60	10,83		11	53	16,52	57,78	25,70
	1	4	18,66	67,80	13,54		11	54	18,33	56,06	25,61
	1	5	14,59	66,99	18,41		11	55	22,01	52,60	25,39
	2	6	22,05	65,12	12,82		12	56	23,50	69,29	7,21
	2	7	17,28	66,88	15,84		12	57	21,16	68,96	9,88
	2	8	23,12	63,04	13,84		12	58	40,71	54,92	4,38
	2	9	14,84	70,51	14,65		12	59	43,09	50,47	6,45
	2	10	15,72	66,31	17,96		12	60	36,03	56,99	6,98
Garden Castle (GC)  Southern Drakensberg (29/12/2017, 04/01/2018)	3	11	9,39	77,56	13,05	Monks Cowl (MC)  Northern Drakensberg (25/01/2018)	13	61	24,92	55,34	19,74
	3	12	8,83	78,73	12,44		13	62	29,14	53,98	16,88
	3	13	8,77	80,40	10,82		13	63	22,13	55,77	22,11
	3	14	9,46	79,52	11,02		13	64	25,55	56,00	18,45
	3	15	10,47	73,29	16,24		13	65	24,73	53,05	22,21
	4	16	10,94	69,70	19,36		14	66	13,36	63,81	22,82
	4	17	10,19	72,54	17,27		14	67	15,32	63,57	21,12
	4	18	12,27	69,26	18,48		14	68	6,82	65,90	27,28
	4	19	19,20	64,24	16,56		14	69	8,93	70,09	20,98
	4	20	5,74	69,95	24,31		14	70	12,62	62,22	25,15
Cobham (CH)  Southern Drakensberg (02/01/2018)	5	21	9,16	61,17	29,68	Cathedral Peak (CP)  Northern Drakensberg (26/01/2018)	15	71	34,03	54,82	11,15
	5	22	3,95	61,44	34,61		15	72	30,39	55,78	13,83
	5	23	4,91	64,38	30,70		15	73	36,35	50,86	12,78
	5	24	4,55	64,41	31,04		15	74	33,69	55,42	10,89
	5	25	1,18	68,72	30,11		15	75	40,18	48,88	10,93
	6	26	3,98	68,21	27,81		16	76	8,59	76,90	14,51
	6	27	9,06	65,78	25,16		16	77	15,09	64,76	20,15
	6	28	0,82	66,67	32,51		16	78	10,30	70,85	18,85
	6	29	4,63	72,60	22,77		16	79	6,96	81,33	11,71
	6	30	12,03	61,37	26,60		16	80	9,18	75,80	15,03
Kamberg (KB)  Central Drakensberg (22/01/2018)	7	31	16,32	64,79	18,89	Royal Natal (RN)  Northern Drakensberg (27/01/2018)	17	81	22,34	56,63	21,02
	7	32	17,33	64,78	17,89		17	82	24,34	58,06	17,61
	7	33	7,32	69,29	23,39		17	83	10,33	67,49	22,18
	7	34	15,44	68,95	15,62		17	84	15,03	64,79	20,19
	7	35	11,72	70,12	18,15		17	85	25,33	57,39	17,27
	8	36	7,85	66,77	25,38						
	8	37	14,08	64,79	21,13						
	8	38	14,05	65,76	20,19						
	8	39	18,64	65,31	16,04						
	8	40	18,50	61,00	20,51						
Giant's Castle (GI)  Central Drakensberg (23/01/2018)	9	41	19,07	65,74	15,19						
	9	42	23,60	61,65	14,75						
	9	43	21,46	62,83	15,71						
	9	44	35,38	51,68	12,94						
	9	45	19,40	63,86	16,74						
	10	46	16,84	61,61	21,55						
	10	47	12,08	63,14	24,78						
	10	48	17,25	58,98	23,77						
	10	49	13,16	60,24	26,61						
	10	50	11,22	60,03	28,74						

## APPENDIX B: SOIL DATA GRAPHS

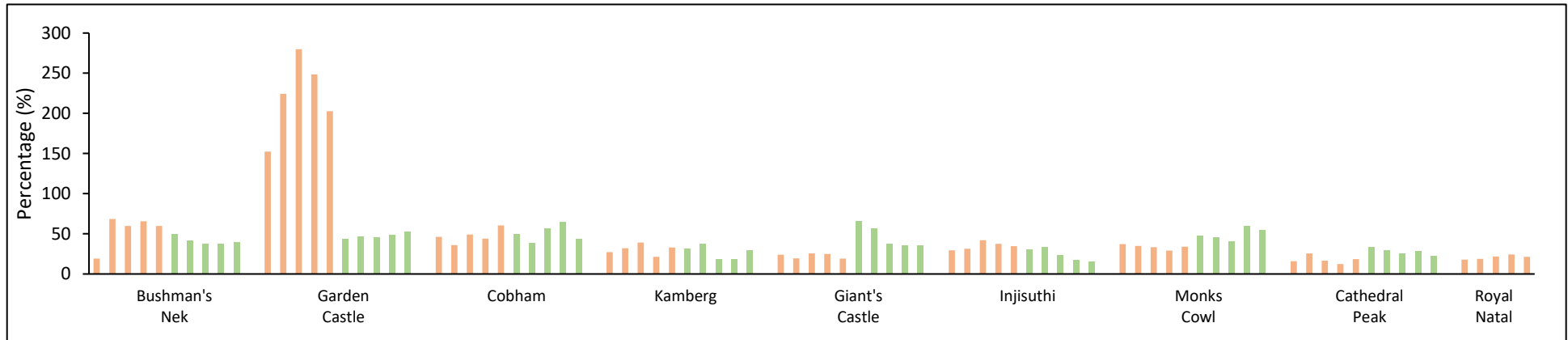


Figure 9.1. Soil moisture values (%) for all sites in the UDP. Orange represents high fire frequency sites and green represents low fire frequency sites.

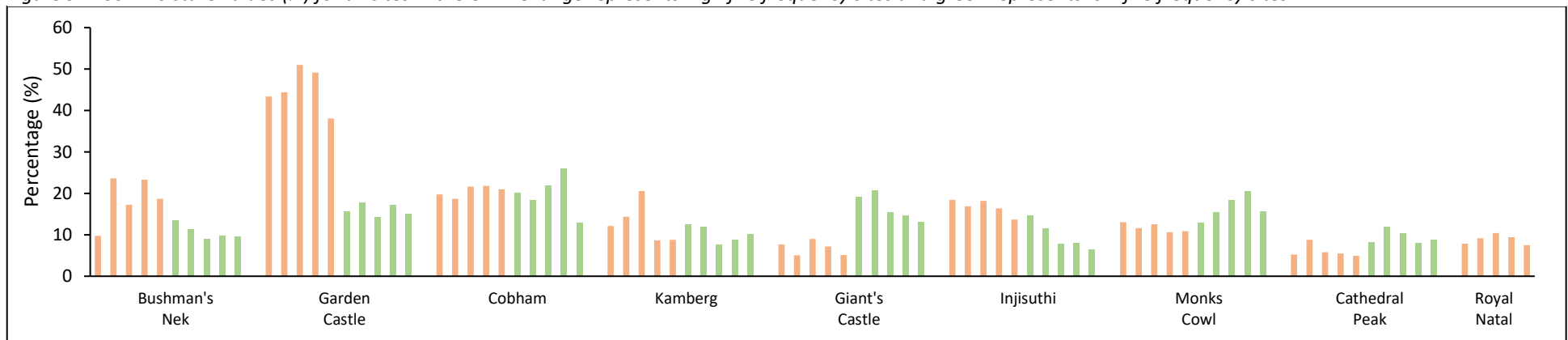


Figure 9.2. Soil organic matter values (pH) for all sites in the UDP. Orange represents high fire frequency sites and green represents low fire frequency sites.

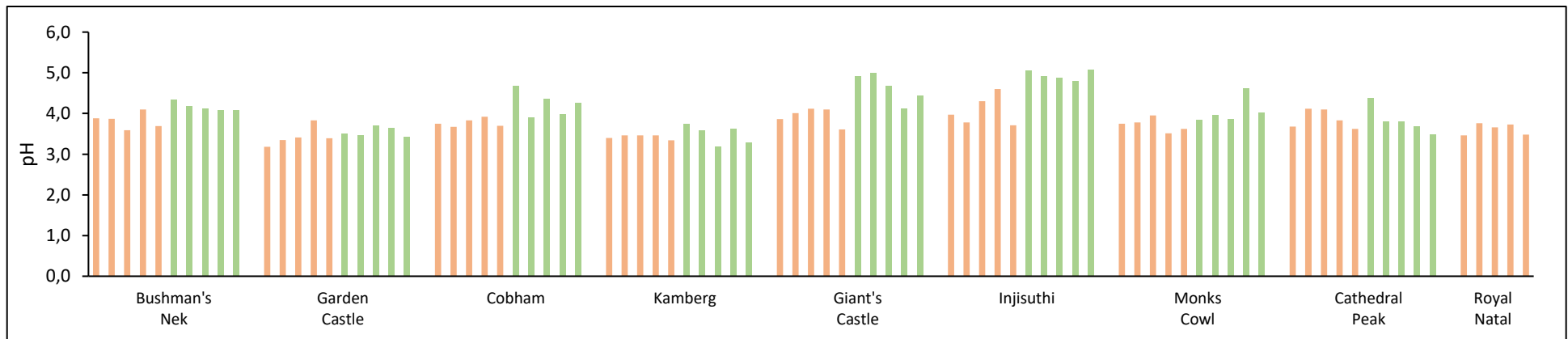


Figure 9.3. Soil pH values for all sites in the UDP. Orange represents high fire frequency sites and green represents low fire frequency sites.





## APPENDIX C: SOIL STATISTICAL DATA

### Regression Models

HP

```
Call:
lm(formula = hp ~ burn + area2 + type + geology1 + aspect2 +
    veg + elevation + slope + sand + clay, data = geo_data)

Residuals:
    Min       1Q   Median       3Q      Max
-1059.87 -366.96   18.26   329.60  1965.83

Coefficients:
                Estimate Std. Error t value Pr(>|t|)
(Intercept)      4376.305  10928.782   0.400  0.6902
burnBurn           32.833    326.733   0.100  0.9203
area2northern    -515.275   1804.109  -0.286  0.7761
area2southern     873.586    945.737   0.924  0.3592
type1            -354.862    163.999  -2.164  0.0343 *
geology1Elliot     54.355    433.357   0.125  0.9006
geology1Karoo Dolerite -299.482    976.542  -0.307  0.7601
geology1Molteno    926.951    774.826   1.196  0.2360
geology1Tarkastad   946.958    475.062   1.993  0.0506 .
aspect2North     -1115.778    542.939  -2.055  0.0440 *
aspect2South     -1850.693   1228.719  -1.506  0.1370
vegNorthern Drakensberg Highland Grassland  1317.746    850.715   1.549  0.1264
vegNorthern KwaZulu-Natal Moist Grassland   315.254   1185.917   0.266  0.7912
vegSouthern Drakensberg Highland Grassland -559.911    513.775  -1.090  0.2800
elevation         -2.095     6.978   -0.300  0.7650
slope              35.675    37.080   0.962  0.3397
sand               17.648    13.050   1.352  0.1811
clay               43.031    28.728   1.498  0.1392

Signif. codes:  0 '***' 0.001 '**' 0.01 '*' 0.05 '.' 0.1 ' ' 1

Residual standard error: 567.3 on 63 degrees of freedom
Multiple R-squared:  0.5498, Adjusted R-squared:  0.4283
F-statistic: 4.526 on 17 and 63 DF,  p-value: 5.219e-06
```

HSV

```
Call:
lm(formula = hsv ~ burn + area2 + type + geology1 + aspect2 +
    veg + elevation + slope + sand + clay, data = geo_data)

Residuals:
    Min       1Q   Median       3Q      Max
 -44.411 -11.897  -4.407   10.656   68.633

Coefficients:
                Estimate Std. Error t value Pr(>|t|)
(Intercept)      457.7352  431.4760   1.061  0.29280
burnBurn          -11.9902   12.8997  -0.929  0.35618
area2northern    -65.4182   71.2275  -0.918  0.36189
area2southern     67.5174   37.3384   1.808  0.07534 .
type1            -2.9674    6.4748  -0.458  0.64831
geology1Elliot     7.0520   17.1092   0.412  0.68161
geology1Karoo Dolerite -7.9839   38.5546  -0.207  0.83661
geology1Molteno    57.6562   30.5907   1.885  0.06408 .
geology1Tarkastad   44.7978   18.7558   2.388  0.01993 *
aspect2North     -43.4010   21.4356  -2.025  0.04714 *
aspect2South     -85.1313   48.5107  -1.755  0.08414 .
vegNorthern Drakensberg Highland Grassland  102.2607   33.5868   3.045  0.00340 **
vegNorthern KwaZulu-Natal Moist Grassland   35.5888   46.8209   0.760  0.45003
vegSouthern Drakensberg Highland Grassland   4.0300   20.2842   0.199  0.84316
elevation         -0.3041    0.2755  -1.104  0.27386
slope              2.7449    1.4639   1.875  0.06543 .
sand               1.4341    0.5152   2.784  0.00709 **
clay               2.3716    1.1342   2.091  0.04057 *

Signif. codes:  0 '***' 0.001 '**' 0.01 '*' 0.05 '.' 0.1 ' ' 1

Residual standard error: 22.4 on 63 degrees of freedom
Multiple R-squared:  0.6135, Adjusted R-squared:  0.5092
F-statistic: 5.882 on 17 and 63 DF,  p-value: 9.268e-08
```

## Soil pH

```
Call:
lm(formula = ph ~ burn + area2 + type + geology1 + aspect2 +
    veg + elevation + slope + sand + clay, data = geo_data)

Residuals:
    Min       1Q   Median       3Q      Max
-0.48749 -0.13391 -0.01167  0.11205  0.50114

Coefficients:
                Estimate Std. Error t value Pr(>|t|)
(Intercept)         6.1857338   4.4560013    1.388 0.169972
burnBurn            -0.2309709   0.1332193   -1.734 0.087851 .
area2northern        0.3602668   0.7355908    0.490 0.626001
area2southern        0.5638632   0.3856063    1.462 0.148636
type1               -0.1744696   0.0668673   -2.609 0.011323 *
geology1Elliot      -0.4554505   0.1766928   -2.578 0.012299 *
geology1Karoo Dolerite -1.0486018   0.3981665   -2.634 0.010617 *
geology1Molteno     -1.2634874   0.3159203   -3.999 0.000169 ***
geology1Tarkastad   -1.1238160   0.1936973   -5.802 2.3e-07 ***
aspect2North         0.0127722   0.2213731    0.058 0.954174
aspect2South         1.0093753   0.5009866    2.015 0.048201 *
vegNorthern Drakensberg Highland Grassland  0.0339226   0.3468629    0.098 0.922403
vegNorthern KwaZulu-Natal Moist Grassland -0.3506256   0.4835351   -0.725 0.471057
vegSouthern Drakensberg Highland Grassland -0.2328461   0.2094819   -1.112 0.270563
elevation            -0.0006974   0.0028452   -0.245 0.807171
slope                -0.0114074   0.0151186   -0.755 0.453346
sand                 0.0020899   0.0053207    0.393 0.695799
clay                 -0.0115715   0.0117134   -0.988 0.326986

Signif. codes:  0 '***' 0.001 '**' 0.01 '*' 0.05 '.' 0.1 ' ' 1

Residual standard error: 0.2313 on 63 degrees of freedom
Multiple R-squared:  0.7886, Adjusted R-squared:  0.7316
F-statistic: 13.83 on 17 and 63 DF, p-value: 3.093e-15
```

## Soil Organic Matter

```
Call:
lm(formula = loss_ig ~ burn + area2 + type + geology1 + aspect2 +
    veg + elevation + slope + sand + clay, data = geo_data)

Residuals:
    Min       1Q   Median       3Q      Max
-10.5270  -2.4175  -0.5472   2.2269  10.7621

Coefficients:
                Estimate Std. Error t value Pr(>|t|)
(Intercept)    -101.88600   84.94721   -1.199 0.234863
burnBurn        11.36780    2.53963    4.476 3.26e-05 ***
area2northern   23.57619   14.02297    1.681 0.097665 .
area2southern  -14.38618    7.35103   -1.957 0.054778 .
type1           -1.28954    1.27473   -1.012 0.315590
geology1Elliot -11.81613    3.36839   -3.508 0.000839 ***
geology1Karoo Dolerite  0.53376    7.59047    0.070 0.944162
geology1Molteno -18.19779    6.02256   -3.022 0.003631 **
geology1Tarkastad -15.63207    3.69256   -4.233 7.62e-05 ***
aspect2North     0.14854    4.22016    0.035 0.972033
aspect2South     14.85207    9.55058    1.555 0.124933
vegNorthern Drakensberg Highland Grassland -18.61481    6.61244   -2.815 0.006500 **
vegNorthern KwaZulu-Natal Moist Grassland -20.63310    9.21790   -2.238 0.028739 *
vegSouthern Drakensberg Highland Grassland  0.42483    3.99347    0.106 0.915618
elevation         0.09758    0.05424    1.799 0.076789 .
slope            -1.11838    0.28821   -3.880 0.000252 ***
sand             -0.80083    0.10143   -7.895 5.44e-11 ***
clay             -0.54391    0.22330   -2.436 0.017700 *

Signif. codes:  0 '***' 0.001 '**' 0.01 '*' 0.05 '.' 0.1 ' ' 1

Residual standard error: 4.41 on 63 degrees of freedom
Multiple R-squared:  0.8229, Adjusted R-squared:  0.7751
F-statistic: 17.22 on 17 and 63 DF, p-value: < 2.2e-16
```

## BIC and AIC Models

HP

```

BIC
BICq equivalent for q in (0.491862424846219, 0.806062978530219)
Best Model:

```

	Estimate	Std. Error	t value	Pr(> t )
(Intercept)	-8629.847388	2084.607306	-4.139795	9.324167e-05
burnBurn	519.723443	135.398029	3.838486	2.634870e-04
area2northern	1438.862971	369.215460	3.897082	2.160147e-04
type1	-354.198819	153.554939	-2.306659	2.395418e-02
geology1Tarkastad	510.101855	154.657445	3.298269	1.513694e-03
aspect2North	-809.653686	253.499217	-3.193910	2.083065e-03
vegSouthern.Drakensberg.Highland.Grassland	-1305.118098	239.405437	-5.451497	6.656394e-07
elevation	6.166561	1.288407	4.786189	8.804705e-06
clay	45.141713	10.746003	4.200791	7.517698e-05

```

Call:
lm(formula = hp ~ burn + area2 + type + geology1 + aspect2 +
    veg + elevation + clay, data = geo_data)

Residuals:
    Min       1Q   Median       3Q      Max
-1042.58  -394.02    8.98   300.32  2252.99

Coefficients:
                Estimate Std. Error t value Pr(>|t|)
(Intercept)    -5870.224   4991.119   -1.176  0.24383
burnBurn         284.044    286.311    0.992  0.32484
area2northern  1300.850    769.443    1.691  0.09570
area2southern   -20.627    491.059   -0.042  0.96662
type1          -321.108    163.199   -1.968  0.05339
geology1Elliot  -19.255    415.989   -0.046  0.96322
geology1Karoo Dolerite  272.381    599.260    0.455  0.65096
geology1Molteno  171.866    593.130    0.290  0.77292
geology1Tarkastad  683.260    434.998    1.571  0.12110
aspect2North   -1283.496    477.816   -2.686  0.00916 **
aspect2South   -925.255    1034.324   -0.895  0.37433
vegNorthern Drakensberg Highland Grassland  461.118    556.702    0.828  0.41053
vegNorthern KwaZulu-Natal Moist Grassland -632.539    764.481   -0.827  0.41103
vegSouthern Drakensberg Highland Grassland -957.020    437.135   -2.189  0.03217 *
elevation         4.907     2.962    1.657  0.10238
clay             24.914     26.193    0.951  0.34504

Signif. codes:  0 '***' 0.001 '**' 0.01 '*' 0.05 '.' 0.1 ' ' 1

Residual standard error: 569.4 on 65 degrees of freedom
Multiple R-squared:  0.532, Adjusted R-squared:  0.424
F-statistic: 4.926 on 15 and 65 DF, p-value: 2.746e-06

```

Soil pH

```

AIC
BICq equivalent for q in (0.531314836889583, 0.789895629252902)
Best Model:

```

	Estimate	Std. Error	t value	Pr(> t )
(Intercept)	7.598766752	0.528448842	14.379380	1.918942e-22
burnBurn	-0.128001442	0.067261412	-1.903044	6.120750e-02
area2southern	0.725056253	0.113036641	6.414347	1.505589e-08
type1	-0.191743092	0.063348352	-3.026805	3.472618e-03
geology1Elliot	-0.512298726	0.142923043	-3.584438	6.254826e-04
geology1Karoo.Dolerite.	-1.348232970	0.180023706	-7.489197	1.714856e-10
geology1Molteno	-1.234132734	0.140524905	-8.782306	7.435062e-13
geology1Tarkastad	-1.195297531	0.133081074	-8.981724	3.221597e-13
aspect2North	0.261977623	0.104976388	2.495586	1.497006e-02
aspect2South	1.292819353	0.166565137	7.761644	5.453529e-11
vegSouthern.Drakensberg.Highland.Grassland	-0.273703093	0.120461251	-2.272126	2.619926e-02
elevation	-0.001825162	0.000305843	-5.967642	9.298255e-08

```

Call:
lm(formula = ph ~ burn + area2 + type + geology1 + aspect2 +
    veg + elevation, data = geo_data)

Residuals:
    Min       1Q   Median       3Q      Max
-0.54724 -0.14306  0.00983  0.11618  0.50280

Coefficients:
                Estimate Std. Error t value Pr(>|t|)
(Intercept)      8.191164   1.886113   4.343 4.95e-05 ***
burnBurn        -0.155161   0.091689  -1.692  0.09531 .
area2northern   -0.060320   0.308994  -0.195  0.84583
area2southern    0.845162   0.193058   4.378 4.38e-05 ***
type1           -0.189835   0.064595  -2.939  0.00454 **
geology1Elliot  -0.465272   0.165790  -2.806  0.00658 **
geology1Karoo Dolerite -1.414008   0.224780  -6.291 2.89e-08 ***
geology1Molteno -1.154229   0.237029  -4.870 7.31e-06 ***
geology1Tarkastad -1.152332   0.175586  -6.563 9.63e-09 ***
aspect2North     0.250859   0.146704   1.710  0.09197 .
aspect2South     1.242962   0.276732   4.492 2.91e-05 ***
vegNorthern Drakensberg Highland Grassland  0.113318   0.217993   0.520  0.60492
vegNorthern KwaZulu-Natal Moist Grassland  0.147839   0.238604   0.620  0.53766
vegSouthern Drakensberg Highland Grassland -0.291577   0.152560  -1.911  0.06032 .
elevation        -0.002223   0.001176  -1.890  0.06313 .

Signif. codes:  0 '***' 0.001 '**' 0.01 '*' 0.05 '.' 0.1 ' ' 1

Residual standard error: 0.2299 on 66 degrees of freedom
Multiple R-squared:  0.7813, Adjusted R-squared:  0.7349
F-statistic: 16.84 on 14 and 66 DF, p-value: < 2.2e-16

```

### Soil Organic Matter

```

BIC
BICq equivalent for q in (0.0244454067636993, 0.508925607443935)
Best Model:

                Estimate Std. Error   t value   Pr(>|t|)
(Intercept)    26.3256989  1.56716541  16.798290 3.927073e-27
burnBurn       5.1200231  1.15858172   4.419216 3.287907e-05
geology1Molteno 6.1792988  1.63970198   3.768550 3.249231e-04
vegSouthern.Drakensberg.Highland.Grassland 6.0944393  1.77966289   3.424491 1.001718e-03
slope          -0.8341280  0.11807578  -7.064345 7.032836e-10
sand           -0.5287806  0.06367861  -8.303896 3.149087e-12

```

```

Call:
lm(formula = loss_ig ~ burn + geology1 + veg + slope + sand,
    data = geo_data)

Residuals:
    Min       1Q   Median       3Q      Max
-9.2287 -2.6511 -0.4082  2.5734 14.6956

Coefficients:
                Estimate Std. Error t value Pr(>|t|)
(Intercept)      32.2353    3.2533   9.909 5.85e-15 ***
burnBurn         6.9037    1.3944   4.951 4.91e-06 ***
geology1Elliot   -7.5122    3.2724  -2.296  0.02470 *
geology1Karoo Dolerite -6.8441    3.6881  -1.856  0.06770 .
geology1Molteno  -1.3634    3.5455  -0.385  0.70173
geology1Tarkastad -6.9762    3.0509  -2.287  0.02525 *
vegNorthern Drakensberg Highland Grassland -2.5392    2.1004  -1.209  0.23077
vegNorthern KwaZulu-Natal Moist Grassland -5.2886    2.8356  -1.865  0.06636 .
vegSouthern Drakensberg Highland Grassland  5.7768    1.8576   3.110  0.00271 **
slope            -0.7701    0.1195  -6.447 1.25e-08 ***
sand             -0.5217    0.0742  -7.030 1.10e-09 ***









Signif. codes:  0 '***' 0.001 '**' 0.01 '*' 0.05 '.' 0.1 ' ' 1









Residual standard error: 4.762 on 70 degrees of freedom
Multiple R-squared:  0.7706, Adjusted R-squared:  0.7378
F-statistic: 23.51 on 10 and 70 DF, p-value: < 2.2e-16

```

APPENDIX D: SITE COMPARISON PHOTOGRAPHS

Table 9.4. Site photographs comparing high and low fire frequency sites.

Site	High fire frequency	Low fire frequency
Bushman's Nek		
Garden Castle		
Cobham		
Kamberg		

Giant's Castle		
Injisuthi		
Monk's Cowl		
Cathedral Peak		
Royal Natal	